CONNECTING BRAIN TUMOR STEM CELLS WITH THEIR PRIMARY TUMOR AND EXPLORING GLYCOGEN SYNTHASE KINASE-3β REGULATION OF CELL FATE

TING HUI LING, ESTHER
(B.Sc. (Hons.), NUS)

A THESIS SUBMITTED

FOR THE DEGREE OF MASTER OF SCIENCE

DEPARTMENT OF PHYSIOLOGY

NATIONAL UNIVERSITY OF SINGAPORE

2011

ACKNOWLEDGEMENTS

Research is a process of discoveries – scientific discoveries and discoveries of oneself. Validating new hypotheses, uncovering novel insights but more to that, there is also the exploration of propelling oneself beyond your potential, to set higher goals that if you believe, would be achievable. I would like to sincerely thank my supervisors Dr Carol Tang Soo Leng, A/Prof Soong Tuck Wah and my co-supervisor A/Prof Ang Beng Ti for their continual guidance and mentorship. My gratitude also to all lab members for striving together in our research pursuits. I would also like to thank our collaborators from Eli Lilly Singapore who have been instrumental in providing materials and technical support. My deep appreciation for my thesis examiners A/Prof Lim Kah Leong and Dr Alan Lee Yiu Wah for kindly availing their precious time to evaluate my thesis. Importantly, my family who are my pillars of support and who are always there for me.

TABLE OF CONTENTS

RESULTS

SUMMARY

Malignant brain tumors such as glioblastoma multiforme (GBM) and oligodendroglial tumors can arise from a subpopulation of cells with stem-like properties, commonly called glioma-propagating cells (GPCs). GPCs exhibit resistance to conventional therapies, hence are the likely culprits of tumor recurrence. These cells are controversial largely because their identity depends on the context of animal assays designed to measure the tumor-initiating cell frequency. Our study describes the derivation of GPCs from a patient with anaplastic oligoastrocytoma, NNI-8. We show that these GPCs displayed stem-like characteristics with extensive self-renewal capability, and preserve the karyotypic integrity of the primary tumor. Importantly, the glioma xenograft phenocopied the patient's original tumor histopathology. We explored if GPCs derived from these glioma variants can serve as reliable *in vitro* culture systems for studies. We utilized gene expression analyses, since GBM and oligodendrogliomas can be molecularly classified. Accordingly, we derived a gene signature distinguishing oligodendroglial GPCs from GBM GPCs collated from different studies, which was enriched for the Wnt, Notch and TGFβ pathways. Using a novel method in glioma biology, the Connectivity Map, we mapped the strength of gene signature association with patient gene expression profiles in 2 independent glioma databases. Our gene signature consistently stratified survival in glioma patients. This data would suggest that *in vitro* low passage GPCs are similarly driven by transcriptomic changes that characterize the favorable outcome of oligodendrogliomas over GBM. Additionally, the gene signature was associated with the 1p/19q co-deletion status, the current clinical indicator of chemosensitivity. Our gene

signature detects molecular heterogeneity in oligodendroglioma patients that cannot be accounted for by histology or the 1p/19q status alone, and highlights the limitation of morphology-based histological analyses in tumor classification, consequently impacting on treatment decisions. Furthermore, these findings highlight the clinical contribution of GPCs to disease progression and survival outcome; thus linking for the first time, the controversial "cancer stem cells" to the primary tumor.

We identified GSK3β as a possible target of GPCs in a collaborative small molecule screen with Eli Lilly. Utilizing a well-known GSK3 inhibitor, BIO, together with shGSK3β knockdown, we show that GSK3β maintains GPC survival, preferentially in the $CD133^+$ population that is frequently associated with tumor-initiating potential. Reduced GSK3β triggers apoptosis and a reduction in c-Myc oncoprotein, with concomitant differentiation. Interestingly, we observed increased proliferation in the $CD133^-$ non-tumor stem cell population. While GSK3β may be crucial to maintain the tumor-propagating fraction, these data indicate that tumor cells interact with their microenvironment, and one needs to target both cellular fractions for an effective therapeutic approach. Our findings thus challenge the "cancer stem cell hypothesis" that only the tumor-initiating fraction is relevant for therapeutic targeting, and further underscores the complexity of the tumorigenic process.

LIST OF TABLES

LIST OF FIGURES

Page Number

LIST OF ABBREVIATIONS

Abbreviations	Definition
ALDH	Aldehyde dehydrogenase
ALV	Avian Leukosis Virus
AP-1	Activator protein 1
APC	Adenomatous polyposis coli
AURKA	Aurora A/TAK1
BDNF	Brain-derived neurotrophic factor
bFGF	Basic fibroblast growth factor
BIO	6-bromoindirubin-3'-oxime
CD133	Complementarity determinant 133
CD15	Complementarity determinant 15
CDK	Cyclin-Dependent Kinase
CLASP	CLIP-associated protein
CREB	Cyclic AMP response element binding protein
CRMP2	Collapsing response mediator protein 2
CSC	Cancer stem cell
DAPI	4'6-diamidino-2-phenylindole
DMEM	Dulbecco's modified Eagle's medium
DMSO	Dimethyl sulfoxide
EGFR	Epidermal growth factor receptor
eIF-2B	Eukaryotic protein synthesis initiation factor-2B
GBM	Glioblastoma multiforme
GFAP	Glial fibrillary acidic protein
GPC	Glioma-propagating cell
GSK3	Glycogen synthase kinase 3
H&E	Hematoxylin and eosin
HRP	Horseradish peroxidase

LIF	Leukemia inhibitory factor
KLC	Kinesin light chain
LRP6	Low-density lipoprotein receptor-related protein 6
MAP	Mitogen-activated protein
MAP1B	Microtubule-associated protein 1B
MMLV	Moloney Murine Leukemia Virus
MOI	Multiplicity of infection
Msi-1	Musashi-1
mTOR	Mammalian target of rapamycin
NF-κB	Nuclear factor-kappaB
NF1	Neurofibromin 1
NFATc	Nuclear factor of activated T cells
NG2	Neuroglial chondroitin sulfate proteoglycan 4
NSG	Non-obese diabetic/severe combined immunodeficiency gamma
Oct4	Octamer-binding transcription factor 4
OPC	Oligodendrocyte progenitor cell
PARP	Poly (ADP-ribose) polymerase
PCA	Principal Component Map
PDGFR	Platelet-derived growth factor receptor
PI3K	Phosphoinositide 3-kinase
PKB	Protein kinase B
PLK	Polo-Like Kinase
PTEN	Phosphatase and tensin homologue
PYK2	Proline-rich tyrosine kinase 2
Rb	Retinoblastoma
REMBRANDT	Repository of Molecular Brain Neoplasia Data
RTK	Receptor Tyrosine Kinase
SP	Side Population
SSEA-1	Stage-specific embryonic antigen 1

TCGA	The Cancer Genome Atlas
TGFβR1	Transforming growth factor beta receptor 1
TRAIL	Tumor necrosis factor-related apoptosis-inducing ligand
TSC2	Tuberous sclerosis 2
TuJ1	Neuron-specific class III beta-tubulin
WHO	World Health Organisation

CHAPTER 1 - INTRODUCTION

1.1 BRAIN TUMORS

1.1.1 Classification of Gliomas

Brain tumors of the astrocytic lineage predominate the spectrum of adult malignant central nervous system disorders. Variants such as glioblastoma multiforme (GBM) portend poor prognosis despite advanced surgical interventions, accompanied by adjuvant radiation therapy and chemotherapy[1, 2]. Gliomas are classified according to the World Health Organization (WHO) scheme[1, 3] which is based upon the absence or presence of 4 criteria; namely nuclear atypia, mitoses, endothelial cell proliferation, and necrosis (Table-1). Importantly, the classification scheme is based on morphology which can be subjective. Clinically, tumor grade is a major factor influencing the type of therapy administered. The designation of grade III describes neoplasms with histological evidence of malignancy, such as nuclear atypia and brisk mitotic activity. Grade IV describes cytologically malignant, mitotically active and necrosis-prone neoplasms, which are usually associated with rapid pre- and postoperative disease progression leading to fatal outcome. Extensive infiltration of surrounding tissue also typifies some grade IV neoplasms[1]. Among the gliomas of better prognosis are the oligodendroglial tumors. These tumors typically respond better to chemotherapies and possess genetic indicators such as the 1p/19q co-deletion status which predicts its chemosensitivity[4]. Traditional anatomic/pathologic categorization of tumors has very limited ability to completely stratify patients into meaningful subgroups for prognosis and intervention.

Table-1. WHO grading of glial tumors is based on histology. WHO grading of glial tumors into grades I-IV is based upon the presence or absence of 4 criteria; namely nuclear atypia, mitoses, endothelial cell proliferation, and necrosis. Adapted from Kleihues *et al*. [5].

WHO Grade	Type of glial tumor	Criteria
WHO I	Pilocytic astrocytoma	Low cellularity Rosenthal fibres May have microvascular proliferation
WHO II	Diffuse astrocytoma	Well differentiated neoplastic astrocytic cells Cellularity moderately increased Mitotic activity absent No microvascular proliferation or necrosis
WHO III	Anaplastic astrocytoma	Distinct nuclei atypia Cellularity increased Marked mitotic activity No microvascular proliferation or necrosis
WHO IV	GBM	Pleomorphic astrocytic tumor cells, marked nuclei atypia Cellularity increased Brisk mitotic activity Microvascular proliferation OR necrosis

1.1.2 Molecular Stratification of Gliomas

In 2006, the National Cancer Institute, USA, initiated a public effort (The Cancer Genome Atlas, TCGA) to collate genomic and clinical data from patients of selected cancers[6]. GBM was one of these cancers because of its poor prognosis and impact to healthcare. The effort was predicated on increasing evidence that showed that the patient's gene expression and genetic makeup drive disease progression and consequently survival outcome[7]. Indeed, recent work highlighted that GBM tumors, despite being histologically

similar, can be subtyped into 4 molecular classes: Proneural, Classical, Neural and Mesenchymal[7]. Each class is distinguished by unique gene expression as well as genetic aberrations. Importantly, GBM tumors are driven by mutations frequently occurring in the 3 key signaling pathways: p53, retinoblastoma (Rb) and Receptor Tyrosine Kinases (RTKs)[6]. These molecular subclasses could thus account for the frequently observed inter-patient variability to treatment response. Similar molecular heterogeneity has been observed in other glioma variants, as well as within oligodendrogliomas[8-10]. These findings thus support a patient-tailored approach to designing effective medicines.

One of the important implications of TCGA is patient heterogeneity. This presents challenges in scientific endeavors, particularly in the lab where cellular systems and animal models must reflect the patient's uniqueness. These challenges form the basis for our investigations described in this thesis.

1.2 ANIMAL MODELS OF GLIOMA

Several models of glioma in mice have been established[11]:

1.2.1 Somatic Cell Gene Transfer Models

Somatic cell gene transfer methods make use of viral vectors to transfer genes to a specific subset of somatic cells postnatally. These methods utilize the replication competent Moloney Murine Leukemia Virus (MMLV)[12], an avian leukosis virus (ALV)-based replication competent virus (RCAS) and its receptor tumor virus-A (tv-a)[13], and a replication-incompetent adenovirus engineered to carry Cre recombinase (Ad-Cre)[14]. Somatic cell mouse models involving key genes have been described; the neurofibromin 1

(NF1), epidermal growth factor receptor (EGFR) and Platelet-derived growth factor receptor (PDGFR) classes[7]. While these models serve as very good tools for preclinical studies, they lack the ability to trace the etiology of the disease.

1.2.2 Transgenic Models

Transgenic models utilize genetic manipulation of signal transduction pathways involved in the development of gliomas, through germline genetic modification techniques, which recapitulate the mechanism of glioma initiation more closely than do transplantation or somatic cell gene transfer models targeting generally diverse cell types. Further refinement of disease etiology can be derived from gene deletions mediated through cell type-specific Cre, which allows for characterization of the cell-of-origin alongside its differentiated progeny, as has been elegantly shown in intestinal cancers[15]. Recent works have highlighted the importance of neural stem cells as the cells-of-origin with mutations in NF1/Pten/p53[14], or p53/Pten[16], as opposed to arising from the more mature progeny such as astrocytes, in contributing to GBM formation. In addition, the clever use of color cassettes tracing different proliferating progeny upon sporadic induction of mutations in the neural stem cell compartment allowed for visualization of the transformation process prior to tumor growth[17], thus challenging for the first time that mutations in initiating cells may confer only transformational powers but may not eventually be the cells forming the tumor bulk. Transgenic models are powerful because they offer a window into the events governing the tumorigenic process.

1.2.3 Orthotopic Transplantation Models

One of the important findings of TCGA was the demonstration that orthotopic xenograft tumors established from surgical material recapitulated the GBM molecular subtypes and patient heterogeneity[7, 18]. Moreover, xenograft models have reliably maintained serially-transplanted, human-derived glioma-propagating cells (GPCs), with preservation of primary tumor transcriptomic and karyotypic hallmarks[19]. Although this model cannot identify the cell-of-origin, and lacks in providing suitable tumor microenvironment interactions and host immune responses, it remains important for several reasons: Implantations of GPCs grown under serum-free condition form tumors that recapitulate the gene expression, phenotypic and karyotypic profiles of their primary tumors[19], these xenografts are thus important "replicas" of human tumors that can be prospectively tested with new candidate compounds, yet have retrospective clinical history, gene expression, and paraffin tissue blocks for mining prognostic indicators. This is an important endeavor as small molecule candidates cannot be currently tested in truly treatment-naïve patients, because doctors do not deny the patient the standard care of drugs (e.g. temozolomide). The mouse "replicas" will thus provide the alternative to testing tumor response to drugs, mirroring as closely as possible the biology of the patient's original tumor.

1.3 GLIOMA STEM CELLS OR -PROPAGATING CELLS

In recent years, the distinction between glioma stem cells, glioma-initiating or –propagating cells has been highlighted. Elegant transgenic models have shed light on the role of neural stem cells as the transformational

cells in GBM formation, hence their accurate terminology as glioma stem cells or -initiating cells[14, 16, 17]. Traditionally, the similar identification of these cells in clinical specimens has followed the studies involving first, leukemic stem cells[20] and now several other tumor systems[21-24]; namely, tumor-initiating capacity was defined as cells which conferred significant tumor initiation in xenografted animals. However, recently, Quintana *et al*.[25] challenged the definition of the tumor-initiating cell by showing that tumor initiation could be altered based on 3 parameters: Addition of matrigel, varying the severity of immune-compromised mice depending on strains used, and extending the time to formation of the tumor. This study thus demonstrated that the tumor-initiating capacity is an artifactual consequence of the conditions employed in the xenograft model. Despite the lack of ability of *in vitro* cultured stem cell-like GPCs to reflect the actual transformational cell in tumorigenesis, these cells remain valuable for several reasons: First, they have been shown to retain transcriptomic and karyotypic features commonly found in the primary tumor, compared to commercially procured serum-grown glioma cells which often contain additional genomic aberrations[19, 26]. Second, only GPCs establish xenograft tumors that recapitulate the patient's original histopathology[19]. Finally, transcriptomic analyses suggest that the stemness properties of GPCs and other cancer stem cells are enriched in high grade, malignant tumors, and contributes to disease progression and survival outcome[27]. These reasons underscore the importance of GPCs as a relevant cellular system to study. The terminology of "glioma-propagating cells" has now been assigned to these *in vitro* passaged cells to illustrate their properties in the context of an animal model (Fig. 1).

Our earlier work described the isolation and characterization of patient-derived GPCs[28]. Two important observations were made: (1) Histologically similar GBM tumors yielded GPCs with very different transcriptomic profiles, suggesting that these underlying differences may account for the frequently observed inter-patient variability to treatment response. In support, Shats *et al*.[27] has shown that a stemness signature derived from embryonic stem cells could predict the breast cancer patient cohort sensitive to small molecules linked to this signature using the Connectivity Map[29], demonstrating the clinical contribution of cancer stem cells to patient outcome; (2) Many investigators have repeatedly derived new GPC lines or serially propagated the cells in animals to maintain their lines. What this means is that GPCs are constantly treated as reproducible entities, even though they're really derived from different patients. In addition, serial propagation in animals has been shown to result in a genetic drift towards highly proliferating genes[18]. The end result is that the original features of these lines are lost. With our novel cryopreservation technique, we have essentially resolved the bottleneck in maintaining these cells. That is, we now have a reliable repository of different patients' lines which can be thawed upon experimental needs, and we have characterized them so we know what each patient's phenotypic and transcriptomic profiles looks like. This greatly enhances any projects that deal with larger patient numbers that addresses the patient stratification hypothesis. Collectively, these findings form the foundation of our work described here: We have suitable xenograft models that recapitulate the patient's original histopathology, and we have GPCs which reflect the patients' molecular heterogeneity.

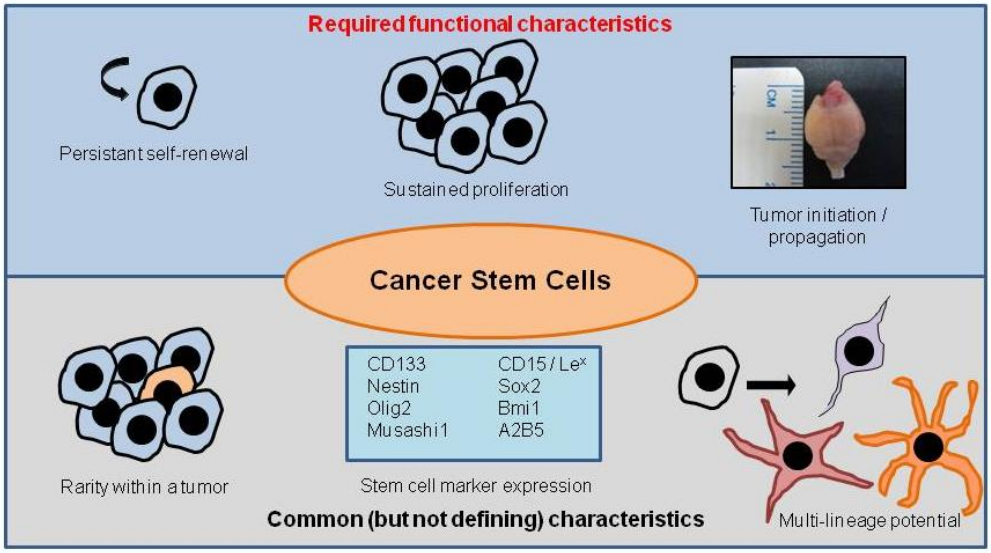

Figure-1. Cancer stem cells (CSCs) are defined by functional characteristics. CSCs are defined by their capacity for sustained self-renewal, persistant proliferation and tumor initiation/propagation. Some characteristics which are commonly but may not be necessarily associated with CSCs are that CSCs constitute only a minority population, can be isolated by cell surface markers, and display multipotency upon induction of differentiation. Adapted from Rich and Eyler[30].

1.3.1 Assays to Define Functional Activity of Glioma-Propagating Cells

In recent years, several markers have been proposed to represent the tumor-initiating or stem cell in brain tumors. These include complementarity determinant 133 (CD133)[31], stage-specific embryonic antigen 1 (SSEA-1)[32], Nestin[33], aldehyde dehydrogenase (ALDH)[33] and the Side Population (SP)[34, 35]. Many of these markers are also present on normal cellular counterparts, hence do not present the best targeting candidates in any therapeutic strategy. Furthermore, markers such as CD133 are debatable as tumors have also been shown to arise from CD133-negative cells in a subset of GBM tumors[36, 37]. In addition, CD133 expression changes with surface sialylation according to disease state and progression[38, 39], further complicating its definition as a marker of *bona fide* tumor-initiating capacity. Thus, the field of cancer stem cells is moving away from heavy reliance on surface markers, to

complementing findings by adopting assays which measure the functional activities of tumor stem cells.

The neurosphere assay is often used to approximate neural stem cell frequency in normal biology[40]. Neurospheres are heterogeneous and comprise long-term, self-renewing neural stem cells, as well as short-term, transiently-amplifying progenitors. Thus, sphere frequency is typically scored over 3-4 generations to measure the activity of *bona fide* neural stem cells, compared to transient progenitors which cease sphere formation typically after 1-2 generations[41]. This sphere frequency has often been shown to translate to *in vivo* animal survival outcome[2, 42]. Sphere size which is also measured represents proliferation. This readout of individual spheres is important because it distinguishes proliferation arising from the stem cell population, which is masked if general 3-(4,5-Dimethylthiazol-2-yl)-2,5-diphenyltetrazolium bromide (MTT)-based viability tests are carried out that also measure the proliferation of progenitors. We utilized these functional assays to complement our current studies and conclusions.

1.4 GAP IN KNOWLEDGE

Our effort described here comprises the following:

1. We derived and characterized GPCs from a high grade oligodendroglial tumor. GPCs have routinely been isolated from such tumors, and more commonly, from GBM. Our oligodendroglial GPCs, NNI-8, established tumor xenografts that were distinct from GBM tumors, and illustrated typical features of oligodendroglial tumors. It is tempting to speculate that such tumor phenotypes are driven by transcriptomic programs residing in

GPCs. By inference, different patients' GPCs would be unique phenocopies of their primary tumors. If so, such a repository of GPCs would be very valuable for recapitulating the tumor profiles of patients and be amenable to preclinical drug compound testing. In addition, we would also be able to study signaling pathways distinguishing GPC subtypes, and therefore possibly targeting more primary tumor subtypes.

2. We embarked on a small molecule screen to look for candidate compounds targeting GPC survival. Several known targets were identified, thus validating our screen. Novel targets included glycogen synthase kinase 3 (GSK3), which was selected for our subsequent studies because of its dual role in cell death and cell fate.
3. We show that GSK3β regulates GPC maintenance and survival. Depletion of GSK3β activity impairs proliferation, triggers apoptosis and reduces tumor stem cell frequency. A pro-differentiation response is also observed.

Collectively, our approach conveys important information that GPCs capture the molecular heterogeneity of primary tumor subtypes and can be effectively targeted by GSK3β inhibition. We further show the importance of a tight balance between cell death and cell fate in maintaining GPCs.

1.5 GSK3 REGULATION AND SIGNALING

Physiological regulation of GSK3 activity by a number of upstream kinases[43-46] in various physiological and pathological conditions has been reported[47]. The activity of GSK3 is controlled by an activating Tyr279/Tyr216 phosphorylation or an inhibitory Ser21/Ser9 phosphorylation. GSK3 is

phosphorylated constitutively and essentially stoichiometrically at a single tyrosine residue (Tyr279 in GSK3α and Tyr216 in GSK3β)[48], and the dephosphorylation of this residue ablates activity *in vitro*[48]. Evidence from mammalian cells has shown that an intramolecular autophosphorylation event may play an important role in stabilizing GSK3[49]. However, tyrosine phosphorylation of GSK3 does not seem to be greatly influenced by extracellular signals[49]. Instead, it is now well published that the activity of GSK3 is inhibited in response to a variety of agonists resulting from the phosphorylation of a single serine residue (Ser21 in GSK3α and Ser9 in GSK3β)[50, 51]. Fig. 2 shows a schematic representation of mammalian GSK3α and GSK3β with the tyrosine and serine phosphorylation sites pointed out by arrowheads (adapted from Doble and Woodgett[47]).

Insulin stimulation of cells results in inactivation of GSK3 through a phosphoinositide 3-kinase (PI 3-kinase)-dependent pathway. PI-kinase-induced activation of protein kinase B (PKB), also known as Akt, results in PKB phosphorylation of Ser9 in GSK3β and Ser21 in GSK3α, thereby inhibiting GSK3 activity[44]. Inhibition of GSK3 activity results in dephosphorylation of substrates such as glycogen synthase and eukaryotic protein synthesis initiation factor-2B (eIF-2B), leading to activation of their functions, with a subsequent enhanced glycogen and protein synthesis[52]. In addition, growth factors like epidermal growth factor (EGF), platelet-derived growth factor (PDGF) and brain-derived neurotrophic factor (BDNF) also inactivate GSK3 through Ser9/Ser21 phosphorylation. These growth factors stimulate the GSK3-inactivating kinase p90 ribosomal S6 kinase (p90RSK) (or MAPKAP-K1) through mitogen-activated protein (MAP) kinases,

activators of p70 ribosomal S6 kinase (p70S6K), activators of cAMP-activated protein kinase (PKA) and PKC activators[47]. Wnt-induced inhibition of GSK3 also occurs but GSK3 does not become phosphorylated at Ser9 upon induction of Wnt signalling. Instead, phosphorylation of proteins in the Wnt pathway such as axin, adenomatous polyposis coli (APC) and β-catenin might involve high-affinity interactions with GSK3 in the Wnt multiprotein signalling complex[51].

Recent work has demonstrated two possible candidates for kinases that might contribute to tyrosine phosphorylation of GSK3, namely the proline-rich tyrosine kinase 2 (PYK2), a calcium-sensitive enzyme and the Fyn tyrosine kinase[47]. GSK3 phosphorylates several transcription factors, such as β-catenin, c-Jun, c-Myc, and cyclic AMP response element binding protein (CREB)[53]. Upon GSK3 phosphorylation, most of these transcription factors transcription factors subsequently undergo proteosomal degradation. Other substrates of GSK3 include the microtubule-associated protein Tau, involved in the control of neuronal polarization and axon growth, and the pro-apoptotic protein Bax[53].

In addition, many proto-oncogenic or tumor suppressing transcription and translation factors are substrates of GSK3β. Tumor suppressor transcription factor p53 is a substrate of GSK3β where the levels as well as intracellular localization of p53 are modulated[54]. Moreover, the activity of transcription factors, activator protein 1 (AP-1) and nuclear factor-κB (NF-κB) are also directly regulated by GSK3β[55-57]. These transcription factors possess a vital role in neoplastic transformation and tumor formation. An illustration of the GSK3 signalling pathway is shown in Fig. 3, while Fig. 4 shows a

summary of proposed substrates of GSK3 involved in various functions in the cell.

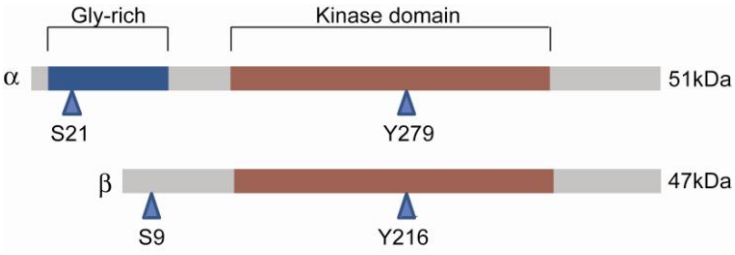

Figure-2. Schematic representation of GSK3α and GSK3β in mammals. The blue arrowheads indicate sites of tyrosine phosphorylation, Tyr279 (GSK3α)/ Tyr216 (GSK3β), and sites of serine phosphorylation, Ser21 (GSK3α)/ Ser9 (GSK3β). (Adapted from Doble and Woodgett[47]).

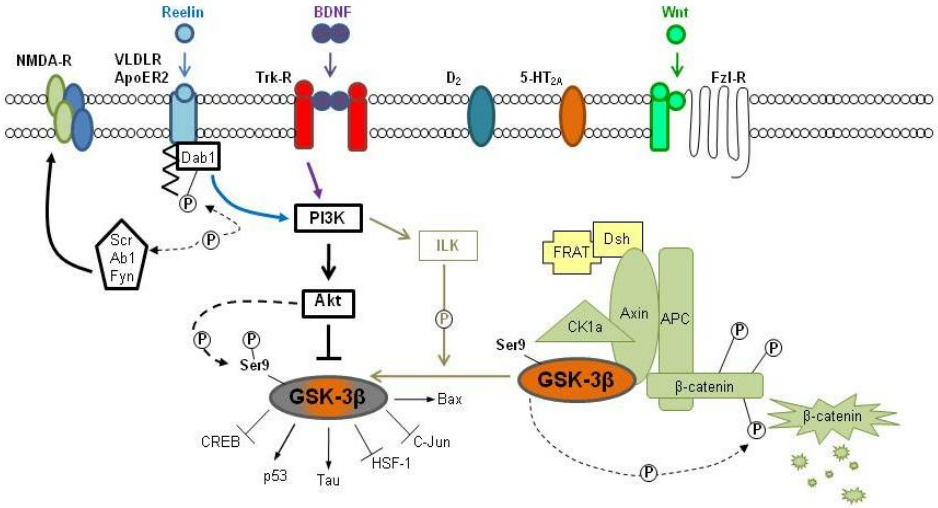

Figure-3. An illustration of the GSK3 signalling pathway. GSK3 inhibition through Ser21/Ser9 phosphorylation occurs upon insulin, growth factor stimulation or via Wnt-induction, leading to the inhibition of phosphorylation of downstream transcription factors. (Adapted from Koros and Dorner-Ciossek[58]).

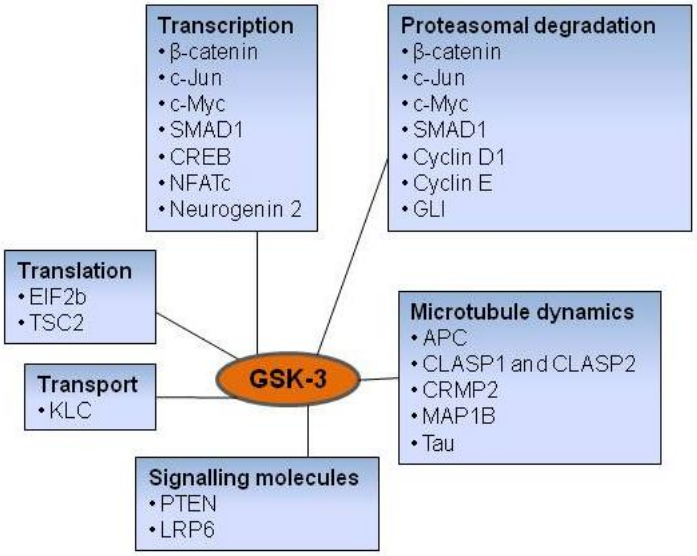

Figure-4. Representative GSK3 substrates involved in various cellular functions. GSK3 phosphorylates several transcription factors including β-catenin, c-Jun, c-Myc, SMAD1, CREB, nuclear factor of activated T cells (NFATc) and neurogenin 2. Upon GSK3 phosphorylation, these transcription factors subsequently undergo proteasomal degradation. GSK3 phosphorylation also influences proteasomal targeting and degradation of other proteins such as cyclin D1 and cyclin E. Microtubule-associated proteins, which are also substrates, include adenomatosis polyposis coli (APC), CLIP-associated protein 1 (CLASP1) and CLASP2, collapsing response mediator protein 2 (CRMP2), microtubule-associated protein 1B (MAP1B) and Tau. Molecules involved in signalling, such as phosphatase and tensin homologue (PTEN) and Wnt co-receptor low-density lipoprotein receptor-related protein 6 (LRP6), are also phosphorylated by GSK3. Other substrates of GSK3 are kinesin light chain (KLC), which function to regulate selective transport, and important elements of the translational machinery, such as eukaryotic initiation factor 2B (EIF2B) and tuberous sclerosis 2 (TSC2). (Adapted from Hur and Zhou[53]).

1.5.1 GSK3β in Tumorigenesis

The dysregulation of GSK3β has been associated with tumorigenesis and cancer progression. However, it remains controversial as to whether GSK3β is a "tumor suppressor" or "tumor promoter"[59]. In certain types of tumors, GSK3β may function as a "tumor suppressor", but enhances the growth and development of yet other kinds of tumors. Reports have shown GSK3β to be a negative regulator of skin tumorigenesis. In a study that utilizes a mouse epidermal multistage carcinogenesis model, it was shown that inactivation of GSK3β takes place during mouse skin carcinogenesis, in that

there was a stark elevation in phosphorylation of Ser9 (inactive form of GSK3β) and drastic drop in Tyr216 phosphorylation (active form of GSK3β) in late papillomas and squamous cell carcinomas[60]. Moreover, a study conducted using human skin cancer tissues showed high pGSK3β(Ser9) expression in squamous cell carcinoma cells[61]. These and other studies indicate that GSK3β plays a role in tumor development during skin carcinogenesis, and inactivation or down-regulation of GSK3β would make it oncogenic for epidermal cells[62].

The role of GSK3β as a tumor suppressor is also evident in mammary tumors. Studies have shown that kinase-inactive GSK3β in mouse mammary glands promotes mammary tumorigenesis, mediated by dysregulation of the Wnt/β-catenin pathway[63]. On the other hand, studies have also provided evidence of GSK3β as a promoter of tumorigenesis and cancer progression. Overexpression of the GSK3β protein has been reported in human ovarian, colon and pancreatic carcinomas[57]. It has been shown that in a mouse model of hepatic carcinogenesis, elevated levels of GSK3β correlating with positive regulation of the proliferation and survival of human ovarian cancer cells both *in vivo* and *in vitro* are observed[64]. In colon cancer cell lines, GSK3β expression has also been demonstrated to be elevated, and ablation of GSK3β by pharmacological inhibition or RNA interference led to a decrease in survival and proliferation of colon cancer cells both *in vitro* and *in vivo*[65]. In addition, GSK3β inhibition reduces pancreatic cancer cell survival and proliferation[66], and studies conducted in hepatocellular, prostate and lymphocytic leukemia cancer cells have also reported that proliferation and

survival is enhanced upon GSK3β activation[67-70], thereby validating GSK3β inhibition as an attractive therapeutic target.

Studies have been conducted to implicate the role of GSK3β in GBMs. Kotliarova *et al.*[71] has shown that GSK3 inhibition reduced glioma cell survival and clonogenicity, through the effects of c-Myc, decrease in NFκB, and alteration of glucose metabolism, leading to apoptosis and cytotoxicity. In addition, Korur *et al.*[72] has demonstrated that Bmi1, the polycomb group gene needed for neural stem cell self-renewal is highly expressed in GBMs, and Bmi1 downregulation led to a concomitant reduction in GSK3β levels, also found to be overexpressed in GBMs. GSK3β inhibition further induced tumor cell differentiation, apoptosis and reduction in clonogenicity. Many of these studies were carried out in commercially procured, serum-grown glioma cells. It remains to be investigated if GPCs, the tumor-initiating cells, can be effectively targeted by GSK3β inhibition.

1.5.2 Investigating the Role of GSK3β in GPCs

In collaboration with Eli Lilly, we carried out a small molecule screen targeting various oncologic pathways, and discovered GSK3β as a potential drug target in our GPCs. Utilizing the GSK3 specific inhibitor BIO as well as lentiviral shGSK3β, we observed the effects of GSK3β inhibition on cell viability, levels of the apoptotic protein cleaved poly (ADP-ribose) polymerase (PARP), oncoprotein c-Myc, as well as the neuronal marker β-tubulin (TuJ1), to assess for pro-differentiation effects upon GSK3β inhibition. The pro-differentiation effect induced by GSK3β inhibition was also validated through immunofluorescence analyses. Subsequently, flow-cytometric

analysis revealed a decrease in the levels of the stem cell marker CD133, and NFκB, and an increase in PARP. We also utlized the neurosphere assay and soft agar assay, and observed an abrogation of self-renewal capability as well as *in vitro* tumorigenic potential. The implication of the GSK3β pathway in regulation of GPCs should provide new insights into the generation of therapeutic interventions targeted at cancer stem cells.

CHAPTER 2 - MATERIALS AND METHODS

GPC cell lines from this study, "Gunther"[73] and "Pollard"[74]; gene expression data processing and the derivation of the oligodendroglial GPC gene signature are described in supplementary methods in the appendix section.

2.1 Tissue Collection and Primary Oligoastrocytoma Neurosphere Culture

Graded brain tumor specimens were obtained with informed consent, as part of a study protocol approved by the institutional review board. In this study, NNI-8 was from a patient with primary anaplastic oligoastrocytoma who was treatment-naive. NNI-1 was from a patient with recurrent GBM (grade IV) who had received radiation therapy, and NNI-4, NNI-5, and NNI-11 were from patients with primary GBM who were treatment-naive. Tumors were processed using methods established in our previous work[28]. Cells were seeded at a density of 2,500 cells per cm^2 in chemically defined serum-free selection growth medium consisting of basic fibroblast growth factor (bFGF; 20 ng/ml; PeproTech, New Jersey), epidermal growth factor (EGF; 20 ng/ml; PeproTech), human recombinant leukemia inhibitory factor (LIF; 20 ng/ml; Chemicon, Temecula, CA), heparin (5 μg/ml; Sigma-Aldrich, St. Louis), and serum-free supplement (B27; 1×; Gibco, Grand Island, NY) in a 3:1 mix of Dulbecco's modified Eagle's medium (DMEM; Sigma-Aldrich) and Ham's F-12 Nutrient Mixture (F-12; Gibco). The cultures were incubated at 37°C in a water-saturated atmosphere containing 5% CO_2 and 95% air. To maintain the undifferentiated state of neurosphere cultures, growth factors were replenished

every 2 days. Differentiation was carried out over 14 days in DMEM/F12 without growth factors, supplemented with 5% fetal bovine serum (FBS; Invitrogen, Carlsbad) and B27. Successful neurosphere cultures (1–2 weeks) were expanded by mechanical trituration using a flame-drawn glass Pasteur pipette, and cells were reseeded at 100,000 cells per milliliter in fresh medium.

2.2 GSK3 inhibitor Treatment *in Vitro*

Compound 14 was kindly provided by Eli Lilly (Indianapolis, IN, USA). The small molecule of 6-bromoindirubin-3'-oxime (BIO), a specific inhibitor of glycogen synthesis kinase-3 (GSK-3), was purchased from Calbiochem (San Diego, CA, USA). All drugs were dissolved in 100% DMSO and used at the concentrations specified in our study.

2.3 Cell Proliferation and Viability Assays

To assess cellular proliferation rates, cells were harvested and plated into 96-well plates at 5000 cells per well. Wells containing media only without cells were used as a background control. Cytotoxicity assay to measure viability of cells after drug treatment was carried out by plating 5000 cells per well into 96-well plates. Wells containing cells and treated with dimethyl sulfoxide (DMSO) (Merck & Co., Whitehouse Station, NY) were used as a control. Cells were then incubated in 10% alamarBlue® (Serotec, Oxford, UK) diluted in normal culture media for 16 hours before each reading was taken. Proliferation rates and cell viability were determined at various timepoints and absorbance readings were measured at 570 and 600nm using the Tecan microplate reader Sunrise™ (Tecan Trading AG, Switzerland).

2.4 Immunofluorescence Analyses

Neurospheres were dissociated into single cells using Accutase™ (eBioscience Inc., San Diego; non-trypsin-based) and seeded at a cell density of 2 $\times 10^4$ cells per well (stemness markers)/ 1 $\times 10^4$ cells per well (differentiation markers) of laminin-coated (Sigma-Aldrich) eight-well culture slides (BD Biosciences, San Diego). Plated cells were fixed with 4% paraformaldehyde (Sigma-Aldrich) for 10 minutes, permeabilised with 0.1% Triton X-100 (Sigma-Aldrich) for 10 minutes, blocked with 5% FBS for 1 hour, all at room temperature and stained for the following markers.

Stemness Markers. The undifferentiated cells (stem state) were stained for Nestin (Chemicon), Oct4 (Santa Cruz Biotechnology Inc., Santa Cruz, CA), Musashi-1 (Chemicon), and Ki-67 (Chemicon). Incubation with a secondary antibody conjugated to Alexa-Fluor-488 or -594 (Molecular Probes, Eugene, OR) was carried out. The cells were then counterstained with 4'6-diamidino-2-phenylindole (DAPI, 100 mg/ml, Sigma-Aldrich) to visualize the nuclei.

Differentiation Markers. Induction of differentiation was carried out with DMEM/F12 in the absence of growth factors and supplemented with 5% FBS and 1× B27. After 14 days, differentiated cells were stained for neurons (neuron-specific class III beta-tubulin, TuJ1; Chemicon), astrocytes (glial fibrillary acidic protein, GFAP; Dako, Glostrup, Denmark), and oligodendrocytes (O4; Chemicon).

2.5 Limiting Dilution Assay and Primary Sphere Formation Assay

Limiting dilution assay was performed as previously described[75, 76]. After primary sphere formation was noted, sphere cells were dissociated with

Accutase™ and plated into 96-well plates in 100 µl of GPC medium. Final cell dilutions ranged from 100 cells/well to 5 cells/well in 100 µl volumes. Growth factors were replenished every 2 days. After 7 days, the percentage of wells not containing spheres for each cell plating density was calculated and plotted against the number of cells per well. Regression lines were plotted and x-intercept values calculated, which represent the number of cells required to form at least 1 tumor sphere in every well.

2.6 Secondary Sphere Formation Assays

Tumor neurospheres were dissociated into single cells by treatment with Accutase™. The cells were then dispensed into each well of a 96-well plate at 30 cells per well. Primary sphere size was scored at day 7 after seeding. To carry out serial passaging, the primary spheres were similarly dissociated into single cells and then dispensed into each well of a 96-well plate at similar cell numbers. Secondary sphere size was scored at day 7 after seeding. This process was carried out for 3 passages to measure long-term self-renewal[77].

2.7 Flow Cytometry

Neurospheres were dissociated with Accutase™ and blocked with FcR blocking reagent (Miltenyi Biotec, Bergisch Gladbach, Germany). For stemness analysis, cells were stained with anti-CD133/2-allophycocyanin (Miltenyi Biotec, Bergisch Gladbach, Germany), anti-CD15 (BD Biosciences, San Diego), anti-neuroglial chondroitin sulfate proteoglycan 4 (NG2, Millipore AB5320, Bedford, MA), anti-Nestin (Chemicon) and detected for aldehyde dehydrogenase activity (ALDH, Stem Cell Technologies,

Vancouver, Canada) according to the manufacturers' instructions. For cleaved PARP and NF-κB expression analysis, cells were stained with PE mouse anti-cleaved PARP (Asp214) (BD Biosciences) and 488 mouse anti-NF-κB p65 (BD Biosciences) according to the manufacturers' instructions and subsequently co-stained with anti-CD133/2-allophycocyanin. A total of 10,000 events were acquired on a FACSCalibur instrument (BD Biosciences). Data were plotted using FlowJo software (Tree Star, Ashland, OR).

2.8 Immunohistochemical Staining of Tumor Tissues

Specimens from the human tumor and from tumors of mice that presented with neurological deficits were fixed in 4% paraformaldehyde, embedded in paraffin wax (Microm AP280-2, Zeiss), and sectioned (4 μm) using the microtome (Microm HM360, Zeiss). Hematoxylin and eosin (H&E) staining was carried out as described in our previous work[28]. For antibody staining, we adapted protocols from Gritti *et al.*[78]. Briefly, sections were mounted on poly-L-lysine-coated slides, and subsequently processed for heat-induced epitope retrieval. The sections were incubated with 5% goat serum for 1 hour at room temperature and then stained with rabbit polyclonal anti-CD133 (Abcam), anti-NG2 (human tissue using Invitrogen 372300, mouse tissue using Millipore AB5320[79]) or mouse anti-Nestin (Chemicon) antibodies overnight, followed by incubation with HRP-conjugated secondary antibody (goat anti-rabbit or anti-mouse IgG). Detection was carried out using the ChemMate Detection Kit (Dako); a positive reaction was indicated by brown color using DAB, and was counterstained with hematoxylin. ALDH activity was detected

according to the manufacturer's instructions (ALDH, Stem Cell Technologies, Vancouver, Canada).

2.9 Stereotaxic Intracranial Implantations of NOD/SCID gamma (NSG) Mice

Mice were treated according to the guidelines of the Institutional Animal Care and Use Committee, National Neuroscience Institute, Singapore. NNI-8 cells from dissociated neurospheres were injected orthotopically into non-obese diabetic/severe combined immunodeficiency gamma (NOD/SCID gamma, NSG, NOD.Cg-*Prkdc*^{scid}*Il2rg*^{tm1Wjl}/SzJ JAX®, The Jackson Laboratory, Maine) mice. Five hundred thousand cells in 2 µl of phosphate-buffered saline were delivered into the right frontal lobe (0.1 µl/minute) by stereotaxic injection through a glass electrode connected to a Hamilton syringe (Narishige, Tokyo). The coordinates used were +2 mm mediolateral, +1 mm anteroposterior and -2.5 mm dorsoventral. Mice were euthanized by means of transcardiac perfusion with 4% paraformaldehyde upon presentation of neurological deficits with ataxia, cachexia, lethargy, or seizure[28]. Where secondary cultures were generated, non-perfused tumors were surgically removed, avoiding mouse tissue and dissociated into single cells using Accutase™ and treated as described in our previous work[28].

2.10 Karyotypic Analysis of Tumor Neurospheres (Conducted by SH Leong and OL Kon, National Cancer Centre)

Two million cells from dissociated neurospheres were cultured in a T-25 flask (BD Biosciences). The cells were then treated within 3–5 days with 0.1 µg/ml

colcemid (Invitrogen) for 24 hours. Metaphase-arrested cells were pelleted (180*g* for 10 minutes) and hypotonic-treated with 0.075 M potassium chloride. Chromosomes were fixed in methanol:acetic acid (3:1), re-centrifuged and resuspended in fixative. Twelve µl of the fixed cell suspension was dropped on a clean, moistened glass slide and placed on a hot plate at 48^{o}C to obtain chromosome spreads. Spectral karyotyping (SkyPaint; Applied Spectral Imaging, Israel) was performed on metaphases according to the manufacturer's instructions.

2.11 Microarray Data Acquisition of Tumor Neurospheres

Total RNA was isolated from neurosphere cells using TRI Reagent® (Molecular Research Center, Cincinnati, OH) and purified with the RNeasy Mini Kit (Qiagen, Hilden, Germany). Reverse transcription and cRNA amplification were performed using an RNA Amplification kit (Ambion, Austin, TX). Microarray hybridization was performed using the Illumina Gene Expression BeadChip (Illumina Inc., San Diego).

2.12 Connectivity Map Analysis (Conducted by F.S.L. Ng, Singapore Institute for Clinical Sciences, A*STAR)

We utilized the Connectivity Map, a method originally used to define the strengths of association of a biological state (represented by a gene signature) to the action of small molecule therapeutics (a database of reference profiles)[29]. Since then, this method has successfully been used to determine the degree of oncogenic pathway activation in gastric cancer[80]. We adapted the

method to score glioma gene expression databases based on the extent of pathway activation associated with our GPC gene signature. (i) First, we defined a "GPC signature" – a set of genes exhibiting altered expression between 2 cell states (oligodendroglial GPC versus GBM GPC), (ii) Second, we generated databases of reference gene expression profiles from 2 major public glioma databases – REMBRANDT and "Gravendeel"[9, 81]. (iii) Third, using a non-parametric, rank-based pattern matching procedure, we mapped the GPC signature onto each patient gene expression profile and calculated activation scores based on the strength of association to the GPC signature, and finally, (iv) The patients were sorted according to their pathway activation scores. Two groups of patients were identified, (+) and (-), where a positive activation score indicates that the patient gene expression profile is positively associated to the gene signature and vice versa. Kaplan-Meier and Cox regression analysis of (+) and (-) groups were done in R using the *survival* package[168]. The two-tailed test p-values associated with each activation score were calculated as described in Lamb *et al.* [29]. Samples with p-value ≤ 0.1 were considered significant.

2.13 Western Blot Analysis

Cells were harvested and pelleted prior to lysis with RIPA buffer (1% sodium deoxycholate (ionic detergent), 1× Triton X-100 (non-ionic detergent), 0.1% SDS (sodium dodecyl sulfate) (ionic detergent), 0.15 M NaCl, 50 mM Tris HCl pH7.2 in deionised water) in the presence of a cocktail of protease inhibitors (1 mM phenylmethylsulphonyl fluoride (PMSF) (Sigma-Aldrich), 10 µg/ml aprotinin (Sigma-Aldrich), 10 µg/ml pepstatin (Sigma-Aldrich) and

10 µg/ml leupeptin (Sigma-Aldrich)). Protein lysates were resolved on denaturing 8% sodium dodecyl sulphate (SDS)-polyacrylamide gel, transferred to a polyvinylidene difluoride (PVDF) membrane (Invitrogen), and probed with the following antibodies: anti-GSK-3α/β (1:300, Santa Cruz Biotechnology Inc.); anti-phospho-GSK3 (Tyr279/Tyr216) (1:1000, Millipore); anti-phospho-GSK3α/β (Ser21/9) (1:1000, Cell Signaling Technologies, Beverly, MA); mouse anti-cleaved PARP (#9546 used to detect both full length and cleaved PARP) (1:2000, Cell Signaling Technologies); rabbit anti-cleaved PARP (#9541 used to detect only cleaved PARP) (1:1000, Cell Signaling Technologies); anti-c-Myc (1:300, Santa Cruz Biotechnology Inc.); anti-tubulin, beta III isoform (TuJ1, 1:1000, Millipore) and β-actin antibody (1: 10,000, Santa Cruz Biotechnology Inc.). Goat anti-mouse horseradish peroxidise (HRP)–conjugated secondary antibody (1: 10,000, ECL Amersham Biosciences, Buckinghamshire, UK), donkey anti-rabbit HRP-linked secondary antibody (1: 10,000, ECL Amersham Biosciences), or goat anti-mouse IgG-HRP (1: 10,000, Santa Cruz Biotechnology Inc.) were used. All antibodies were diluted in blocking buffer [5% w/v bovine serum albumin (Sigma), 10 mmol/L Tris-HCl, 100 mmol/L NaCl, 0.1% (v/v) Tween 20]. Membranes were visualized using the chemiluminescence detection kit ECL plus (Amersham Biosciences), SuperSignal West Pico (Thermo Scientific, Rockford, USA) or SuperSignal West Pico (Thermo Scientific) according to the manufacturer's instructions. Protein bands were quantified with Quantity One® software (Bio-Rad Laboratories, CA, USA). Results were normalized to actin levels.

2.14 Sorting of $CD133^+$ and $CD133^-$ GPC Cell Populations

GPCs were harvested, blocked with FcR blocking reagent (Miltenyi Biotec) and stained with allophycocyanin (APC)-conjugated anti-CD133/2 (Miltenyi Biotec) and mouse IgG2b-APC isotype control antibody (Abcam, Cambridge, UK). Cells were subsequently sorted with a FACS Aria™ (BD Biosciences).

2.15 Colony Formation Assay

For each GPC, 30 cells were flow-sorted into $CD133^+$, $CD133^-$ and total populations as described in section 2.14 and plated in triplicate into 96-well plates containing 100µl of DMEM/F12 culture medium supplemented with growth factors. Cells were treated with BIO after a recovery period of 4 days post-sorting. Cells were grown for up to 21 days at 37^0C and 5% CO_2, during which period the drugs were topped up and growth factors were supplemented twice a week. Cells were then scored for number of colonies formed and colony size under a Nikon® microscope (Nikon Instruments Inc., Melville, USA) at days 7, 14 and 21.

2.16 Lentiviral Infections

Human GIPZ lentiviral shRNAmir target gene set was obtained from Open Biosystems (Huntsville, AL) consisting of a set of 3 clones (Clone ID. V2LHS_114290, V2LHS_114293 and V2LHS_114291). Non-silencing-GIPZ lentiviral shRNAmir control (Open Biosystems) and the lentiviral vectors targeting GSK3β were transfected into HEK-293T cells together with plasmids encoding the packaging (psPAX2) and envelope proteins (pMD2-VSV-G) (Addgene, Cambridge, USA) using FuGENE® 6 transfection reagent

(Roche Applied Biosciences, Indianapolis, IN, USA). The concentration of infectious particles in the supernatant was titred using the Lenti-X^{TM} p24 Rapid Titer Kit (Clontech, CA, USA) according to the manufacturer's instructions. Glioma cells were transduced with infectious viral particles. Stably transfected clones were selected with 2 µg/ml puromycin.

2.17 Soft Agar Assay

Equal volumes of melted 1% Agar (DNA grade) (Vivantis, CA, USA) and 2× DMEM/F12, supplemented with growth factors were mixed to give 0.5% Agar, 1× DMEM/F12 and added into each of the wells in a 24-well culture plate (Nunc, Denmark). The agar was allowed to set to constitute the base agar. Following that, equal volumes of melted 0.8% Agar (DNA grade agarose) and 2× DMEM/F12 supplemented with growth factors was prepared to give a final dilution of 0.4% Agar, 1× DMEM/F12; and 2,000 cells were resuspended and immediately plated into each of the wells in the 24-well culture plate precast with the base agar. Cells were incubated at 37^0C and fed weekly by overlaying the soft agar with 0.4% Agar, 1× DMEM/F12 supplemented with growth factors. The colonies were counted after 14 days of plating and the colony sizes determined under phase contrast.

2.18 Statistical Analysis

Data are expressed as means ± SEM of at least three independent experiments. Student's *t* test or the Mann-Whitney *U* test was used where appropriate. Values of $p \leq 0.05$ were accepted as statistically significant.

RESULTS

CHAPTER 3 – A NOVEL METHOD TO INTERROGATE THE CONTRIBUTION OF STEM-LIKE GLIOMA-PROPAGATING CELLS TO MOLECULAR HETEROGENEITY AND SURVIVAL OUTCOME IN GLIOMAS

Gliomas are heterogeneous and can arise from neural precursors such as stem cells[14, 16] or oligodendrocyte progenitor cells (OPCs)[79, 82], depending on the initial cell type-specific mutations created in transgenic mouse models. As lineage-tracing studies can be performed, transgenic mouse models allow us to identify the cell-of-origin, its subsequent progeny and consequently pinpoint events in the etiology of gliomas. Although these mouse models demonstrate tumor formation that resembles the patient's original histopathology, we now know that they often do not recapitulate the diverse molecular heterogeneity characterizing human specimens. This highlights the limitation of using transgenic mouse models for glioma studies[83]. Recent work by The Cancer Genome Atlas (TCGA)[6, 7], Erasmus Medical Centre[9] and REMBRANDT[81] illustrate the complexity of human gliomas. Accordingly, these studies defined molecular sub-groups distinguished by gene expression, genetic aberrations and clinical profiles. These findings indicate that gene expression drives disease progression and survival outcome. In addition, the different sub-groups could be distinguished by recurring mutations in key signaling mechanisms such as the RTK, p53 and Rb pathways[6]. An important observation from the TCGA effort was the ability of xenografted surgical material to recapitulate patient tumor heterogeneity[7, 18].

Such findings underlie the foundation of our current study. We had previously characterized GPCs derived from GBM[28, 84], and demonstrated their extensive self-renewal and multi-lineage potential, accompanied by their ability to form orthotopic xenograft tumors that recapitulate the patient's original pathophysiology. Importantly, we showed that histologically similar tumors yielded GPCs with very different transcriptomic profiles, thus offering a possible explanation for the frequently observed inter-patient variability to treatment response. Here, we characterized NNI-8 GPCs derived from a different high grade glioma variant with oligodendroglial features. Oligodendroglial tumors are well-documented to have better prognosis than GBM[14]; in particular, the presence of the 1p/19q co-deletion status predicts their sensitivity to chemotherapy[4]. We thus explored the following: (1) We asked if NNI-8 GPCs displayed stem cell-like properties, and could re-establish xenograft tumors that mirrored the patient's original histopathology, which would be expected to differ from GBM tumors. This information would shed light on whether GPCs represent a reliable cellular model for recapitulating the tumor class; (2) By collating oligodendroglial GPCs and GBM GPCs from different investigators[28, 73, 74], we asked if differentially regulated genes characterized these tumor classes. Next, we derived clinical relevance of this gene signature by mapping its strength of association with gene expression profiles of patients from major public glioma databases, REMBRANDT[81] and "Gravendeel"[9]. We utilized a novel method in glioma biology, the "Connectivity Map"[29] to draw these associations. This method has the advantage of allowing us to make connections between different data platforms and biological information through the common vocabularly of

genome-wide expression profiling. Our question was to ascertain if the gene signature could stratify patients for survival outcome, and thus highlight the clinical contribution of GPCs to disease outcome.

3.1 An Anaplastic Oligoastrocytoma, NNI-8, Expresses Stemness Markers, Displays Extensive Self-Renewal and Multipotentiality

3.1.1 Patient magnetic resonance imaging (MRI) and histopathology

The patient from which the tumor specimen and subsequent GPC line was derived, was a 49 year old Chinese man who presented with progressive headaches over 3 months. The magnetic reasonance (MR) images were consistent with that of a high grade glioma – specifically, there was a lobulated left temporal intra-parenchymal mass lesion with irregular rim-enhancing borders which demonstrated inhomogeneous contrast enhancement accompanied by surrounding vasogenic edema and local mass effect (Fig. 5A-C). In addition, a satellite lesion with similar morphology could be seen in the posterior temporal lobe. On histopathological analysis following surgical resection, it was revealed to be a highly cellular neoplasm with juxtaposed regions of astrocytic and oligodendroglial differentiation. The astrocytic component was fibrillary in nature and the oligodendroglial component showed the typical dense network of branching capillaries and also tumor cells with clear cytoplasm, well-defined plasma membranes, hyperchromatic nuclei and peri-nuclear halos. Features of malignancy such as increased cellularity, marked cytologic atypia and high mitiotic activity were present as well. There was extensive hemorrhaging and the tumor exhibited a “fried egg”

morphology with “chicken wire” patterning of the stroma, typical of tumors with an oligodendroglial component (Fig. 5D)[85].

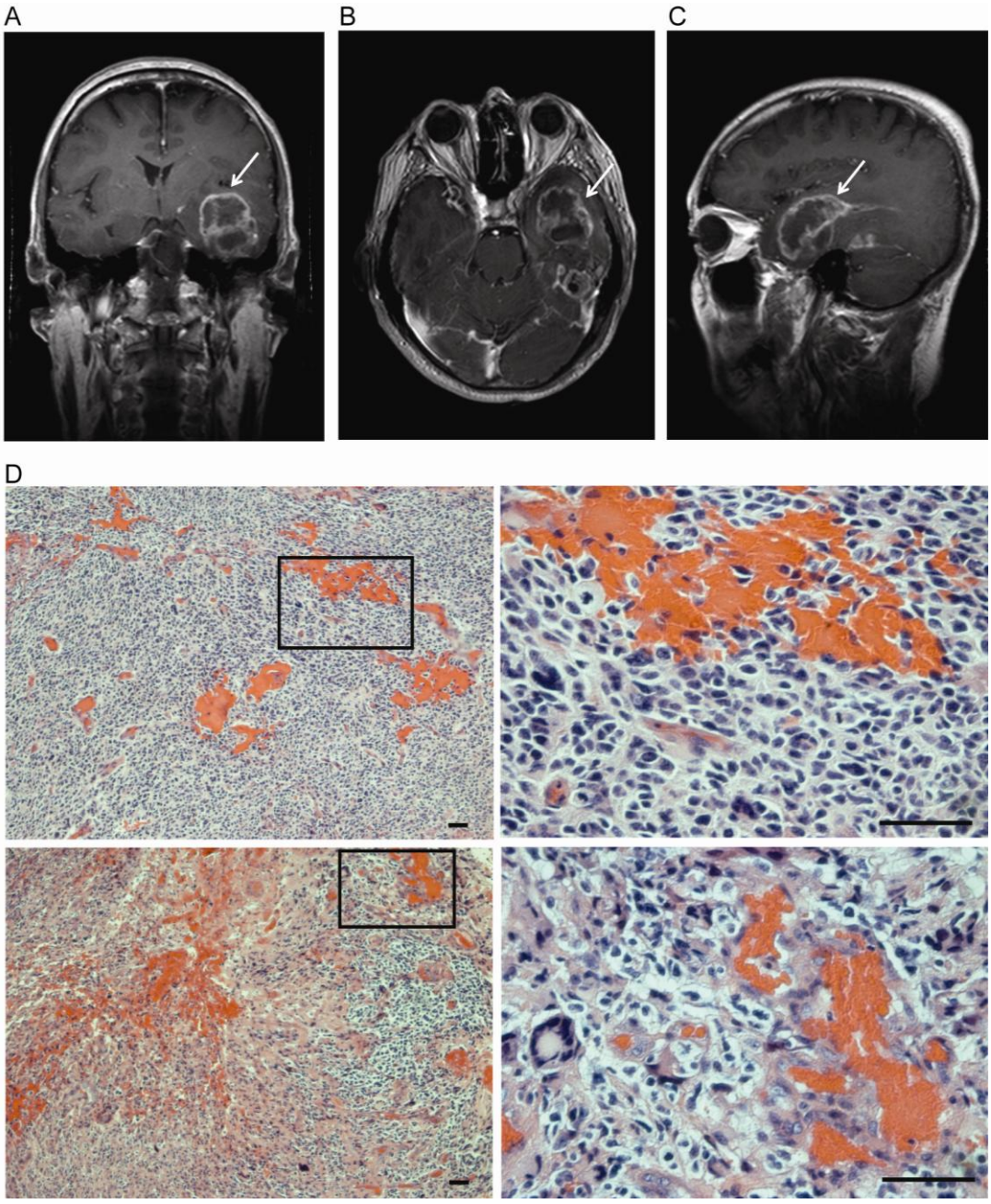

Figure-5. Magnetic resonance images, histopathology and immunohistochemistry of a case of anaplastic oligoastrocytoma. (A) Coronal, **(B)** Axial, and **(C)** Sagittal sections. White arrows denote tumor mass. **(D)** Representative H&E staining of primary tumor tissue, exhibiting the characteristic clear halo “fried-egg” appearance of oligodendroglial cells with “chicken wire” patterning of the stroma, and extensive haemorrhaging. Scale bar = 50 μm. Abbreviations: H&E, hematoxylin and eosin.

3.1.2 Anaplastic oligoastrocytoma-derived GPCs (NNI-8) display stemness expression and extensive self-renewal capability

GPCs from GBM, ependymoma and medulloblastoma have previously been characterized[86-88]. Here, we investigated the expression of common GPC surface markers based on our hypothesis that similar cells exist in anaplastic oligoastrocytoma. We evaluated the appearance of CD133, CD15 (SSEA-1), ALDH and Nestin, all frequently associated with the brain tumor stem cell[2, 31, 33, 89]. NNI-8 GPCs doubled in approximately 5 days (Fig. 6A) and displayed ~80% CD133, ~0.4% CD15, ~5% ALDH and ~100% Nestin expression (Fig. 6Bi, ii). To assess *in vitro* self-renewal potential, we utilized the neurosphere assay adapted from normal neural stem cell biology which approximates the tumor stem cell frequency[40]. As neurospheres are heterogeneous, we carried out long-term serial passage (up to 3 generations) to measure self-renewal capacity originating from *bona fide* tumor stem/propagating cells which can be distinguished from short-term, transit amplifying progenitors[41]. We show that the GPC frequency was maintained at ~1.25% for up to 3 generations (Fig. 6Ci). Sphere size, which is an indication of GPC cell proliferation, remained constant at ~54.16 ± 1.44 μm for up to 3 generations (Fig. 6Cii)[90]. A slight but significant increase was observed in passage 2 compared to passage 1. Our data suggests that NNI-8 GPCs possess common brain tumor stem cell surface markers and their abundance can be reliably maintained *in vitro* for up to 3 passages. In support, we previously demonstrated that by mechanical trituration, we were able to expand GPCs for up to 10 passages with preservation of transcriptomic profile, stemness/differentiation expression, key karyotypic hallmarks and tumorigenicity[28]. This method of mechanical

expansion without the use of harsh enzymatic dissociation solution is analogous to expansion of normal neural stem cells as a batch colony and best preserves the cytogenetic profile of stem cells[91, 92].

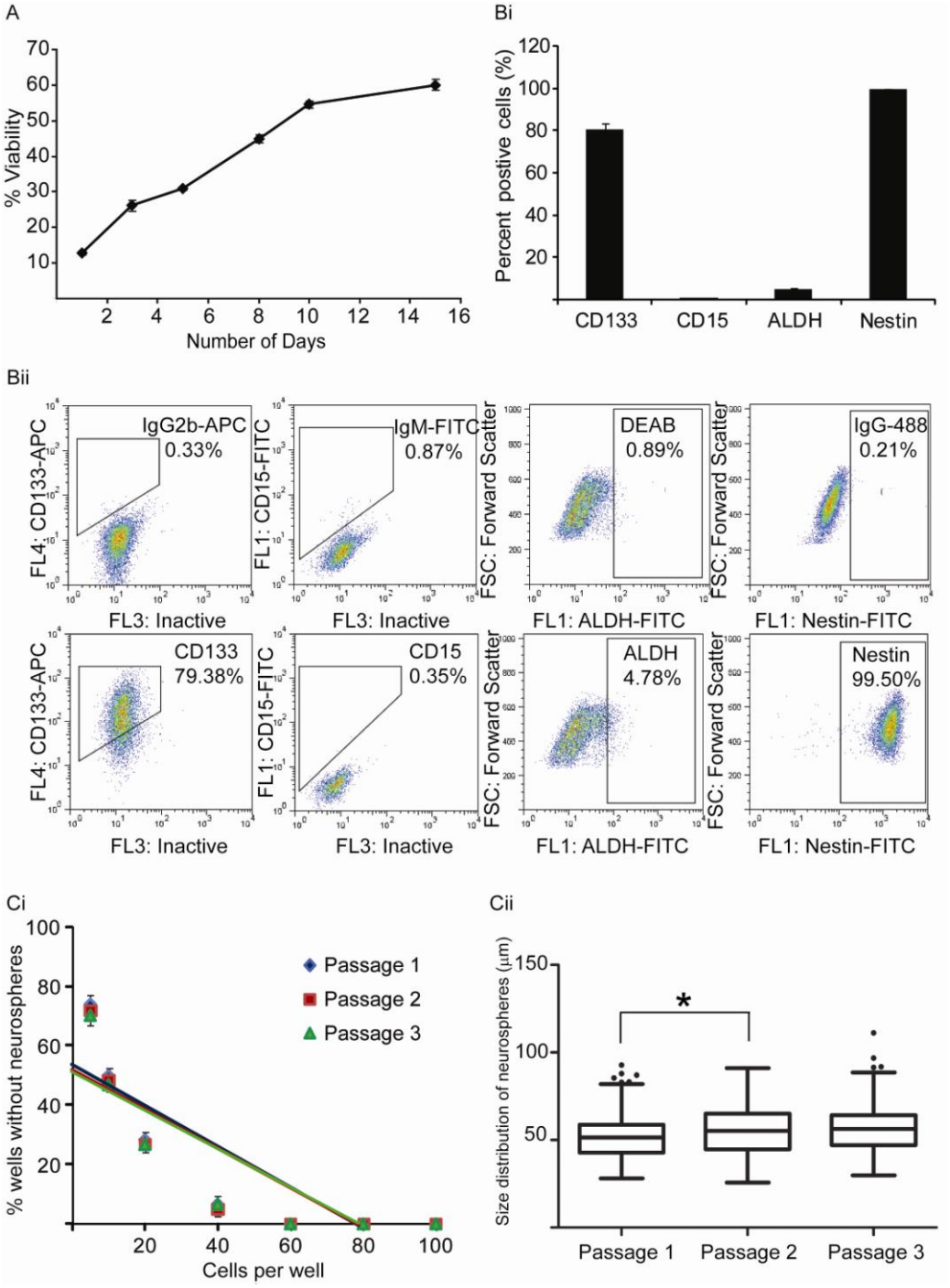

Figure-6. NNI-8 glioma propagating cells exhibit stemness expression and extensive self-renewal. (A) Proliferation curve measured by alamarBlue®, showing a doubling time of about 5 days. **(Bi)** Graphical representation for the percentages of CD133, CD15, ALDH and Nestin expressions. **(Bii)** Representative flow cytometric plots of data shown in **(Bi)**. **(Ci)** Limiting dilution analysis of GPCs at first, second and third passages, illustrating the maintenance of GPC frequency. **(Cii)** Sphere sizes at first, second and third passages indicating a constant proliferation rate. Abbreviations: CD133, complementarity determinant 133; CD15, complementarity determinant 15; ALDH, aldehyde dehydrogenase.

3.1.3 NNI-8 displays stem-like cell phenotypes and are multipotent

We evaluated NNI-8 GPCs for cell type-specific phenotypes previously demonstrated in GPCs of other brain tumor types. The GPC neurospheres were dissociated into single cells and seeded on to laminin-coated wells mounted on glass slides. After a recovery phase of 2-3 days was allowed, the cells were stained for various antigens. GPCs grown as adherent layers on laminin have previously been shown to preserve their biological profiles and function[74, 93].

We observed that nearly all GPCs displayed Nestin, Musashi-1 (Msi-1) and octamer-binding transcription factor 4 (Oct4) expression, with ~30% Ki-67-positive cells (Fig. 7A, B). Nestin is expressed in neural precursors; Msi-1 is a marker for self-renewal and Oct4 is a transcription factor essential for the maintenance of an undifferentiated state[94-97]. Ki-67 marks actively dividing cells[98]. These data suggest that NNI-8 GPCs are actively-dividing and possess stemness markers commonly associated with pluripotency and self-renewal ability.

Next, we subjected our GPCs to growth factor withdrawal, accompanied by serum addition over a period of 14 days. As cell morphology changes accompany the induction of differentiation of neural stem cells, we assessed multipotentiality by scoring for neurons (neuron-specific class III beta-tubulin, TuJ1), astrocytes (glial fibrillary acidic protein, GFAP) and oligodendrocytes (O4). In addition, we scored for differentiated cells staining positive for Nestin and Msi-1 stemness markers. Our data indicate that upon induction of differentiation, most cells retained Nestin and Msi-1 positivity, suggesting the preservation of a primitive neural precursor state with

continued self-renewal, otherwise distinct from normal terminally differentiated neural cells (Fig. 7A, C). The differentiated cells also nearly all stained positive for the astrocytic and oligodendroglial lineages, with ~20% staining positive for the neuronal lineage. Interestingly, ~10% of cells stained positive for both TuJ1 and GFAP, reflecting an aberrant developmental pathway otherwise absent in normal terminally differentiated neurons or astrocytes (Fig. 7A, C). Our data suggest that NNI-8 GPCs are multipotent and retain some degree of self-renewal potential, however, the extent of self-renewal capacity requires more rigorous assays.

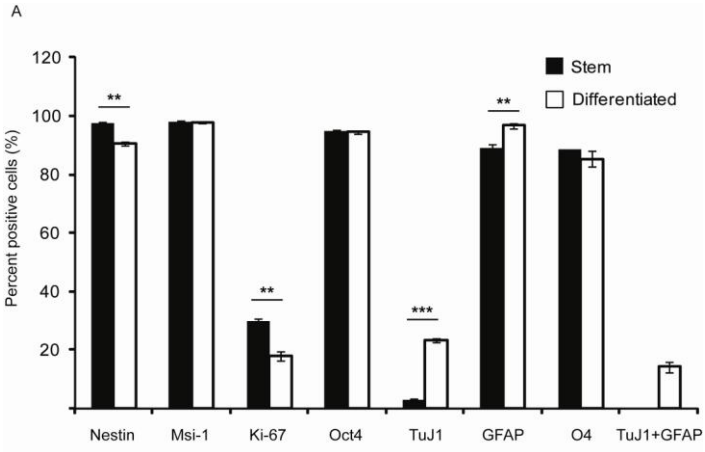

Figure-7. NNI-8 expresses stem-like cell phenotypes and multipotentiality. (A) Graphical representation of GPCs stained with stemness markers Nestin, Msi-1, Ki-67, Oct4, and assessed for neurons (TuJ1), astrocytes (GFAP) and oligodendrocytes (O4) before (stem) and after (differentiated for 14 days) the addition of serum. Cells co-stained for TuJ1 and GFAP were also assessed as well as neural precursor cells marked by Nestin and cells staining for Msi-1 after serum addition, indicating self-renewal potential. Abbreviations: Msi-1, Musashi-1; Ki-67, antigen identified by monoclonal antibody Ki-67; Oct4, octamer-binding transcription factor 4; TuJ1, neuronspecific class III beta-tubulin; GFAP, glial fibrillary acidic protein. $^{**}p < 0.01$, $^{***}p < 0.001$

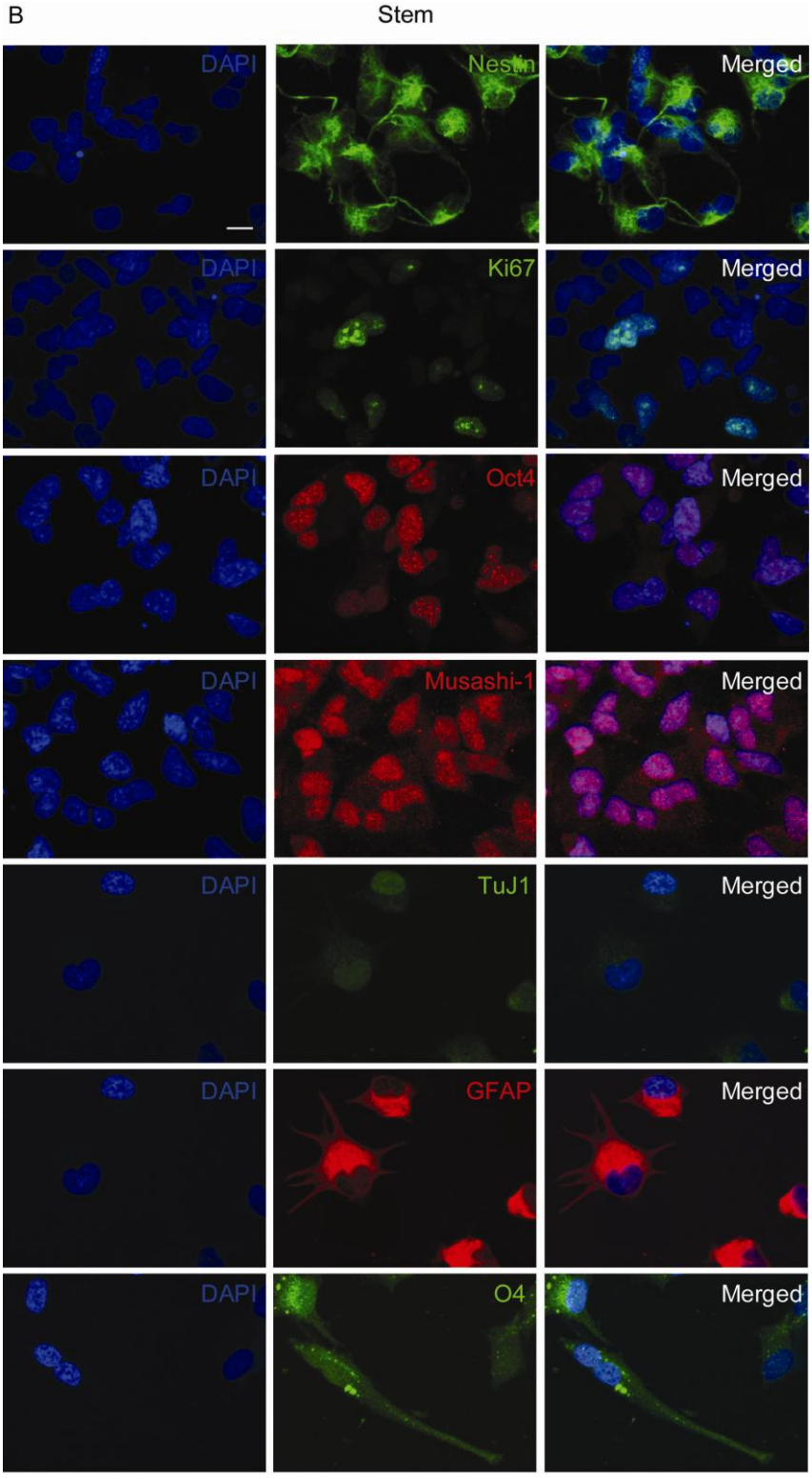

Figure-7. NNI-8 expresses stem-like cell phenotypes and multipotentiality. (B) Representative immunofluorescent images of data shown in **(A)**, before serum addition. Scale bar = 20 μm.

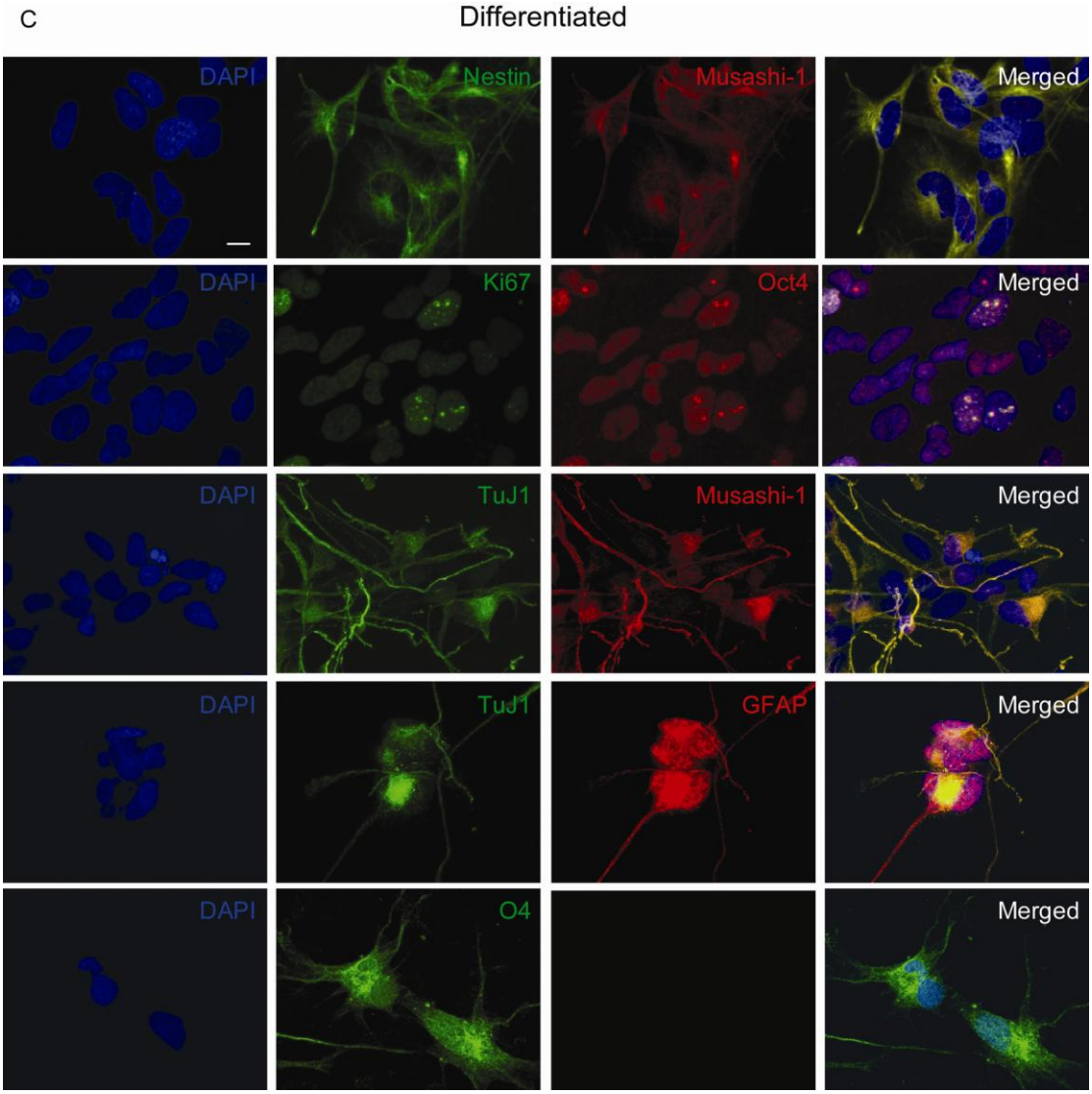

Figure-7. NNI-8 expresses stem-like cell phenotypes and multipotentiality. (C) Representative immunofluorescent images of data shown in **(A)**, after serum addition. Scale bar = 20 μm.

3.2 NNI-8 Orthotopic Xenograft Recapitulates Original Patient Tumor Pathophysiology and Retains Key Karyotypic Hallmarks upon Serial Passage

3.2.1 NNI-8 orthotopic xenograft phenocopies original patient tumor pathophysiology

One of the cardinal features of tumor-propagating cells is their ability to reform serially transplantable tumors which phenocopy the original primary tumor morphology[99]. Such tumor sustaining capacity reflects the extensive self-renewal capability of stem-like cells whereas the more committed, transit-amplifying cells such as progenitors tend to form tumors that cannot be serially transplanted with time[100]. In addition, the ability of GPCs to give rise to all neural lineages (that is, multipotency); namely astrocytes, oligodendrocytes and neurons, is important in reconstituting the tumor phenotype. We stereotaxically implanted 500,000 dissociated GPC single cells into the right frontal cortex of NOD-SCID gamma mice and monitored the time to development of neurological deficits. NNI-8 GPC cells typically formed large tumors within 4.5-6 months (Fig. 8Ai-iii). These tumors were highly invasive and infiltrated along white matter tracts such as the corpus callosum (Fig. 8Ai). Extensive hemorrhaging was common, and microscopic analyses revealed cells with a “fried egg” morphology and “chicken wire” patterning of the stroma, typical of tumors with an oligodendroglial component[85]. The morphology of the mouse tumor xenograft was identical to the human primary tumor; in addition, its molecular expression profile associated it with the oligodendroglial lineage[101], thus confirming the initial diagnosis (Fig. 5D, Fig. 8Ai-iii, Fig. 9). To assess self-renewal capacity, we

derived secondary GPC cultures from these first generation xenografts, and re-implanted a second set of animals. We were able to obtain similar tumors in comparable time periods in the second generation mice, suggesting that our GPCs possessed self-renewal capability (Fig. 8B). In addition, we noted that in both human and xenografted tumors, the expressions of CD133 and Nestin were maintained (Fig. 8C, Fig. 9). The strong ALDH "positive" staining in the primary tumor was confirmed by the pathologist to arise from reactive astrocytes, a reaction not seen in the immune-compromised mouse xenograft model. Neuroglial chondroitin sulphate proteoglycan 4 (NG2) expression has recently been implicated as the marker for progenitor cells-of-origin in a mouse model of oligodendroglioma[102]. NG2 staining was negligible in both human and xenografted tumors (Fig. 9). Furthermore, primary GPCs derived from patient material and GPCs derived from xenografted tumors both maintained similar levels of expression of ALDH and Nestin, while CD133 and CD15 were slightly but significantly elevated in xenografted GPCs (Fig. 8Di, ii). While it is attractive to postulate that *in vivo* serial passaging positively enriches for CD133 and CD15-expressing GPCs, this would require further robust clonality assays to be carried out. In contrast, we observed a significant increase in abundance of NG2-positive cells in primary GPCs (Fig. 10)[102]. We noted that this pattern was reversed in GPCs cultivated in serum-free medium supplemented with leukemia inhibitory factor (LIF), another culture condition frequently used by several teams (Fig. 10)[103]. Thus, NG2 expression, at least *in vitro*, appears to vary in accordance with the presence of LIF, explaining the discrepancy with results obtained from the tumor

immunohistochemistry data. This indicates that *in vitro* cultures cannot be used to assess the enrichment of NG2-expressing tumor-propagating cells.

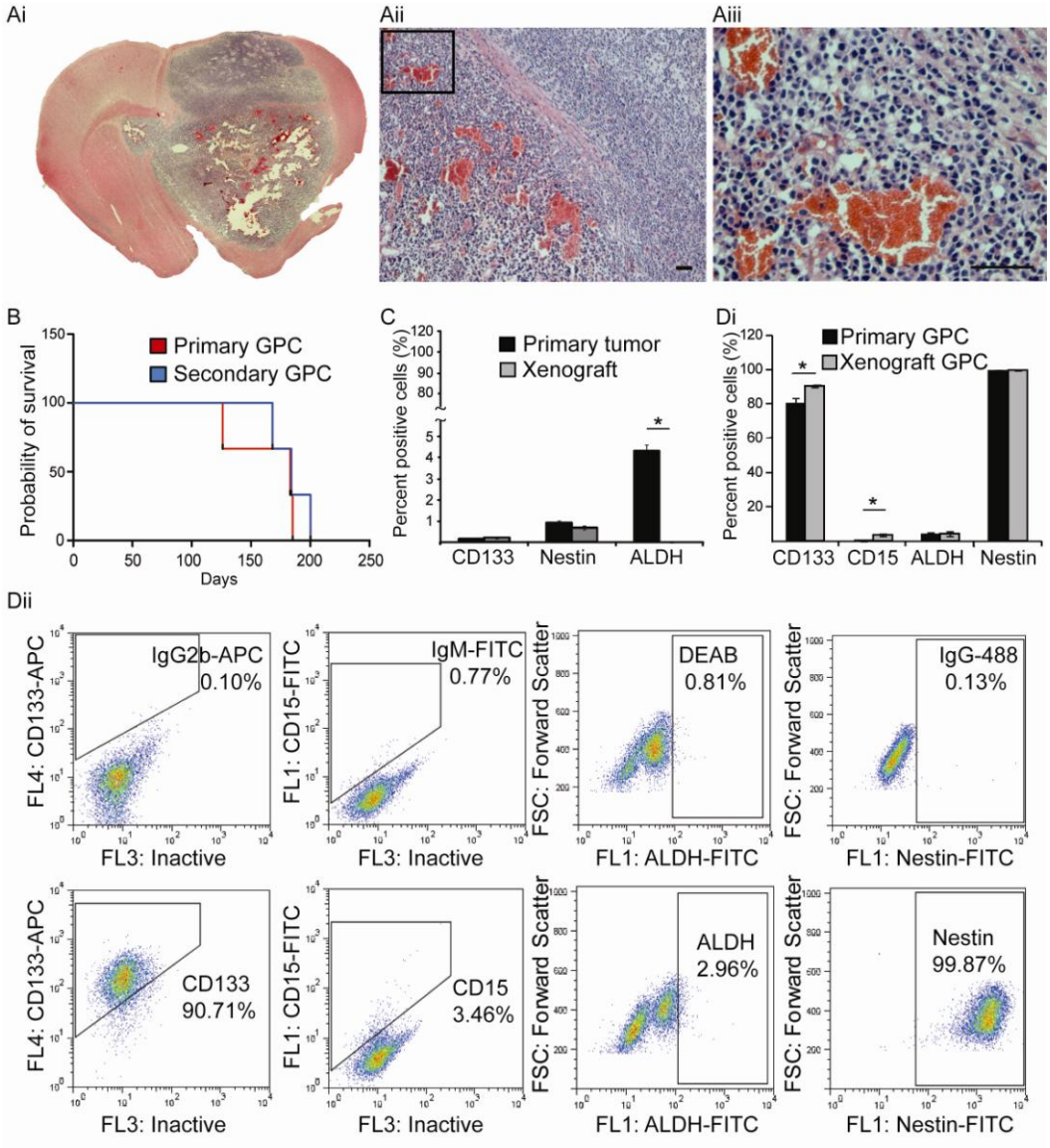

Figure-8. NNI-8 orthotopic xenograft recapitulates patient tumor pathophysiology. (Ai-iii) Tumor xenograft section showing extensive hemorrhaging, "fried egg" morphology and "chicken wire" patterning of the stroma via H&E staining. Scale bar = 50 μm. **(B)** Tumorigenicity and animal survival arising from implanted primary and secondary GPCs. **(C)** Graphical representation of CD133, ALDH and Nestin expressions in the primary and xenografted tumors derived from immunohistochemical staining; *, $p < 0.05$. NG2 had negligible expression. Note that CD15 expression was not evaluated as the anti-CD15 antibody cross-reacts strongly with mouse tissue, thereby confounding analysis. **(Di)** Graphical representation of CD133, CD15, ALDH and Nestin expressions in primary and secondary GPCs; *, $p < 0.05$. **(Dii)** Representative flow cytometric plots of data illustrated in **(Di)**. Abbreviations: H&E, hematoxylin and eosin; GPCs, glioma-propagating cells; CD133, complementarity determinant 133; ALDH, aldehyde dehydrogenase; NG2, neuroglial chondroitin sulphate proteoglycan 4; CD15, complementarity determinant 15.

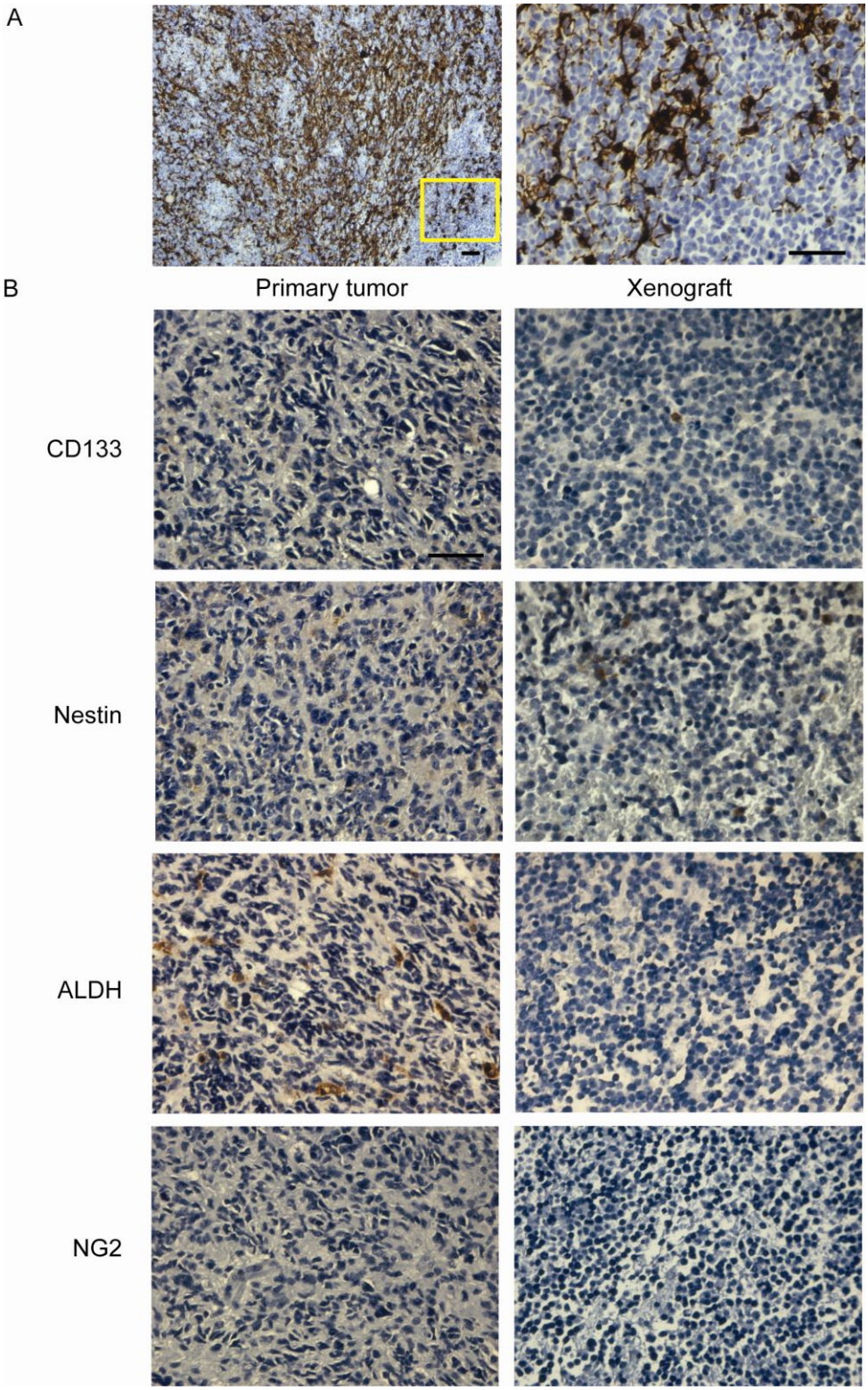

Figure-9. Xenografted tumor maintains common stemness marker expressions compared to the primary tumor. (A) Immunohistochemical staining detecting for the presence of ALDH in primary tumor **(B)** Immunohistochemical staining detecting for the presence of CD133, Nestin, ALDH and NG2. Note that the "positive" staining pattern of ALDH in the primary tumor was confirmed by the pathologist to arise from reactive astrocytes, a reaction not seen in the immunecompromised mouse xenograft model. Scale bar = 50 μm. Abbreviations: CD133, complementarity determinant 133; ALDH, aldehyde dehydrogenase; NG2, neuroglial chondroitin sulfate proteoglycan 4

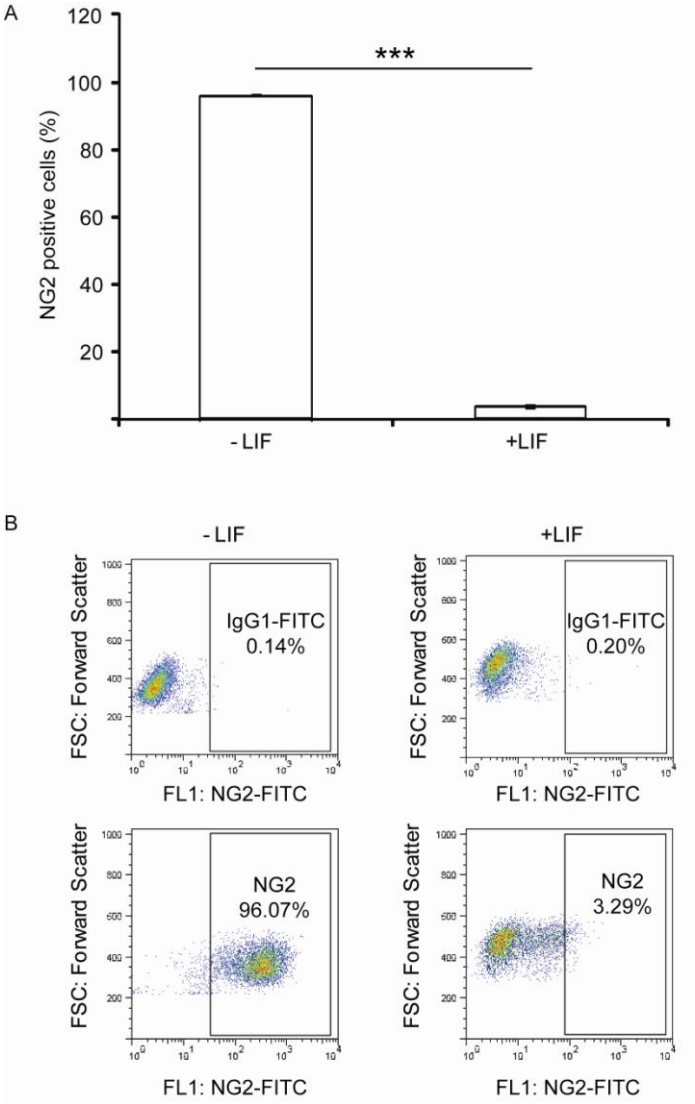

Figure-10. Leukemia inhibitory factor (LIF) influences the level of NG2 expression. (A) The addition of LIF in the culture medium leads to a significant reduction in NG2 expression; ***, $p < 0.001$. **(B)** Representative flow cytometric plots of data illustrated in **(A)**. Abbreviations: LIF, leukemia inhibitory factor; NG2, neuroglial chondroitin sulfate

3.2.2 *In vivo* serial passage maintains key karyotypic hallmarks (Conducted by SH Leong and OL Kon, National Cancer Centre)

We previously showed that we were able to maintain key karyotypic hallmarks of GPCs derived from patients with GBM that were *in vitro* expanded for 10 passages[28]. To our knowledge, no work exists that has studied the progression of GPC karyotypes when the cells have been serially transplanted in animals. Work by Lee *et al*. has suggested that GPCs cultured under serum-free condition supplemented with growth factors contained karyotypic patterns similar to the primary tumor, however, their preservation through *in vivo* passaging remains to be verified[19]. We thus evaluated karyotypes of NNI-8 GPCs within 10 passages after derivation from clinical material ("primary GPCs"), and within 10 passages after harvesting from the first generation animal implantations ("secondary GPCs"). Our motive was to ascertain if any karyotypic hallmarks were preferentially selected for or obliterated upon *in vivo* tumor propagation. This is an important endeavor as it addresses the reliability of *in vivo* serial transplantation to maintain such GPCs.

Our data are illustrated in Fig. 11A, B. The structural rearrangements in black font in the figure legend were retained in both primary and secondary GPCs, indicating that the majority of chromosomal rearrangements were preserved in first generation mouse transplantations. The structural rearrangement, i(7q), and the diploid Y chromosome status (both shown in red font) were obliterated in the secondary GPCs. Whether these obliterations occurred as a result of selection of tumor-propagation activity, or accidental clone loss remains to be followed up in subsequent work. Interestingly, the translocation at t(5;10) was no longer balanced, suggesting that the copy

numbers of 5p and 10q were likely to be altered. Our data suggest that *in vivo* serial passage maintains the overall karyotypic integrity of NNI-8 GPCs.

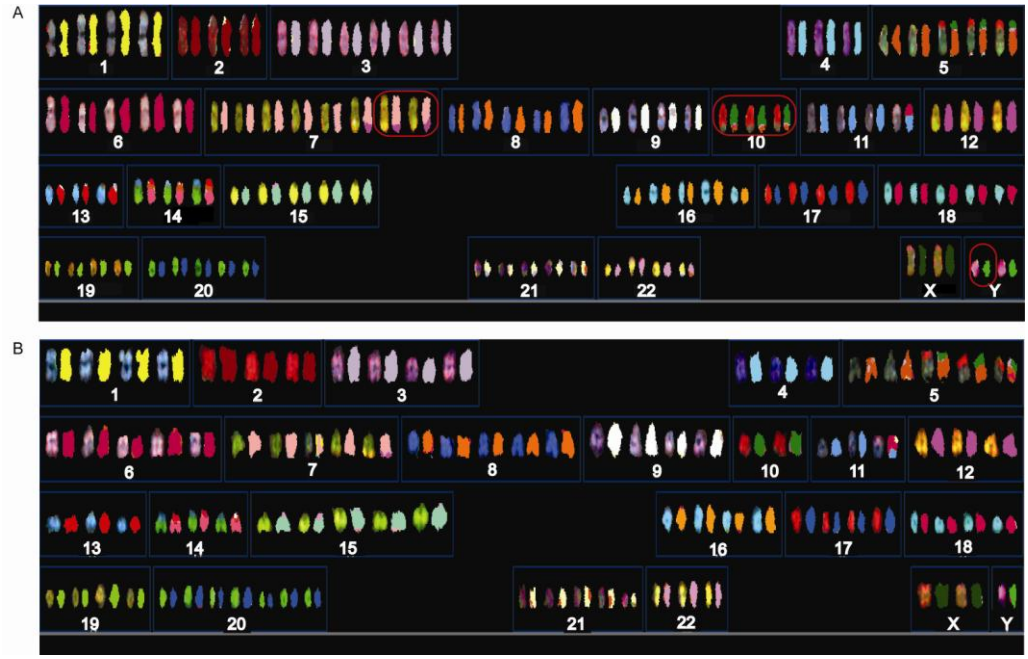

Figure-11. Majority of karyotypic hallmarks in GPCs are maintained upon serial transplantation. (A) Primary GPCs derived from clinical material. Karyotype: 93~102, XXYY[10], +1x2[10], +2[10], +3x3~4[8], +4[9], +t(10;5)(10qter → q23::5p13 → 5qter;10pter → 10q23:5p13 → pter)x3[9],, +6x2~3[8], +7x1~2[10], +i(7q)[5], +t(7;12)(7pter → 7q31::12?)x3[9], +8x2~3[10], +9x2[8], +t(6;11)(6qter → ?6q22::11p23 → 11qter)[9], +12[10], +13[10], +14[10], +15x2~3[9], +16x3[9], +17x2[9], +18x3[9], +19x2~3[9], +20x4~5[9], +21x3[7], +22x3[7], cp10. Parentheses indicate number of metaphases with observed structural rearrangement; cp10 indicates total number of 10 metaphases scored. **(B)** Secondary GPCs derived from first generation tumor xenograft showed similar karyotype except for obliteration of structural rearrangements in red font above; Y and +i(7q)[5]. Note that the translocation at t(5;10) was also no longer balanced, suggesting that the copy numbers of 5p and 10q were likely altered. Abbreviation: cp, composite.

3.3 An Oligodendroglial GPC Gene Signature Stratifies Patient Survival in Gliomas (Conducted by F.S.L. Ng, Singapore Institute for Clinical Sciences, A*STAR)

3.3.1 An oligodendroglial GPC gene signature is defined

We first determined genes differentially regulated between 2 cell groups: Oligodendroglial GPCs (NNI-8, GS-2, G174) and 17 GBM GPCs collectively obtained from this study plus Gunther[73] and Pollard[74] as previously described (Fig. 12). We used a linear model that selected for differentially expressed genes while batch variation was normalized. A $\log_2$ fold change of 0.8 with p-value of 0.05 were maintained. Eighty-four genes corresponding to 95 probes were selected as the top-ranking candidates. We called this the "oligodendroglial GPC gene signature" which was enriched in the Notch, Wnt and TGFβ signaling pathways (Table S1, Fig. S1 in appendices).

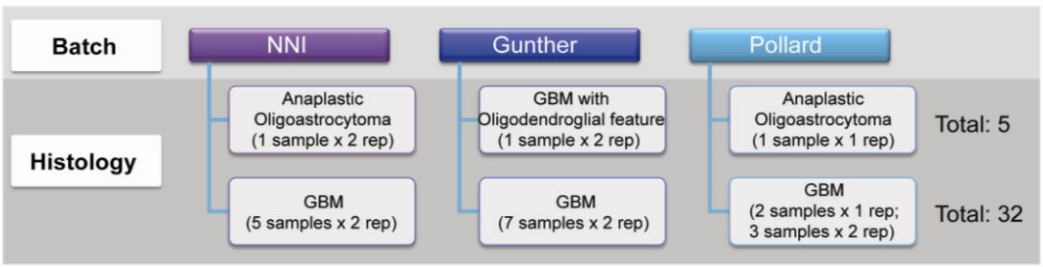

Figure-12. Study flowchart for derivation of oligodendroglial GPC gene signature. Oligodendroglial GPCs (NNI-8, GS-2, G174) and 17 GBM GPCs were collectively obtained from this study plus Gunther[73] and Pollard[74]. The number of samples and replicate microarray data are indicated.

3.3.2 The oligodendroglial GPC gene signature stratifies patient survival in all gliomas

Next, we analyzed the strength of association of this gene signature with patient gene expression data from 2 public glioma databases – REMBRANDT and Gravendeel[9, 81]. We assigned positive "(+)" and negative "(-)" activation scores with significant p-values where (+) refers to a strong enrichment of the gene signature in similar direction in the clinical database, while an inverse correlation is defined as (-) (Table S2 in appendices). We observed that the gene signature separated (+) and (-) patient cohorts with approximately 30-50% in each category (Table 2). Importantly, the gene signature stratified patient survival (Fig. 13). Patients with better survival comprised of (+) association (more oligodendroglial GPC association) whereas poorly surviving patients tended to be (-) (i.e. more GBM GPC association) (REMBRANDT p-value, 1.93E-05; Gravendeel p-value, 0.0082). The (+) activation score also contained more low grade gliomas, especially enriched for oligodendrogliomas, while the (-) activation score enriched for high grade gliomas with mainly GBMs. A univariate Cox regression model indicated that the gene signature could serve as an alternate indicator of patient prognosis in addition to age, histology and tumor grade (Tables 2, 3; REMBRANDT p-value, 2.90E-05; Gravendeel p-value, 0.009). In the larger database REMBRANDT, the gene signature predicted survival better than age, histology and grade (Table 3; p-value, 2.22E-05).

Next, we attempted to strengthen our findings that tumor grade inversely correlates with the oligodendroglial GPC gene signature. We applied the "Phillips" classification of gliomas[10] which molecularly categorizes the

tumors into 3 sub-classes: Proneural, Proliferative and Mesenchymal. We found that the (+) activation score enriched for the Proneural sub-class, while the (-) activation score tended to be Proliferative or Mesenchymal (Fig. 13). Proneurals are typically lower grade gliomas with oligodendroglial features, frequently associated with better prognosis; in contrast, the Mesenchymal sub-class characterizes highly aggressive, recurrent gliomas such as GBM. Interestingly, recent work has suggested that oligodendrogliomas are more chemosensitive because their cells-of-origin are OPCs, compared to the more resistant neural stem cells in GBM[102]. Although this conclusion arose from transgenic mouse models, we find it intriguing that all *in vitro* cultured GPCs from different studies maintained the phenotypes of these purported cells-of-origin; however, we are not able to definitively pinpoint the identity of GPCs due to its human origin. Furthermore, to eliminate the possibility that we were biasing the gene signature selection towards better surviving oligodendroglial tumors by our filtering procedure, we additionally derived a gene signature by comparing NNI-8 GPCs to its primary tumor (Tables S3, S4, S5 in appendices). This gene signature similarly stratified patient survival, with the (+) class enriching for lower grade tumors of Proneural classification, while the (-) class enriched for higher grade tumors with Mesenchymal features (Fig. S2 in appendices). The data collectively suggest that oligodendroglial GPCs contribute to a favorable prognosis, likely mediated by more chemosensitive OPC-like properties (Fig. S3 in appendices).

Table-2. Summary of results from Connectivity Maps, Logrank and Cox Regression Analysis for all patient samples.

Dataset	Connectivity Maps Analysis						Log Rank *p*-value	Multivariate Cox		Univariate Cox	
	# of probes	# of samples	(+)	(-)	total (+)(-)	%(+)(-)		Hazard Ratio	*p*-value	Hazard Ratio	*p*-value
REMBRANDT	95	298	86	61	147	49.33	1.93E-05	0.440 (0.301-0.643)	2.22E-05	0.462 (0.322-0.664)	2.90E-05
Gravendeel	95	276	58	34	92	33.33	0.0082	0.851 (0.504-1.436)	0.546	0.535 (0.334-0.856)	0.009

(+) represent patients with concordance to GPC signature; (-) represent patients with inverse gene expression relationship to GPC signature

Table-3A. Multivariate cox regression model for all patient samples.

Dataset	variable	coef	exp(coef)	exp(-coef)	lower .95	upper .95	se(coef)	z	Pr(>|z|)	Significance
REMBRANDT	age	0.019326	1.0195	0.9809	1.007	1.032	0.00628	3.076	0.0021	**
	grade	0.710044	2.0341	0.4916	1.393	2.97	0.19307	3.678	0.00024	***
	class	-0.82114	0.4399	2.2731	0.301	0.643	0.19359	-4.242	2.22E-05	***
Gravendeel	age	0.04299	1.044	0.9579	1.0235	1.065	0.01008	4.267	1.98E-05	***
	grade	1.02668	2.792	0.3582	1.5974	4.879	0.28485	3.604	0.00031	***
	class	-0.16141	0.851	1.1752	0.5041	1.436	0.26714	-0.604	0.54572	-

Multivariate Cox Regression:
REMBRANDT: coxph(formula = Surv(survival, status) ~ age + grade + class, data = dat)
Gravendeel: coxph(formula = Surv(survival, status) ~ age + grade + class, data = dat)

Table-3B. Univariate cox regression model for all patient samples.

Dataset	variable	coef	exp(coef)	exp(-coef)	lower .95	upper .95	se(coef)	z	Pr(>|z|)	Significance
REMBRANDT	class	-0.7715	0.4623	2.163	0.322	0.6638	0.1845	-4.181	2.90E-05	***
Gravendeel	class	-0.6252	0.5351	1.869	0.3344	0.8563	0.2399	-2.607	0.00914	**

Univariate Cox Regression:
REMBRANDT: coxph(formula = Surv(survival, status) ~ class, data = dat)
Gravendeel: coxph(formula = Surv(survival, status) ~ class, data = dat)

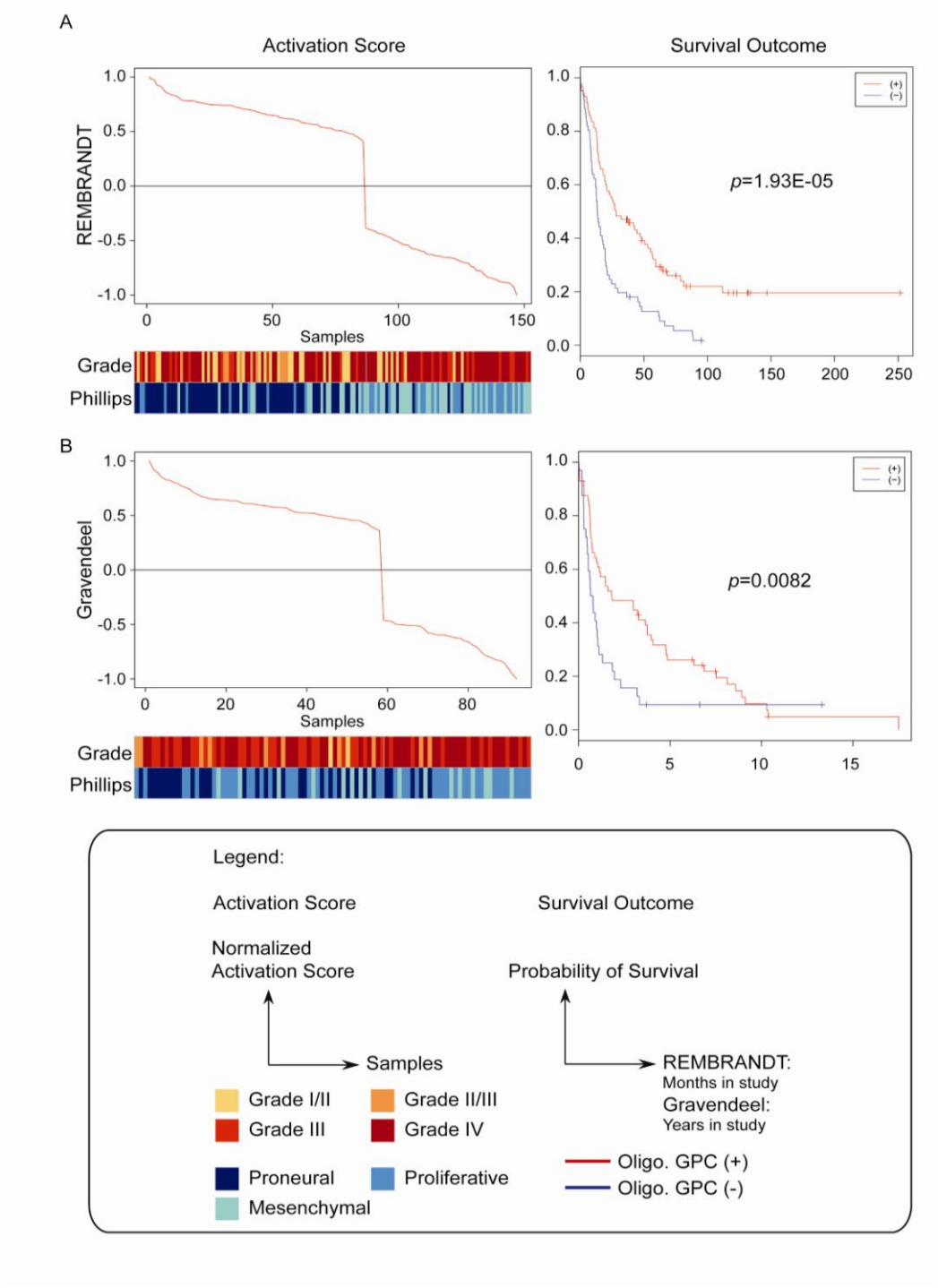

Figure-13. Oligodendroglial GPC gene signature stratifies patient survival. Patient survival is shown in all glioma patients. Tumor grade ("Grade") and molecular classification ("Phillips"[10]) distribution corresponding to (+) and (-) classes is shown below the activation score graphs. Patients with better survival comprised of + association (more oligodendroglial GPC association) whereas poorly surviving patients tended to be - (i.e. more GBM GPC association). The + activation score also contained more low grade gliomas, especially enriched for oligodendrogliomas; and was enriched for the Proneural sub-class.

3.3.3 The oligodendroglial GPC gene signature defines molecular heterogeneity within oligodendrogliomas

We next interrogated this GPC gene signature in oligodendroglioma patients. The (+) class enriched for lower tumor grades associated with patients exhibiting the 1p/19q co-deletion (Fig. 14). Interestingly, patients without loss-of-heterozygosity at 1p/19q were spread throughout the (+) and (-) classes, indicating that the gene signature detected molecular heterogeneity that cannot be accounted for by the 1p/19q co-deletion status alone.

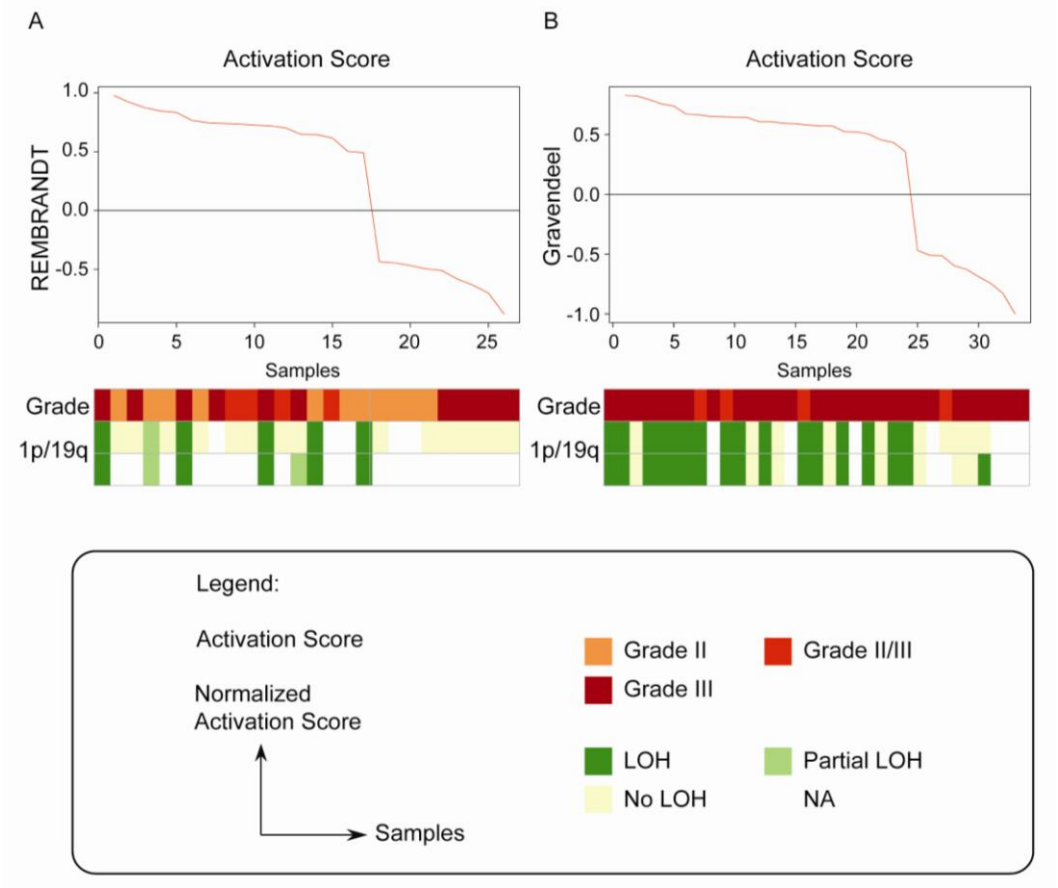

Figure-14. Oligodendroglial GPC gene signature is associated with lower tumor grade and 1p/19q co-deletion. Tumor grade ('Grade") and 1p/19q co-deletion distribution corresponding to (+) and (-) classes is shown below the activation score graphs.

SUMMARY

Following the characterization of GBM GPCs in our previous manuscript[28], we describe the derivation of GPCs from a patient with anaplastic oligoastrocytoma, NNI-8. These GPCs displayed stem cell-like characteristics; notably, extensive self-renewal capacity and multi-lineage potential. Importantly, orthotopically implanted cells formed tumors that phenocopied the patient's original tumor histopathology. These data suggest that NNI-8 GPCs do preserve the ability to reform tumors that mirror the original primary tumor pathological diagnosis. To address the clinical relevance of GPCs, transcriptomic analyses were carried out on 2 major groups of GPCs derived from GBM and oligodendroglial tumors. Our data show that tumor classes and their survival outcome can be predicted by transcriptomic information residing in GPCs, thus validating these cells as relevant cellular models for glioma studies.

CHAPTER 4 – IDENTIFICATION OF GSK3β AS A DRUG CANDIDATE FROM ELI LILLY SCREEN

4.1 Identification of GSK3β as a Possible Drug Candidate in GPCs

4.1.1 Drug screening from 50 Eli Lilly compounds reveals key signaling pathways in gliomas

In recent years, evidence is mounting that indicates that brain tumor variants such as GBM[6, 7], oligodendrogliomas[8] and medulloblastomas[104] are molecularly heterogeneous among patients even if their tumor histologies are similar. These findings underscore the limitation of morphology-based histological analyses in diagnosing tumor class/grading and consequently treatment regimen. Efforts from The Cancer Genome Atlas (TCGA)[6, 7], Eramus Medical Centre[9] and REMBRANDT[81] suggest that gene expression drives disease progression and survival outcome. These public efforts show that brain tumors such as GBM can be classified into 4 subtypes based on gene expression, with each class containing unique genetic aberrations and clinical outcome[7]. In addition, TCGA efforts mapped the 3 major signaling mechanisms most frequently altered in GBM: RTKs, p53 and Rb tumor suppressor pathways.

Accordingly, to identify the mechanisms promoting self-renewing and tumorigenic GPCs (i.e. to target the relevant tumor-propagating fraction in the heterogeneous tumor mass), we selected 50 small molecules (Table S7 in appendices) targeting common oncologic pathways. Each pathway was targeted by more than 1 compound to ensure that data implicating specific pathways could be reproduced. We screened these small molecules in 4 GPC

lines: NNI-1, 4, 5 (previously published[28, 84]) and NNI-8 (this study). From our previous work, we showed that NNI-1 and NNI-5 GPCs clustered together in a Principal Component Map (PCA) analysis (S cluster); while NNI-4, a semi-adherent sphere subtype clustered away, closer to the primary tumor, thus confirming that it also differs transcriptomically from the S cluster spheres, and may contain more differentiated progeny found in the primary tumor (T cluster))[3, 28]. Interestingly, all 3 spheres were derived from histologically similar GBM primary tumors, once again confirming the inadequacy of morphological approaches in tumor grading. In contrast, NNI-8 which represents GPCs derived from a high grade glioma with oligodendroglial features remained transcriptomically distinct from all others, consistent with our earlier findings that the transcriptomic changes driving the primary tumor phenotype are "hardwired" into the GPCs (Fig. 15). Our choice of GPC lines reflects our rationale for identifying small molecules that inhibit all glioma GPCs irrespective of morphology and transcriptomic differences. Intuitively, the inability of certain molecules to target different GPC subtypes may reflect underlying differences that regulate these subtypes.

We adapted our screening protocol from previous investigators[105, 106]. Briefly, we carried out the small molecule screen with suspension GPC spheres and assayed for their viability upon drug treatment. Viability rather than functional sphere formation assays which reflect GPC frequency was used initially due to its relative ease in screening 50 compounds quickly. We used two criteria: First, we winnowed down candidate compounds that reduced viability by at least 2-fold. Second, we selected only compounds that demonstrated greater specificity for GPCs compared to normal mouse

astrocyte cells, C8-D1A[106]. Ideally, the use of normal human neural stem cells or astrocytes would offer better alternatives but ethical issues may preclude their use. This is because (i) Bioinformatics data in this thesis carried out by bioinformaticians at Eli Lilly and company do not approve the use of human fetal cell-related research (ii) Normal human neural stem cells are immortalized and not entirely representative of the stem cells we are studying (iii) Normal human astrocytes (NHA) or human neural stem cells procured commercially are of higher passages, thus these cells might possess *in-vitro* passage artifacts.

The specificity of compounds was assessed using the following "selectivity ratio": % viability $_{(astrocytes)}$ / % viability $_{(GPCs)}$. Thus, a good GPC inhibitor would be reflected as a high selectivity ratio. Using this approach, we grouped our data to show compounds that are consistent with GPC literature, and compounds that are novel in GPC sustenance that may potentially represent areas of exploration (Fig. 16). Interestingly, inhibitors targeting the PI3K/Akt/mammalian target of rapamycin (mTOR)[3], transforming growth factor beta receptor 1 (TGFβR1)[42, 107] and Jak2/Stat3[108, 109] pathways identify signalling elements existent in GBM GPCs. These data validate our screening procedure. In contrast, we saw no effects with inhibitors targeting Hedgehog/Smoothened[33] or Notch[110], likely because their regulation involves paracrine feedback which is not present in our screening system[111, 112]. Inhibitors against Polo-Like Kinase (PLK), Aurora A/TAK1 (AURKA), Cyclin-Dependent Kinase (CDK) and Glycogen Synthase Kinase 3 beta (GSK3β) were identified in this screen and their roles in GPC maintenance are currently unknown. We thus focused on investigating the GSK3β signalling

pathway for 3 reasons: Firstly, inhibitors against PLKs, CDKs and AURKA tend to target the proliferative aspects of tumor growth (i.e. cell cycle machinery)[113, 114]. We rationalized that GPC self-renewal and tumorigenic properties would comprise more than proliferation alone; for example, cell fate (aberrant stem cells versus lineage-committed progenitors in the transformation process) determines tumorigenic potential[100]. Consequently, targeting these unique properties would more likely be specific towards tumor cells than targeting cell cycle machinery as normal cells would be similarly affected. Secondly, previous work suggested that GSK3 inhibitors may target primary glioma cells via a novel apoptotic machinery, but its impact on tumor-initiating GPCs is unknown[71]. Thirdly, recent work has implicated GSK3 regulation with cell fate[72]. We thus hypothesized that GSK3β specifically, may control GPC self-renewal and consequently tumor growth by regulating cell fate. We focused on the beta isoform since GSK3α-null mice exhibited no defects; furthermore, GSK3α could not rescue embryonically lethal GSK3β-null mice[115].

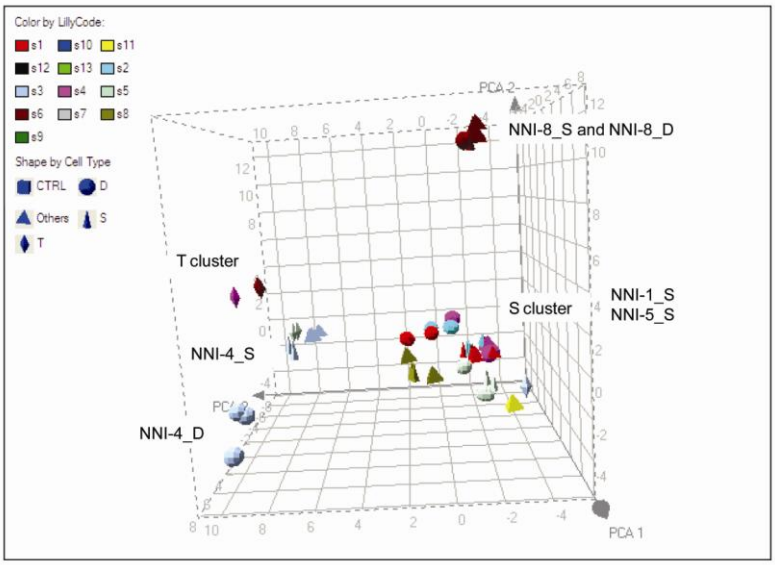

Figure-15. GBMs exhibit different phenotypic and genotypic subtypes. PCA of NNI-1, NNI-4, NNI-5 and NNI-8 showing the distinct genetic profiles of S, D, and T clusters. NNI-4 tumor spheres associated with the T cluster. NNI-8 shows a distinct transcriptome profile from the S cluster. Abbreviations: D, differentiated; PCA, principal component analysis; S, serum- free; T, tumor

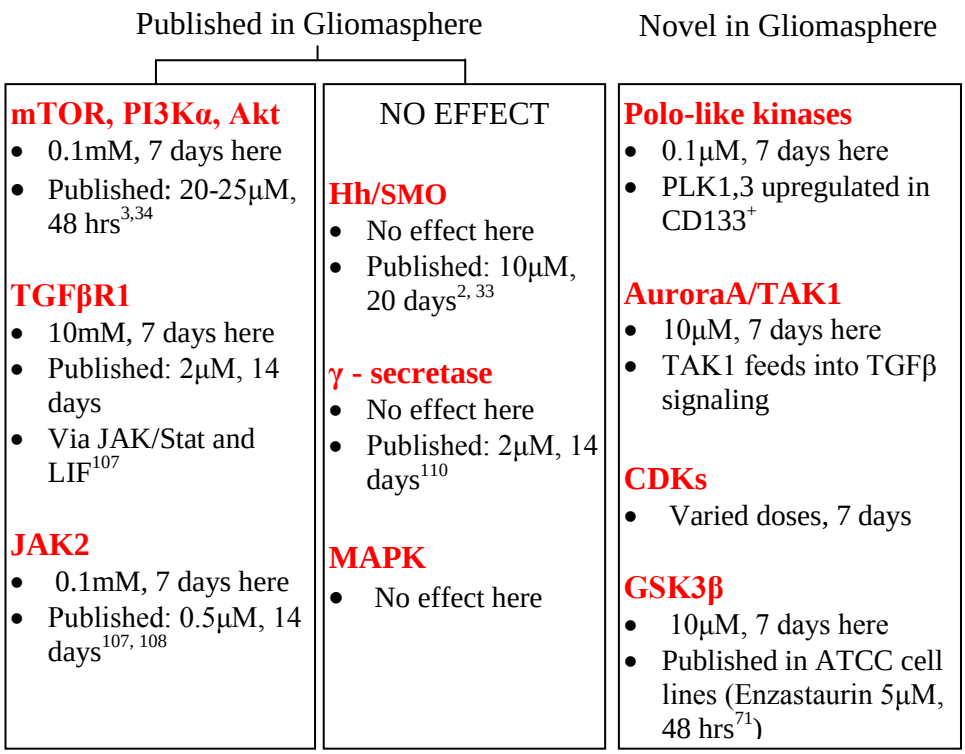

Figure-16. Compound groups from Eli Lilly screen published and novel in GPCs. Consistent with literature, the mTOR/PI3K/Akt, TGFβR1 and JAK2 pathways were identified. The roles of PLKs, AURKA, CDKs and GSK3β are currently unknown in GPCs.

4.1.2 Investigation of GSK3β as a Drug Target in GPCs

The GSK3β inhibitor accessed from Eli Lilly is designated as Compound 14 (Table S7, Fig. 17), selected based on its ability to reduce cell viability by at least 2-fold at 10μM and exhibiting a selectivity ratio of 2-fold or more across the 4 GPC lines. Compound 14 further demonstrated an interesting toxicity profile in the free-floating neurospheres (NNI-1, NNI-5 and NNI-8), demonstrating cell viabilities of 28.64%, 59.57% and 13.92% respectively; but displayed little toxicity towards NNI-4, a semi-adherent GBM sphere subtype with 85.51% cell viability (Fig. 17). Interestingly, this data would be consistent with Compound 14 targeting the relatively more undifferentiated NNI-1, 5 and 8 GPCs compared to the more differentiated NNI-4 GPCs as predicted by the PCA map (Fig. 15), further strengthening its mechanism through cell fate.

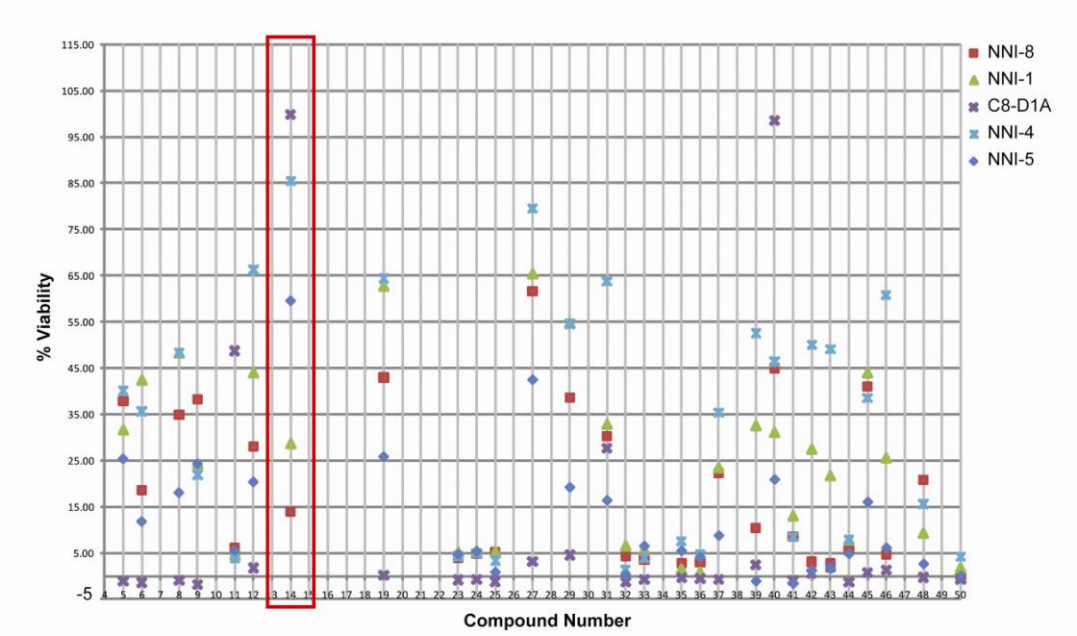

Figure-17. Compound 14 reduces cell viability of free-floating neurospheres by 2-fold or more and displays a selectivity ratio greater than 2. Compound 14 (boxed in red) demonstrates greater toxicity in the free-floating neurospheres (NNI-1, NNI-5 and NNI-8) as compared to the semi-adherent neurosphere (NNI-4). Preferential targeting of GPCs over mouse astrocytes is also observed.

4.1.3 Half Maximal Inhibitory Concentration (IC_{50}) of Compound 14 in Relation to Kinase Selectivity Profiles of Well-Published GSK3β Inhibitors

To further characterize Compound 14 effects on GPCs, we established dose response curves to determine the half maximal inhibitory concentrations (IC_{50}) needed to reduce viability by 50%. We observed that NNI-1, 5 and 8 showed IC_{50} values of 8.4, 14.3 and 15.8μM respectively (Fig. 18). In contrast, the more resistant GPC line, NNI-4 showed an IC_{50} value of 25.4μM. These data suggest that Compound 14 effectively targets the relatively undifferentiated, free-floating sphere subtype.

We referenced these concentrations to well-published GSK3β inhibitors to generate an understanding of whether these concentrations reflect the potency of Compound 14 (Table 4). The kinase selectivity profile of 6-bromoindirubin-3'-oxime (BIO), a potent GSK3 inhibitor, revealed an IC_{50} of 0.005μM for GSK3 kinase activity, indicating a strong selectivity of BIO for GSK3α/β[116]. *In vitro* experiments involving BIO utilized concentrations ranging from 5nm-5μM BIO[116-118], exhibiting a greater specificity than lithium chloride (LiCl). LiCl is the most frequently used pharmacological inhibitor of GSK3, despite its effects being in the 10-20mM range in cell-based assays[119]. Under conditions that approximate the intracellular environment (free concentration of Mg^{2+} 0.5mM and isotonic KCl 150mM), lithium exhibits an IC_{50} of 2mM[120]. Korur *et al.*[72] utilized another GSK3 inhibitor, SB216763, at 20μM in commercially procured, serum-grown glioma cell lines. Taken together, our data suggests that Compound 14 may target GSK3 selectively in our GPCs but that its relatively weaker potency precludes its utility as an

investigational tool in further work. We further substantiate this conclusion below.

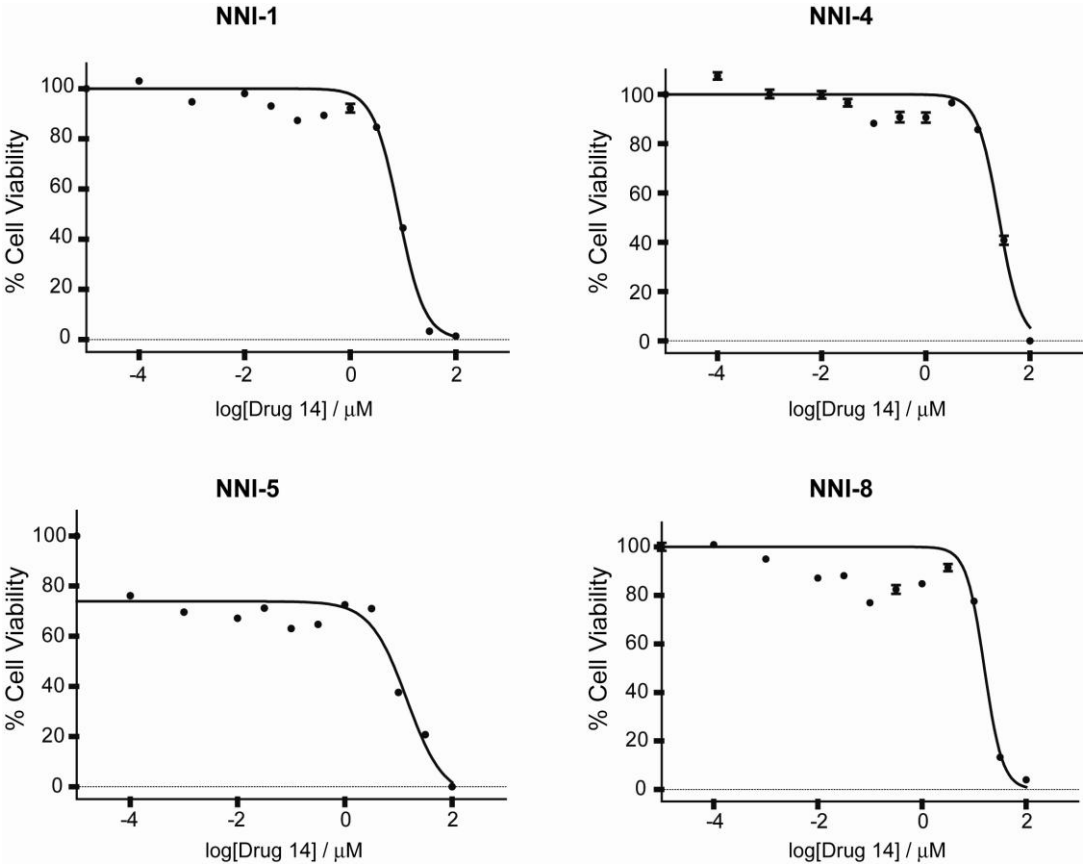

Figure-18. Dose-response curves of GPCs treated with Drug 14 over 5 days. NNI-4 displays higher IC_{50} value of 25.4μM as compared to 8.4μM, 14.3μM and 15.8μM in NNI-1, NNI-5 and NNI-8 respectively.

Table-4. Inhibitory concentrations (IC_{50}) of well-published GSK3β inhibitors in biochemical and cell-based context. IC_{50} values of commonly used GSK3β inhibitors in published literature, with LiCl being the most frequently used but least specific inhibitor.

Compound	IC_{50}	Context
BIO[116-118]	0.005μM	Biochemical
	5nM - 5μM	Cell-based
LiCl[119, 120]	2mM	Biochemical
	10-20mM	Cell-based
SB216763[72]	20μM	Cell-based

4.1.4 Compound 14 Acts as an Initial Lead in Exploration of GSK3β Modulation of GPCs

GSK3 exists as two isoforms – GSK3α and GSK3β. GSK3α is an enzyme originally isolated from tissues as a 51kDa protein, while GSK3β is a 46kDa polypeptide exhibiting similar catalytic properties as GSK3α[121]. Studies have shown that GSK3 is highly phosphorylated on tyrosine *in vivo*, which is functionally essential. The activating phosphorylation occurs on Tyr279 of GSK3α and Tyr216 of GSK3β[48]. Phosphorylation by protein kinases such as PKB/AKT leads to inhibitory phosphorylation of GSK3 at a serine residue near its amino terminus, which is serine 21 (Ser21) in GSK3α and Ser9 in GSK3β, hence inhibiting GSK3 activity[51].

We assessed of the levels of Tyr279/Tyr216 and Ser21/Ser9 phosphorylation after treating the GPCs with Compound 14 at their IC_{50} concentrations. We rationalized that such changes in phosphorylation would have to occur for Compound 14 to act specifically through GSK3-related mechanisms. We observed a slight decrease in Tyr216 of GSK3β in the GPCs, and a drastic increase in Ser21 of GSK3α phosphorylation for NNI-4, which has the highest IC_{50} of 25.4μM (Fig. 19). This difference is due to NNI-1, NNI-4 and NNI-8 representing different patient-specific cell lines. This specific assay for GSK3 activity suggests that Compound 14 is a weak GSK3 inhibitor and could have likely reduced cell viability by additional off-target, toxic effects. Nevertheless, we obtained consistent viability-reducing data with other compounds in the cluster targeting GSK3 (Table S7, Fig. 17), thus we believe that its initial value at implicating this pathway in GPCs is valid. We

thus focused on the use of well-published and more specific GSK3 inhibitors for the characterization of GSK3β regulation in our GPCs.

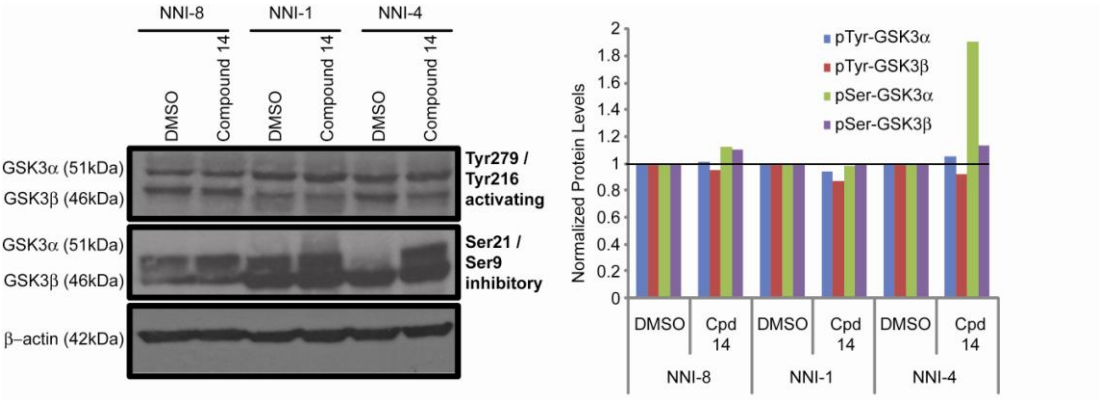

Figure-19. Compound 14 exhibits slight effects in modulation of GSK3β activity in GPCs. Assessment of activating Tyr279/Tyr216 and inhibitory Ser21/Ser9 phosphorylations revealed only a slight decrease in Tyr216 in GPCs and increase in Ser21/Ser9 phosphorylation in NNI-4 and NNI-8.

SUMMARY

Small molecule inhibitor screening with Eli Lilly compounds revealed drug targets in our GPCs consistent with previously characterized pathways such as the mTOR/PI3K/Akt, TGFβR1 and JAK/STAT signaling pathways, thus aligning our cells with international brain tumor stem cell efforts. GSK3β was identified as an interesting potential drug target due to a reduction in cell viability in our GPCs that was selective over normal mouse astrocytes, and a purported role in regulation of cell fate. Compound 14, however, was not the best candidate to elucidate GSK3β modulation of GPCs and therefore, we relied on the well-published and more specific inhibitor BIO as a probing tool for our investigation.

CHAPTER 5 – BIO IS A SELECTIVE GSK3 INHIBITOR

5.1 BIO (6-bromoindirubin-3'-oxime) selectively inhibits glycogen synthase kinase-3 (GSK3)

Studies have recently shown that 6-bromoindirubin derived from Tyrian purple, a natural dye produced by the gastropod mollusks, is a potent GSK3 inhibitor. Its synthetic derivative, 6-bromoindirubin-3'-oxime (BIO), constitutes a cell-permeable, potent and selective inhibitor of GSK3[116]. The kinase selectivity profile of BIO indicates a biochemical IC_{50} value of 0.005μM for GSK3 activity (Table 5)[116]. Specifically, the study showed that as much as 1μM BIO significantly reduced tyrosine phosphorylation (at Tyr279 and Tyr216) levels of both GSK3α/β isoforms respectively. We thus proceeded to assess BIO effects on our GPCs with a range of 5nM to 1μM.

We treated all GPC lines with increasing concentrations of BIO from 5nM to 1μM for 48 hours, and assessed the phosphorylation status of activating Tyr279 (GSK3α), Tyr216 (GSK3β) and inhibitory Ser21 (GSK3α), Ser9 (GSK3β) (Fig. 20). Previous work implicates the role of these phosphorylation sites at regulating GSK3 activity[51]. We observed a dose-dependent decrease in the levels of Tyr279/216 phosphorylation with as little as 50nM BIO treatment. Conversely, no dose-dependent increase in Ser21/9 phosphorylation was observed in NNI-1, 4 and 8 (Fig. 20A-C), implying that BIO inhibits GSK-3 activity by suppressing the activating Tyr279/216 phosphorylation sites. The inhibitory phosphorylation of GSK3α Ser21 was upregulated in NNI-11, suggesting additional GSK3 inhibition by this mode (Fig. 20D).

We thus utilized 500nM BIO for our subsequent experiments because significant ablation of Tyr279/216 phosphorylation of GSK3α/β was observed (Fig. 20). Following, we observed a time-dependent reduction in cell viability with 500nM BIO (Fig. 21). Interestingly, by day 15, viability decreased by approximately 20% in all GPC lines, suggesting that the process of cell death and cell proliferation must be balanced to maintain this small change upon BIO treatment. Accordingly, we explored 2 possible mechanisms previously associated with GSK3 inhibition[71, 72]: apoptosis (cell death) and induction of differentiation (limited cell proliferation compared to *bona fide* tumor stem cells).

Table-5. Biochemically-derived kinase selectivity profile of BIO, showing strong selectivity of BIO for GSK3α/β. Kinases were assayed using various concentrations of each compound. IC_{50} values, generated from the dose-response curves, are expressed in μM. Data from Meijer *et al.*[116].

Protein Kinases	BIO
GSK3α/β	0.005
CDK1/cyclin B	0.32
CDK2/cyclin A	0.30
CDK4/cyclin D1	10
CDK5/p35	0.08
erk1	> 10
erk2	> 10
MAPKK	10
protein kinase C α	12
protein kinase C β1	> 10
protein kinase C β2	> 10
protein kinase C γ	> 10
protein kinase C σ	> 10
protein kinase C ε	> 10
protein kinase C η	> 10
protein kinase C ξ	> 10
cAMP-dependent PK	> 10
cGMP-dependent PK	> 10
casein kinase 2	> 10
insulin receptor Tyr kinase	> 10

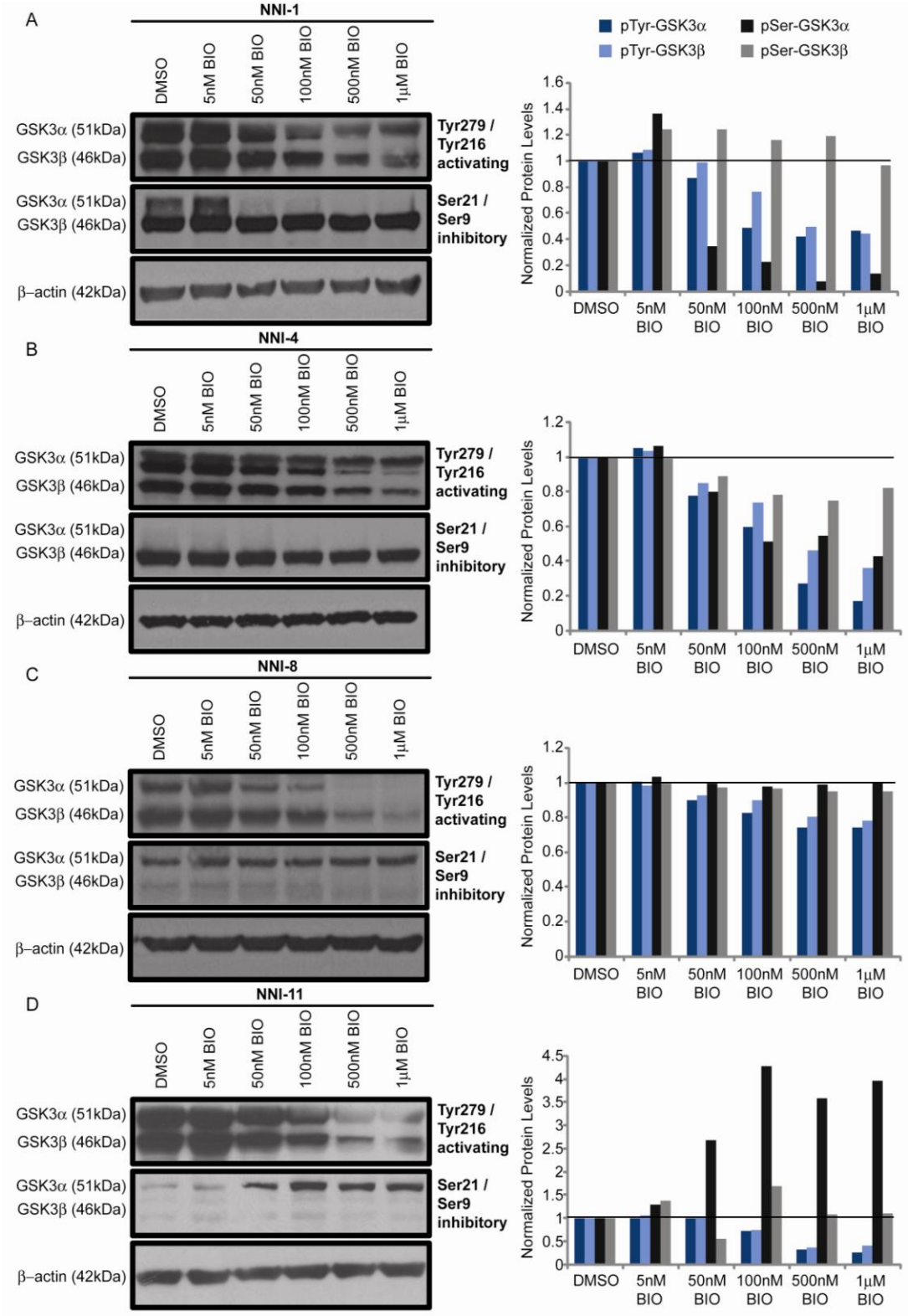

Figure-20. BIO selectively inhibits GSK3*α*/β by suppressing Tyr279/216 phosphorylation. BIO causes a dose-dependent decrease in activating Tyr279/216 phosphorylation in NNI-1, NNI-4, NNI-8 and NNI-11, while also promoting inhibitory Ser21 phosphorylation in NNI-11. 500nM BIO was utilized for subsequent experiments due to significant ablation of Tyr279/216 observed. **(Right Panel)** Quantitation using Quantity One of protein levels in Western blot **(Left Panel)**

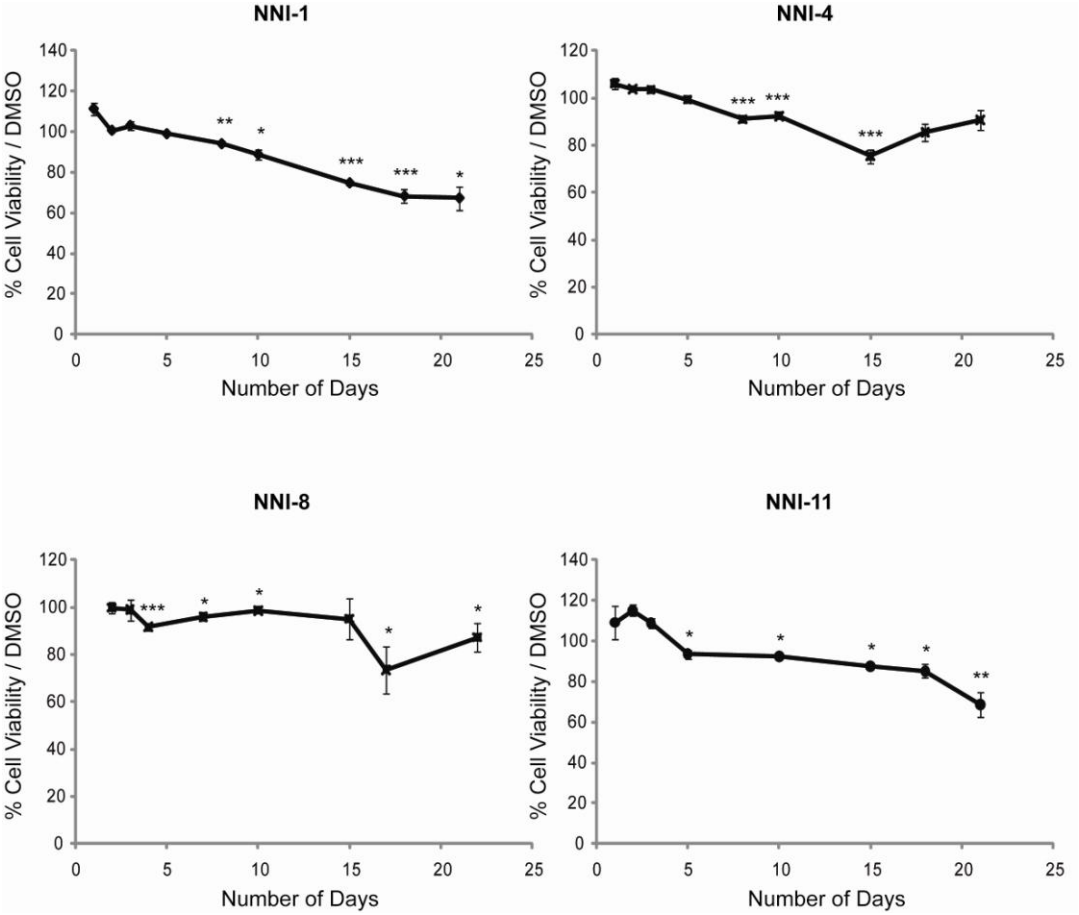

Figure-21. GSK3 inhibition by BIO treatment decreases GPCs cell viability. Treatment of GPCs at increasing timepoints leads to a significant decrease in cell viability in NNI-8 and NNI-11 by 5 days BIO treatment; and in NNI-1 and NNI-4 by 8 days BIO treatment.

5.2 GSK3 inhibition by BIO specifically targets the stem cell population defined by the CD133 marker

5.2.1 GSK3 inhibition depletes clonogenicity in GPCs and preferentially targets towards the CD133$^+$ population

The study of tumor stem cells is complicated by the fact that conventional assays tend to reflect the activity of majority cells, thus masking that of a fractional population. GPCs are grown as spheroid structures and recent work highlights their heterogeneous make-up[77, 122]. To determine the activity of specific cellular populations, we utilized flow cytometry to evaluate the sphere-forming ability of CD133-expressing cells, a marker frequently associated with tumor-initiating capacity in certain GBM subtypes[36, 37]. The neurosphere assay estimates *bona fide* tumor stem cell frequency, while sphere size indicates proliferative capacity[123]. This assay provides an *in vitro* readout of tumor stem cell activity that often correlates with survival outcome in orthotopic mouse models[2, 107].

GPCs were flow-sorted into CD133$^+$ and CD133$^-$ populations and seeded at clonal densities that distinguish true stem cell-originated spheres from cell aggregations[90]. Thirty cells per well were seeded into 96-well plates and the percentage of neurospheres formed, as well as neurosphere size were assessed. Colonies greater than 20μm were scored as spheres[124]. In all GPC lines, we observed the following trends (Figs. 22A-D; Tables 6A, B): (1) Sphere number in unsorted cells decreased by day 21 post-BIO treatment (Figs. 22A-Di), indicating that the tumor stem cell frequency was diminished; (2) BIO treatment reduced sphere number in specifically CD133$^+$ cells compared to CD133$^-$ cells (Figs. 22A-Di), suggesting that *bona fide* tumor stem cells

were effectively targeted; (3) Sphere size, an indicator of proliferation, was diminished in BIO-treated $CD133^+$ cells, whereas $CD133^-$ spheres tended to increase in size (Figs. 22A-D,ii-iv). These data suggest that GSK3 inhibition is effective against tumor stem cells, causing cellular disintegration, leading to the appearance of more small spheres; while $CD133^-$ cells were unaffected and continued to proliferate. This underscores the importance of designing therapies that target both tumor-initiating and other majority cells to completely eradicate tumor growth. The data challenges that while the "cancer stem cell hypothesis" accurately pinpoints the etiology of the tumor, targeting the supporting cells may also be crucial to remove the microenvironmental niche[125]. Interestingly, recent evidence supports that $CD133^+$ GBM cells are capable of differentiating into endothelial cells which in turn provide the vasculogenic niche to maintain the tumor stem cell fraction[24, 126, 127]. Such findings highlight the delicate interplay between various cellular fractions in the heterogeneous tumor mass.

Table-6A. Average percentage neurospheres formed normalized to DMSO control for GPCs treated with BIO. GPCs were seeded at 30 cells per well into 96-well plates, treated with BIO, and colonies were scored at Days 7, 14 and 21. Values are expressed as mean±SEM.

	Total Population			**$CD133^+$ -flow sorted fraction**			**$CD133^-$-flow sorted fraction**		
BIO treatment (Days)	7	14	21	7	14	21	7	14	21
NNI-1	1.024± 0.035	0.981± 0.035	0.824± 0.069	0.752± 0.048	0.675± 0.062	0.785± 0.057	0.980± 0.053	1.324± 0.074	1.383± 0.086
NNI-4	0.908± 0.093	0.941± 0.157	0.574± 0.079	0.752± 0.040	0.923± 0.026	0.743± 0.060	1.134± 0.171	1.000± 0.143	0.849± 0.144
NNI-8	0.958± 0.023	0.766± 0.027	0.833± 0.088	0.890± 0.024	0.799± 0.022	0.859± 0.067	1.166± 0.030	1.153± 0.091	1.318± 0.196
NNI-11	0.931± 0.056	0.900± 0.095	0.569± 0.117	0.882± 0.053	0.979± 0.089	0.575± 0.076	1.435± 0.095	0.996± 0.089	0.795± 0.063

Table-6B. Average neurosphere size normalized to DMSO control for GPCs treated with BIO. GPCs were seeded at 30 cells per well into 96-well plates, treated with BIO, and colonies were scored at Days 7, 14 and 21. Values are expressed as mean±SEM.

	Total Population			**$CD133^+$ -flow sorted fraction**			**$CD133^-$-flow sorted fraction**		
BIO treatment (Days)	7	14	21	7	14	21	7	14	21
NNI-1	1.153± 0.015	0.955± 0.035	0.910± 0.004	0.913± 0.029	0.851± 0.019	0.854± 0.023	1.211± 0.020	1.428± 0.061	1.166± 0.030
NNI-4	1.035± 0.033	0.726± 0.054	0.604± 0.083	0.923± 0.047	0.698± 0.045	0.562± 0.033	1.304± 0.076	1.064± 0.054	0.856± 0.109
NNI-8	0.911± 0.084	0.898± 0.044	0.763± 0.034	0.862± 0.070	0.859± 0.054	0.668± 0.049	1.383± 0.111	1.314± 0.151	0.793± 0.068
NNI-11	0.932± 0.015	0.865± 0.090	0.779± 0.071	0.917± 0.033	0.854± 0.047	0.726± 0.011	1.305± 0.039	1.516± 0.144	0.995± 0.044

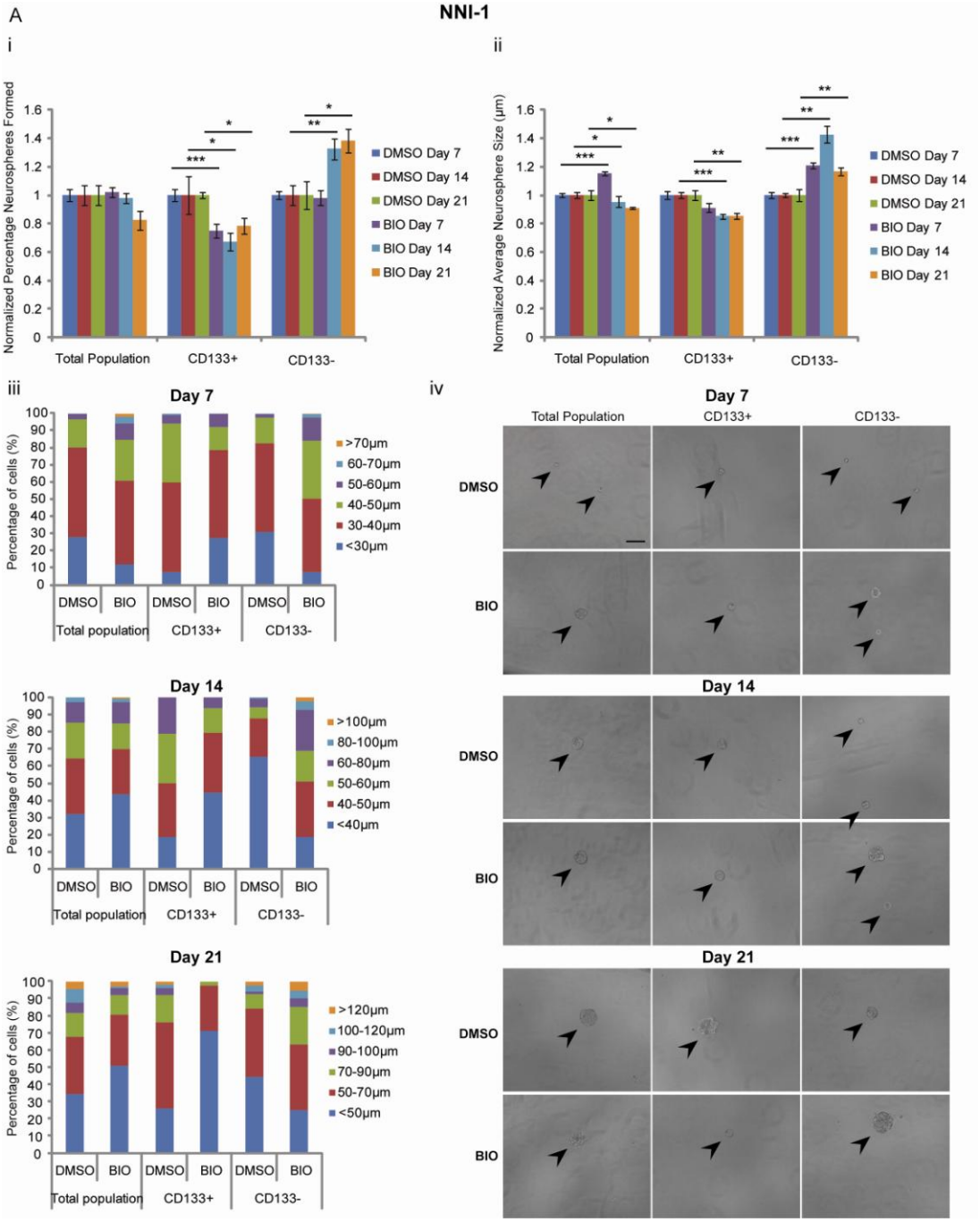

Figure-22A. GSK3 inhibition by BIO depletes self-renewal potential of GPCs preferentially in the CD133$^+$ population in NNI-1. (i) BIO treatment reduces average percentage neurospheres formed and **(ii)** average neurosphere size in the CD133$^+$ subpopulation. **(iii)** Distribution of neurosphere size showing a reduction in spheres of larger sizes and increase in spheres exhibiting smaller sizes in the CD133$^+$ subpopulation as compared to the total and CD133$^-$ subpopulations upon BIO treatment. **(iv)** Representative colonies at days 7, 14 and 21 in the DMSO-control and BIO-treated NNI-1 GPCs. Scale bar = 100µm. *$p < 0.05$, **$p < 0.01$, ***$p < 0.001$

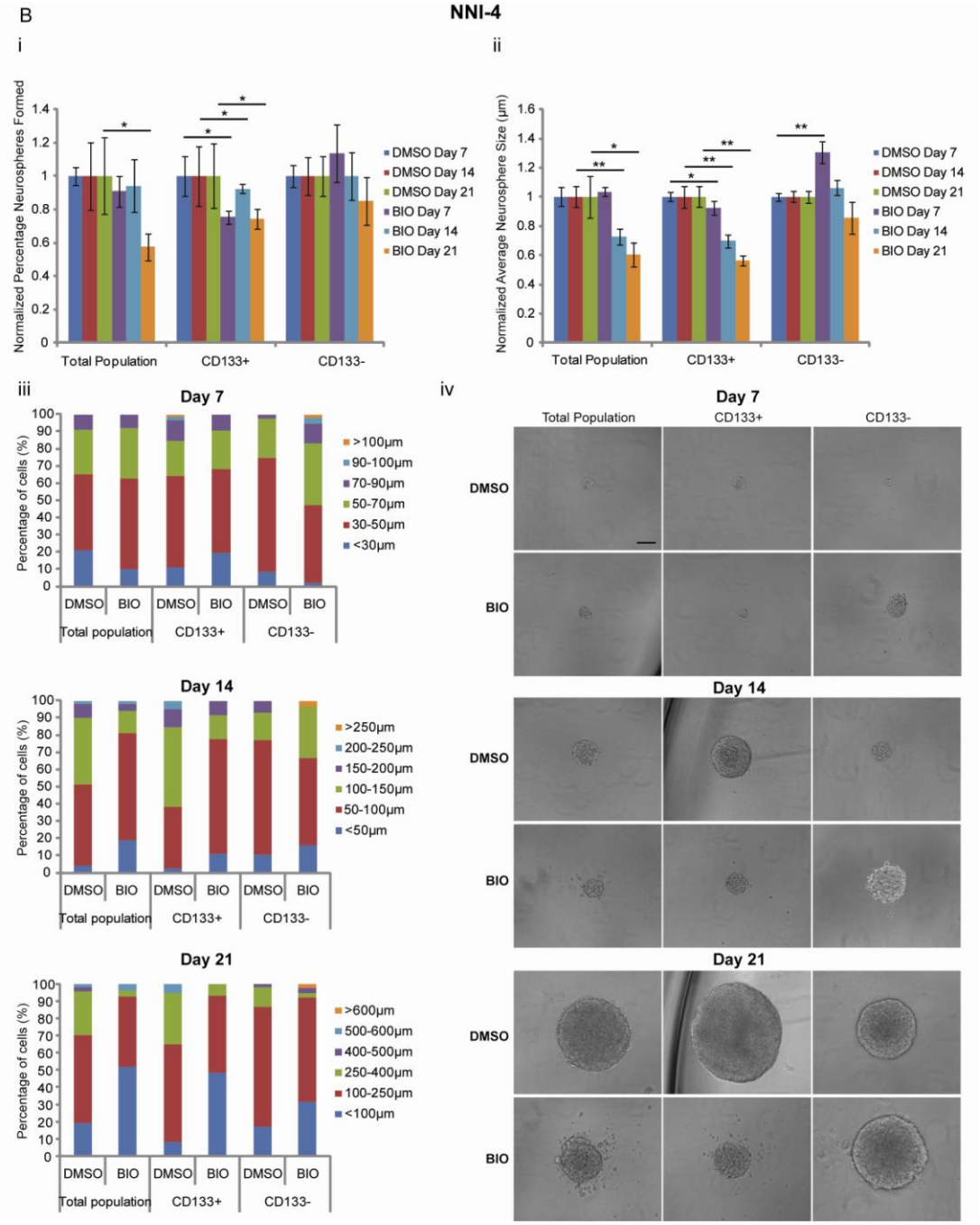

Figure-22B. GSK3 inhibition by BIO depletes self-renewal potential of NNI-4 GPCs preferentially in the CD133$^+$ population. (i) BIO treatment reduces average percentage neurospheres formed and **(ii)** average neurosphere size in the CD133$^+$ subpopulation. **(iii)** Distribution of neurosphere size showing a reduction in spheres of larger sizes and increase in spheres exhibiting smaller sizes in the CD133$^+$ subpopulation as compared to the total and CD133$^-$ subpopulations upon BIO treatment. **(iv)** Representative colonies at days 7, 14 and 21 in the DMSO-control and BIO-treated NNI-4 GPCs. Disintegration of neurospheres was observed upon BIO treatment in the CD133$^+$ and total populations at days 14 and 21. Scale bar = 100µm. *$p < 0.05$, **$p < 0.01$, ***$p < 0.001$

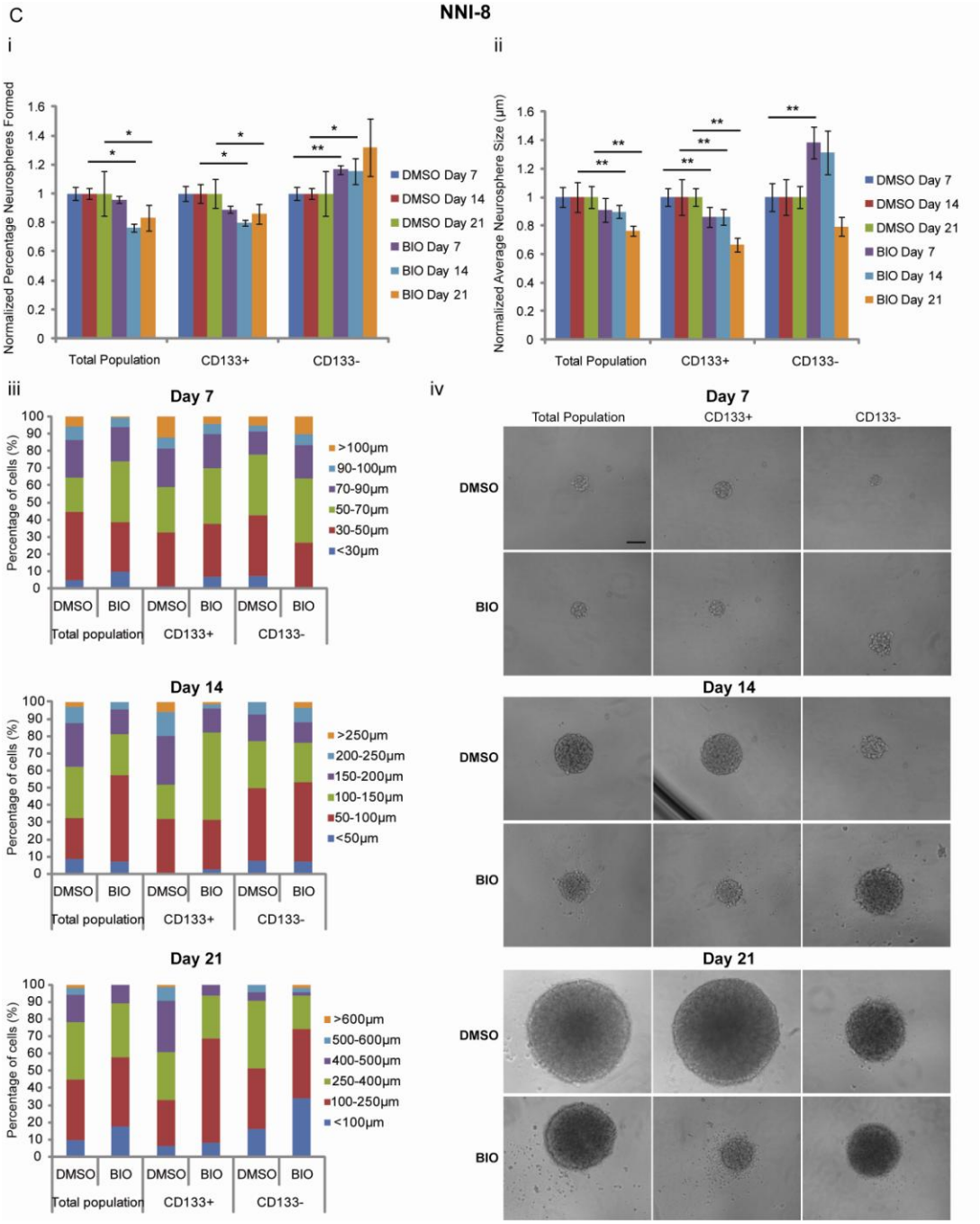

Figure-22C. GSK3 inhibition by BIO depletes self-renewal potential of NNI-8 GPCs preferentially in the CD133$^+$ population. (i) BIO treatment reduces average percentage neurospheres formed and **(ii)** average neurosphere size in the CD133$^+$ subpopulation. **(iii)** Distribution of neurosphere size showing a reduction in spheres of larger sizes and increase in spheres exhibiting smaller sizes in the CD133$^+$ subpopulation as compared to the total and CD133$^-$ subpopulations upon BIO treatment. **(iv)** Representative colonies at days 7, 14 and 21 in the DMSO-control and BIO-treated NNI-8 GPCs. Disintegration of neurospheres was observed upon BIO treatment in the CD133$^+$ and total populations at days 14 and 21. Scale bar = 100µm. *$p < 0.05$, **$p < 0.01$, ***$p < 0.001$

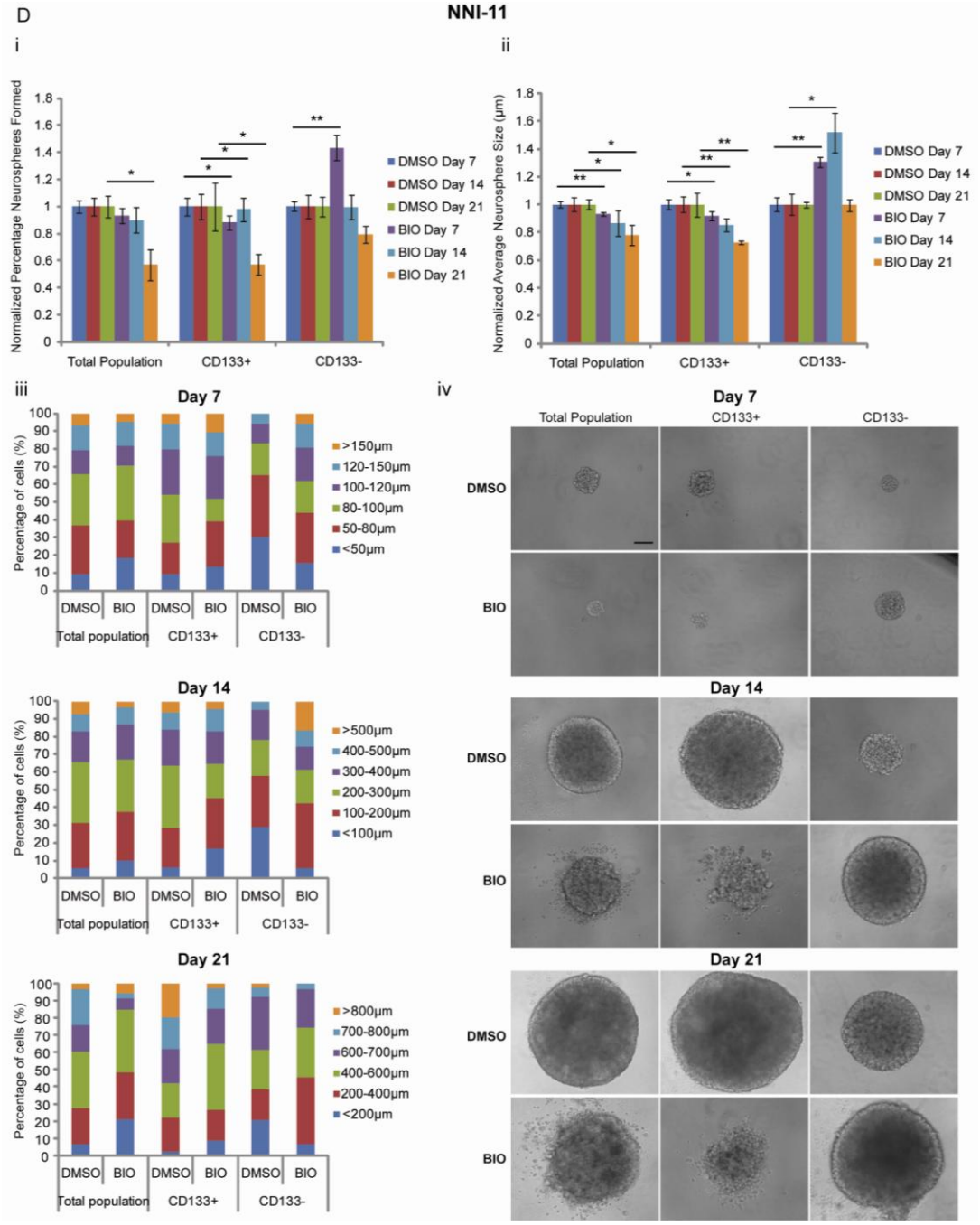

Figure-22D. GSK3 inhibition by BIO depletes self-renewal potential of NNI-11 GPCs preferentially in the CD133$^+$ population. (i) BIO treatment reduces average percentage neurospheres formed and **(ii)** average neurosphere size in the CD133$^+$ subpopulation. **(iii)** Distribution of neurosphere size showing a reduction in spheres of larger sizes and increase in spheres exhibiting smaller sizes in the CD133$^+$ subpopulation as compared to the total and CD133$^-$ subpopulations upon BIO treatment. **(iv)** Representative colonies at days 7, 14 and 21 in the DMSO-control and BIO-treated NNI-11 GPCs. Disintegration of neurospheres was observed upon BIO treatment in the CD133$^+$ and total populations at days 14 and 21. Scale bar = 100µm. *$p < 0.05$, **$p < 0.01$, ***$p < 0.001$

5.2.2 GSK3 inhibition leads to an increase in cleaved PARP-positive cells specifically in the CD133^{+} population

Due to apparent cell death from data in our sphere assays, we explored the possibility of apoptosis occurring upon BIO treatment. Previous literature implicates the role of GSK3 inhibition in triggering apoptosis of common serum-grown glioma cells[71]. We explored this phenomenon in GPCs by capitalizing on the ability of flow cytometry to detect multiple parameters in single cell populations. Accordingly, we evaluated cleaved poly(ADP-ribose) polymerase (PARP) in CD133$^{+/-}$ GPC fractions. PARP has been implicated in DNA repair[128] and is the main cleavage target of caspase-3, thereby separating the 24kDa PARP amino-terminal DNA binding domain from the 89kDa carboxy-terminal catalytic domain[129]. PARP is required for maintenance of cell viability, and its cleavage aids in cell disassembly, thus serving as a marker of apoptotic cells[130].

We observed in all GPC lines the following trends (Figs. 23A-H): (1) Apoptosis as measured by cleaved PARP-expressing cells increased by 1.5 to 3-fold after 5 days of treatment with 500nM BIO; (2) This increase in cleaved PARP-expressing cells coincided with CD133-marked cells. In contrast, the changes in cleaved PARP levels in CD133^{-} cells were insignificant. These data suggest that GSK3 inhibition by BIO triggers apoptosis in specifically CD133^{+} tumor-initiating cells, further supporting that GSK3 regulation may be more crucial in maintaining the CD133^{+} phenotype.

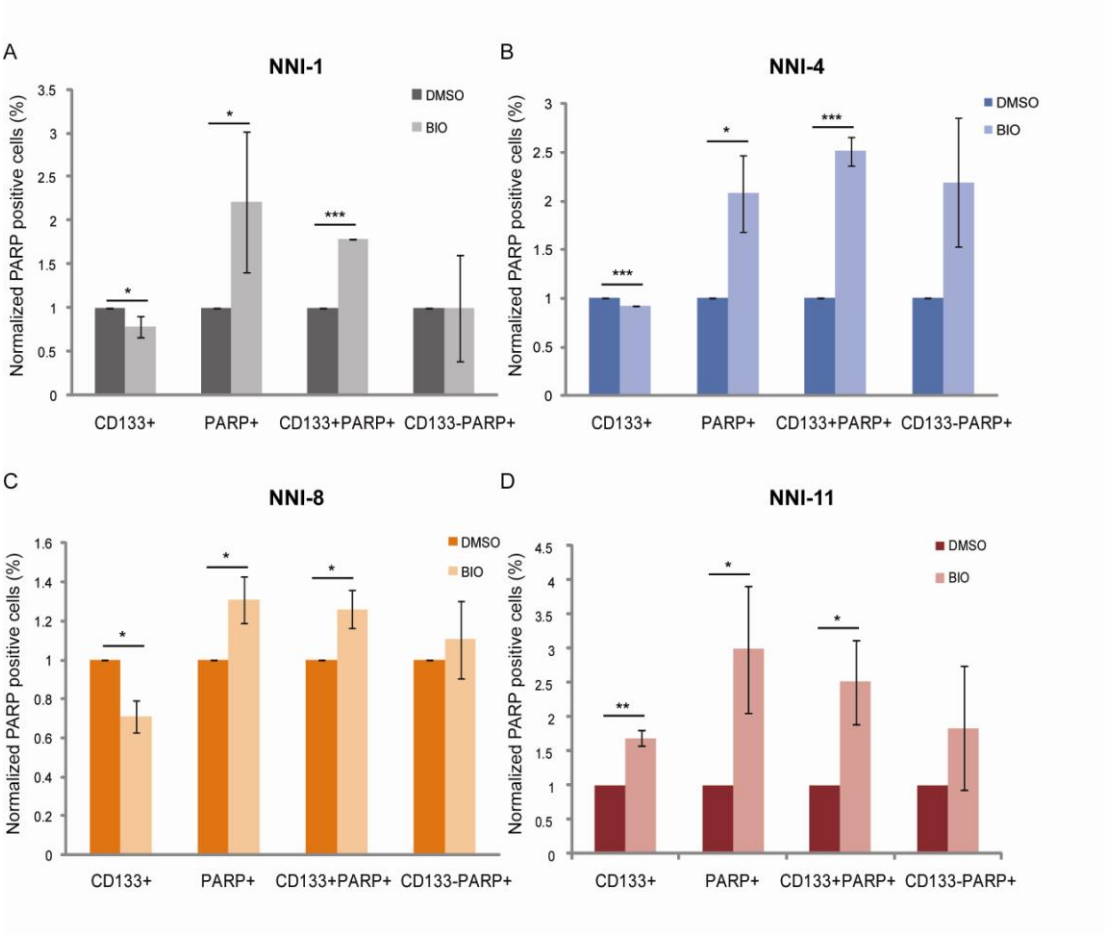

Figure-23A-D. GSK3 inhibition induces a significant increase in cleaved PARP-positive cells, preferentially targeting the CD133$^+$ fraction. Graphs showing percentage of cleaved PARP-positive and CD133-positive cells in GPCs treated with BIO for 5 days normalized to DMSO control. *$p < 0.05$, **$p < 0.01$, ***$p < 0.001$

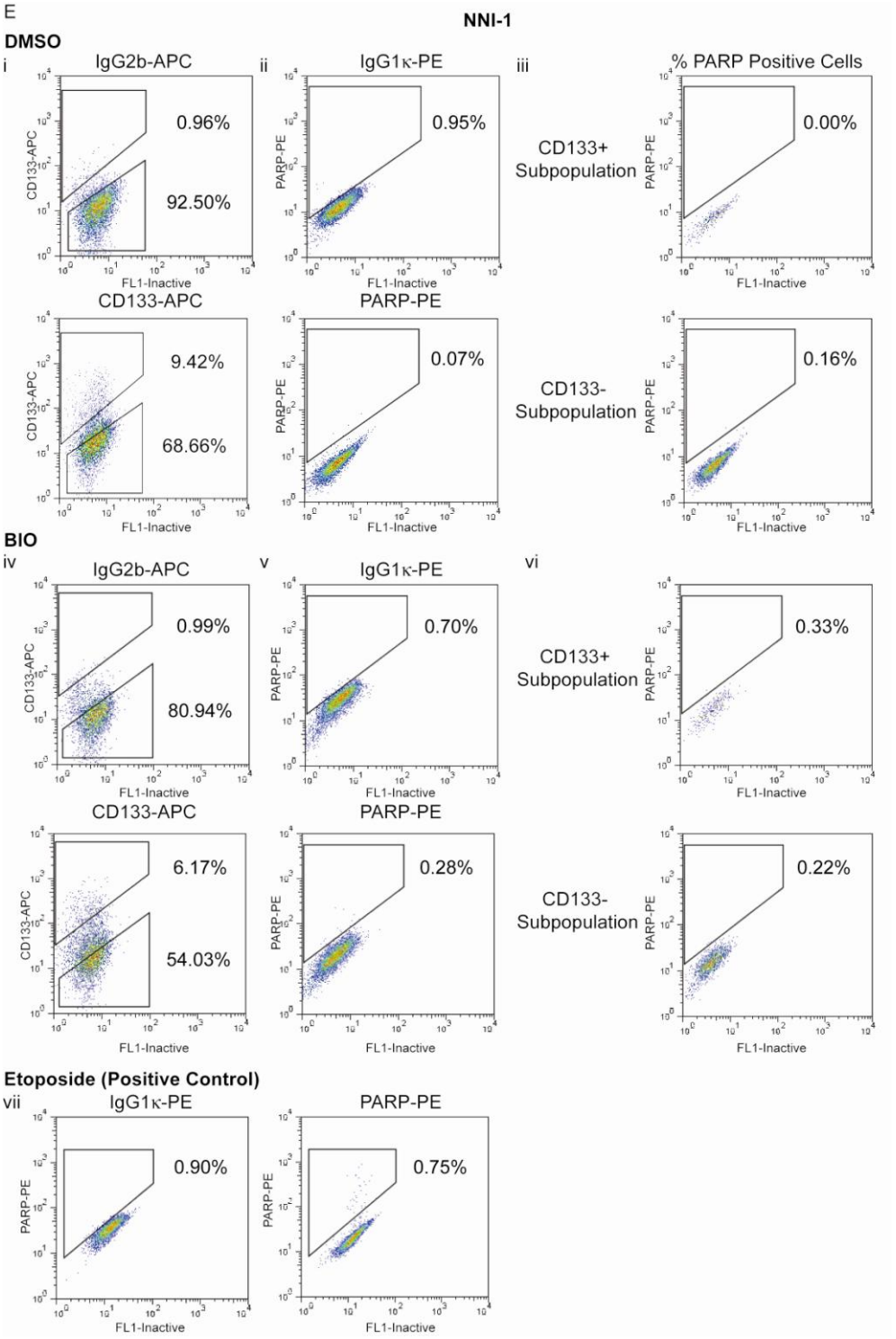

Figure-23E. GSK3 inhibition induces a significant increase in cleaved PARP-positive cells, preferentially targeting the CD133$^+$ fraction in NNI-1. Representative FACS plots of the data in **(A)** showing changes in CD133 percentage, cleaved PARP percentages and cleaved PARP expression in the CD133$^+$ and CD133$^-$ fraction in NNI-1. **(i, ii, iv, v)(Bottom panels)** Percentages of CD133 and cleaved PARP-positive cells gated on their respective isotype controls **(i, ii, iv, v)(Top panels)**. **(iii, vi)** Percentage of cleaved PARP-expressing cells in the CD133$^+$ and CD133$^-$ subpopulations of DMSO and BIO-treated cells respectively. **(viii)** Etoposide-treated cells as a positive control for assessment of cleaved PARP-positive cells.

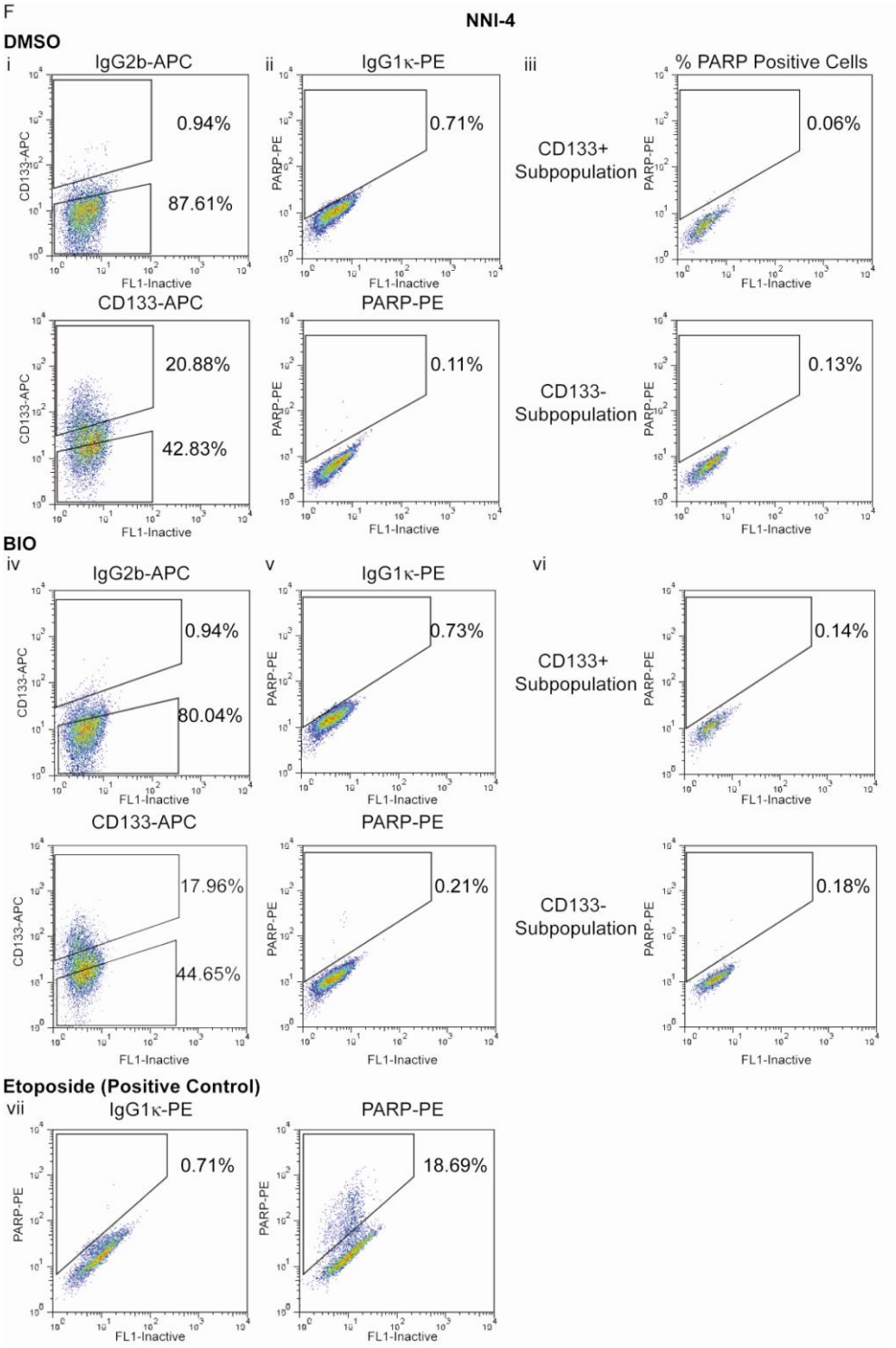

Figure-23F. GSK3 inhibition induces a significant increase in cleaved PARP-positive cells, preferentially targeting the CD133^{+} fraction in NNI-4. Representative FACS plots of the data in **(B)** showing changes in CD133 percentage, cleaved PARP percentages and cleaved PARP expression in the CD133^{+} and CD133^{-} fraction in NNI-4. **(i, ii, iv, v)(Bottom panels)** Percentages of CD133 and cleaved PARP-positive cells gated on their respective isotype controls **(i, ii, iv, v)(Top panels)**. **(iii, vi)** Percentage of cleaved PARP-expressing cells in the CD133^{+} and CD133^{-} subpopulations of DMSO and BIO-treated cells respectively. **(viii)** Etoposide-treated cells as a positive control for assessment of cleaved PARP-positive cells.

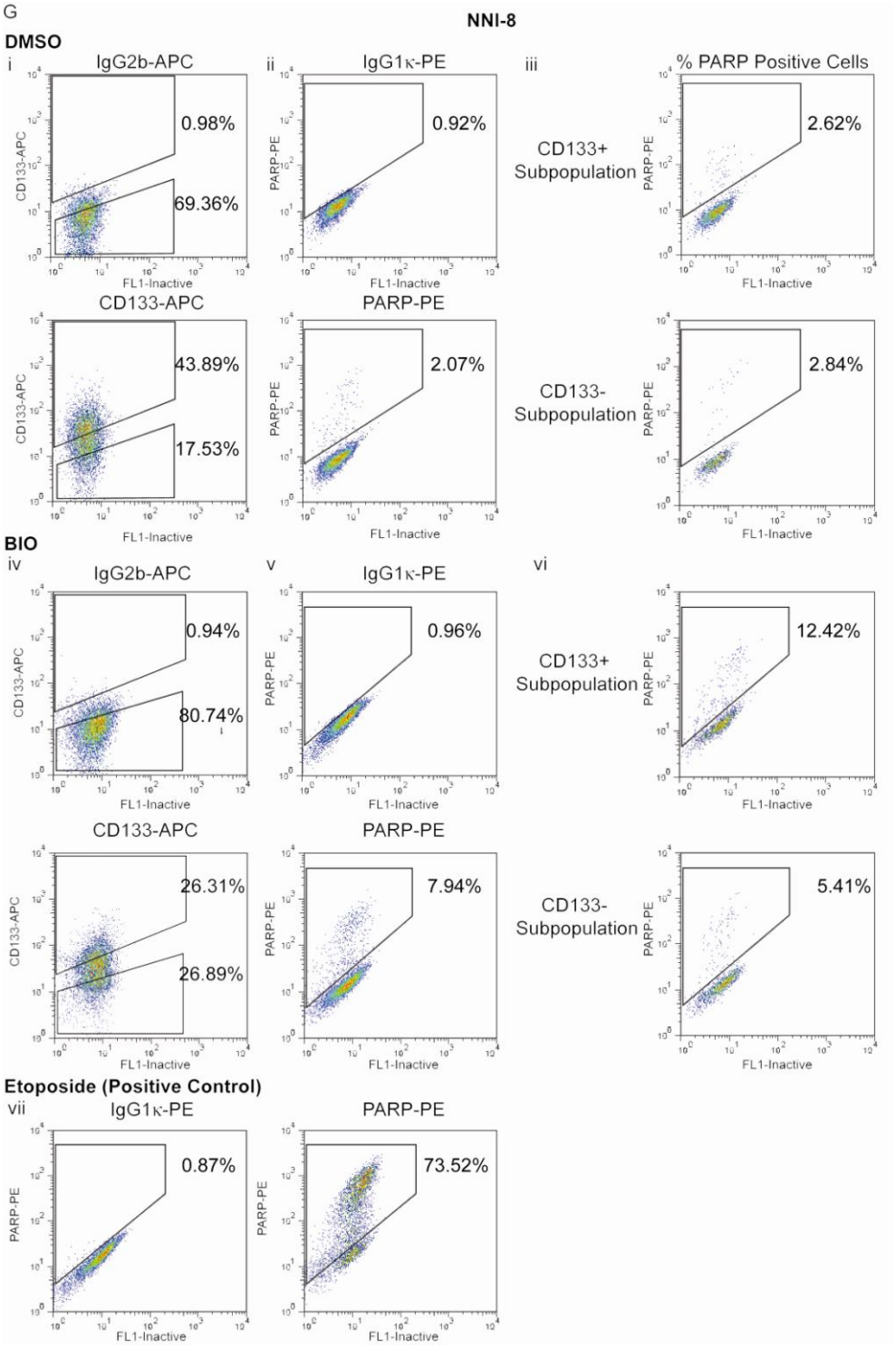

Figure-23G. GSK3 inhibition induces a significant increase in cleaved PARP-positive cells, preferentially targeting the CD133^{+} fraction in NNI-8. Representative FACS plots of the data in **(C)** showing changes in CD133 percentage, cleaved PARP percentages and cleaved PARP expression in the CD133^{+} and CD133^{-} fraction in NNI-8. **(i, ii, iv, v)(Bottom panels)** Percentages of CD133 and cleaved PARP-positive cells gated on their respective isotype controls **(i, ii, iv, v)(Top panels)**. **(iii, vi)** Percentage of cleaved PARP-expressing cells in the CD133^{+} and CD133^{-} subpopulations of DMSO and BIO-treated cells respectively. **(viii)** Etoposide-treated cells as a positive control for assessment of cleaved PARP-positive cells.

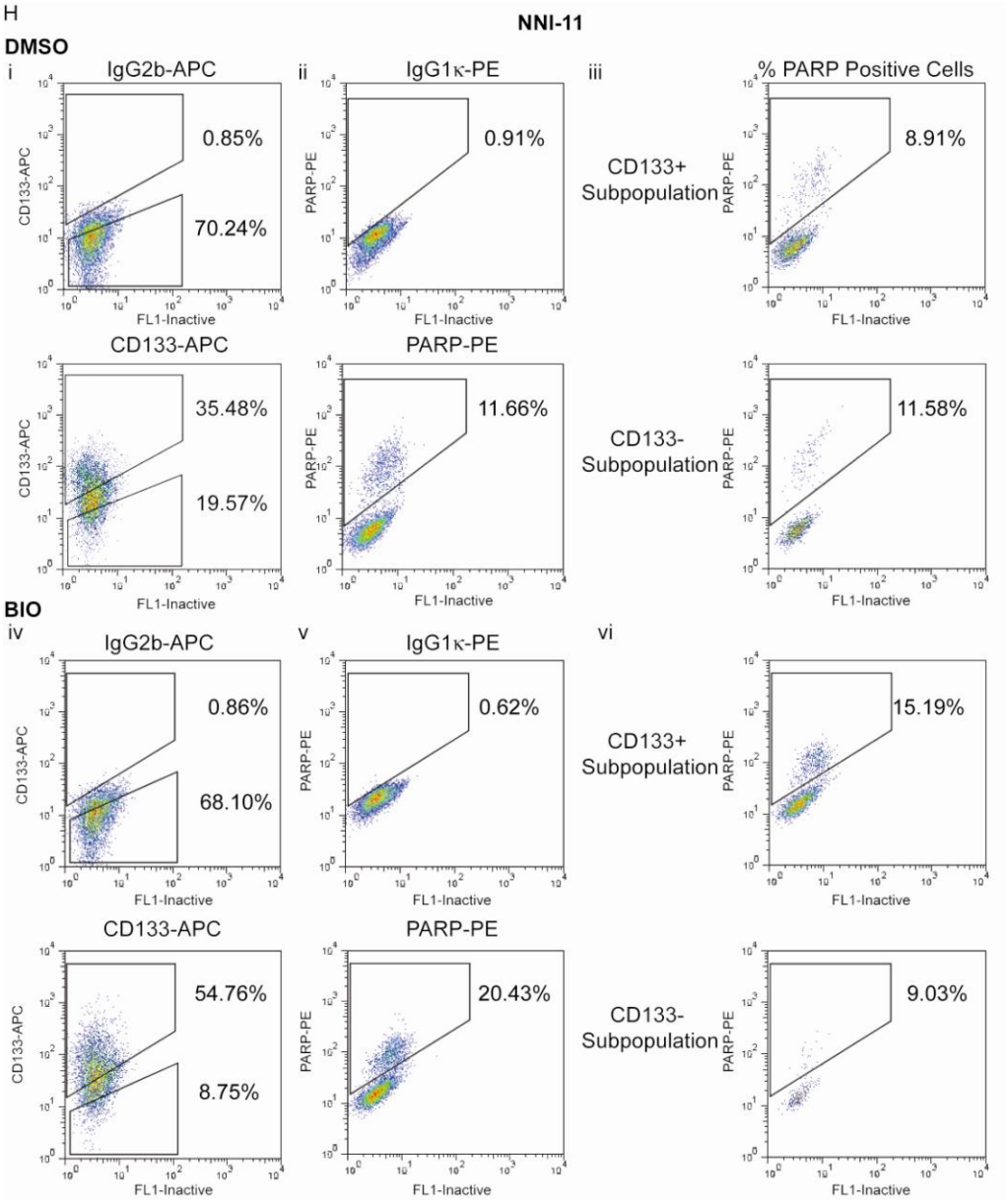

Figure-23H. GSK3 inhibition induces a significant increase in cleaved PARP-positive cells, preferentially targeting the CD133$^+$ fraction in NNI-11. Representative FACS plots of the data in **(D)** showing changes in CD133 percentage, cleaved PARP percentages and cleaved PARP expression in the CD133$^+$ and CD133$^-$ fraction in NNI-11. **(i, ii, iv, v)(Bottom panels)** Percentages of CD133 and cleaved PARP-positive cells gated on their respective isotype controls **(i, ii, iv, v)(Top panels)**. **(iii, vi)** Percentage of cleaved PARP-expressing cells in the CD133$^+$ and CD133$^-$ subpopulations of DMSO and BIO-treated cells respectively.

5.2.3 GSK3 inhibition depletes NF-κB-positive cells, preferentially in the CD133^{+} fractions in NNI-8 and NNI-11

Reports have implicated nuclear factor-kappaB (NF-κB) in pro-survival activities of glioma: NF-κB activation protected against tumor necrosis factor-related apoptosis-inducing ligand (TRAIL)–induced cell death in glioma cells[131]; NF-κB inhibition induced apoptosis in GBM cell lines and primary cultures and inhibited tumor growth in nude mice brains[132]; and overexpression of mitogen-activated protein kinase/extracellular-regulated kinase kinase kinase-3 (MEKK3) conferred resistance to apoptosis through NF-κB activation[133]. Furthermore, GSK3 ablation was shown to inhibit NF-κB activity, leading to reduced glioma cell survival *in vitro* and extended tumor latency[71].

We sought to investigate the effects of BIO treatment on changes in levels of NF-κB specifically in CD133$^{+/-}$ cells. We show that GSK3 inhibition significantly decreased NF-κB-expressing cells, preferentially in the CD133^{+} fractions (Figs. 24C, D, G, H). NNI-1 and NNI-4 however did not show this trend in the CD133^{+} fraction (Figs. 24A, B, E, F), indicating that GSK3 inhibition of CD133^{+} cells was likely occurring through a NFκB-independent mechanism. This is not unexpected because CD133 as a marker of tumor-initiating capacity has been controversial and shown to vary according to the state of disease progression[134]. Furthermore, tumor-initiating capacity has been found in CD133^{-} cells as well[36, 37], highlighting the complexity of relying on surface markers to assign tumorigenic properties to populations of cells. This emphasizes the need to adopt complementary assays to measure the functional aspects of tumor stem cells, as previously described in our sphere assays.

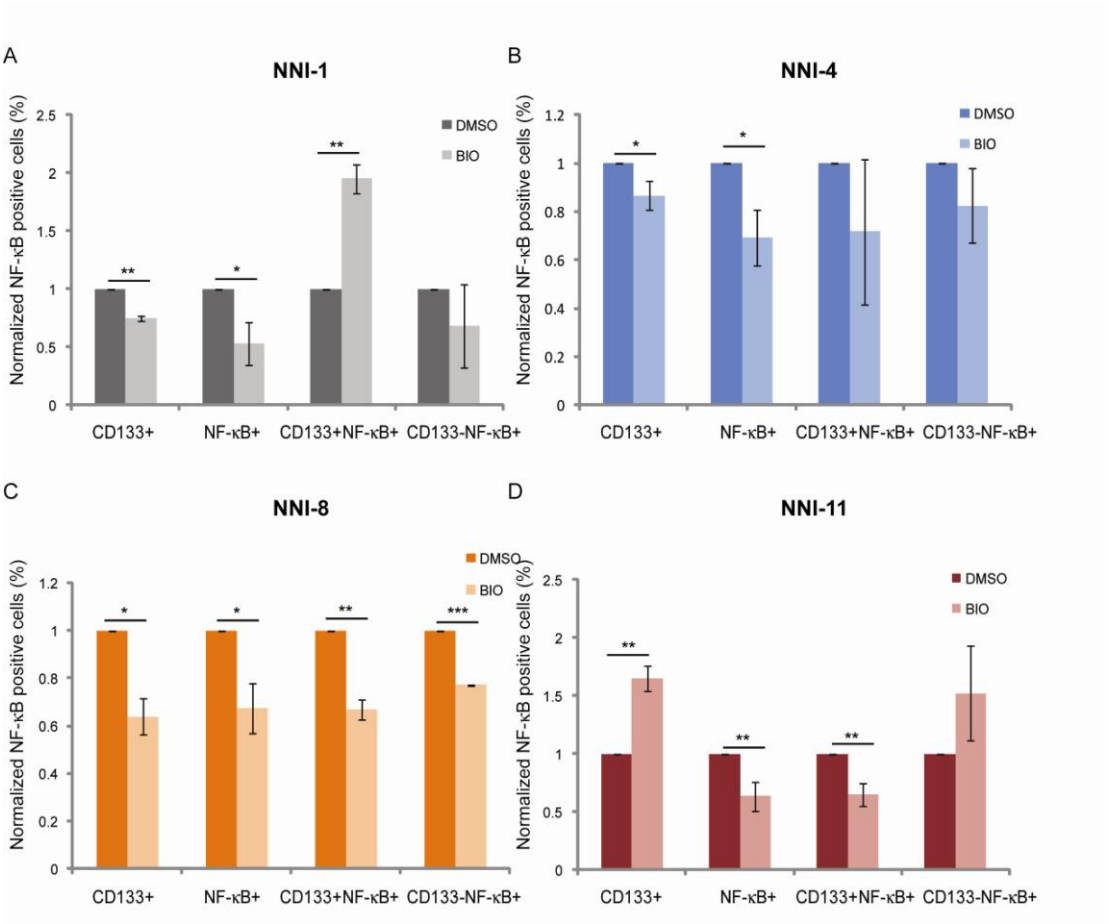

Figure-24A-D. GSK3 inhibition induces a significant decrease in NF-κB-positive cells, preferentially targeting the CD133$^+$ fraction in NNI-8 and NNI-11. Graphs showing of percentage NF-κB-positive and CD133-positive cells in GPCs treated with BIO for 5 days normalized to DMSO control. *$p < 0.05$, **$p < 0.01$, ***$p < 0.001$

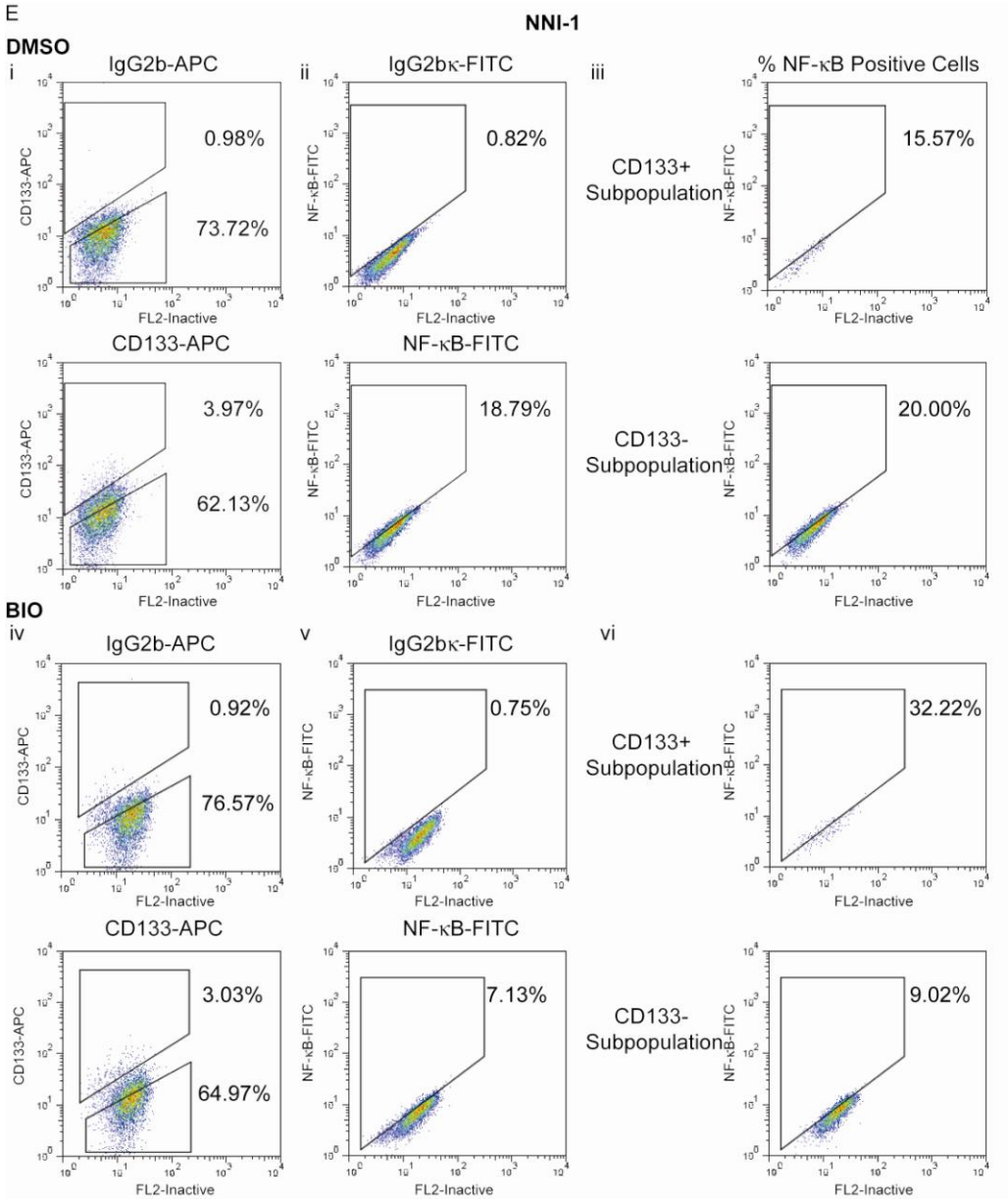

Figure-24E. GSK3 inhibition induces a significant decrease in NF-κB-positive cells, preferentially targeting the CD133$^+$ fraction in NNI-8 and NNI-11. Representative FACS plots of the data in **(A)** showing changes in CD133 percentage, NF-κB percentages and NF-κB expression in the CD133$^+$ and CD133$^-$ fraction in NNI-1. **(i, ii, iv, v)(Bottom panels)** Percentages of CD133 and NF-κB-positive cells gated on their respective isotype controls **(i, ii, iv, v)(Top panels)**. **(iii, vi)** Percentage of NF-κB-expressing cells in the CD133$^+$ and CD133$^-$ subpopulations of DMSO and BIO-treated cells respectively.

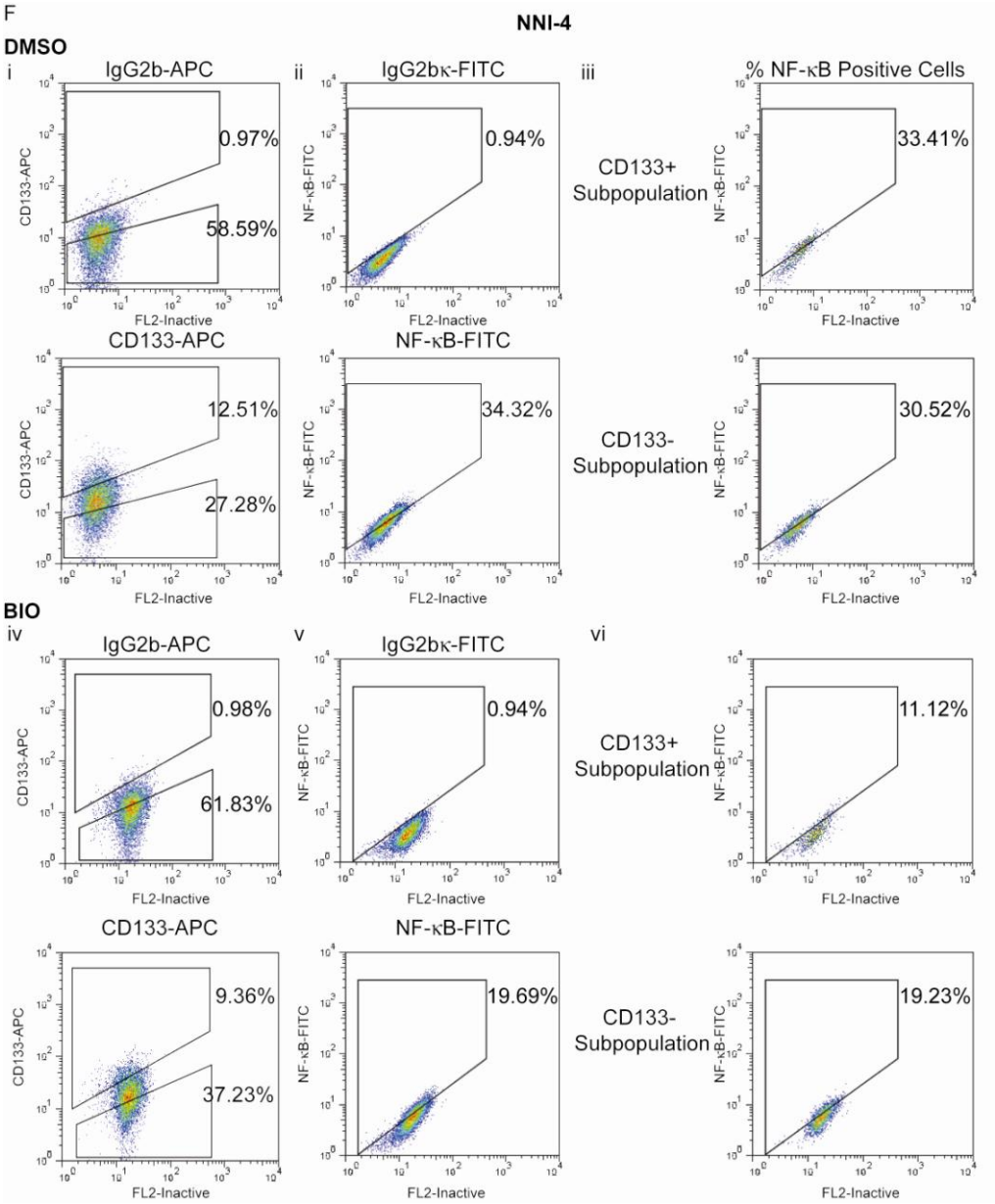

Figure-24F. GSK3 inhibition induces a significant decrease in NF-κB-positive cells, preferentially targeting the CD133^{+} fraction in NNI-8 and NNI-11. Representative FACS plots of the data in **(B)** showing changes in CD133 percentage, NF-κB percentages and NF-κB expression in the CD133^{+} and CD133^{-} fraction in NNI-4. **(i, ii, iv, v)(Bottom panels)** Percentages of CD133 and NF-κB-positive cells gated on their respective isotype controls **(i, ii, iv, v)(Top panels)**. **(iii, vi)** Percentage of NF-κB-expressing cells in the CD133^{+} and CD133^{-} subpopulations of DMSO and BIO-treated cells respectively.

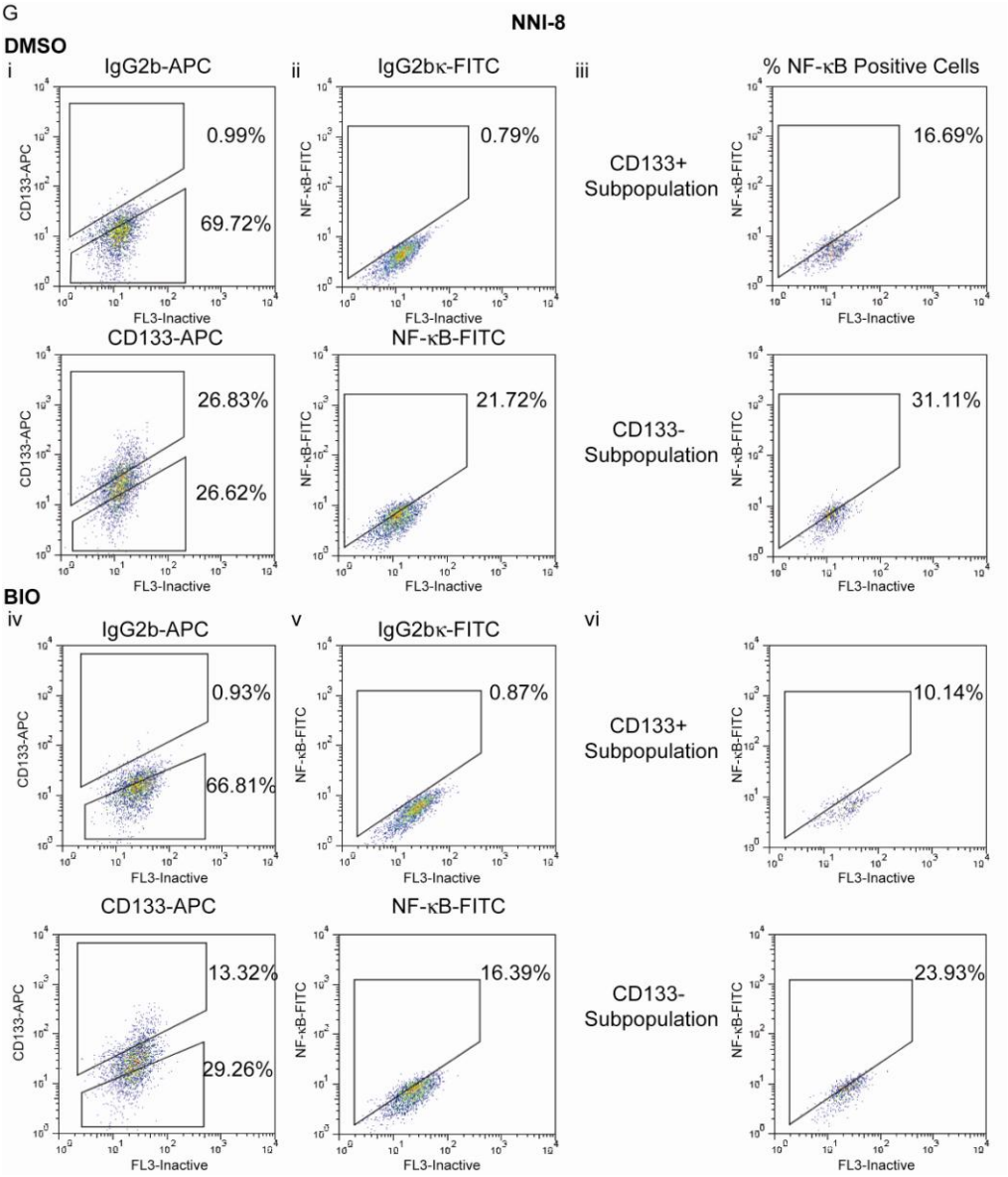

Figure-24G. GSK3 inhibition induces a significant decrease in NF-κB-positive cells, preferentially targeting the CD133^{+} fraction in NNI-8 and NNI-11. Representative FACS plots of the data in **(C)** showing changes in CD133 percentage, NF-κB percentages and NF-κB expression in the CD133^{+} and CD133^{-} fraction in NNI-8. **(i, ii, iv, v)(Bottom panels)** Percentages of CD133 and NF-κB-positive cells gated on their respective isotype controls **(i, ii, iv, v)(Top panels)**. **(iii, vi)** Percentage of NF-κB-expressing cells in the CD133^{+} and CD133^{-} subpopulations of DMSO and BIO-treated cells respectively.

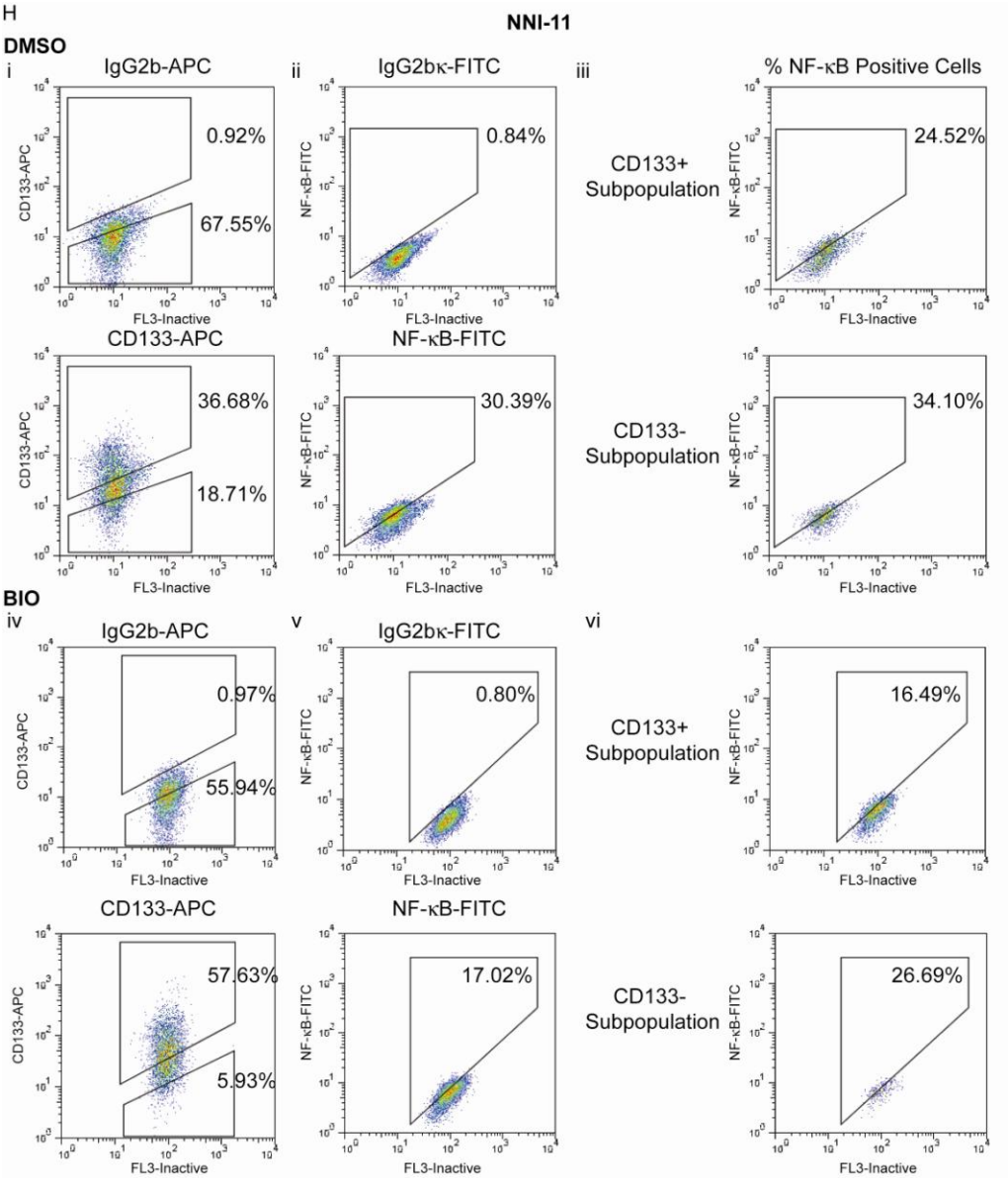

Figure-24H. GSK3 inhibition induces a significant decrease in NF-κB-positive cells, preferentially targeting the CD133$^+$ fraction in NNI-8 and NNI-11. Representative FACS plots of the data in **(D)** showing changes in CD133 percentage, NF-κB percentages and NF-κB expression in the CD133$^+$ and CD133$^-$ fraction in NNI-11. **(i, ii, iv, v)(Bottom panels)** Percentages of CD133 and NF-κB-positive cells gated on their respective isotype controls **(i, ii, iv, v)(Top panels)**. **(iii, vi)** Percentage of NF-κB-expressing cells in the CD133$^+$ and CD133$^-$ subpopulations of DMSO and BIO-treated cells respectively.

5.3 BIO causes GPC cell death through the effects of cleaved PARP, c-Myc and leads to a pro-differentiation response

5.3.1 BIO induces a time-dependent increase in cleaved PARP, and a decrease in c-Myc protein levels

The c-Myc oncoprotein has recently been implicated in the regulation of cell proliferation, differentiation and apoptosis and has been reported to be deregulated in various human tumors[135, 136]. c-Myc was previously reported to regulate GPC maintenance and self-renewal[137]. GPCs with reduced c-Myc levels showed diminished proliferation, increased apoptosis, and were unable to form neurospheres *in vitro* or generate tumors in mice. Accordingly, we explored the timing of events occurring after BIO treatment, specifically the induction of apoptosis, as well as the onset of differentiation (subsequent section). We treated the GPCs with BIO at increasing time-points of 48 hours, 72 hours and 5 days and probed for levels of cleaved PARP and c-Myc. These time periods were chosen to reflect the average time needed for doubling as well as to allow other phenotypic changes such as differentiation to occur[28] (Fig. 25). As a positive control for apoptosis, GPCs were treated with 10μM etoposide for 72 hours. Etoposide, a chemotherapeutic drug, is a topoisomerase II inhibitor known to induce apoptosis by promoting DNA double strand breaks, thereby leading to p53 activation[138]. We noted a time-dependent increase in cleaved PARP after 5 days, indicating an induction of apoptosis upon GSK3 inhibition by BIO (Fig. 26). This data mirrors the timing of the earlier flow-acquired data on PARP distribution in $CD133^{+/-}$ cellular fractions (Fig. 23). In addition, we also observed a decrease in c-Myc

after 5 days of BIO treatment (Fig. 26). These results provide evidence of apoptosis triggered by GSK3 inhibition.

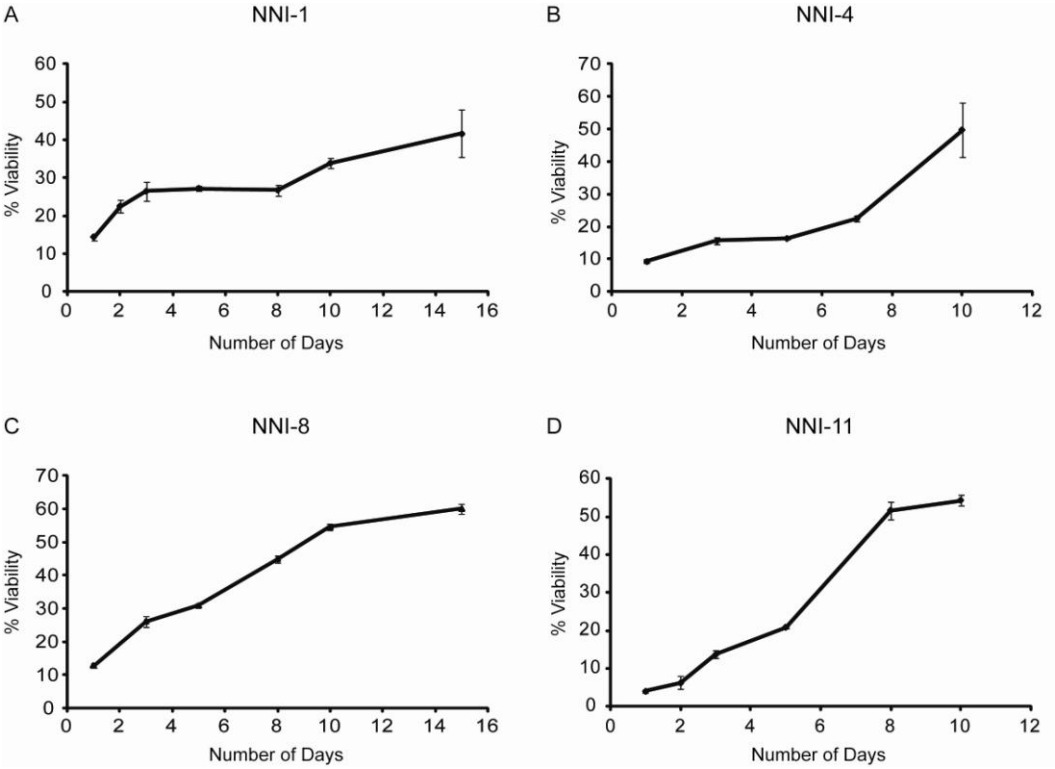

Figure-25. Proliferation curves of GPCs. (A) Proliferation curve of NNI-1 **(B)** NNI-4 and **(C)** NNI-8, showing doubling times of approximately 5 days **(D)** Proliferation curve of NNI-11 with a doubling time of about 2 days.

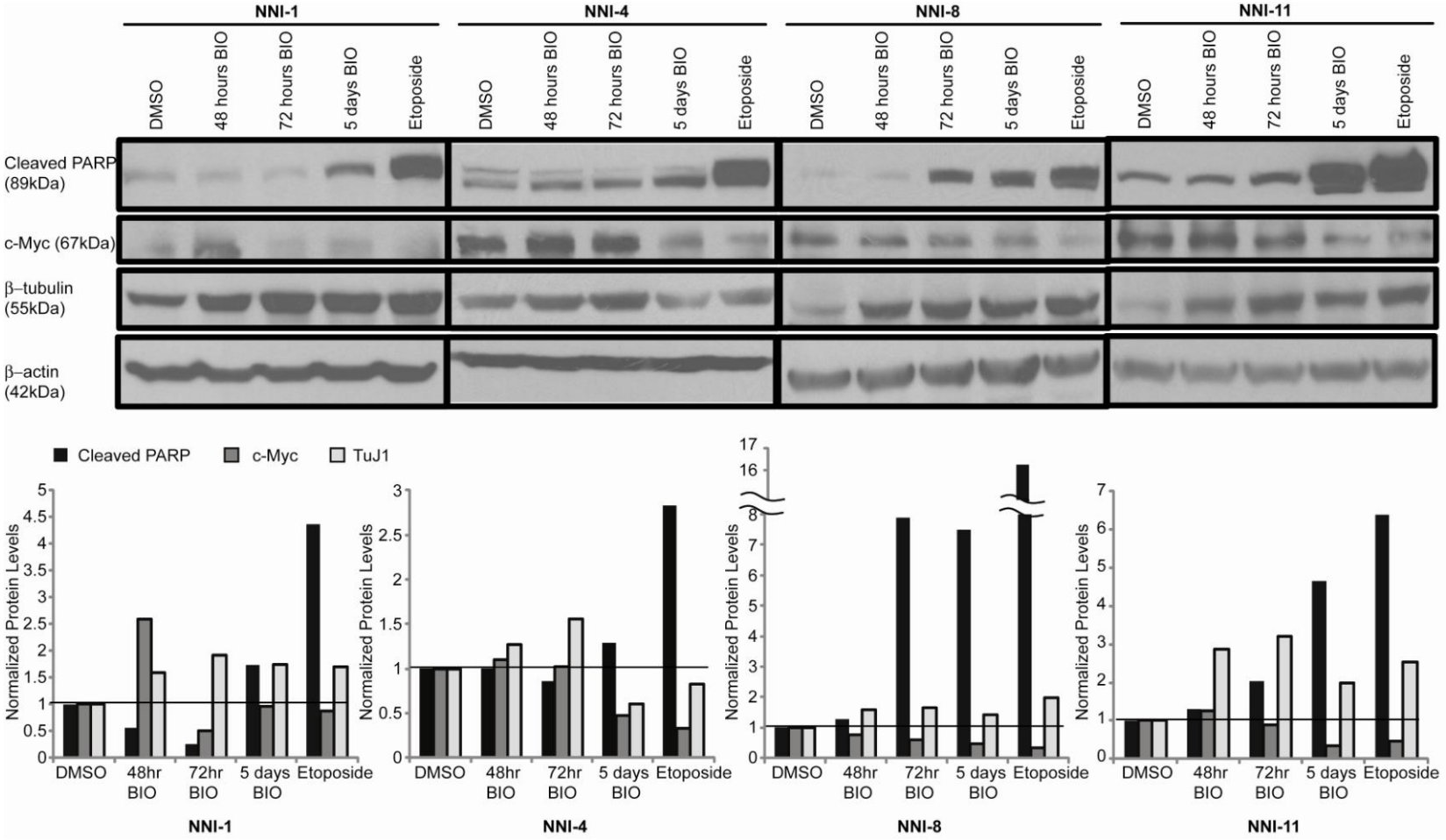

Figure-26. GSK3 inhibition leads to a pro-apoptotic and pro-differentiation response. Treatment of GPCs with BIO showed a time-dependent increase in levels of cleaved PARP and a decrease in c-Myc (except for NNI-1) protein levels. Protein levels of β-tubulin increased for NNI-1, NNI-8 and NNI-11 but this was not evident in NNI-4. **(Bottom panel)** Quantitation by Quantity One of Western blots **(Top panel)**

5.3.2 GSK3 inhibition induces a pro-differentiation response

Recent findings implicate the role of cell fate in the tumorigenicity of GPCs[100]. Accordingly, relatively undifferentiated, *bona fide* tumor stem cells retain tumor-initiating and propagating activity; in contrast, the more differentiated progenitors exit mitosis and eventually cease cell division, resulting in tumor involution. Enforced differentiation of GPCs has thus been proposed as a viable therapeutic strategy. As GSK3 inhibition has been associated with changes in cell fate[72], we explored this possible mode of regulation in our GPCs.

We first assessed the protein levels of β-tubulin III (TuJ1) which marks neuronal cells, and then scored for the differentiated phenotypes by immunofluorescent analyses. We observed in all GPC lines a general trend of time-dependent, elevated TuJ1 expression upon BIO treatment for up to 72 hours, except for NNI-4 at day 5 (explained below; Fig. 26). Etoposide which acted as a positive control for apoptosis similarly induced TuJ1 expression, consistent with its role at inducing differentiation[139]. This protein blot analysis allowed us to correlate the time of appearance of TuJ1 increase with the appearance of the apoptotic process, as illustrated by cleaved PARP and c-Myc (Fig. 26). Our data suggests that BIO treatment induces apoptosis, a post-mitotic event that accompanies cellular differentiation[72].

To substantiate our initial findings, we carried out immunofluorescent analyses to document the induction of differentiated phenotypes after BIO treatment. We analyzed changes in the stemness markers, Nestin, Musashi-1 (Msi-1), Oct4 and Ki-67; as well as changes in the differentiation markers, TuJ1, glial fibrillary acidic protein (GFAP) and O4. Nestin is expressed in

neural precursors[94], Msi-1 is a marker for self-renewal[95], Oct4 is a transcription factor involved in maintaining the pluripotency of stem cells[96, 97] and Ki-67 is a marker of dividing cells. TuJ1 marks neurons, GFAP is an astroglial marker, and O4 marks oligodendrocytes. Our data are summarized in Table 7; Fig. 27 (NNI-1); Fig. 28 (NNI-4); Fig. 29 (NNI-8) and Fig. 30 (NNI-11). Briefly, we observed a slight but significant decrease in stemness markers of all GPCs except for NNI-4 (not significant). Nestin expression was decreased in NNI-1, NNI-8 and NNI-11 (Fig. 27, 29, 30); Oct4 expression was decreased in NNI-1 and NNI-11 (Fig. 27, 30); while Msi-1 expression was decreased in NNI-8 (Fig. 29). Ki-67 expression was also decreased in all GPCs except for NNI-4, and correlated with the drop in cell viability upon BIO treatment (Fig. 21). Analysis of differentiation markers revealed that in BIO-treated cells except for NNI-4, TuJ1 and GFAP were increased while O4 was increased in only NNI-8 and 11 cells (Fig. 27-30). The differentiation capacity to various neural lineages can differ for patients' lines[74, 140], consistent with our observations. Taken together, these data provide strong evidence for the pro-differentiation effect of GSK3 inhibition by BIO. Interestingly, NNI-4 did not demonstrate significant differentiation, likely because it already contained the more differentiated cell types of the primary tumor (Fig. 15)[139].

Table-7. Immunofluorscent analysis of percent positive cells for stemness and differentiation markers in GPCs treated with BIO for 5 days. Significant decrease in stemness markers Nestin, Msi-1 Oct4 and Ki-67 percentages and increase in differentiation markers TuJ1, GFAP and O4 was observed upon GSK3 inhibition.

	% positive cells	**Nestin**	**Msi-1**	**Oct4**	**Ki-67**	**TuJ1**	**GFAP**	**O4**
NNI-1	DMSO	97.42±0.20	99.14±0.20	97.83±0.45	37.09±0.43	2.81±0.28	21.54±1.15	6.04±1.34
	BIO	95.52±0.34	96.17±1.37	94.20±0.27	19.67±0.78	31.42±0.10	31.15±0.09	4.57±1.39
	p - value	0.00706	0.0914	0.00320	0.000930	0.00003	0.00608	0.264
NNI-4	DMSO	97.45±0.17	98.72±0.11	96.29±0.32	30.84±1.45	14.52±0.49	41.38±1.40	68.32±0.91
	BIO	96.58±0.23	98.58±0.14	96.40±0.16	30.59±1.35	14.92±0.61	39.69±0.85	68.33±0.84
	p - value	0.0762	0.192	0.419	0.449	0.289	0.252	0.497
NNI-8	DMSO	97.17±0.17	98.96±0.13	94.89±0.33	31.15±0.79	29.21±1.21	91.30±0.49	89.53±1.37
	BIO	94.81±0.63	97.39±0.07	92.73±0.86	18.39±3.62	55.98±3.84	93.98±0.50	94.52±0.14
	p - value	0.0326	0.000642	0.0975	0.0259	0.0167	0.0000430	0.0328
NNI-11	DMSO	56.19±0.42	98.24±0.44	96.87±0.11	65.29±1.23	2.75±0.70	13.12±0.56	86.76±0.26
	BIO	41.16±4.73	98.34±0.16	95.28±0.15	49.63±1.38	25.20±1.60	43.06±3.43	95.16±0.64
	p - value	0.0367	0.400	0.00139	0.0105	0.00190	0.00469	0.00552

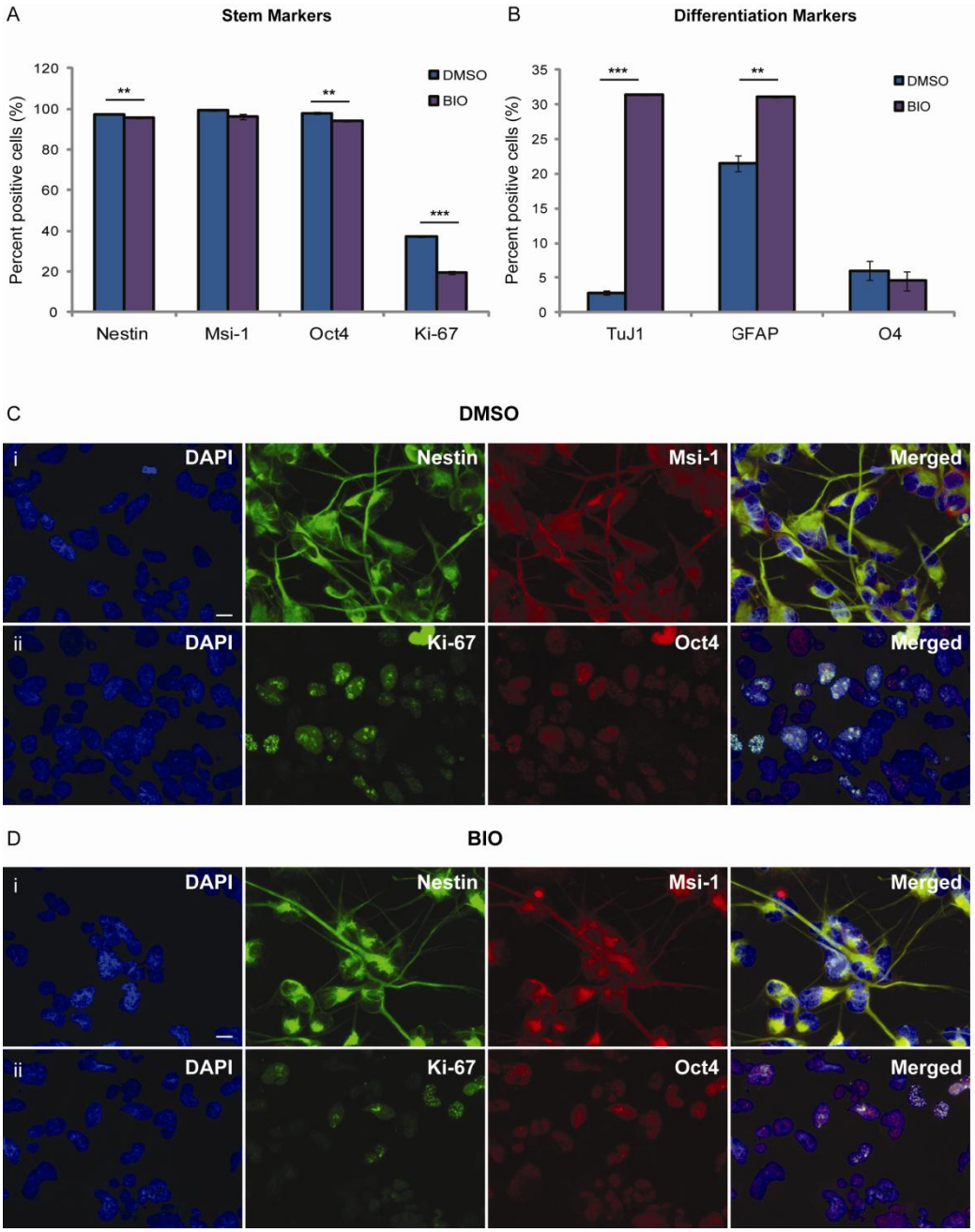

Figure-27. GSK3 inhibition by BIO reduces stemness expression and induces differentiation in NNI-1. (A, B) Graphical representation of NNI-1 GPCs stained for stem and differentiation marker upon BIO treatment as compared to DMSO control. **(C, D)** Representative images of the graph in **(A)**, showing changes in stemness marker expression in DMSO **(C)** and BIO-treated cells **(D).** Scale bar = 10μm; *$p < 0.05$, **$p < 0.01$, ***$p < 0.001$

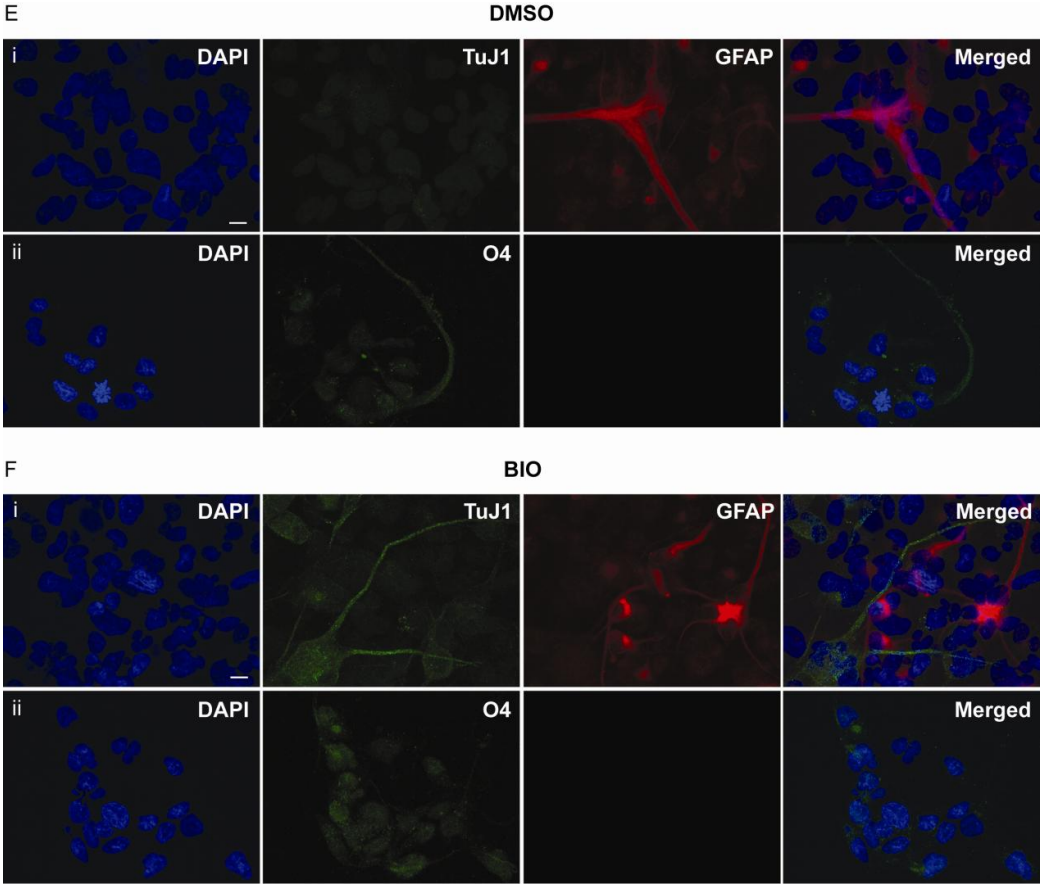

Figure-27. GSK3 inhibition by BIO reduces stemness expression and induces differentiation in NNI-1. (E, F) Representative images of the graph in **(B)**, showing changes in differentiation marker expression in DMSO **(E)** compared to BIO-treated cells **(F)**. Scale bar = 10μm

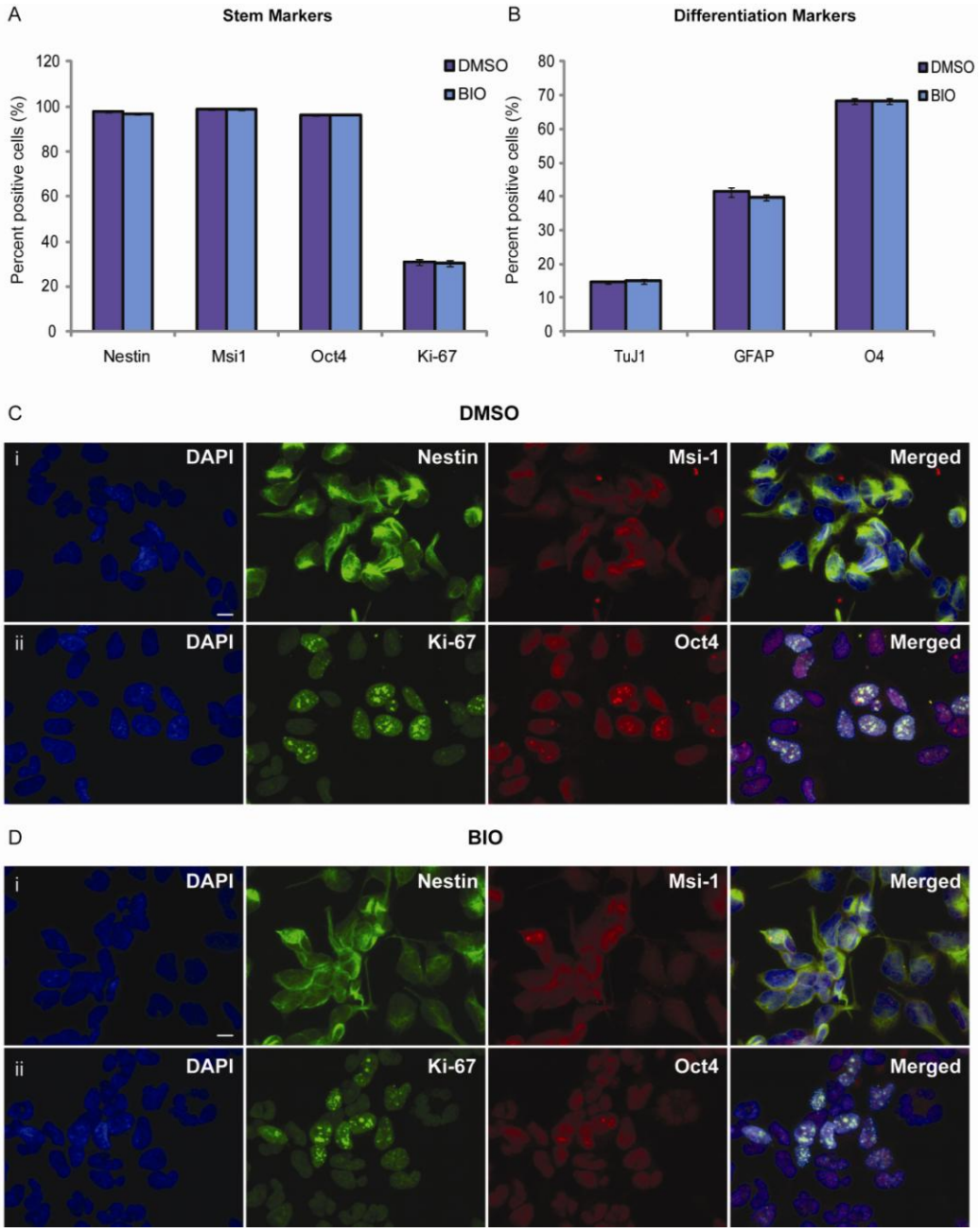

Figure-28. GSK3 inhibition by BIO does not affect stemness and differentiation expression in NNI-4. (A, B) Graphical representation of NNI-4 GPCs stained for stem and differentiation marker upon BIO treatment as compared to DMSO control. **(C, D)** Representative images of the graph in **(A)**, showing changes in stemness marker expression in DMSO **(C)** and BIO-treated cells **(D).** Scale bar = 10µm

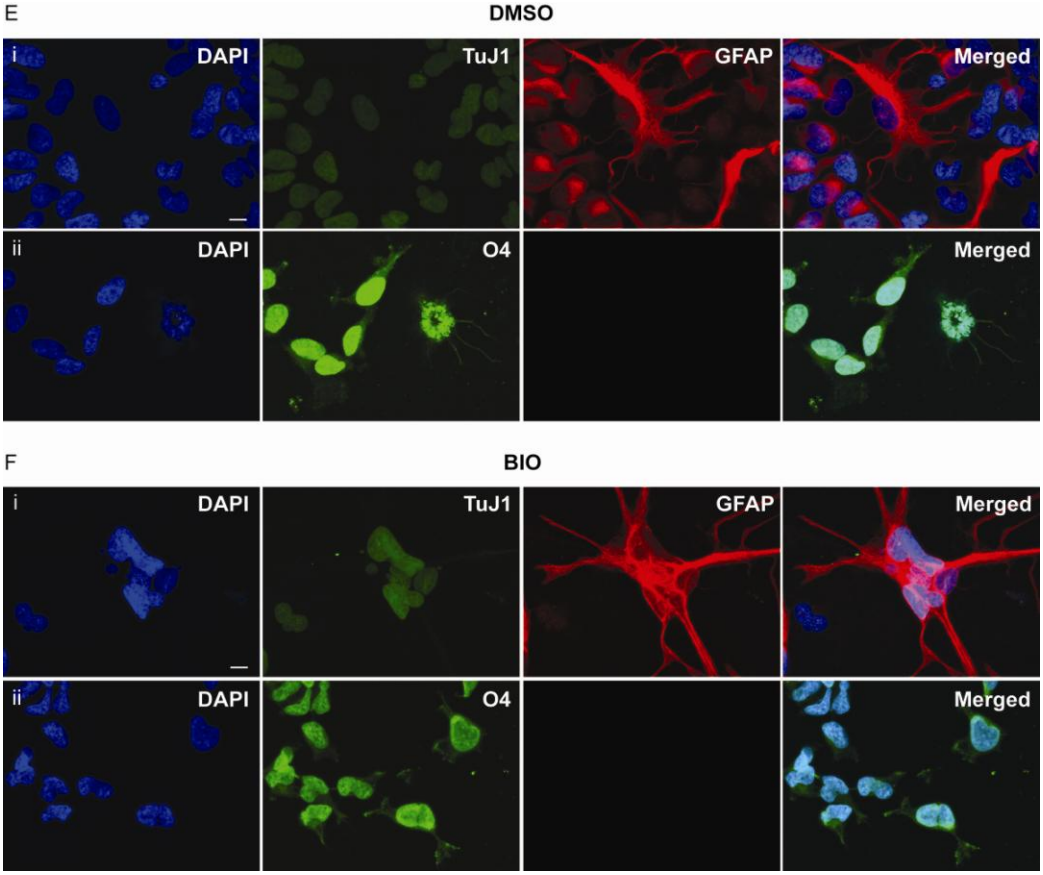

Figure-28. GSK3 inhibition by BIO does not affect stemness and differentiation expression in NNI-4. (E, F) Representative images of the graph in **(B)**, showing changes in differentiation marker expression in DMSO **(E)** compared to BIO-treated cells **(F)**. Scale bar = 10μm

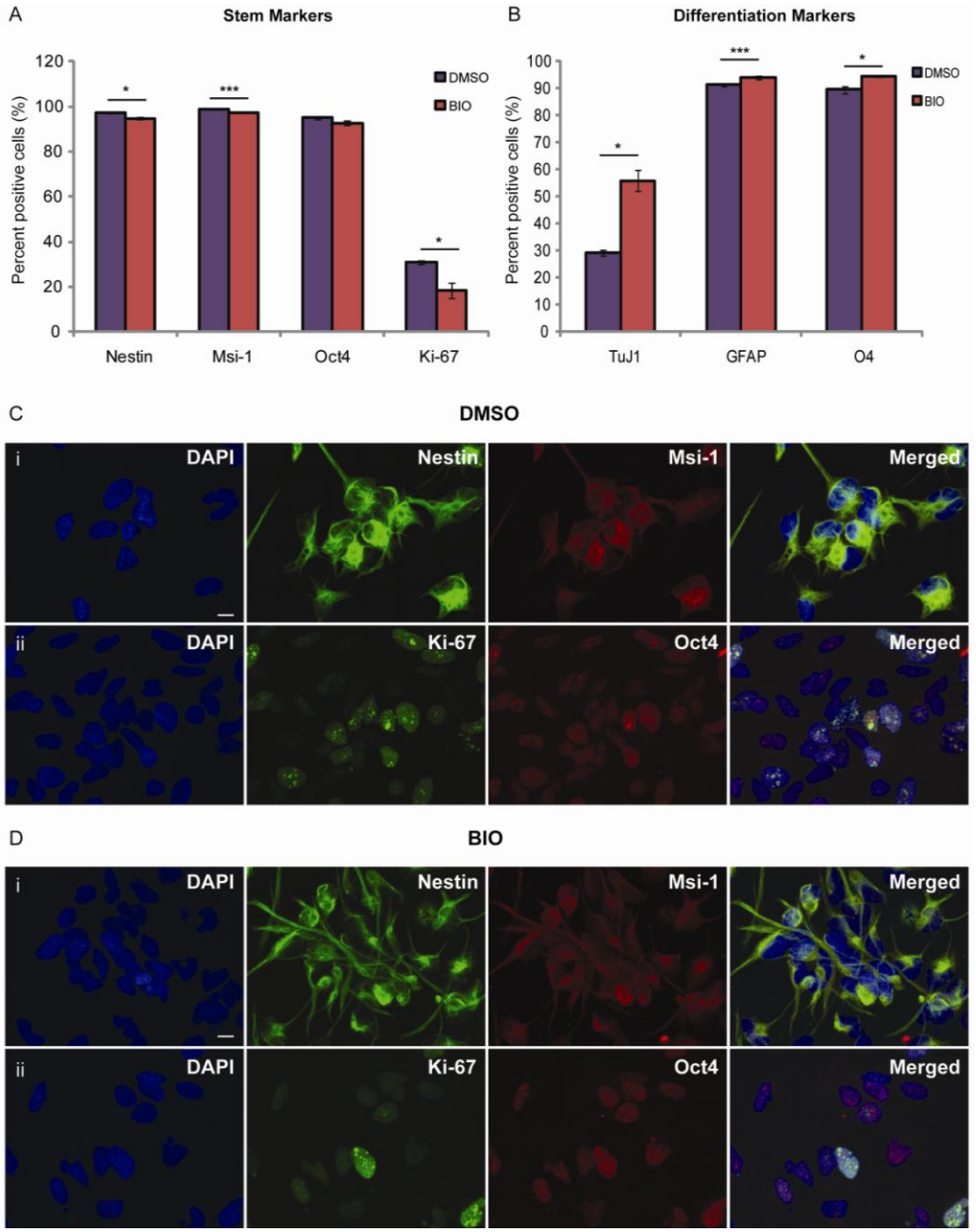

Figure-29. GSK3 inhibition by BIO reduces stemness expression and induces differentiation in NNI-8. (A, B) Graphical representation of NNI-8 GPCs stained for stem and differentiation marker upon BIO treatment as compared to DMSO control. **(C, D)** Representative images of the graph in **(A)**, showing changes in stemness marker expression in DMSO **(C)** and BIO-treated cells **(D).** Scale bar = 10μm; *$p < 0.05$, **$p < 0.01$, ***$p < 0.001$

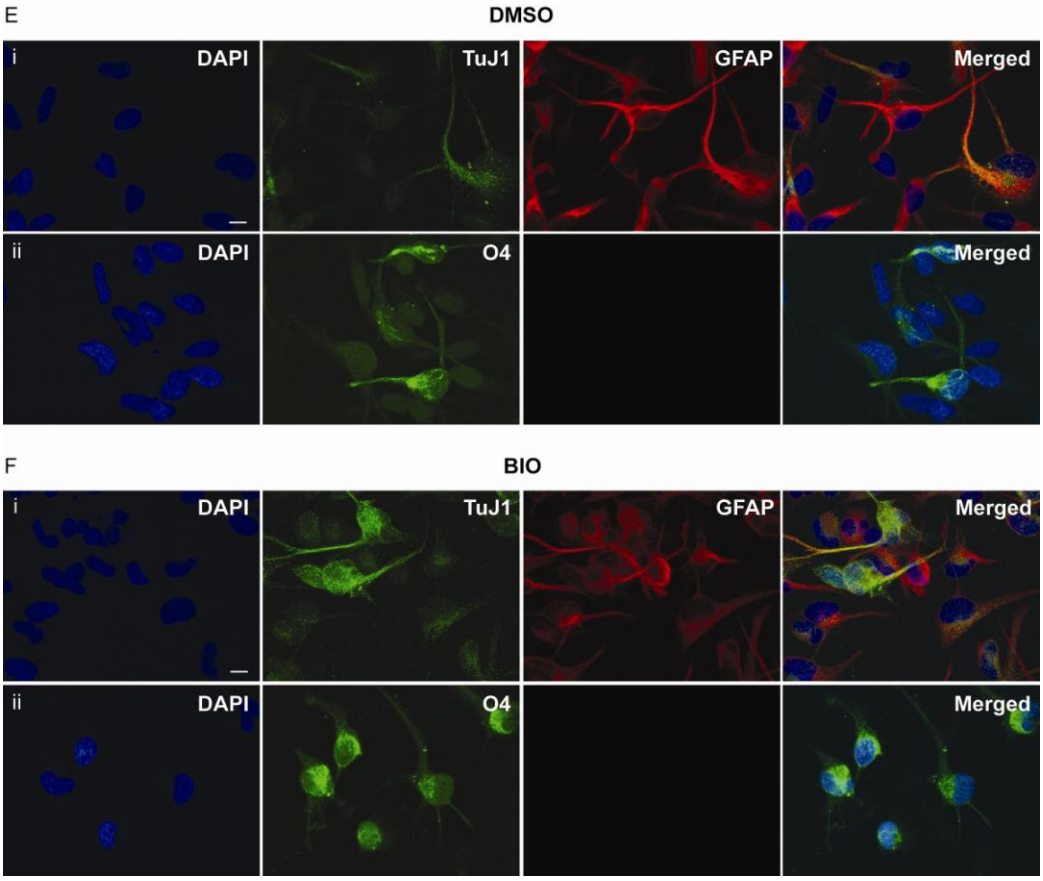

Figure-29. GSK3 inhibition by BIO reduces stemness expression and induces differentiation in NNI-8. (E, F) Representative images of the graph in **(B)**, showing changes in differentiation marker expression in DMSO **(E)** compared to BIO-treated cells **(F)**. Scale bar = 10μm

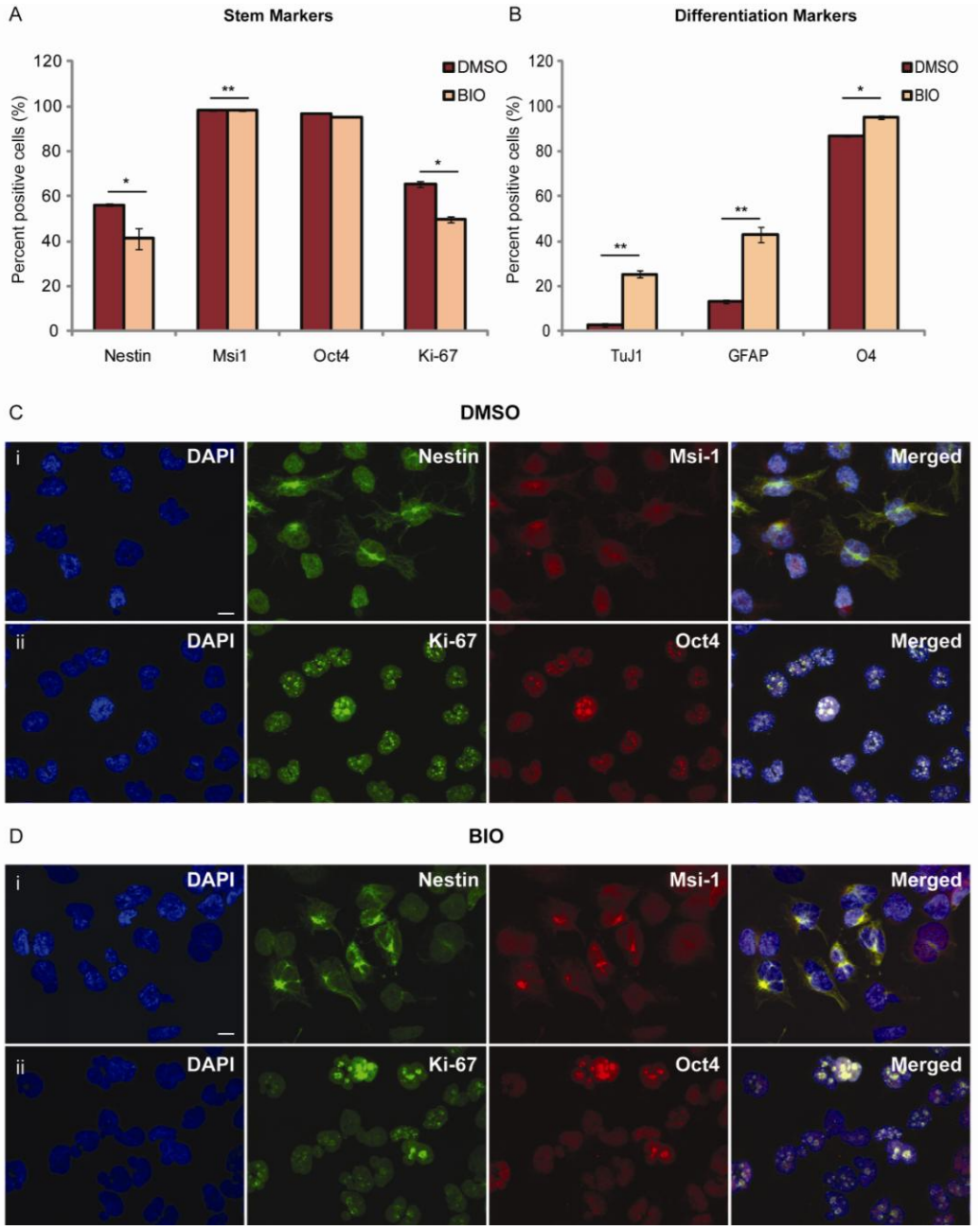

Figure-30. GSK3 inhibition by BIO reduces stemness expression and induces differentiation in NNI-11. (A, B) Graphical representation of NNI-11 GPCs stained for stem and differentiation marker upon BIO treatment as compared to DMSO control. **(C, D)** Representative images of the graph in **(A)**, showing changes in stemness marker expression in DMSO **(C)** and BIO-treated cells **(D).** Scale bar = 10μm; *$p < 0.05$, **$p < 0.01$, ***$p < 0.001$

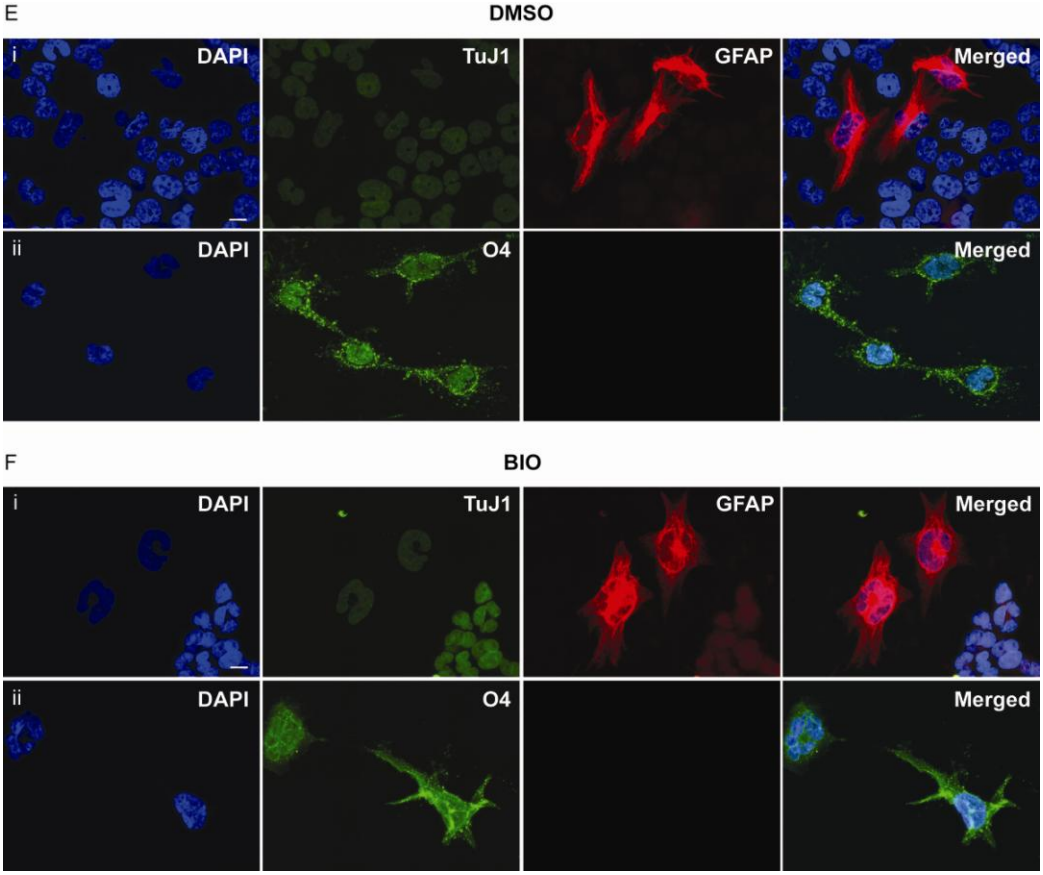

Figure-30. GSK3 inhibition by BIO reduces stemness expression and induces differentiation in NNI-11. (E, F) Representative images of the graph in **(B)**, showing changes in differentiation marker expression in DMSO **(E)** compared to BIO-treated cells **(F)**. Scale bar = 10μm

SUMMARY

We have chosen BIO as the probing tool of choice at elucidating GSK3 regulation in our GPCs. We show that BIO targets preferentially $CD133^{+}$ cells, inducing apoptosis with concomitant reduction in oncoprotein c-Myc and pro-survival protein NFκB. In addition, this apoptotic process follows an induction of differentiation.

CHAPTER 6 – GENETIC MANIPULATION BY GSK3β shRNA ABOLISHES *IN VITRO* TUMORIGENIC POTENTIAL

6.1 GPCs lentivirally transduced with shGSK3β exhibit high transduction efficiencies and diminished GSK3β activity

6.1.1 High transduction efficiency

As GSK3α-null mice are viable and GSK3α cannot rescue the embryonically lethal GSK3β-null mice[115]; along with the evidence that GSK3β maintains the growth of several commercially procured serum-grown glioma cells[71, 72], we explored if GPCs were similarly regulated. Our work is not merely a replication of GSK3β's role in a different cellular context for the following reasons: (1) GPCs represent the tumor-initiating fraction in the heterogeneous tumor mass; consequently, their effective targeting is crucial; (2) Serum-grown glioma cells, in contrast with GPCs, have been shown to contain karyotypic aberrations not found in the primary tumor. Furthermore, they are transcriptomically very distinct from GPCs and the primary tumor[19], suggesting that they may be driven by different signalling pathways. In addition, they form orthotopic xenograft tumors that exhibit well-delineated margins and are non-hemorrhagic[19]. These features are not reflective of the actual patient's tumor morphology. Thus, the validation of GSK3β's role in GPCs would be important to ensure that these signalling mechanisms are indeed present. Importantly, we will specifically implicate GSK3β's role in regulating GPCs by lentiviral knockdown of the gene.

GPCs are slowly-dividing cells and thus amendable to genetic manipulation via lentiviral vectors[141, 142]. This method also yields stably transduced cells, necessary for our long-term *in vitro* assays to detect tumor

stem cell activity. We utilized the human pGIPZ lentiviral shRNAmir target gene set from Open Biosystems (Huntsville, AL) consisting of 3 clones which we termed clone 1 (V2LHS_114290), clone 2 (V2LHS_114293) and clone 3 (V2LHS_114291). The microRNA-adapted shRNAs (shRNAmir) incorporate the gene-specific silencing sequence into a microRNA scaffold, leading to greater specificity due to endogenous processing of the hairpin and also exhibits lower cellular toxicity, hence is advantageous over classic stem-loop designed shRNAs[143, 144]. In addition, the pGIPZ vector contains turbo-GFP (tGFP), enabling visualization and quantification (Fig. 31).

We carried out lentiviral transductions in NNI-4 and 8 because these GPC lines form tumor xenografts reproducibly[28, 84] (NNI-8, this study), and therefore, would be crucial for future *in vivo* experimentation. GPCs were transduced for 4 days at a multiplicity of infection (MOI) of 50[2], and then clonally selected at 5µg/ml puromycin for at least 2 passages. Stably transduced clones were further maintained in media containing 2µg/ml puromycin. Visual analysis showed green fluorescent cells (data not shown), with high transduction efficiencies confirmed by flow cytometry (Fig. 32). Briefly, in both GPC lines, we observed close to 95% GFP-positive cells, compared to non-transduced and non-silencing controls for all 3 shGSK3β clones 1-3.

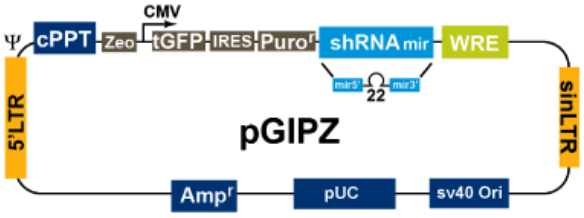

Figure-31. Vector map of pGIPZ lentiviral backbone. The vector is driven by a CMV promoter, a turbo GFP marker to track shRNAmir expression and a puromycin mammalian selectable marker.

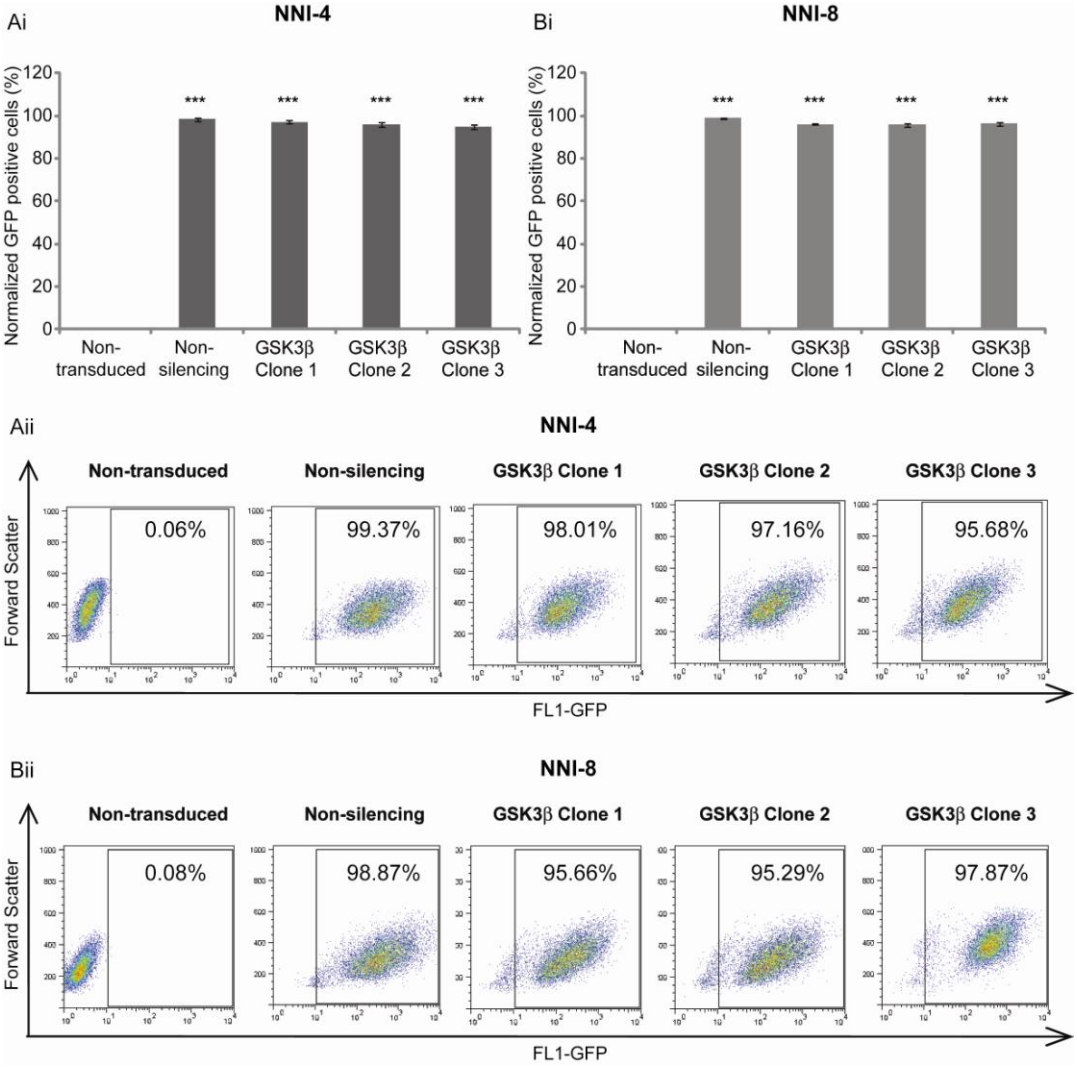

Figure-32. NNI-4 and NNI-8 GPCs transduced with GSK3β shRNA Clones 1 to 3 and non-silencing control displays high transduction efficiencies. (Ai) NNI-4 GPCs transduced with GSK3β shRNA and non-silencing construct exhibits transduction efficiencies greater than 95%. Non-transduced GPCs was used as a negative control. **(Aii)** Representative FACS plots of the data in (Ai). **(Bi)** NNI-8 GPCs transduced with GSK3β shRNA and non-silencing construct displays transduction efficiencies greater than 95%. Non-transduced GPCs was used as a negative control. **(Bii)** Representative FACS plots of the data in (Bi). ***$p < 0.001$

6.1.2 GSK3β activity is diminished in shGSK3β cells

Following lentiviral transductions, we observed that effective knockdown of GSK3β was confirmed in all GPC lines (Fig. 33). Next, we assessed GSK3 activity by probing for the activating Tyr279(α)/Tyr216(β) and inhibitory Ser21(α)/Ser9(β) phosphorylation status. In both NNI-4 and 8 GPC lines, we observed the following trends: (1) Phosphorylation at Tyr216 (β) was significantly reduced while negligible change was seen with Tyr279 (α); and (2) Negligible change was observed at inhibitory Ser21(α)/9(β) phosphorylation sites (Fig. 33). BIO-treated cells were used as the positive control and displayed diminished GSK3 activity at both α and β phosphorylation sites, consistent with its kinase selectivity profile of being non-selective over the α and β forms (Table 5). These data suggest that specific knockdown of GSK3β could be achieved. This is important as it would allow us to distinguish the effects of the β-form from the α-form.

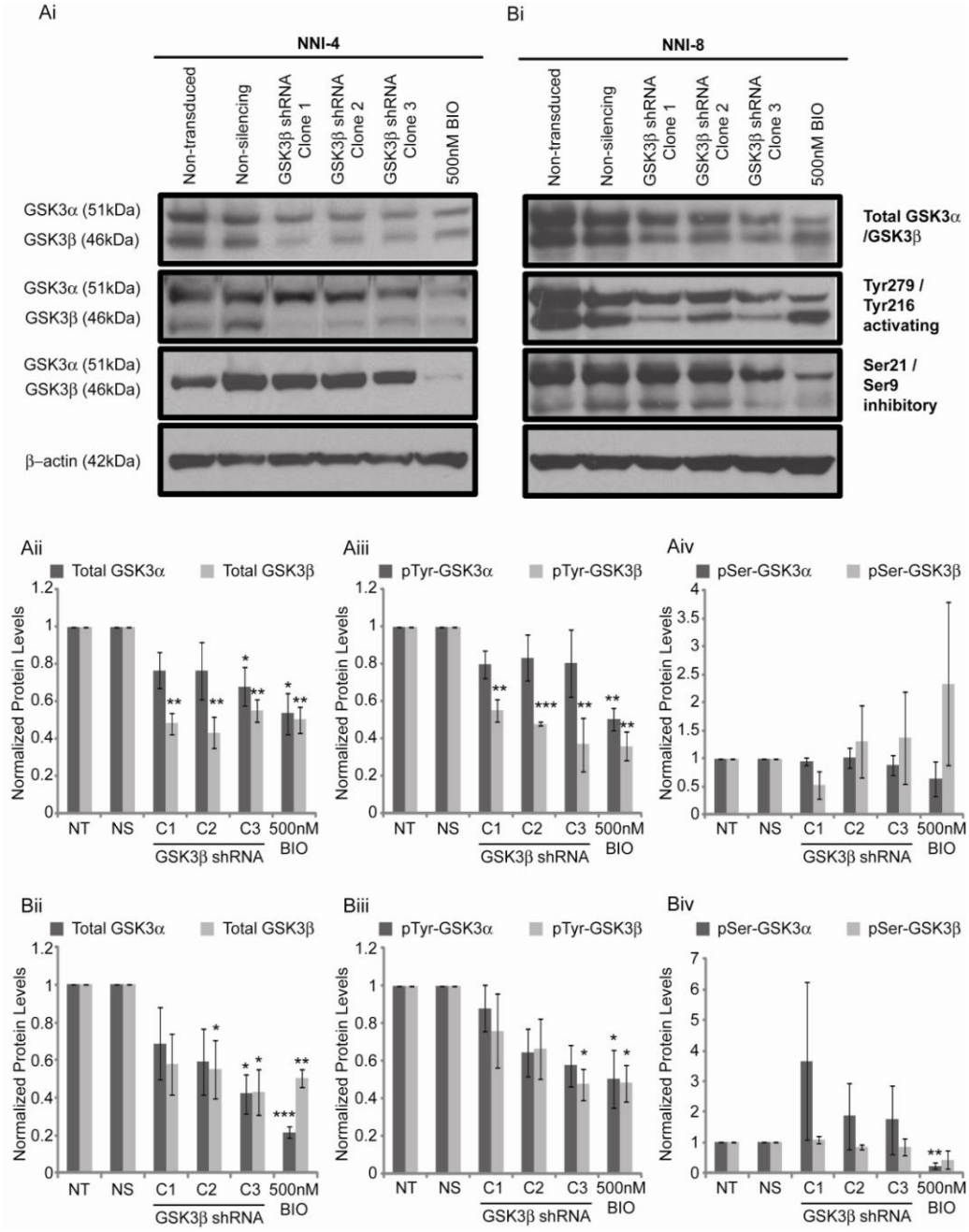

Figure-33. Transduction of NNI-4 and NNI-8 GPCs with GSK3β shRNA results in an ablation of total GSK3β and activating phosphorylated Tyr216 (GSK3β) **(Ai)** Representative western blot showing reduction of total GSK3β and activating pTyr216 levels in NNI-4. **(Aii-iv)** Quantitation of total GSK3α/β, activating tyrosine 279/216 phosphorylation and inhibitory serine 21/9 phosphorylation levels respectively for the data in **(Ai)**. **(Bi)** Representative western blot showing reduction of total GSK3β and activating pTyr216 levels in NNI-8. **(Bii-iv)** Quantitation of total GSK3α/β, tyrosine 279/216 and serine 21/9 phosphorylation levels respectively for the data in **(Bi)**. All values are normalized to the non-silencing control and non-transduced cells for cells transduced with shGSK3β clones and cells treated with BIO respectively, and are performed in triplicates. *$p < 0.05$, **$p < 0.01$, ***$p < 0.001$ Abbreviations: Non-transduced (NT), Non-silencing (NS), Clones 1-3 (C1-C3)

6.2 GSK3β inhibition reduces cell viability and CD133 expression, mediated by PARP, c-Myc and a pro-differentiation response, leading to diminished soft agar colony formation

6.2.1 shGSK3β knockdown reduces cell viability

We assessed cell viability after lentiviral transduction of shGSK3β clones 1-3. Generally, we observed reduced cell viability by 1.8-fold for up to 10 days (NNI-4) and 1.4-fold for up to 15 days (NNI-8) (Fig. 34). The data suggest that GSK3β maintains GPC proliferation.

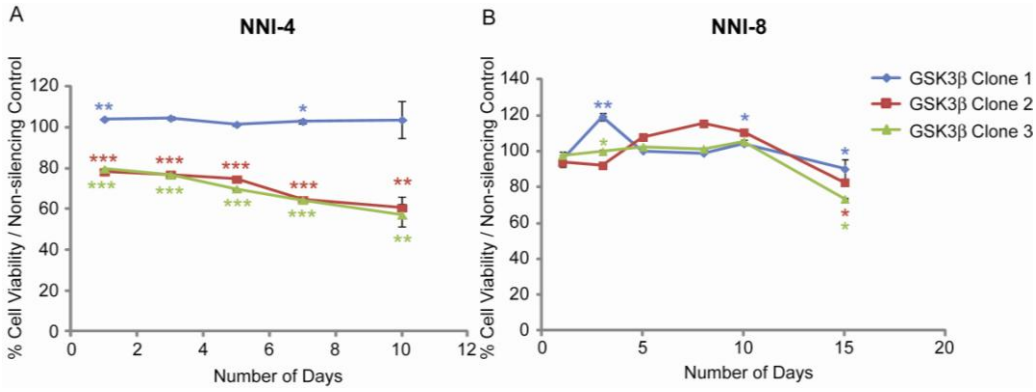

Figure-34. Ablation of GSK3β reduces cell viability in NNI-4 and NNI-8. (A) Cell viability curve of NNI-4 showing reduced cell viability in cells transduced with shGSK3β clones 2 and 3 as compared to the non-silencing control. **(B)** Cell viability curve of NNI-8 demonstrating reduced cell viability for cells transduced with shGSK3β clone 3. *$p < 0.05$, **$p < 0.01$, ***$p < 0.001$

6.2.2 shGSK3β knockdown reduces CD133-expressing cells

Next, we assessed the effects of shGSK3β knockdown on the frequency of CD133-expressing cells, bearing in mind that our previous experiments suggested that BIO preferentially targeted $CD133^+$ tumor-initiating cells. Accordingly, we observed up to 2-fold reduction in CD133 in NNI-4 for clones 2 and 3; while NNI-8 demonstrated ~ 2-3-fold CD133 reduction for clones 1-3 (Fig. 35). It should be noted that the CD133% in NNI-4 was already low (~3%) in initial cultures hence a clear reduction is less obvious. Nevertheless, other works have indicated that mere 2-fold changes in CD133% can result in significant differences in tumor latency[145] due to enrichment of the relevant tumor-initiating cell fraction.

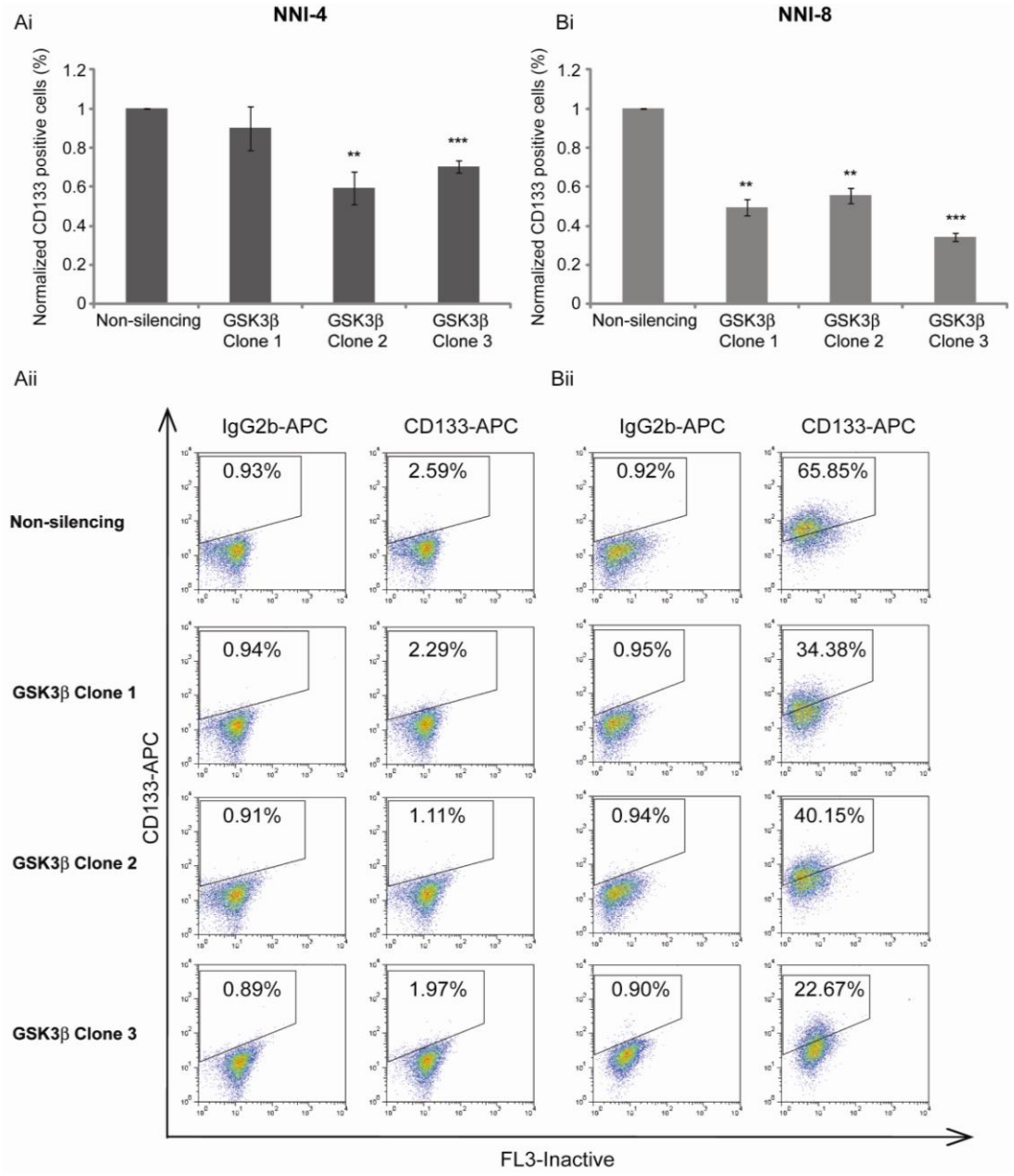

Figure-35. GSK3β ablation depletes the CD133-expressing GPCs. (Ai) NNI-4 transduced with GSK3βshRNA clones 2 and 3 showed a significant reduction in CD133-percentage when normalized to the non-silencing control. **(Aii)** Representative FACS plots of the data in **(Ai). (Bi)** NNI-8 transduced with GSK3βshRNA clones 1-3 displayed a significant decrease in CD133-percentage when normalized to the non-silencing control. **(Bii)**Representative FACS plots of the data in **(Bi).** $^{**}p < 0.01$, $^{***}p < 0.001$

6.2.3 shGSK3β knockdown leads to increased cleaved PARP and correlates with decreased c-Myc, and the induction of differentiation

Next, we evaluated the levels of cleaved PARP, c-Myc and TuJ1 in shGSK3β knocked down GPCs. Although the result was less clear in NNI-4 (Fig. 36A), we generally noted with shGSK3β clone 3 that cleaved PARP was increased, with concomitant decrease in oncoprotein c-Myc. In addition, TuJ1 was induced. We noted that this clone also generated the most obvious phenotypic change in the soft agar colony assay described in a later section (Section 6.2.5). This would be accounted for by the extent of efficient GSK3β knockdown. BIO- and etoposide-treated GPCs were included as positive controls of apoptosis. Our data further strengthens previous findings with BIO that GSK3 inhibition, specifically the β form, results in apoptosis with concomitant induction of differentiation.

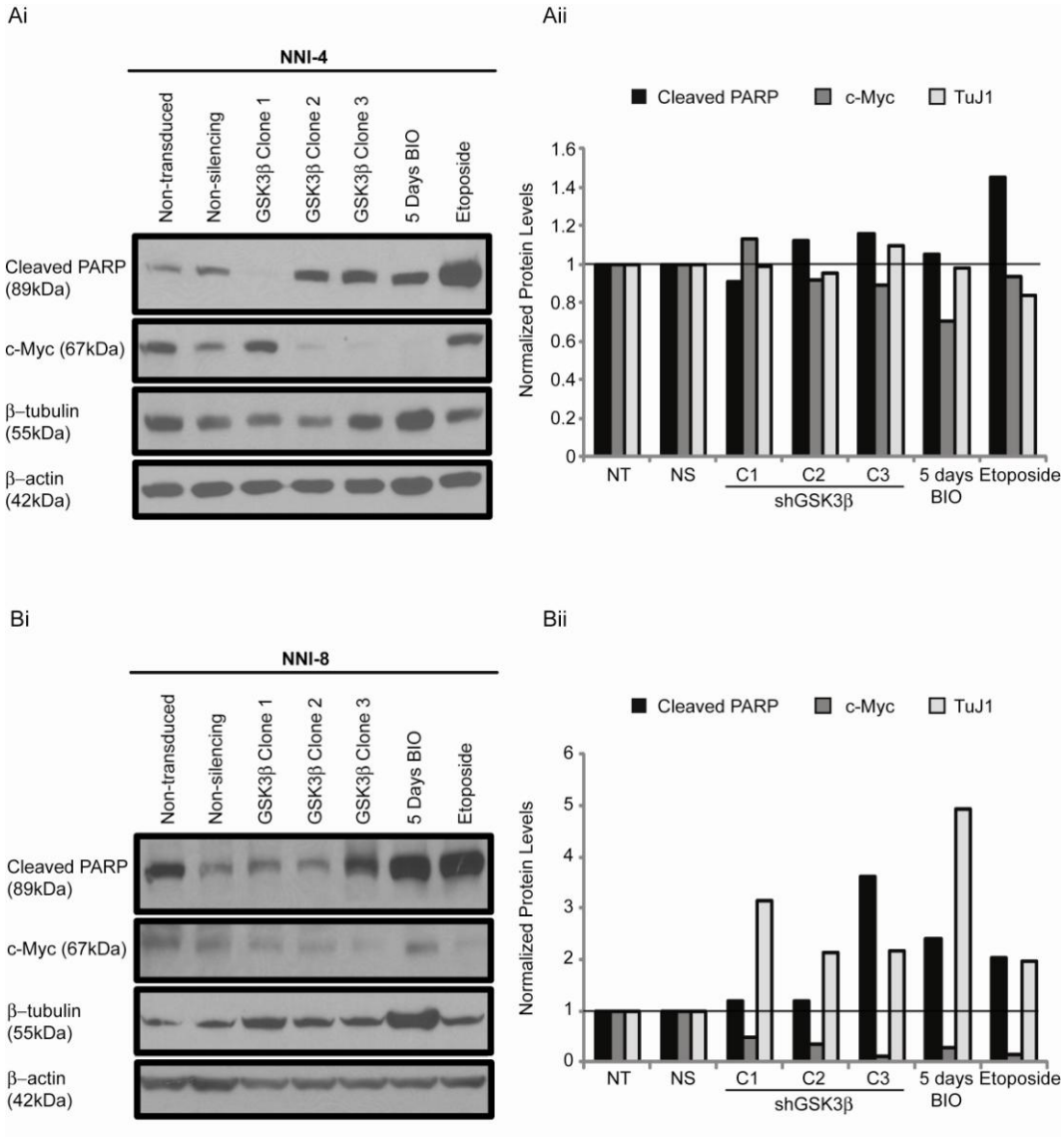

Figure-36. NNI-4 and NNI-8 GPCs transduced with GSK3β shRNA exhibitied an increase in cleaved PARP, correlated with a decrease in c-Myc and also leads to elevated TuJ1 expression levels. (A) NNI-4 GPCs transduced with GSK3β shRNA Clones 2 and 3 exhibitied an increase in cleaved PARP, correlated with a decrease in c-Myc and an increase in TuJ1 expression for clone 3. **(Ai)** Western blot analysis of NNI-4 transduced with GSK3β shRNA with etoposide as a positive control. **(Aii)** Quantitation of Western blot results by Quantity One. **(B)** NNI-8 GPCs transduced with GSK3β shRNA exhibitied an increase in cleaved PARP, correlated with a decrease in c-Myc and also leads to elevated TuJ1 expression levels. **(Bi)** Western blot analysis of NNI-8 transduced with GSK3β shRNA with etoposide as a positive control. **(Bii)** Quantitation of Western blot results by Quantity One. Abbreviations: Non-transduced (NT), Non-silencing (NS), Clones 1-3 (C1-C3)

6.2.4 GSK3β inhibition leads to induction of differentiation

To substantiate our observation that shGSK3β (clone 3 in particular) knockdown leads to the induction of differentiation, we scored for differentiated cell types: Neurons (TuJ1), astrocytes (GFAP) and oligodendrocytes (O4). In addition, we examined the retention of stemness markers such as Nestin, Msi-1 and Oct4. Ki67 indicates dividing cells. In both GPC lines, we observed negligible changes in the levels of stemness markers (Figs. 37, 38), consistent with the notion that GPCs maintain self-renewal properties typical of *bona fide* stem cells, and may represent a state of de-differentiation[146]. However, our studies with cells of human origin preclude that analysis. In NNI-4, significant increases were observed in O4 cells, while proliferation was diminished (Fig. 37A). On the other hand, NNI-8 displayed an increase in mainly TuJ1 cells, similarly with diminished proliferation (Fig. 38A). The ability of patients' GPCs to give rise to varied lineages has been previously documented[28, 74]. Collectively, our data provides strong support that GSK3β inhibition leads to the induction of differentiation, with concomitant reduction in proliferation. This finding would be consistent with the notion that enforced differentiation of GPCs may be a way to blunt the tumorigenic potential of these cells[100]. By targeting GSK3β critically required for GPC maintenance, we could potentially control tumor growth at its "root".

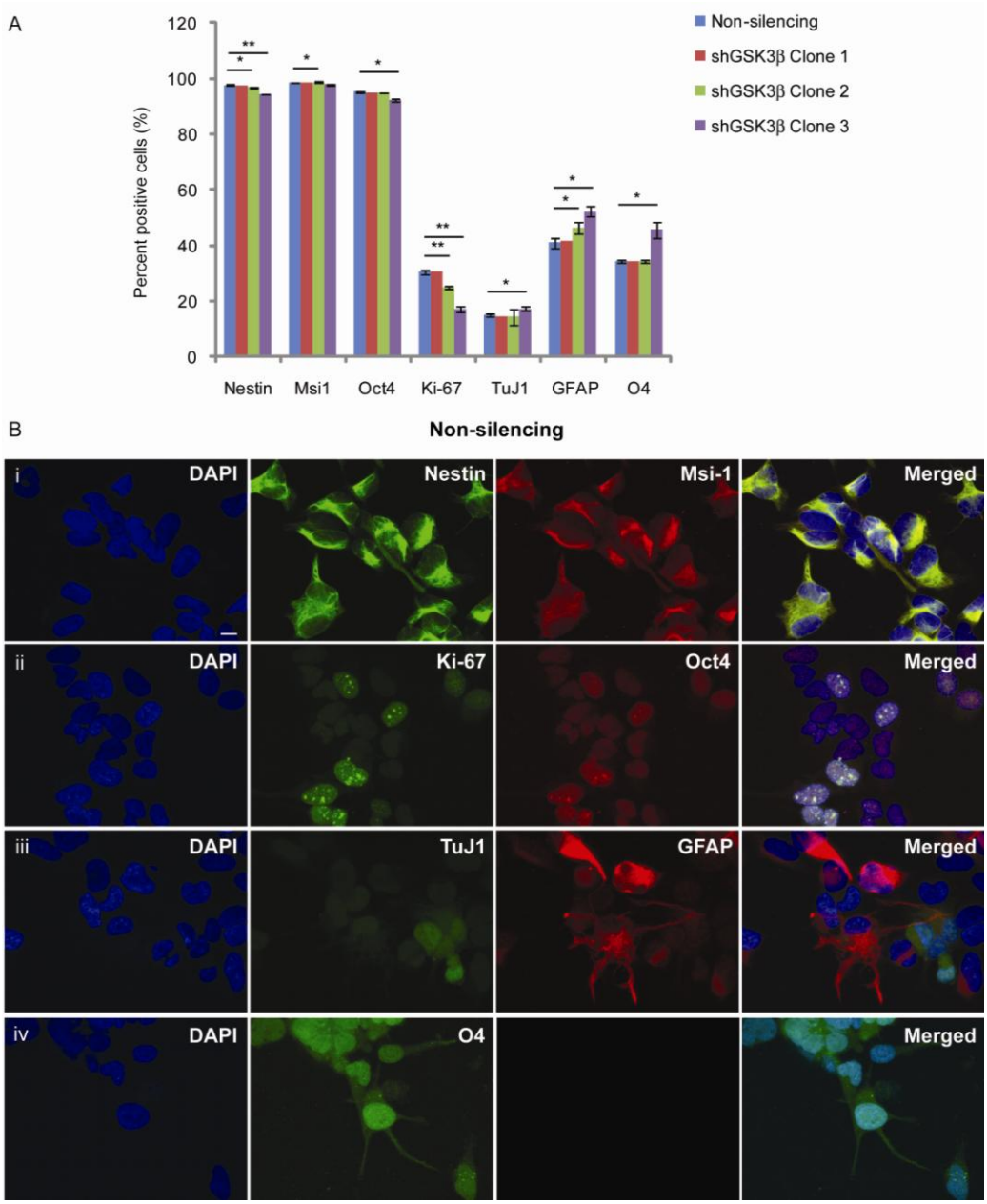

Figure-37. GSK3β downregulation by shGSK3β reduces stemness expression and induces differentiation in NNI-4. (A) Graphical representation of NNI-4 GPCs stained for stem and differentiation markers upon shGSK3β transduction as compared to GPCs transduced with the non-silencing control construct. **(B)** Representative images of the graph in **(A)**, showing changes in stemness and differentiation marker expression in non-silencing construct -transduced cells**.** Scale bar = 10μm; *$p < 0.05$, **$p < 0.01$, ***$p < 0.001$

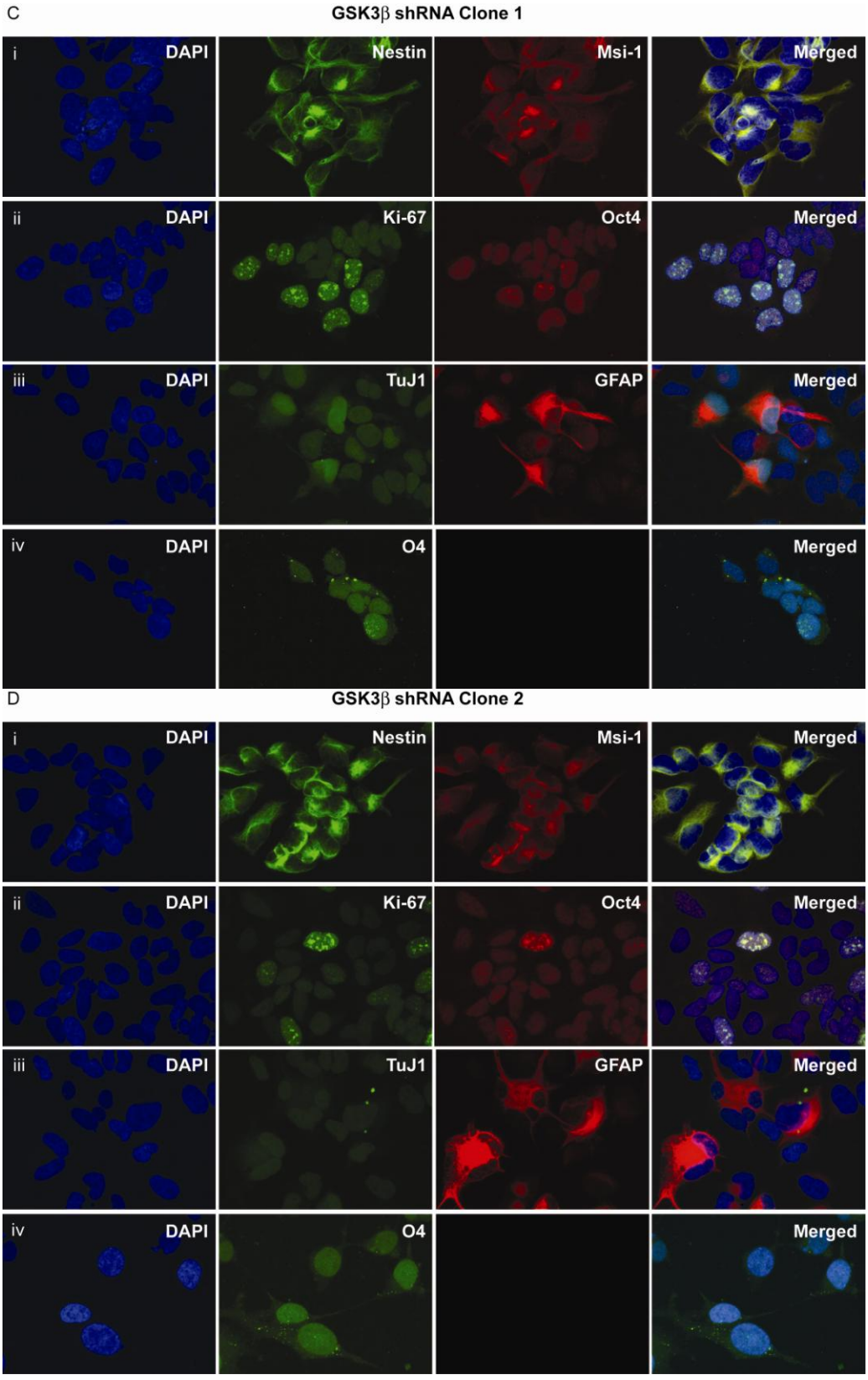

Figure-37. GSK3β downregulation by shGSK3β reduces stemness expression and induces differentiation in NNI-4. Representative images of the graph in **(A)**, showing changes in stemness and differentiation marker expression in shGSK3β Clone 1 **(C)**, shGSK3β Clone 2 **(D)** -transduced cells**.**

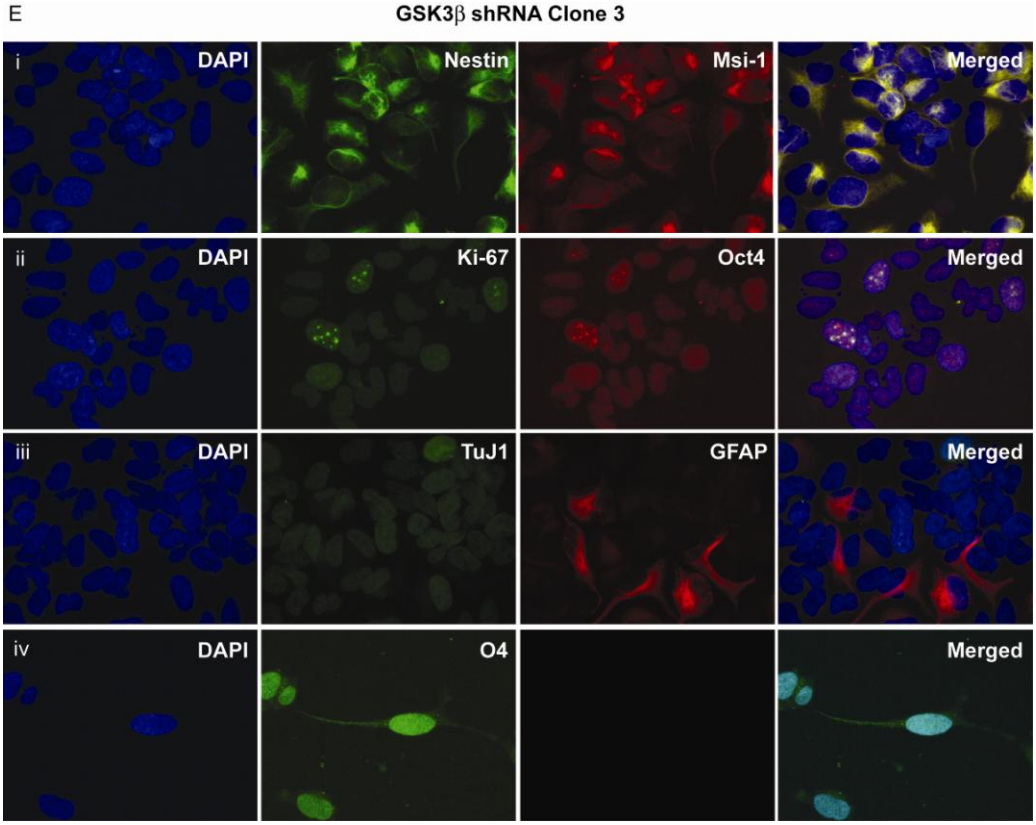

Figure-37. GSK3β downregulation by shGSK3β reduces stemness expression and induces differentiation in NNI-4. Representative images of the graph in **(A)**, showing changes in stemness and differentiation marker expression in shGSK3β Clone 3 **(E)** -transduced cells**.**

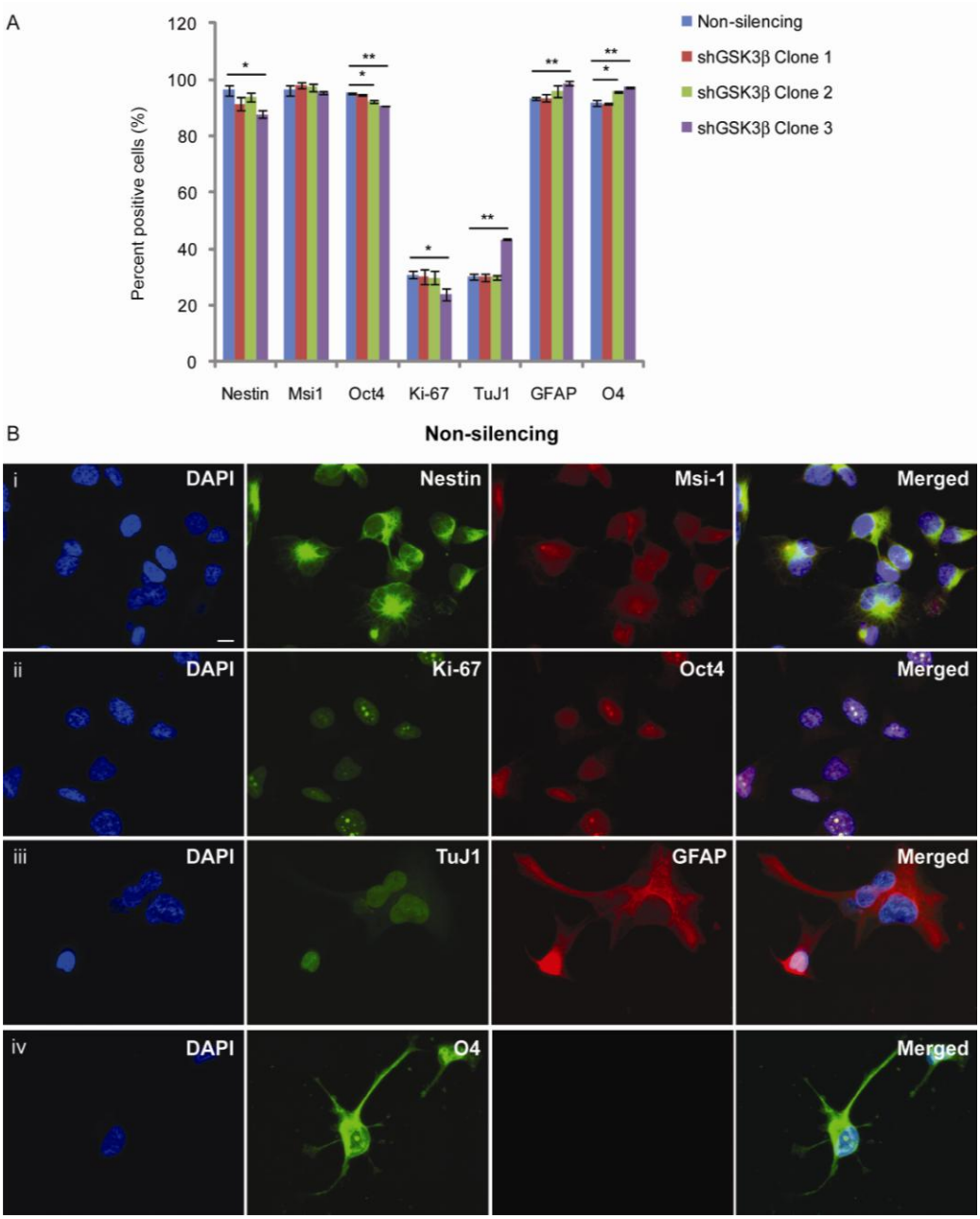

Figure-38. GSK3β downregulation by shGSK3β reduces stemness expression and induces differentiation in NNI-8. (A) Graphical representation of NNI-8 GPCs stained for stem and differentiation markers upon shGSK3β transduction as compared to GPCs transduced with the non-silencing control construct. **(B)** Representative images of the graph in **(A)**, showing changes in stemness and differentiation marker expression in non-silencing construct -transduced cells**.** Scale bar = 10µm; *$p < 0.05$, **$p < 0.01$, ***$p < 0.001$

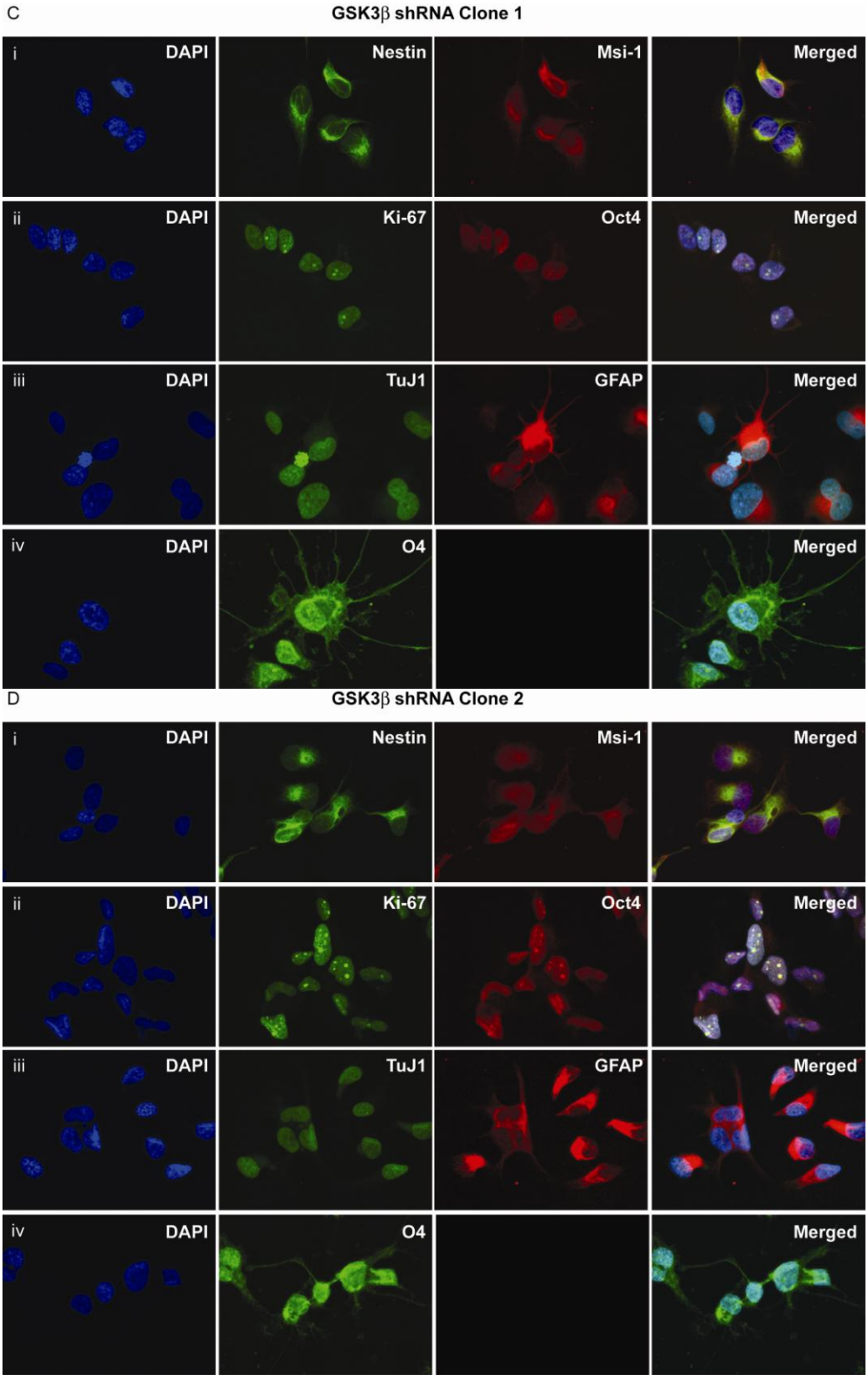

Figure-38. GSK3β downregulation by shGSK3β reduces stemness expression and induces differentiation in NNI-8. Representative images of the graph in **(A)**, showing changes in stemness and differentiation marker expression in shGSK3β Clone 1 **(C)**, shGSK3β Clone 2 **(D)** -transduced cells**.**

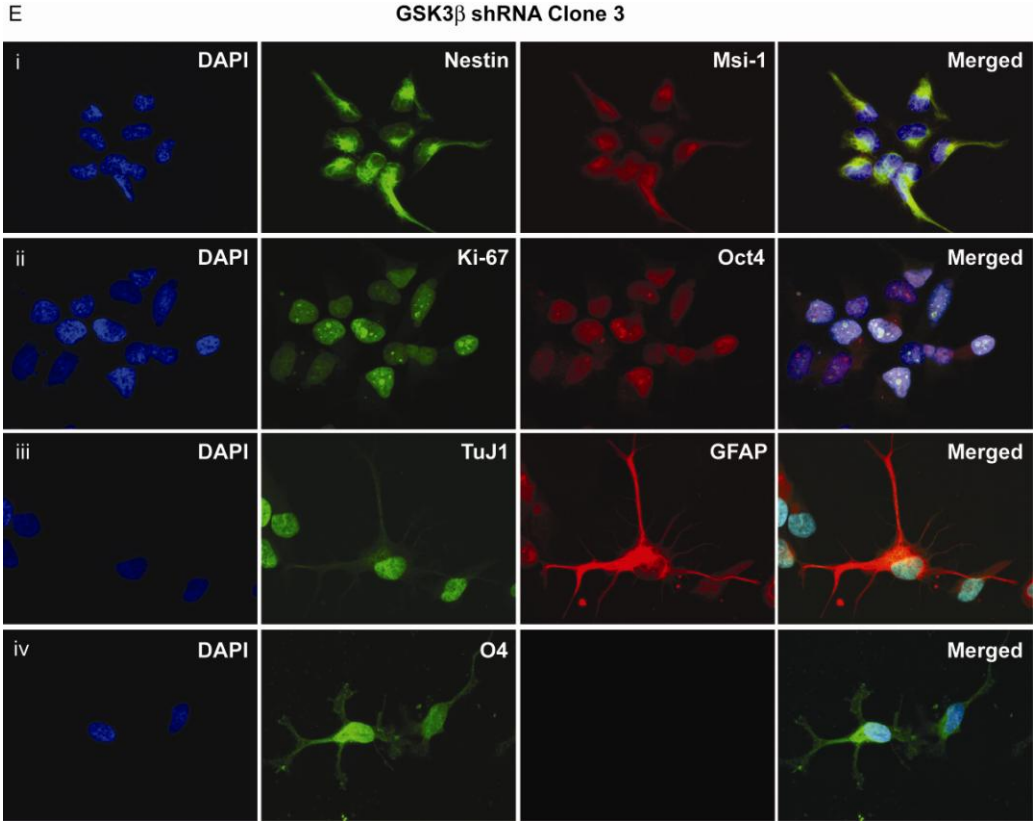

Figure-38. GSK3β downregulation by shGSK3β reduces stemness expression and induces differentiation in NNI-8. Representative images of the graph in **(A)**, showing changes in stemness and differentiation marker expression in shGSK3β Clone 3 **(E)** -transduced cells**.**

6.2.5 shGSK3β knockdown diminishes colony formation in soft agar

The soft agar assay is an *in vitro* correlate of transformation and detects malignant cell transformation[147, 148]. It is often an accurate prediction of *in vivo* tumorigenesis[147, 148]. Colony formation was measured to determine the anchorage-independent growth potential of GPCs following transduction with shGSK3β.

We observed, except with clone 1 in NNI-4, that GSK3β knockdown in general led to reduced colony numbers and sizes (Fig. 39). Notably, clone 3 which we earlier documented to show the greatest changes in PARP, c-Myc and TuJ1 proteins, significantly abrogated colony growth. Our data provides

strong evidence that GSK3β maintains GPC survival, and its ablation leads to diminished tumorigenic potential.

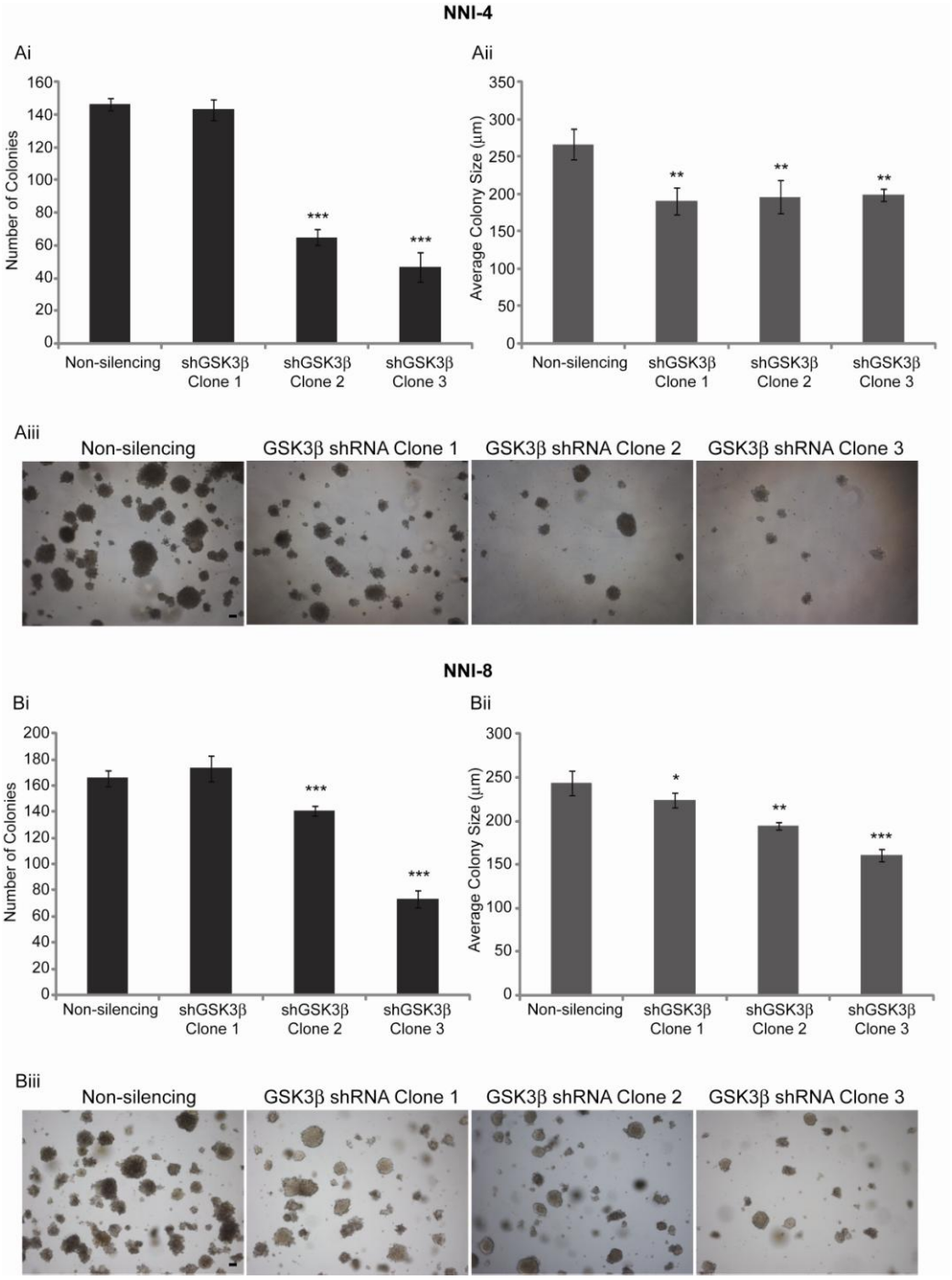

Figure-39. GSK3β inhibition depletes *in vitro* tumorigenic potential in GPCs. (A) NNI-4 GPCs showed a **(i)** decrease in number of colonies and **(ii)** reduction in colony size when transduced with GSK3β shRNA clones 2 and 3 **(iii)** Representative soft agar images (4× magnification) illustrating the data in **(Ai,ii)**. **(B)** NNI-8 GPCs also showed an inhibition in soft agar colonization with a **(i)** decrease in number of colonies as well as **(ii)** reduction in colony size when transduced with GSK3β shRNA clones 2 and 3 **(iii)** Representative soft agar images (4× magnification) illustrating the data in **(Bi,ii)**. Scale bar = 100μm; *$p < 0.05$, **$p < 0.01$, ***$p < 0.001$

SUMMARY

To definitively prove the role of GSK3β in GPC regulation, we employed lentiviral-mediated transduction of shGSK3β in our GPCs. We show that ablation of GSK3β activity depletes CD133 expression, leading to apoptosis with concomitant increase in PARP and reduction in c-Myc, further resulting in induction of differentiation, cumulating in diminished soft agar colonization.

CHAPTER 7 – DISCUSSION

Cancer stem cells are controversial because their definition as the cells-of-origin of the tumor can be interpreted as an artifactual consequence of the animal model when prospectively isolated[25]. Thus, GPCs isolated from clinical specimens cannot reflect the etiology of the disease although they may contain characteristics that perpetuate the tumor. It is critical to realize that the molecular characteristics supporting the malignant traits of GPCs are not necessarily the same molecular alterations that permit transformation and thus generation of tumors *de novo*[149]. To reveal cellular compartments necessary for transformation, lineage-tracing models with suitable cell type-specific promoters would have to be utilized to identify the tumor-initiating cell, and its subsequent progeny which reconstitutes the tumor mass[14, 16]. This poses a question as to how reliable GPCs are as cellular models for investigations. Previous works have highlighted that GPCs grown in serum-free media supplemented with growth factors retain transcriptomic and karyotypic hallmarks typically found in the primary tumor[19], whereas commercially procured serum-grown glioma cells contain many additional aberrations[19, 150]. In addition, their respective xenograft tumors differ with only GPCs capable of recapitulating the patient's original histopathology[19]. Such findings underscore the relevance of GPCs, but do not shed light on how these cells might contribute to disease outcome and patient survival profiles. The link between GPCs and the primary tumor thus remains unresolved.

Our work initially described the isolation and characterization of GPCs from GBM and oligodendroglial tumors. These tumors are molecularly distinct; furthermore, have very different clinical profiles where patients with

oligodendrogliomas typically respond better to chemotherapy and survive longer[4]. We thus sought to establish if these phenotypic differences were driven at the gene expression level in GPCs. This is an important endeavor as it would suggest that GPCs retain similar properties to the primary tumor, and potentially mirror the primary tumor molecular classification systems established in The Cancer Genome Atlas (TCGA)[6, 7], REMBRANDT[81], Phillips[10] and Gravendeel[9]. It would further suggest that to target a tumor effectively, the selective disruption of key signaling pathways predicted by gene expression would become imperative. Accordingly, we observed an enrichment of the oligodendroglial GPC gene signature in better surviving, lower grades of gliomas including oligodendrogliomas, while the GBM GPC signature predominated the higher grades. These data would strongly imply that neural precursor type differences underlie their survival outcome. In support, Persson *et al*. showed using transgenic mouse models that GPCs derived from oligodendrogliomas were more sensitive to chemotherapeutic agents than GPCs derived from GBM[102]. These oligodendroglioma GPCs exhibited features of oligodendrocyte progenitor cells (OPCs), as opposed to GBM GPCs which displayed neural stem cell features. Thus, our findings validate Persson *et al*.'s conclusions in a clinical setting. Surprisingly when we looked at the performance of the gene signature within oligodendrogliomas, patients who fared better were enriched for this signature, which seemed to contradict the conventional belief that cancer stem cells drive the aggressiveness and grade of tumors as had been shown by a recent work that the abundance of $CD133^{+}$ cells correlates with oligodendroglioma grade[151]. Our findings could be reconciled by recognizing that in our work, we were

observing entire transcriptomic changes related to the oligodendroglial GPC which could be independent of the CD133 status. Extensive sialylation which tends to characterize tumor invasiveness was found to modify CD133 surface expression[39], implying that CD133 may represent yet another aspect of the tumor phenotype as distinct from the tumor-propagating functions specified in the gene signature. Nevertheless, our data provide strong evidence that the primary tumor phenotype and patient survival outcome are "hardwired" into the GPCs, thus underscoring their use as relevant cellular models for further investigations. In particular, knowing their regulatory and maintenance pathways would aid greatly in therapeutic targeting strategies.

Our small molecule screen consistently identified known signaling pathways promoting the survival of GPCs; namely TGFβ[42, 107], Jak/Stat[108, 152], PI3K/Akt/mTOR[3], all of which have been shown to be critical for maintaining GPCs *in vitro*, resulting in tumor growth. However, the lack of efficacy of Hh/SMO[111] and γ-secretase[153] inhibitors suggests that such screens cannot reflect an aspect of tumor biology, that is, paracrine feedback loops. In addition, in enabling a greater speed at performing these initial screens with a larger number of compounds, viability which was used as an endpoint may not reflect the survival of *bona fide* tumor stem cells. These frequently minority cells would be masked by the transiently proliferating progenitors. Consequently, candidates from such screens have to be further validated with functional assays. GSK3β emerged as a novel regulatory pathway of GPC survival. We focused our attention on this pathway as clinical stage candidates are in trials and the demonstration of its inhibition efficacy on GPCs would be instrumental. Initially thought to have a role only in glycogen metabolism,

GSK3 has recently been reported to be an important enzymatic modulator of a wide array of cellular functions including cell survival, metabolism and structure[154, 155]. The involvement of GSK3 in the regulation of apoptosis is controversial. While studies have implicated a role of GSK3 as a pro-survival factor, yet others have reported a role of GSK3 as pro-apoptotic. GSK3β knockout mice have been shown to develop an embryonic lethal phenotype, and the embryonic fibroblasts from these knockout mice are sensitized to apoptosis[115]. GSK3 has also been shown to be a pro-survival factor in pancreatic tumor cells, through the modulation of NF-κB[66]. Moreover, reports have provided evidence for GSK3β inhibition in the promotion of p53-dependent apoptosis mediated by Bax in colorectal cancer cells[156]. On the other hand, studies have shown that overexpression of catalytically active GSK3 induced apoptosis in both Rat-1 and PC12 cells, and dominant-negative GSK3 protected cells from apoptosis upon inhibition of phosphatidylinositol (PI) 3-kinase, thereby proving a role of GSK3 in the PI 3-kinase/Akt cell survival pathway[157]. A role of GSK3β has also been reported in neuronal apoptosis[158], and apoptosis of cardiomyocytes using the GSK3 inhibitor BIO[159]. These data point to the complex involvement of GSK3 in apoptosis and suggest that the biological outcome of GSK3 signaling is tissue and cell type context dependent. The complexity of GSK3β is heightened by reports implicating its role both as a tumor promoter and tumor suppressor. Studies have shown a role of GSK3β as a tumor suppressor in skin tumorigenesis, where down-regulation or inactivation of GSK3β would render it oncogenic for epidermal cells[62]. Kinase-inactive GSK3β in mouse mammary glands also plays a role in promoting mammary tumorigenesis[63]. However, the

function of GSK3β as a tumor promoter has been evident in tumorigenesis of ovarian, colon and pancreatic carcinomas[57].

Studies have provided an insight into the role of GSK3β in GBM, demonstrating that GSK3 inhibition reduced glioma cell survival and clonogenicity, through the effects of c-Myc, decrease in NFκB, and alteration of glucose metabolism, leading to apoptosis and cytotoxicity[71]. Studies have also provided a role for GSK3β inhibition in the promotion of tumor cell differentiation, apoptosis and reduction in clonogenicity in serum-grown glioma cells[72]. These data point to a pro-survival and tumor promoter involvement of GSK3β in GBMs, providing the basis for our investigations in GPCs. Specifically, we asked how GSK3β inhibition affected tumor stem cell activity defined by complementary means; CD133 expression and sphere formation which reflects extended self-renewal potential. Our data suggest that GSK3β inhibition induces differentiation of GPCs, accompanied by apoptotic responses consistent with cell cycle exit. Interestingly, we noted that while $CD133^+$ cells were preferentially inhibited, $CD133^-$ cells which comprised more lineage-committed progenitors generally continued to proliferate. Such observations challenge the "cancer stem cell hypothesis" in therapeutic targeting, and suggests that equal targeting of other non-stem cells may be crucial to fully eradicate tumor growth. Indeed, we had observed that GSK3 inhibition resulted in elevated β-catenin protein expression in our GPCs (data not shown). The Wnt pathway has been shown vital to maintain self-renewing stem cells, and hyperactivated Wnt signaling initiates and sustains intestinal cancers[15]. It is thus plausible that while GSK3β maintains the $CD133^+$ tumor stem cell population, its inhibition may induce differentiation and a

concomitant loss of CD133 expression (thus scoring as $CD133^-$ cells) which then proliferate owing to the self-renewing properties of an activated Wnt signaling mechanism. Supporting our hypothesis, we leveraged on REMBRANDT and observed that GSK3β mRNA expression was able to stratify patient survival. Fig. 40A shows the Kaplan-Meier survival plot for all gliomas with differential GSK3β gene expression, where significant difference was observed between the GSK3β upregulated versus downregulated samples ($p = 0.0212$). An investigation into the clinical reports of patients with GSK3β upregulation revealed that most of the samples belonged to Grades II and III astrocytoma and oligodendroglioma, whereas Grade IV GBMs only constituted 3 out of 19 of the patient samples. In the group of patients with GSK3β downregulation, an increased number of patients belonged to Grade IV GBMs, with 11 out of 23 patients. An analysis of the gene expression plot in all gliomas indeed shows that GBMs show significant downregulation of GSK3β gene expression ($p = 0.0224$) compared to the insignificant change in GSK3β gene expression in other gliomas ($p > 0.05$) when evaluated against the non-tumor samples (Fig. 40B). These observations would be consistent with our postulation of GSK3β inhibition at inducing differentiation with elevated β-catenin, consistent with GBM being of a mixed cell type tumor. From our results in this thesis however, we would have expected a reversed trend in which low GSK3β expression correlates with better survival and high GSK3β expression portends poorer survival by promoting GPC growth. Interestingly, Clement *et al.* demonstrated that embryonic stem cell-like genes tended to be enriched in glioma grades II-III, further strengthening our notion that GBM represents a more differentiated state where *bona fide* stem cell

numbers are diluted. GSK3 has been shown to negatively regulate the Wnt, Notch and Hh pathways, which exhibit aberrant activation in various cancers[160, 161]. This suggests that GSK3 inhibitors could have a therapeutically negative, pro-survival impact on tumor cells by activating the Wnt pathway. In contrast, although the induction of differentiation by itself has been suggested as a therapeutic strategy, the use of morphogens introduces the potential problem of interfering with the highly regulated adult stem cell niches, and therefore should be monitored for any undesired effects on the adult stem cell population.

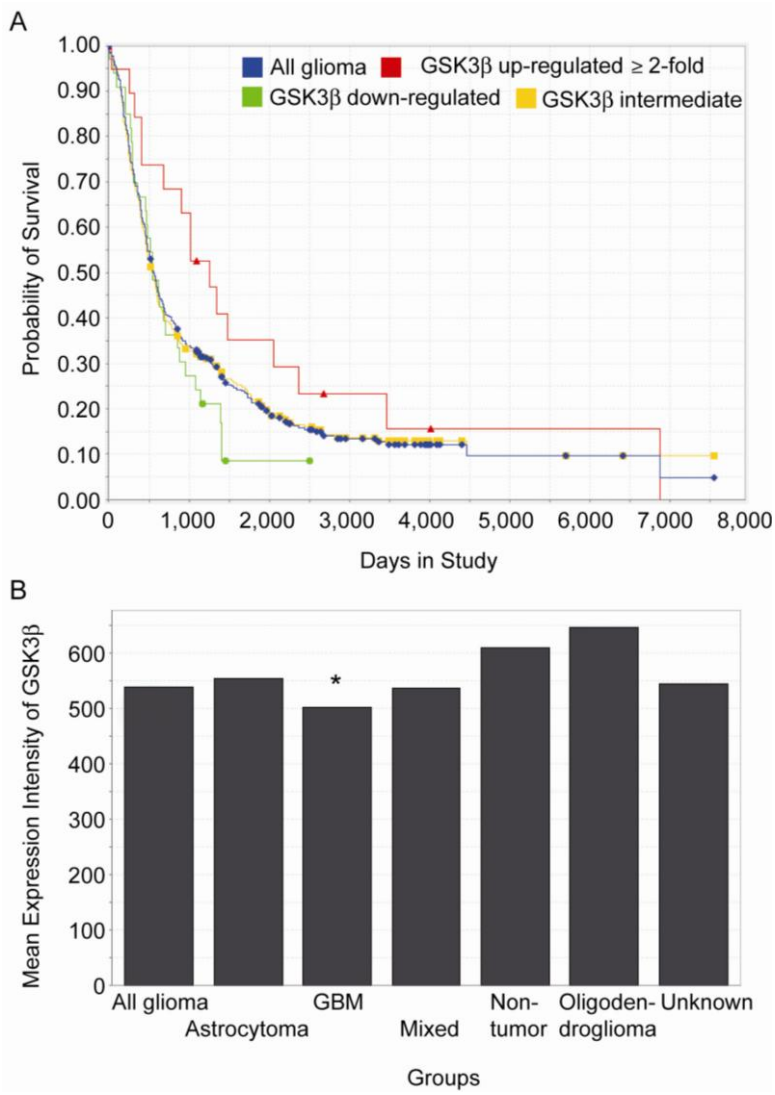

Figure-40. Kaplan-Meier survival plot for gliomas with differential GSK3β gene expression and gene expression intensity in gliomas. (A) Kaplan-Meier plot for all gliomas displaying up- and down-regulated GSK3β expression **(B)** Gene expression intensity of GSK3β in gliomas showing significant down-regulation in GBMs versus non-tumor. *$p < 0.05$

7.1 FUTURE WORK

Moving forward, the validation of GSK3β inhibition in GPCs requires further *in vivo* work, specifically, populations of cells must be colored to allow for single cell tracking. Varnat *et al.* has recently developed a novel 'red/green' competition assay to test stem cell self-renewal *in vivo*[162]. This method has the advantage in that it does not select cell populations for analysis (e.g. implantation), resulting in a biased, expected survival outcome. Instead, mixed, colored cell populations are allowed to interact in tumor formation, and the ratio of colors determines the mechanism between $CD133^+$ and $CD133^-$ cells. Adapting this method, we can isolate $CD133^+$ GBM cells from primary tumors and transduce these cells with shGSK3β lentiviral vectors expressing RFP (TomatoRED). Similarly for $CD133^-$ cells, we can sort these cells and 129ransducer them with shGSK3β lentiviral vectors expressing GFP. We can then proceed to inject these cells into immunocompromised mice. Competition occurs between the RFP^+ and GFP^+ populations, where altered self-renewal of $CD133^+RFP^+$ /$CD133^-GFP^+$ cells *in vivo* in a tumor context is postulated to change the size of the RFP^+ and GFP^+ populations. Compared to xenograft models with GPCs transduced with non-silencing control vectors, we can then generate a survival Kaplan-Meier curve in which we would expect the shGSK3β transduced GPCs to exhibit better survival. Relative population size changes of sorted $CD133^+$ and $CD133^-$ cells can then be measured by FACS analysis following tumor dissociation where relative expression of RFP- and GFP-positive cells can be determined. A greater percentage of RFP^+ cells would suggest that the stem $CD133^+$ cells are responsible for tumor growth and are not eradicated by GSK3β inhibition. Conversely, a greater percentage

of GFP^+ cells as compared to RFP^+ cells would suggest a contribution by the more differentiated $CD133^-$ cells. This would help us validate if GSK3β inhibition indeed causes a differentiation in the $CD133^+$ population. The contribution of proliferation of these sorted GPCs can be determined by IHC staining of Ki-67.

7.2 CONCLUSIONS

In vitro passaged GPCs contribute to molecular heterogeneity and survival outcome of glioma patients. GSK3β promotes GPC survival while its inhibition abrogates tumor stem cell frequency and induces differentiation. However, non-tumor stem cells continue to proliferate, signaling a need for caution in determining efficacy of GSK3β inhibition by focusing on only GPC activity alone. Better animal models allowing single cell tracking by colors will be needed to definitively implicate GSK3β inhibition as a viable therapeutic strategy.

BIBLIOGRAPHY

1. Louis, D. N. et al. The 2007 WHO classification of tumours of the central nervous system. Acta Neuropathol 114, 97-109 (2007).
2. Clement, V., Sanchez, P., de Tribolet, N., Radovanovic, I. & Ruiz i Altaba, A. HEDGEHOG-GLI1 signaling regulates human glioma growth, cancer stem cell self-renewal, and tumorigenicity. Curr Biol 17, 165-72 (2007).
3. Eyler, C. E. et al. Brain cancer stem cells display preferential sensitivity to Akt inhibition. Stem Cells 26, 3027-36 (2008).
4. Cairncross, J. G. et al. Specific genetic predictors of chemotherapeutic response and survival in patients with anaplastic oligodendrogliomas. J Natl Cancer Inst 90, 1473-9 (1998).
5. Kleihues, P. et al. The WHO classification of tumors of the nervous system. J Neuropathol Exp Neurol 61, 215-25; discussion 226-9 (2002).
6. Comprehensive genomic characterization defines human glioblastoma genes and core pathways. Nature 455, 1061-8 (2008).
7. Verhaak, R. G. et al. Integrated genomic analysis identifies clinically relevant subtypes of glioblastoma characterized by abnormalities in PDGFRA, IDH1, EGFR, and NF1. Cancer Cell 17, 98-110.
8. French, P. J. et al. Gene expression profiles associated with treatment response in oligodendrogliomas. Cancer Res 65, 11335-44 (2005).
9. Gravendeel, L. A. et al. Intrinsic gene expression profiles of gliomas are a better predictor of survival than histology. Cancer Res 69, 9065-72 (2009).

10. Phillips, H. S. et al. Molecular subclasses of high-grade glioma predict prognosis, delineate a pattern of disease progression, and resemble stages in neurogenesis. Cancer Cell 9, 157-73 (2006).
11. Wee, B., Charles, N. & Holland, E. C. Animal models to study cancer-initiating cells from glioblastoma. Front Biosci 17, 2243-58.
12. Uhrbom, L., Hesselager, G., Nister, M. & Westermark, B. Induction of brain tumors in mice using a recombinant platelet-derived growth factor B-chain retrovirus. Cancer Res 58, 5275-9 (1998).
13. Holland, E. C., Hively, W. P., DePinho, R. A. & Varmus, H. E. A constitutively active epidermal growth factor receptor cooperates with disruption of G1 cell-cycle arrest pathways to induce glioma-like lesions in mice. Genes Dev 12, 3675-85 (1998).
14. Alcantara Llaguno, S. et al. Malignant astrocytomas originate from neural stem/progenitor cells in a somatic tumor suppressor mouse model. Cancer Cell 15, 45-56 (2009).
15. Barker, N. et al. Crypt stem cells as the cells-of-origin of intestinal cancer. Nature 457, 608-11 (2009).
16. Zheng, H. et al. p53 and Pten control neural and glioma stem/progenitor cell renewal and differentiation. Nature 455, 1129-33 (2008).
17. Jacques, T. S. et al. Combinations of genetic mutations in the adult neural stem cell compartment determine brain tumour phenotypes. Embo J 29, 222-35.

18. Hodgson, J. G. et al. Comparative analyses of gene copy number and mRNA expression in glioblastoma multiforme tumors and xenografts. Neuro Oncol 11, 477-87 (2009).

19. Lee, J. et al. Tumor stem cells derived from glioblastomas cultured in bFGF and EGF more closely mirror the phenotype and genotype of primary tumors than do serum-cultured cell lines. Cancer Cell 9, 391-403 (2006).

20. Bonnet, D. & Dick, J. E. Human acute myeloid leukemia is organized as a hierarchy that originates from a primitive hematopoietic cell. Nat Med 3, 730-7 (1997).

21. Al-Hajj, M., Wicha, M. S., Benito-Hernandez, A., Morrison, S. J. & Clarke, M. F. Prospective identification of tumorigenic breast cancer cells. Proc Natl Acad Sci U S A 100, 3983-8 (2003).

22. O'Brien, C. A., Pollett, A., Gallinger, S. & Dick, J. E. A human colon cancer cell capable of initiating tumour growth in immunodeficient mice. Nature 445, 106-10 (2007).

23. Prince, M. E. et al. Identification of a subpopulation of cells with cancer stem cell properties in head and neck squamous cell carcinoma. Proc Natl Acad Sci U S A 104, 973-8 (2007).

24. Ricci-Vitiani, L. et al. Identification and expansion of human colon-cancer-initiating cells. Nature 445, 111-5 (2007).

25. Quintana, E. et al. Efficient tumour formation by single human melanoma cells. Nature 456, 593-8 (2008).

26. Li, A. et al. Genomic changes and gene expression profiles reveal that established glioma cell lines are poorly representative of primary human gliomas. Mol Cancer Res 6, 21-30 (2008).

27. Shats, I. et al. Using a stem cell-based signature to guide therapeutic selection in cancer. Cancer Res 71, 1772-80 (2011).

28. Chong, Y. K. et al. Cryopreservation of neurospheres derived from human glioblastoma multiforme. Stem Cells 27, 29-39 (2009).

29. Lamb, J. et al. The Connectivity Map: using gene-expression signatures to connect small molecules, genes, and disease. Science 313, 1929-35 (2006).

30. Rich, J. N. & Eyler, C. E. Cancer stem cells in brain tumor biology. Cold Spring Harb Symp Quant Biol 73, 411-20 (2008).

31. Singh, S. K. et al. Identification of human brain tumour initiating cells. Nature 432, 396-401 (2004).

32. Son, M. J., Woolard, K., Nam, D. H., Lee, J. & Fine, H. A. SSEA-1 is an enrichment marker for tumor-initiating cells in human glioblastoma. Cell Stem Cell 4, 440-452 (2009).

33. Bar, E. E. et al. Cyclopamine-mediated hedgehog pathway inhibition depletes stem-like cancer cells in glioblastoma. Stem Cells 25, 2524-33 (2007).

34. Bleau, A. M. et al. PTEN/PI3K/Akt pathway regulates the side population phenotype and ABCG2 activity in glioma tumor stem-like cells. Cell Stem Cell 4, 226-35 (2009).

35. Chua, C. et al. Characterization of a side population of astrocytoma cells in response to temozolomide. J Neurosurg 109, 856-66 (2008).

36. Beier, D. et al. CD133(+) and CD133(-) glioblastoma-derived cancer stem cells show differential growth characteristics and molecular profiles. Cancer Res 67, 4010-5 (2007).

37. Sakariassen, P. O. et al. Angiogenesis-independent tumor growth mediated by stem-like cancer cells. Proc Natl Acad Sci U S A 103, 16466-71 (2006).

38. Kemper, K. et al. The AC133 epitope, but not the CD133 protein, is lost upon cancer stem cell differentiation. Cancer Res 70, 719-29.

39. Zhou, F. et al. Alpha2,3-Sialylation regulates the stability of stem cell marker CD133. J Biochem 148, 273-80.

40. Reynolds, B. A., Tetzlaff, W. & Weiss, S. A multipotent EGF-responsive striatal embryonic progenitor cell produces neurons and astrocytes. J Neurosci 12, 4565-74 (1992).

41. Reynolds, B. A. & Rietze, R. L. Neural stem cells and neurospheres-re-evaluating the relationship. Nat Methods 2, 333-6 (2005).

42. Anido, J. et al. TGF-beta Receptor Inhibitors Target the CD44(high)/Id1(high) Glioma-Initiating Cell Population in Human Glioblastoma. Cancer Cell 18, 655-68.

43. Fang, X. et al. Phosphorylation and inactivation of glycogen synthase kinase 3 by protein kinase A. Proc Natl Acad Sci U S A 97, 11960-5 (2000).

44. Cross, D. A., Alessi, D. R., Cohen, P., Andjelkovich, M. & Hemmings, B. A. Inhibition of glycogen synthase kinase-3 by insulin mediated by protein kinase B. Nature 378, 785-9 (1995).

45. Stambolic, V. & Woodgett, J. R. Mitogen inactivation of glycogen synthase kinase-3 beta in intact cells via serine 9 phosphorylation. Biochem J 303 (Pt 3), 701-4 (1994).

46. Sutherland, C., Leighton, I. A. & Cohen, P. Inactivation of glycogen synthase kinase-3 beta by phosphorylation: new kinase connections in insulin and growth-factor signalling. Biochem J 296 (Pt 1), 15-9 (1993).

47. Doble, B. W. & Woodgett, J. R. GSK-3: tricks of the trade for a multi-tasking kinase. J Cell Sci 116, 1175-86 (2003).

48. Hughes, K., Nikolakaki, E., Plyte, S. E., Totty, N. F. & Woodgett, J. R. Modulation of the glycogen synthase kinase-3 family by tyrosine phosphorylation. Embo J 12, 803-8 (1993).

49. Cole, A., Frame, S. & Cohen, P. Further evidence that the tyrosine phosphorylation of glycogen synthase kinase-3 (GSK3) in mammalian cells is an autophosphorylation event. Biochem J 377, 249-55 (2004).

50. Cohen, P. The Croonian Lecture 1998. Identification of a protein kinase cascade of major importance in insulin signal transduction. Philos Trans R Soc Lond B Biol Sci 354, 485-95 (1999).

51. Cohen, P. & Frame, S. The renaissance of GSK3. Nat Rev Mol Cell Biol 2, 769-76 (2001).

52. Cohen, P., Alessi, D. R. & Cross, D. A. PDK1, one of the missing links in insulin signal transduction? FEBS Lett 410, 3-10 (1997).

53. Hur, E. M. & Zhou, F. Q. GSK3 signalling in neural development. Nat Rev Neurosci 11, 539-51.

54. Beurel, E. & Jope, R. S. The paradoxical pro- and anti-apoptotic actions of GSK3 in the intrinsic and extrinsic apoptosis signaling pathways. Prog Neurobiol 79, 173-89 (2006).

55. Grimes, C. A. & Jope, R. S. The multifaceted roles of glycogen synthase kinase 3beta in cellular signaling. Prog Neurobiol 65, 391-426 (2001).

56. Manoukian, A. S. & Woodgett, J. R. Role of glycogen synthase kinase-3 in cancer: regulation by Wnts and other signaling pathways. Adv Cancer Res 84, 203-29 (2002).

57. Ougolkov, A. V. & Billadeau, D. D. Targeting GSK-3: a promising approach for cancer therapy? Future Oncol 2, 91-100 (2006).

58. Koros, E. & Dorner-Ciossek, C. The role of glycogen synthase kinase-3beta in schizophrenia. Drug News Perspect 20, 437-45 (2007).

59. Luo, J. Glycogen synthase kinase 3beta (GSK3beta) in tumorigenesis and cancer chemotherapy. Cancer Lett 273, 194-200 (2009).

60. Leis, H., Segrelles, C., Ruiz, S., Santos, M. & Paramio, J. M. Expression, localization, and activity of glycogen synthase kinase 3beta during mouse skin tumorigenesis. Mol Carcinog 35, 180-5 (2002).

61. Ding, Q. et al. Myeloid cell leukemia-1 inversely correlates with glycogen synthase kinase-3beta activity and associates with poor prognosis in human breast cancer. Cancer Res 67, 4564-71 (2007).

62. Ma, C. et al. The role of glycogen synthase kinase 3beta in the transformation of epidermal cells. Cancer Res 67, 7756-64 (2007).

63. Farago, M. et al. Kinase-inactive glycogen synthase kinase 3beta promotes Wnt signaling and mammary tumorigenesis. Cancer Res 65, 5792-801 (2005).

64. Cao, Q., Lu, X. & Feng, Y. J. Glycogen synthase kinase-3beta positively regulates the proliferation of human ovarian cancer cells. Cell Res 16, 671-7 (2006).

65. Shakoori, A. et al. Deregulated GSK3beta activity in colorectal cancer: its association with tumor cell survival and proliferation. Biochem Biophys Res Commun 334, 1365-73 (2005).

66. Ougolkov, A. V., Fernandez-Zapico, M. E., Savoy, D. N., Urrutia, R. A. & Billadeau, D. D. Glycogen synthase kinase-3beta participates in nuclear factor kappaB-mediated gene transcription and cell survival in pancreatic cancer cells. Cancer Res 65, 2076-81 (2005).

67. Erdal, E., Ozturk, N., Cagatay, T., Eksioglu-Demiralp, E. & Ozturk, M. Lithium-mediated downregulation of PKB/Akt and cyclin E with growth inhibition in hepatocellular carcinoma cells. Int J Cancer 115, 903-10 (2005).

68. Liao, X., Zhang, L., Thrasher, J. B., Du, J. & Li, B. Glycogen synthase kinase-3beta suppression eliminates tumor necrosis factor-related apoptosis-inducing ligand resistance in prostate cancer. Mol Cancer Ther 2, 1215-22 (2003).

69. Mazor, M., Kawano, Y., Zhu, H., Waxman, J. & Kypta, R. M. Inhibition of glycogen synthase kinase-3 represses androgen receptor activity and prostate cancer cell growth. Oncogene 23, 7882-92 (2004).

70. Ougolkov, A. V., Bone, N. D., Fernandez-Zapico, M. E., Kay, N. E. & Billadeau, D. D. Inhibition of glycogen synthase kinase-3 activity leads to epigenetic silencing of nuclear factor kappaB target genes and induction of apoptosis in chronic lymphocytic leukemia B cells. Blood 110, 735-42 (2007).

71. Kotliarova, S. et al. Glycogen synthase kinase-3 inhibition induces glioma cell death through c-MYC, nuclear factor-kappaB, and glucose regulation. Cancer Res 68, 6643-51 (2008).

72. Korur, S. et al. GSK3beta regulates differentiation and growth arrest in glioblastoma. PLoS One 4, e7443 (2009).

73. Gunther, H. S. et al. Glioblastoma-derived stem cell-enriched cultures form distinct subgroups according to molecular and phenotypic criteria. Oncogene 27, 2897-909 (2008).

74. Pollard, S. M. et al. Glioma stem cell lines expanded in adherent culture have tumor-specific phenotypes and are suitable for chemical and genetic screens. Cell Stem Cell 4, 568-80 (2009).

75. Bellows, C. G. & Aubin, J. E. Determination of numbers of osteoprogenitors present in isolated fetal rat calvaria cells in vitro. Dev Biol 133, 8-13 (1989).

76. Tropepe, V. et al. Distinct neural stem cells proliferate in response to EGF and FGF in the developing mouse telencephalon. Dev Biol 208, 166-88 (1999).

77. Reynolds, B. A. & Rietze, R. L. Neural stem cells and neurospheres--re-evaluating the relationship. Nat Methods 2, 333-6 (2005).

78. Gritti, A. et al. Multipotential stem cells from the adult mouse brain proliferate and self-renew in response to basic fibroblast growth factor. J Neurosci 16, 1091-100 (1996).

79. Persson, A. I. et al. Non-stem cell origin for oligodendroglioma. Cancer Cell 18, 669-82.

80. Ooi, C. H. et al. Oncogenic pathway combinations predict clinical prognosis in gastric cancer. PLoS Genet 5, e1000676 (2009).

81. Madhavan, S. et al. Rembrandt: helping personalized medicine become a reality through integrative translational research. Mol Cancer Res 7, 157-67 (2009).

82. Liu, C. et al. Mosaic Analysis with Double Markers Reveals Tumor Cell of Origin in Glioma. Cell.

83. Wee, B., Charles, N. & Holland, E. C. Animal models to study cancer-initiating cells from Glioblastoma. Front Biosci 17, 2243-58 (2011).

84. Foong, C. S. et al. Cryopreservation of cancer-initiating cells derived from glioblastoma. Front Biosci (Schol Ed) 3, 698-708.

85. He, J. et al. Glioblastomas with an oligodendroglial component: a pathological and molecular study. J Neuropathol Exp Neurol 60, 863-71 (2001).

86. Galli, R. et al. Isolation and characterization of tumorigenic, stem-like neural precursors from human glioblastoma. Cancer Res 64, 7011-21 (2004).

87. Singh, S. K. et al. Identification of a cancer stem cell in human brain tumors. Cancer Res 63, 5821-8 (2003).

88. Taylor, M. D. et al. Radial glia cells are candidate stem cells of ependymoma. Cancer Cell 8, 323-35 (2005).

89. Son, M. J., Woolard, K., Nam, D. H., Lee, J. & Fine, H. A. SSEA-1 is an enrichment marker for tumor-initiating cells in human glioblastoma. Cell Stem Cell 4, 440-52 (2009).

90. Kalani, M. Y. et al. Wnt-mediated self-renewal of neural stem/progenitor cells. Proc Natl Acad Sci U S A 105, 16970-5 (2008).

91. Pera, M. F. Unnatural selection of cultured human ES cells? Nat Biotechnol 22, 42-3 (2004).

92. Svendsen, C. N. et al. A new method for the rapid and long term growth of human neural precursor cells. J Neurosci Methods 85, 141-52 (1998).

93. Lottaz, C. et al. Transcriptional profiles of CD133+ and CD133- glioblastoma-derived cancer stem cell lines suggest different cells of origin. Cancer Res 70, 2030-40.

94. Cai, J. et al. Properties of a fetal multipotent neural stem cell (NEP cell). Dev Biol 251, 221-40 (2002).

95. Kaneko, Y. et al. Musashi1: an evolutionally conserved marker for CNS progenitor cells including neural stem cells. Dev Neurosci 22, 139-53 (2000).

96. Mountford, P., Nichols, J., Zevnik, B., O'Brien, C. & Smith, A. Maintenance of pluripotential embryonic stem cells by stem cell selection. Reprod Fertil Dev 10, 527-33 (1998).

97. Ying, Q. L., Nichols, J., Chambers, I. & Smith, A. BMP induction of Id proteins suppresses differentiation and sustains embryonic stem cell self-renewal in collaboration with STAT3. Cell 115, 281-92 (2003).

98. Schluter, C. et al. The cell proliferation-associated antigen of antibody Ki-67: a very large, ubiquitous nuclear protein with numerous repeated elements, representing a new kind of cell cycle-maintaining proteins. J Cell Biol 123, 513-22 (1993).

99. Vescovi, A. L., Galli, R. & Reynolds, B. A. Brain tumour stem cells. Nat Rev Cancer 6, 425-36 (2006).

100. Piccirillo, S. G. et al. Bone morphogenetic proteins inhibit the tumorigenic potential of human brain tumour-initiating cells. Nature 444, 761-5 (2006).

101. Cahoy, J. D. et al. A transcriptome database for astrocytes, neurons, and oligodendrocytes: a new resource for understanding brain development and function. J Neurosci 28, 264-78 (2008).

102. Persson, A. I. et al. Non-stem cell origin for oligodendroglioma. Cancer Cell 18, 669-82 (2010).

103. Chaichana, K., Zamora-Berridi, G., Camara-Quintana, J. & Quinones-Hinojosa, A. Neurosphere assays: growth factors and hormone differences in tumor and nontumor studies. Stem Cells 24, 2851-7 (2006).

104. Northcott, P. A. et al. Medulloblastoma comprises four distinct molecular variants. J Clin Oncol 29, 1408-14.

105. Danovi, D. et al. Imaging-based chemical screens using normal and glioma-derived neural stem cells. Biochem Soc Trans 38, 1067-71.

106. Diamandis, P. et al. Chemical genetics reveals a complex functional ground state of neural stem cells. Nat Chem Biol 3, 268-73 (2007).

107. Penuelas, S. et al. TGF-beta increases glioma-initiating cell self-renewal through the induction of LIF in human glioblastoma. Cancer Cell 15, 315-27 (2009).

108. Sherry, M. M., Reeves, A., Wu, J. K. & Cochran, B. H. STAT3 is required for proliferation and maintenance of multipotency in glioblastoma stem cells. Stem Cells 27, 2383-92 (2009).

109. Wang, J. et al. A reproducible brain tumour model established from human glioblastoma biopsies. BMC Cancer 9, 465 (2009).

110. Fan, X. et al. Notch pathway inhibition depletes stem-like cells and blocks engraftment in embryonal brain tumors. Cancer Res 66, 7445-52 (2006).

111. Yauch, R. L. et al. A paracrine requirement for hedgehog signalling in cancer. Nature 455, 406-10 (2008).

112. Zhu, T. et al. Endothelial cells create a stem cell niche in glioblastoma by providing Notch ligands that nurture self-renewal of cancer stem-like cells. Cancer Res.

113. Kelly, K. R. et al. Targeting Aurora Kinases in Cancer Treatment. Curr Drug Targets.

114. Strebhardt, K. Multifaceted polo-like kinases: drug targets and antitargets for cancer therapy. Nat Rev Drug Discov 9, 643-60.

115. Hoeflich, K. P. et al. Requirement for glycogen synthase kinase-3beta in cell survival and NF-kappaB activation. Nature 406, 86-90 (2000).

116. Meijer, L. et al. GSK-3-selective inhibitors derived from Tyrian purple indirubins. Chem Biol 10, 1255-66 (2003).

117. Sato, N., Meijer, L., Skaltsounis, L., Greengard, P. & Brivanlou, A. H. Maintenance of pluripotency in human and mouse embryonic stem cells through activation of Wnt signaling by a pharmacological GSK-3-specific inhibitor. Nat Med 10, 55-63 (2004).

118. Noda, T. et al. Activation of Wnt/beta-catenin signalling pathway induces chemoresistance to interferon-alpha/5-fluorouracil combination therapy for hepatocellular carcinoma. Br J Cancer 100, 1647-58 (2009).

119. Patel, S., Yenush, L., Rodriguez, P. L., Serrano, R. & Blundell, T. L. Crystal structure of an enzyme displaying both inositol-polyphosphate-1-phosphatase and 3'-phosphoadenosine-5'-phosphate phosphatase activities: a novel target of lithium therapy. J Mol Biol 315, 677-85 (2002).

120. Davies, S. P., Reddy, H., Caivano, M. & Cohen, P. Specificity and mechanism of action of some commonly used protein kinase inhibitors. Biochem J 351, 95-105 (2000).

121. Hughes, K., Pulverer, B. J., Theocharous, P. & Woodgett, J. R. Baculovirus-mediated expression and characterisation of rat glycogen synthase kinase-3 beta, the mammalian homologue of the Drosophila melanogaster zeste-white 3sgg homeotic gene product. Eur J Biochem 203, 305-11 (1992).

122. Jessberger, S., Clemenson, G. D., Jr. & Gage, F. H. Spontaneous fusion and nonclonal growth of adult neural stem cells. Stem Cells 25, 871-4 (2007).

123. Deleyrolle, L. P. et al. Determination of somatic and cancer stem cell self-renewing symmetric division rate using sphere assays. PLoS One 6, e15844 (2011).

124. Deleyrolle, L. P. et al. Evidence for label-retaining tumour-initiating cells in human glioblastoma. Brain 134, 1331-43.

125. Lathia, J. D., Heddleston, J. M., Venere, M. & Rich, J. N. Deadly teamwork: neural cancer stem cells and the tumor microenvironment. Cell Stem Cell 8, 482-5 (2011).

126. Soda, Y. et al. Transdifferentiation of glioblastoma cells into vascular endothelial cells. Proc Natl Acad Sci U S A 108, 4274-80.

127. Wang, R. et al. Glioblastoma stem-like cells give rise to tumour endothelium. Nature 468, 829-33.

128. Satoh, M. S. & Lindahl, T. Role of poly(ADP-ribose) formation in DNA repair. Nature 356, 356-8 (1992).

129. Nicholson, D. W. et al. Identification and inhibition of the ICE/CED-3 protease necessary for mammalian apoptosis. Nature 376, 37-43 (1995).

130. Oliver, F. J. et al. Importance of poly(ADP-ribose) polymerase and its cleavage in apoptosis. Lesson from an uncleavable mutant. J Biol Chem 273, 33533-9 (1998).

131. Kasuga, C. et al. Sensitization of human glioblastomas to tumor necrosis factor-related apoptosis-inducing ligand (TRAIL) by NF-kappaB inhibitors. Cancer Sci 95, 840-4 (2004).

132. Robe, P. A. et al. In vitro and in vivo activity of the nuclear factor-kappaB inhibitor sulfasalazine in human glioblastomas. Clin Cancer Res 10, 5595-603 (2004).

133. Samanta, A. K., Huang, H. J., Bast, R. C., Jr. & Liao, W. S. Overexpression of MEKK3 confers resistance to apoptosis through activation of NFkappaB. J Biol Chem 279, 7576-83 (2004).

134. Mazzoleni, S. et al. Epidermal growth factor receptor expression identifies functionally and molecularly distinct tumor-initiating cells in human glioblastoma multiforme and is required for gliomagenesis. Cancer Res 70, 7500-13.

135. Nesbit, C. E., Tersak, J. M. & Prochownik, E. V. MYC oncogenes and human neoplastic disease. Oncogene 18, 3004-16 (1999).

136. Oster, S. K., Ho, C. S., Soucie, E. L. & Penn, L. Z. The myc oncogene: MarvelouslY Complex. Adv Cancer Res 84, 81-154 (2002).

137. Wang, J. et al. c-Myc is required for maintenance of glioma cancer stem cells. PLoS ONE 3, e3769 (2008).

138. Karpinich, N. O., Tafani, M., Rothman, R. J., Russo, M. A. & Farber, J. L. The course of etoposide-induced apoptosis from damage to DNA and p53 activation to mitochondrial release of cytochrome c. J Biol Chem 277, 16547-52 (2002).

139. Perez, C., Vilaboa, N. E. & Aller, P. Etoposide-induced differentiation of U937 promonocytic cells: AP-1-dependent gene expression and protein kinase C activation. Cell Growth Differ 5, 949-55 (1994).

140. Hemmati, H. D. et al. Cancerous stem cells can arise from pediatric brain tumors. Proc Natl Acad Sci U S A 100, 15178-83 (2003).

141. Eyler, C. E. et al. Glioma stem cell proliferation and tumor growth are promoted by nitric oxide synthase-2. Cell 146, 53-66.

142. Fuerer, C. & Nusse, R. Lentiviral vectors to probe and manipulate the Wnt signaling pathway. PLoS One 5, e9370.

143. McBride, J. L. et al. Artificial miRNAs mitigate shRNA-mediated toxicity in the brain: implications for the therapeutic development of RNAi. Proc Natl Acad Sci U S A 105, 5868-73 (2008).

144. Beer, S. et al. Low-level shRNA cytotoxicity can contribute to MYC-induced hepatocellular carcinoma in adult mice. Mol Ther 18, 161-70.

145. Fan, X. et al. NOTCH pathway blockade depletes CD133-positive glioblastoma cells and inhibits growth of tumor neurospheres and xenografts. Stem Cells 28, 5-16.

146. Park, D. M. & Rich, J. N. Biology of glioma cancer stem cells. Mol Cells 28, 7-12 (2009).

147. Casalbore, P. et al. Tumorigenic potential of olfactory bulb-derived human adult neural stem cells associates with activation of TERT and NOTCH1. PLoS One 4, e4434 (2009).

148. Thepot, A. et al. Assessment of transformed properties in vitro and of tumorigenicity in vivo in primary keratinocytes cultured for epidermal sheet transplantation. J Skin Cancer 2011, 936546.

149. Visvader, J. E. Cells of origin in cancer. Nature 469, 314-22 (2011).

150. Clark, M. J. et al. U87MG decoded: the genomic sequence of a cytogenetically aberrant human cancer cell line. PLoS Genet 6, e1000832.

151. Beier, D. et al. CD133 expression and cancer stem cells predict prognosis in high-grade oligodendroglial tumors. Brain Pathol 18, 370-7 (2008).

152. Wang, H. et al. Targeting interleukin 6 signaling suppresses glioma stem cell survival and tumor growth. Stem Cells 27, 2393-404 (2009).

153. Zhu, T. et al. Endothelial cells create a stem cell niche in glioblastoma by providing Notch ligands that nurture self-renewal of cancer stem-like cells. Cancer Res (2011).

154. Cohen, P. & Goedert, M. GSK3 inhibitors: development and therapeutic potential. Nat Rev Drug Discov 3, 479-87 (2004).

155. Jope, R. S. & Johnson, G. V. The glamour and gloom of glycogen synthase kinase-3. Trends Biochem Sci 29, 95-102 (2004).

156. Tan, J. et al. Pharmacologic modulation of glycogen synthase kinase-3beta promotes p53-dependent apoptosis through a direct Bax-mediated mitochondrial pathway in colorectal cancer cells. Cancer Res 65, 9012-20 (2005).

157. Pap, M. & Cooper, G. M. Role of glycogen synthase kinase-3 in the phosphatidylinositol 3-Kinase/Akt cell survival pathway. J Biol Chem 273, 19929-32 (1998).

158. Hetman, M., Cavanaugh, J. E., Kimelman, D. & Xia, Z. Role of glycogen synthase kinase-3beta in neuronal apoptosis induced by trophic withdrawal. J Neurosci 20, 2567-74 (2000).

159. Tseng, A. S., Engel, F. B. & Keating, M. T. The GSK-3 inhibitor BIO promotes proliferation in mammalian cardiomyocytes. Chem Biol 13, 957-63 (2006).

160. Wang, Z. et al. Glycogen synthase kinase 3 in MLL leukaemia maintenance and targeted therapy. Nature 455, 1205-9 (2008).

161. Foltz, D. R., Santiago, M. C., Berechid, B. E. & Nye, J. S. Glycogen synthase kinase-3beta modulates notch signaling and stability. Curr Biol 12, 1006-11 (2002).

162. Varnat, F. et al. Human colon cancer epithelial cells harbour active HEDGEHOG-GLI signalling that is essential for tumour growth, recurrence, metastasis and stem cell survival and expansion. EMBO Mol Med 1, 338-51 (2009).

163. Gentleman, R. C. et al. Bioconductor: open software development for computational biology and bioinformatics. Genome Biol 5, R80 (2004).

164. Tibshirani, R., Hastie, T., Narasimhan, B. & Chu, G. Diagnosis of multiple cancer types by shrunken centroids of gene expression. Proc Natl Acad Sci U S A 99, 6567-72 (2002).

165. Li, C. & Wong, W. H. Model-based analysis of oligonucleotide arrays: expression index computation and outlier detection. Proc Natl Acad Sci U S A 98, 31-6 (2001).

166. Lin, M. et al. dChipSNP: significance curve and clustering of SNP-array-based loss-of-heterozygosity data. Bioinformatics 20, 1233-40 (2004).

167. Briancon-Marjollet, A. et al. NG2-expressing glial precursor cells are a new potential oligodendroglioma cell initiating population in N-ethyl-N-nitrosourea-induced gliomagenesis. Carcinogenesis 31, 1718-25.

168. survival: Survival analysis, including penalised likelihood. R package version 2.36-9. http://CRAN.R-project.org/package=survival. Terry Therneau and original Splus->R port by Thomas Lumley. 2011

169. Gentleman R CV, Dudoit S, Irizarry R, Huber W, ed. Smyth, G.K.Limma: linear models for microarray data. In: 'Bioinformatics and Computational Biology Solutions using R and Bioconductor': Springer, New York; 2005.

APPENDICES

SUPPLEMENTARY METHODS

Tissue collection and primary glioma-propagating cell culture

Graded brain tumor specimens were obtained with informed consent, as part of a study protocol approved by the institutional review board. NNI-1, 2, 3, 4 and 5 were derived from patients with GBM as previously described[28, 84]. NNI-8 is a new GPC line derived from a patient with anaplastic oligoastrocytoma, and characterized according to previous methods (Fig. S2)[28]. "Gunther" lines: GS-1, 3, 4, 5, 6, 7 and 8 are GBM-propagating cells while GS-2 was derived from a high grade tumor with oligodendroglial features as previously described[73]. "Pollard" lines: G144, 144ED, 166, 179 and GliNS2 are GBM-propagating cells while G174 was derived from a patient with anaplastic oligoastrocytoma as previously described[74].

Processing of Microarray Data and Gene Signature Generation (Conducted by F.S.L. Ng, Singapore Institute for Clinical Sciences, A*STAR)

Affymetrix U133 Plus 2.0 CEL files were mas5 processed and quantile normalized in the R statistical software using the *affy* packages[163]. Probes with 'Absent' call in all samples were removed. Microarray data was obtained from the Gunther[73] and Pollard[73, 74] publications and were processed similarly. To obtain a GPC gene signature, a linear model was fitted with batch correction using the *limma* package[169]. Additionally, the NNI-8 Stemness signature was obtained using the limma package by comparing the GPC cells

to primary tumor. For both signatures, probesets with adjusted p-value ≤ 0.05 were considered significant.

Prediction of Phillips Classification in Rembrandt and Gravendeel datasets

To classify the Rembrandt and Gravendeel samples according to the Phillips *et al.* classification[10], Affymetrix U133A probes from the Phillips classification signature genes were mapped to U133 Plus 2.0 GeneChip using BioMart (http://www.biomart.org/). Classification of the Rembrandt and Gravendeel datasets was then performed with the R package *pamr* using the signature gene class centroids [164].

Rembrandt SNP Array Processing and 1p19q LOH Analysis

CEL files from the Affymetrix 100K SNP Arrays of Oligodendroglioma and Oligoastrocytoma patients were downloaded from the Rembrandt database and all samples were normalized in dChip[165, 166]. Chromosome 1p and 19q loss of heterozygosity inference was performed in dChip using default parameters.

SUPPLEMENTARY TABLES

Table-S1. Probesets in the GPC signature. 95 probes were used to generate the oligodendroglial GPC gene signature of oligodendroglial GPCs versus the GBM GPCs.

Probeset ID	Entrez Gene ID	Gene Symbol	Description	Log Fold Change
212507_at	23505	TMEM131	transmembrane protein 131	-0.931307621
241612_at	27022	FOXD3	forkhead box D3	1.372986027
201368_at	678	ZFP36L2	zinc finger protein 36, C3H type-like 2	-1.105289687
201369_s_at	678	ZFP36L2	zinc finger protein 36, C3H type-like 2	-0.904474969
201564_s_at	6624	FSCN1	fascin homolog 1, actin-bundling protein (Strongylocentrotus purpuratus)	-1.072722937
220231_at	10842	C7orf16	chromosome 7 open reading frame 16	2.645835821
228035_at	65975	STK33	serine/threonine kinase 33	-1.243243529
215241_at	63982	ANO3	anoctamin 3	1.090294876
218163_at	28985	MCTS1	malignant T cell amplified sequence 1	1.017692402
231840_x_at	90624	LYRM7	Lyrm7 homolog (mouse)	0.891245471
206067_s_at	7490	WT1	Wilms tumor 1	0.827289917
218988_at	55508	SLC35E3	solute carrier family 35, member E3	1.67648345
205386_s_at	4193	MDM2	Mdm2 p53 binding protein homolog (mouse)	1.884030655
211832_s_at	4193	MDM2	Mdm2 p53 binding protein homolog (mouse)	1.788934315
1553426_at	285668	C5orf64	chromosome 5 open reading frame 64	-1.147145398
211138_s_at	8564	KMO	kynurenine 3-monooxygenase (kynurenine 3-hydroxylase)	1.260883191
205306_x_at	8564	KMO	kynurenine 3-monooxygenase (kynurenine 3-hydroxylase)	1.335650833
241765_at	1368	CPM	carboxypeptidase M	3.226405764
243403_x_at	1368	CPM	carboxypeptidase M	2.660052824
225591_at	26260	FBXO25	F-box protein 25	1.023236638
1557260_a_at	84911	ZNF382	zinc finger protein 382	1.763574339
209565_at	7737	RNF113A	ring finger protein 113A	0.993408597
235502_at	5515	PPP2CA	protein phosphatase 2, catalytic subunit, alpha isozyme	1.026294597
243282_at	54520	CCDC93	coiled-coil domain containing 93	-0.893187785
226462_at	29091	STXBP6	syntaxin binding protein 6 (amisyn)	1.408107909
236290_at	220164	DOK6	docking protein 6	0.808537521

214440_at	9	NAT1	N-acetyltransferase 1 (arylamine N-acetyltransferase)	1.762236745
50400_at	196743	PAOX	polyamine oxidase (exo-N4-amino)	1.059361819
237029_at	3081	HGD	homogentisate 1,2-dioxygenase	0.971522564
244829_at	--	C6orf218	chromosome 6 open reading frame 218	1.411926375
227109_at	120227	CYP2R1	cytochrome P450, family 2, subfamily R, polypeptide 1	1.414119526
225846_at	54845	ESRP1	epithelial splicing regulatory protein 1	1.270624793
219121_s_at	54845	ESRP1	epithelial splicing regulatory protein 1	1.120675543
213638_at	221692	PHACTR1	phosphatase and actin regulator 1	1.535840464
215000_s_at	9637	FEZ2	fasciculation and elongation protein zeta 2 (zygin II)	-0.957606762
242989_at	6801	STRN	striatin, calmodulin binding protein	-1.055129989
204077_x_at	9583	ENTPD4	ectonucleoside triphosphate diphosphohydrolase 4	0.815264939
218870_at	55843	ARHGAP15	Rho GTPase activating protein 15	1.017607164
221427_s_at	81669	CCNL2	cyclin L2	-0.850386591
222999_s_at	81669	CCNL2	cyclin L2	-0.954468271
205512_s_at	9131	AIFM1	apoptosis-inducing factor, mitochondrion-associated, 1	0.954516011
207344_at	10566	AKAP3	A kinase (PRKA) anchor protein 3	2.654311598
244825_at	57477	SHROOM4	shroom family member 4	1.054431061
205281_s_at	5277	PIGA	phosphatidylinositol glycan anchor biosynthesis, class A	0.836793751
226764_at	152485	ZNF827	zinc finger protein 827	-0.996757033
1554509_a_at	80013	FAM188A	family with sequence similarity 188, member A	1.293780634
206334_at	8513	LIPF	lipase, gastric	1.947198374
204644_at	10495	ENOX2	ecto-NOX disulfide-thiol exchanger 2	0.879076665
218807_at	10451	VAV3	vav 3 guanine nucleotide exchange factor	-1.573828653
223423_at	26996	GPR160	G protein-coupled receptor 160	1.266788929
215153_at	9722	NOS1AP	nitric oxide synthase 1 (neuronal) adaptor protein	-0.882741057
1563512_at	9722	NOS1AP	nitric oxide synthase 1 (neuronal) adaptor protein	-1.07867364
37512_at	8630	HSD17B6	hydroxysteroid (17-beta) dehydrogenase 6 homolog (mouse)	1.128384226
212631_at	8417	STX7	syntaxin 7	1.113525058
225308_s_at	85461	TANC1	tetratricopeptide repeat, ankyrin repeat and coiled-coil containing 1	-0.854227497
200665_s_at	6678	SPARC	secreted protein, acidic, cysteine-rich (osteonectin)	-1.027737524
229000_at	58492	ZNF77	zinc finger protein 77	0.944812365
204759_at	1102	RCBTB2	regulator of chromosome condensation (RCC1) and BTB (POZ) domain containing protein 2	-1.668131465

221289_at	1750	DLX6	distal-less homeobox 6	1.041848794
206552_s_at	6863	TAC1	tachykinin, precursor 1	1.705027503
222767_s_at	79794	C12orf49	chromosome 12 open reading frame 49	0.808709328
204713_s_at	2153	F5	coagulation factor V (proaccelerin, labile factor)	1.431619627
204714_s_at	2153	F5	coagulation factor V (proaccelerin, labile factor)	1.504311671
206426_at	2315	MLANA	melan-A	0.890635292
206427_s_at	2315	MLANA	melan-A	1.431212371
206135_at	9705	ST18	suppression of tumorigenicity 18 (breast carcinoma) (zinc finger protein)	1.131230985
206058_at	6539	SLC6A12	solute carrier family 6 (neurotransmitter transporter, betaine/GABA), member 12	1.091850355
1561969_at	131368	ZPLD1	zona pellucida-like domain containing 1	1.316003453
224999_at	1956	EGFR	epidermal growth factor receptor	-1.990616663
201983_s_at	1956	EGFR	epidermal growth factor receptor	-2.165112816
204238_s_at	10591	C6orf108	chromosome 6 open reading frame 108	1.111934072
242727_at	221079	ARL5B	ADP-ribosylation factor-like 5B	1.32300753
235356_at	374354	NHLRC2	NHL repeat containing 2	0.931504627
231569_at	203562	TMEM31	transmembrane protein 31	1.032880572
205647_at	5893	RAD52	RAD52 homolog (S. cerevisiae)	-0.833601355
202746_at	9452	ITM2A	integral membrane protein 2A	3.632094429
202747_s_at	9452	ITM2A	integral membrane protein 2A	3.720860606
228891_at	10507	SEMA4D	sema domain, immunoglobulin domain (Ig), transmembrane domain (TM) and short cytoplasmic domain, (semaphorin) 4D	0.981611103
207540_s_at	6850	SYK	spleen tyrosine kinase	1.381598219
204011_at	10253	SPRY2	sprouty homolog 2 (Drosophila)	-0.96891126
221035_s_at	56155	TEX14	testis expressed 14	0.988947099
209848_s_at	6490	PMEL	premelanosome protein	1.830948971
215643_at	223117	SEMA3D	sema domain, immunoglobulin domain (Ig), short basic domain, secreted, (semaphorin) 3D	0.977345169
203122_at	51112	TTC15	tetratricopeptide repeat domain 15	-1.208989641
231068_at	146802	SLC47A2	solute carrier family 47, member 2	-1.501602291
239738_at	117154	DACH2	dachshund homolog 2 (Drosophila)	1.361110621
225651_at	7325	UBE2E2	ubiquitin-conjugating enzyme E2E 2 (UBC4/5 homolog, yeast)	1.451235296
244419_at	2487	FRZB	frizzled-related protein	1.045474278
219212_at	51182	HSPA14	heat shock 70kDa protein 14	0.825224502
206375_s_at	8988	HSPB3	heat shock 27kDa protein 3	1.769496044

219099_at	57103	C12orf5	chromosome 12 open reading frame 5	1.237422609
222613_at	57102	C12orf4	chromosome 12 open reading frame 4	1.105505079
212954_at	8798	DYRK4	dual-specificity tyrosine-(Y)-phosphorylation regulated kinase 4	1.57075808
226066_at	4286	MITF	microphthalmia-associated transcription factor	2.334568409
208606_s_at	54361	WNT4	wingless-type MMTV integration site family, member 4	0.859407907

Table-S2A. Activation scores, associated p-value and metadata of Rembrandt samples identified as (+) or (-) based on the OA GPC signature

Samples	Activation Score	Normalized Score	p-value	Age	Survival (mths)	Status	Histology	Grade
HF0505	0.749457969	1	0.0271	35	3.2	1	GBM	IV
HF1246	0.732100118	0.976839461	0.003	65	0.2	1	ASTROCYTOMA	II
E08021	0.731966357	0.976660984	0.0097	40	81.5	1	OLIGODENDROGLIOMA	III
HF1269	0.694346941	0.926465486	0.0014	55	13	1	GBM	IV
HF0599	0.688132241	0.918173226	0.0444	70	42.8	1	OLIGODENDROGLIOMA	II
E10193	0.680597094	0.908119098	0.0269	50	34.2	NA	GBM	IV
HF1502	0.654386806	0.873146771	0.0595	70	6.4	1	OLIGODENDROGLIOMA	III
HF1032	0.640376005	0.854452194	0.0471	40	28.1	1	ASTROCYTOMA	III
HF1227	0.632969918	0.844570269	0.018	50	251.7	0	OLIGODENDROGLIOMA	II
E09688	0.624472362	0.833232	0.0144	55	50.8	1	MIXED	II
E09787	0.622652421	0.830803657	6.00E-04	55	86.5	0	GBM	IV
HF0180	0.616102353	0.822063916	0.0479	35	0.3	1	GBM	IV
E09956	0.603754355	0.805588012	0.001	70	21	1	GBM	IV
HF1587	0.590356299	0.787711017	0.0511	30	75.3	0	ASTROCYTOMA	III
E10184	0.586292819	0.782289125	0.0947	30	28.3	1	GBM	IV
HF0087	0.586151619	0.782100723	0.0099	60	78.8	1	ASTROCYTOMA	III
E09606	0.584952923	0.780501305	0.0162	30	13.3	1	GBM	IV
E09515	0.584812915	0.780314493	0.0474	35	65.4	0	ASTROCYTOMA	II/III
E09278	0.58381164	0.778978494	0.0363	40	36.6	0	GBM	IV
HF0963	0.575711213	0.768170114	0.04	10	10.6	1	GBM	IV
HF1493	0.57332728	0.764989237	0.0684	65	41.9	1	OLIGODENDROGLIOMA	III
E10252	0.569847595	0.760346302	0.0644	55	53	1	GBM	IV

E09670	0.566785165	0.756260108	0.0575	75	14.2	1	GBM	IV
E09454	0.565155368	0.754085474	0.0828	55	18	1	GBM	IV
E09846	0.559234143	0.746184798	0.0508	65	14.3	1	GBM	IV
HF0285	0.558833826	0.745650656	0.0393	80	14.4	1	OLIGODENDROGLIOMA	II
E10312	0.557733116	0.744181981	0.0856	35	37.9	1	GBM	IV
HF1677	0.557606793	0.744013429	0.0491	50	63.5	0	ASTROCYTOMA	II
E09930	0.557353343	0.743675251	0.0686	50	5.1	1	GBM	IV
HF0026	0.554987055	0.740517919	0.0633	60	57.1	1	ASTROCYTOMA	II
HF0252	0.554987055	0.740517919	0.0552	35	123.1	0	ASTROCYTOMA	II
E09938	0.554812915	0.740285564	0.0303	45	25.2	1	GBM	IV
E09893	0.554807183	0.740277916	0.0153	40	111.9	1	OLIGODENDROGLIOMA	III
E10072	0.550695692	0.734791963	0.0179	65	37.2	0	OLIGODENDROGLIOMA	II/III
E09513	0.544168132	0.726082255	0.0911	55	13.4	1	OLIGODENDROGLIOMA	II/III
HF0251	0.5391027	0.719323462	0.0012	65	22.7	1	OLIGODENDROGLIOMA	III
E09920	0.537674994	0.717418476	0.0367	25	59.4	1	ASTROCYTOMA	III
HF1058	0.530737231	0.708161435	0.0242	40	18	1	GBM	IV
HF1511	0.526839197	0.702960298	0.0256	25	56.6	1	ASTROCYTOMA	II
E09262	0.525938162	0.701758049	0	50	13.6	1	MIXED	II/III
HF0434	0.52223726	0.696819944	0.0083	60	6.1	1	ASTROCYTOMA	II
HF1667	0.519023712	0.692532115	0.0019	60	2.5	1	GBM	IV
HF0445	0.515744412	0.688156552	0.0388	40	47.2	1	GBM	IV
E09212	0.507821892	0.677585553	0	40	7.1	1	ASTROCYTOMA	II/III
E09601	0.503894105	0.672344716	0.0034	70	13.2	1	GBM	IV
E09921	0.497126104	0.663314188	0.0602	40	36.4	0	ASTROCYTOMA	II/III
HF1489	0.496517546	0.662502191	0.0539	50	68.3	1	ASTROCYTOMA	II
E10258	0.488339677	0.651590479	0.0539	50	20.6	1	GBM	IV
HF0936	0.488324253	0.651569899	0.0039	55	5.1	1	ASTROCYTOMA	II
E09988	0.484443639	0.646392006	0.0127	70	64.6	1	OLIGODENDROGLIOMA	III
HF0962	0.483030037	0.644505839	0.0278	45	116.5	0	OLIGODENDROGLIOMA	II
E09605	0.480872441	0.641626964	0.0053	45	59.3	1	GBM	IV
HF1492	0.468710079	0.625398754	0.0344	30	2.2	1	GBM	IV
HF0953	0.466790317	0.622837219	0.0829	35	44.6	1	ASTROCYTOMA	II
E09818	0.464049666	0.619180375	0.0338	30	38.1	0	ASTROCYTOMA	II/III

E09531	0.462403898	0.61698443	8.00E-04	55	19.3	1	ASTROCYTOMA	II/III
E09664	0.461318096	0.615535648	0.0155	40	27.1	1	OLIGODENDROGLIOMA	II/III
HF0022	0.459908744	0.613655152	0.0678	20	133.9	0	ASTROCYTOMA	II
HF0914	0.452628786	0.603941522	0.032	40	146.9	0	ASTROCYTOMA	II
E10551	0.451868661	0.602927288	0.0669	65	12.3	1	GBM	IV
E09907B	0.443791064	0.59214937	0.0024	60	55.2	1	GBM	IV
HF1345	0.433641331	0.578606606	0.0145	15	83.5	0	ASTROCYTOMA	II
HF1588	0.431310239	0.575496235	0.0735	40	75.2	0	ASTROCYTOMA	II
E09802	0.429940365	0.573668415	0.0306	80	32.2	1	GBM	IV
HF1585	0.425210527	0.567357403	0.031	25	19.9	1	GBM	IV
HF0520	0.422798129	0.564138546	0.0122	40	8.7	1	GBM	IV
E09852	0.422437933	0.563657938	0.0288	50	48.3	1	GBM	IV
HF0108	0.420665649	0.561293184	0.0404	35	132	0	ASTROCYTOMA	III
E09192	0.404265925	0.53941107	0.0641	75	13.4	1	GBM	IV
HF0024	0.4034404	0.538309574	0.0562	45	5.8	1	GBM	IV
E09471	0.399568094	0.533142766	0.0065	70	27.2	1	ASTROCYTOMA	II
E10026	0.398363859	0.531535958	0.0281	65	15.4	1	GBM	IV
HF0608	0.398032902	0.531094363	0.0107	50	10.6	1	ASTROCYTOMA	II
E09690	0.389382233	0.519551795	0.0354	75	62.3	0	GBM	IV
E09647	0.382230723	0.510009552	0.0426	55	19.3	1	GBM	IV
E10144	0.380705674	0.507974683	0.0099	50	25.9	1	GBM	IV
HF1409	0.379186615	0.505947806	0.0143	50	12.7	1	ASTROCYTOMA	III
E09661	0.376503249	0.502367397	0.0076	65	48.5	0	OLIGODENDROGLIOMA	II
E09867	0.368241369	0.49134359	0.0267	75	38.7	0	OLIGODENDROGLIOMA	II
HF0778	0.363984009	0.485663005	0.0013	65	8.1	1	ASTROCYTOMA	II
HF1262	0.357766443	0.477366921	0.0163	30	23.7	1	GBM	IV
HF1178	0.356451664	0.475612614	0.0369	35	15.8	1	GBM	IV
HF0152	0.341086864	0.455111398	0.0564	30	131.5	0	ASTROCYTOMA	III
HF0543	0.334896186	0.44685119	0.049	30	67.6	0	GBM	IV
HF0996	0.322142945	0.429834571	0.0493	50	120.5	0	GBM	IV
HF0138	0.306071311	0.408390229	0.0594	60	1.2	1	GBM	IV
HF1509	-0.299523658	-0.386689141	0.0852	40	2.7	1	GBM	IV
HF1517	-0.304781874	-0.393477569	0.0358	55	8.3	1	GBM	IV

HF1078	-0.31280225	-0.403831985	0.0685	50	22.8	1	GBM	IV
HF0790	-0.317019359	-0.40927633	0.0439	45	7.5	1	GBM	IV
HF0855	-0.323567174	-0.417729649	0.0293	55	13.7	1	ASTROCYTOMA	II
HF0510	-0.336784038	-0.434792801	0.0494	45	19.6	1	OLIGODENDROGLIOMA	II
HF0894	-0.337132125	-0.435242187	0.0477	40	14.1	1	GBM	IV
HF0835	-0.34490649	-0.445278998	0.0021	20	45.3	1	OLIGODENDROGLIOMA	II
E10031	-0.352909446	-0.455610923	0.0213	55	27.5	1	GBM	IV
HF0327	-0.362469071	-0.467952531	0.0057	75	19.6	1	OLIGODENDROGLIOMA	II
E09917	-0.367243861	-0.47411685	0.0036	50	6.1	1	GBM	IV
HF0960	-0.383971676	-0.495712688	0.033	45	88.7	1	OLIGODENDROGLIOMA	II
HF0408	-0.387273163	-0.499974953	4.00E-04	30	15.8	1	GBM	IV
HF1090	-0.395275411	-0.510305964	0.0306	50	8.5	1	OLIGODENDROGLIOMA	III
HF0450	-0.407202966	-0.525704601	0.0508	30	29.5	1	ASTROCYTOMA	II
E09791	-0.416213927	-0.537337876	0.0619	60	13.4	1	GBM	IV
E09730	-0.419038557	-0.540984511	0.0168	40	61.7	1	GBM	IV
HF0442.5	-0.422172569	-0.545030563	0.0252	30	19.6	1	GBM	IV
HF1122	-0.440157815	-0.568249762	0.0091	40	7.3	1	GBM	IV
HF1534	-0.445761091	-0.575483669	0.0165	20	7.8	1	GBM	IV
HF1057	-0.450285554	-0.581324812	1.00E-04	55	24.5	1	OLIGODENDROGLIOMA	III
HF1671	-0.453315816	-0.585236922	0.0711	50	13.3	1	GBM	IV
HF0031	-0.462637223	-0.597270985	0.0601	35	0.5	1	GBM	IV
E10300	-0.46358746	-0.598497754	0.0218	60	9.4	1	GBM	IV
HF0702	-0.480207693	-0.619954703	0.0205	50	8.5	1	ASTROCYTOMA	III
E10102	-0.485464009	-0.626740679	0.014	45	38.8	0	GBM	IV
E10271	-0.485974839	-0.627400166	0.0716	30	12.5	1	GBM	IV
HF0460	-0.491378375	-0.634376206	0.0796	45	10.7	1	OLIGODENDROGLIOMA	III
E09348	-0.496743594	-0.641302777	0.0536	35	18.5	1	GBM	IV
E09139	-0.497586056	-0.642390407	0.028	45	36.5	1	GBM	IV
HF1186	-0.500533627	-0.646195762	0.0111	30	20.1	1	ASTROCYTOMA	III
HF1185	-0.506307341	-0.653649705	0.0285	25	95.2	0	ASTROCYTOMA	III
HF1344	-0.506640166	-0.654079386	0.061	60	9	1	ASTROCYTOMA	II
HF0990	-0.508177096	-0.656063585	0	NA	88.3	1	GBM	IV
HF1608	-0.510846262	-0.659509514	0.0827	60	7.9	1	GBM	IV

E10483	-0.513600598	-0.663065399	0.0754	25	66.4	1	ASTROCYTOMA	II
HF1538	-0.521697579	-0.673518713	0.0756	55	3.2	1	GBM	IV
HF1286	-0.530642368	-0.685066558	0.0333	75	13.2	1	ASTROCYTOMA	III
HF1618	-0.537184	-0.693511895	0.022	50	2.4	1	GBM	IV
HF0816	-0.543687185	-0.701907595	0.0361	60	46.7	1	OLIGODENDROGLIOMA	III
E50074	-0.546405102	-0.705416463	0.0368	50	5.4	1	GBM	IV
HF1382	-0.551104735	-0.711483754	0.0141	35	48.3	1	GBM	IV
E09967	-0.574153706	-0.741240291	0.002	45	4.4	1	GBM	IV
E09610	-0.57500937	-0.742344965	0.0061	55	12.5	1	GBM	IV
E10227	-0.601182757	-0.776135166	0.008	45	12.6	1	GBM	IV
HF0066	-0.601470694	-0.776506897	0.0016	50	9.1	1	GBM	IV
HF0986	-0.603858685	-0.779589825	2.00E-04	15	62.4	1	GBM	IV
HF1139	-0.628805522	-0.811796533	0.0117	40	15.8	1	GBM	IV
HF1191	-0.64276171	-0.829814163	7.00E-04	25	0.3	1	GBM	IV
HF1150	-0.651136485	-0.840626112	0	70	21.2	1	ASTROCYTOMA	III
HF0142	-0.6526464	-0.842575432	0.0021	25	0.3	1	GBM	IV
E09833B	-0.661856328	-0.854465576	0.0192	45	20.8	1	GBM	IV
HF1297	-0.665978187	-0.859786953	0	60	17.2	1	GBM	IV
E09966	-0.678273537	-0.875660417	0.0042	55	17.7	1	ASTROCYTOMA	III
HF0184	-0.681526594	-0.879860159	0	65	12	1	OLIGODENDROGLIOMA	III
HF1628	-0.684914765	-0.884234334	0.084	70	14.6	1	GBM	IV
E10284	-0.686683443	-0.886517721	0.0026	55	4.8	1	GBM	IV
E10267	-0.686925784	-0.886830587	0.004	75	12	1	GBM	IV
HF1077	-0.702421737	-0.906836074	5.00E-04	45	73.4	1	GBM	IV
HF1490	-0.722523361	-0.932787546	0.073	65	4	1	ASTROCYTOMA	III
HF1589	-0.774585129	-1	0.0162	25	3.3	1	GBM	IV

Table-S2B. Activation scores, associated p-value and metadata of Gravendeel samples identified as (+) or (-) based on the OA GPC signature

Samples	Activation Score	Normalized Score	p-value	Age	Survival (yrs)	Status	Histology	Grade	CHR1p	CHR19q	EGFR
GSM405355	0.801064034	1	0.0074	73	1.19	1	ASTROCYTOMA	II	NA	NA	NA
GSM405256	0.737876569	0.921120582	0.0866	38	4.79	1	ASTROCYTOMA	II	no LOH	no LOH	wild type
GSM405461	0.716299484	0.894185051	0.0947	49	0.76	1	GBM	IV	LOH	LOH	wild type
GSM405246	0.682859857	0.852441038	0.0305	33	6.31	1	GBM	IV	LOH	LOH	NA
GSM405203	0.66280444	0.827405066	0.0025	39	8.92	1	OLIGODENDROGLIOMA	III	LOH	LOH	wild type
GSM405212	0.658658913	0.82223004	0.02	23	17.49	1	OLIGODENDROGLIOMA	III	LOH	LOH	wild type
GSM405370	0.643329952	0.803094291	0.0192	47	1.61	1	GBM	IV	no LOH	no LOH	wild type
GSM405318	0.634974336	0.792663644	0.0118	62	6.21	0	OLIGODENDROGLIOMA	III	no LOH	no LOH	NA
GSM405216	0.615021607	0.76775586	0.0045	52	3.28	1	GBM	IV	NA	no LOH	wild type
GSM405207	0.605455573	0.755814201	0.0052	44	8.12	1	OLIGODENDROGLIOMA	III	LOH	LOH	wild type
GSM405409	0.59181949	0.738791739	0.0477	54	10.36	1	OLIGODENDROGLIOMA	III	LOH	LOH	NA
GSM405324	0.566705887	0.707441431	0.0436	14	0.67	1	GBM	IV	no LOH	no LOH	amplification
GSM405234	0.554016145	0.691600324	4.00E-04	58	0.62	1	GBM	IV	NA	NA	NA
GSM405283	0.538231934	0.671896267	0.0183	38	4.07	1	OLIGOASTROCYTOMA	III	LOH	LOH	wild type
GSM405205	0.533253927	0.665682023	0.0317	48	3.24	1	OLIGODENDROGLIOMA	III	LOH	LOH	wild type
GSM405386	0.521886757	0.651491935	0.0114	54	3.76	1	OLIGODENDROGLIOMA	II	LOH	LOH	wild type
GSM405325	0.519420906	0.648413715	0.0449	43	3.65	1	OLIGOASTROCYTOMA	III	NA	NA	wild type
GSM405441	0.517104497	0.64552205	0.0178	45	3.27	0	OLIGODENDROGLIOMA	II	LOH	LOH	wild type
GSM405204	0.516167462	0.644352312	0.0954	34	8.59	1	OLIGODENDROGLIOMA	III	LOH	LOH	wild type
GSM405320	0.515438603	0.643442448	0.017	70	0.6	1	GBM	IV	NA	NA	wild type
GSM405411	0.507483079	0.633511251	5.00E-04	38	0.05	1	ASTROCYTOMA	III	LOH	no LOH	NA
GSM405217	0.506733901	0.632576024	0.0389	33	6.77	0	GBM	IV	NA	no LOH	wild type
GSM405314	0.504431242	0.629701523	2.00E-04	54	0.65	1	GBM	IV	no LOH	LOH	wild type
GSM405343	0.489292619	0.610803379	0.0816	67	NA	0	GBM	IV	NA	NA	wild type
GSM405457	0.486971348	0.607905645	0.0523	71	0.3	1	OLIGODENDROGLIOMA	III	no LOH	no LOH	wild type
GSM405287	0.486856457	0.607762221	0.0345	44	6.87	1	OLIGODENDROGLIOMA	III	LOH	LOH	wild type
GSM405330	0.483717775	0.603844081	0.0869	33	0.71	1	GBM	IV	no LOH	NA	wild type
GSM405261	0.476668599	0.595044314	0.0015	60	0.98	1	OLIGODENDROGLIOMA	III	no LOH	no LOH	NA
GSM405227	0.47341699	0.590985202	0.07	48	4.77	1	OLIGODENDROGLIOMA	III	NA	NA	NA

GSM405243	0.470390141	0.587206667	0.0156	61	0.88	1	GBM	IV	NA	NA	NA
GSM405395	0.464586642	0.579961928	0.0425	55	3.76	1	OLIGOASTROCYTOMA	II	LOH	LOH	wild type
GSM405382	0.459041423	0.573039611	0.0015	44	4.86	1	OLIGOASTROCYTOMA	III	LOH	LOH	NA
GSM405420	0.458788616	0.572724023	0.0413	50	3	1	OLIGODENDROGLIOMA	III	no LOH	no LOH	wild type
GSM405278	0.458173812	0.571956538	2.00E-04	58	0.73	1	GBM	IV	NA	NA	amplification
GSM405462	0.454461768	0.567322647	0.0601	50	7.52	1	ASTROCYTOMA	II	LOH	LOH	NA
GSM405415	0.438470443	0.547360042	0.0062	67	0.5	1	GBM	IV	no LOH	no LOH	NA
GSM405301	0.426132041	0.531957526	0.0979	65	0.3	1	GBM	IV	NA	NA	NA
GSM405465	0.420244949	0.524608435	0.0242	69	0.63	1	GBM	IV	NA	no LOH	NA
GSM405211	0.419707136	0.523937062	0.0445	35	1.83	1	OLIGODENDROGLIOMA	III	LOH	LOH	NA
GSM405342	0.417912408	0.521696632	0.0872	47	2.99	1	OLIGODENDROGLIOMA	III	NA	NA	wild type
GSM405396	0.416841065	0.520359231	0.0331	77	0.02	1	GBM	IV	no LOH	no LOH	NA
GSM405403	0.415940255	0.519234715	0.0034	38	0.04	1	ASTROCYTOMA	III	NA	NA	NA
GSM405333	0.40417074	0.504542362	0.0697	58	9.11	1	OLIGODENDROGLIOMA	III	LOH	LOH	wild type
GSM405249	0.40304092	0.503131964	0.002	23	0.04	1	GBM	IV	NA	NA	wild type
GSM405475	0.39505561	0.493163584	0.0501	34	1.05	1	GBM	IV	NA	NA	wild type
GSM405481	0.392048822	0.489410092	0.0018	34	10.37	0	PILOCYTIC ASTROCYTOMA	I	NA	NA	NA
GSM405268	0.385988137	0.481844298	0.0039	48	0.64	1	GBM	IV	no LOH	no LOH	amplification
GSM405311	0.381022431	0.47564541	0.0427	43	7.48	0	ASTROCYTOMA	II	NA	NA	NA
GSM405265	0.377448173	0.471183522	0.0795	32	1.81	1	ASTROCYTOMA	III	NA	NA	wild type
GSM405483	0.373761793	0.466581668	0.0012	32	0.19	0	PILOCYTIC ASTROCYTOMA	I	NA	NA	NA
GSM405334	0.364091978	0.454510454	0.0214	57	1.47	1	OLIGODENDROGLIOMA	III	no LOH	no LOH	wild type
GSM405321	0.363960116	0.454345846	0.0406	34	3.97	1	ASTROCYTOMA	III	NA	NA	wild type
GSM405459	0.36310793	0.453282028	0.0099	64	1.14	1	GBM	IV	no LOH	no LOH	NA
GSM405210	0.348355938	0.434866532	0.0782	39	10.28	1	OLIGODENDROGLIOMA	III	LOH	LOH	wild type
GSM405464	0.340105521	0.424567209	0.0132	55	0.56	1	GBM	IV	NA	NA	NA
GSM405250	0.317464016	0.39630292	0.0848	31	1.48	1	ASTROCYTOMA	II	NA	NA	NA
GSM405466	0.302478925	0.377596437	0.0725	67	0.28	1	GBM	IV	no LOH	no LOH	NA
GSM405377	0.28692836	0.35818405	0.0854	42	0.6	1	OLIGODENDROGLIOMA	III	LOH	LOH	NA
GSM405356	-0.342749828	-0.460064457	0.0371	43	0.18	1	GBM	IV	NA	no LOH	wild type
GSM405298	-0.349169162	-0.468680968	0.0271	43	1.96	1	OLIGOASTROCYTOMA	III	no LOH	no LOH	NA

GSM405240	-0.351520541	-0.471837164	0.0206	33	6.62	0	GBM	IV	no LOH	no LOH	NA
GSM405391	-0.371763333	-0.499008553	0.0328	56	1.05	1	GBM	IV	no LOH	no LOH	NA
GSM405339	-0.373760087	-0.501688746	0.0043	78	NA	0	GBM	IV	NA	NA	amplification
GSM405436	-0.375071936	-0.503449608	0.0199	79	0.48	1	GBM	IV	NA	NA	NA
GSM405450	-0.379106436	-0.508865015	0.0134	37	13.3	0	OLIGOASTROCYTOMA	III	NA	NA	NA
GSM405372	-0.380450453	-0.510669056	0.0961	37	3.32	1	GBM	IV	LOH	LOH	NA
GSM405439	-0.381414955	-0.511963683	0.0096	33	3.7	0	OLIGOASTROCYTOMA	II	no LOH	NA	wild type
GSM405384	-0.383888277	-0.515283561	0.0174	70	0.02	0	GBM	IV	no LOH	no LOH	NA
GSM405424	-0.401716738	-0.539214255	0.0365	33	3.2	1	ASTROCYTOMA	II	no LOH	no LOH	wild type
GSM405230	-0.430676082	-0.578085652	0.0297	63	0.47	1	GBM	IV	no LOH	no LOH	NA
GSM405438	-0.433696491	-0.582139871	0.0301	43	2.3	1	GBM	IV	LOH	LOH	NA
GSM405388	-0.444215467	-0.596259227	0.0413	79	0.53	1	OLIGOASTROCYTOMA	III	no LOH	no LOH	amplification
GSM405337	-0.445057768	-0.597389827	0.0197	15	0.28	1	GBM	IV	NA	NA	amplification
GSM405440	-0.445411877	-0.597865138	0.0352	70	0.53	1	GBM	IV	NA	NA	wild type
GSM405326	-0.450820952	-0.605125604	0.0235	75	0.27	1	GBM	IV	NA	NA	amplification
GSM405422	-0.459443511	-0.616699447	0.034	71	0.91	1	GBM	IV	no LOH	no LOH	NA
GSM405294	-0.465957579	-0.625443117	0.0319	56	0.8	1	GBM	IV	partial LOH	partial LOH	amplification
GSM405476	-0.466653593	-0.626377359	0.0131	65	1.31	1	OLIGOASTROCYTOMA	III	no LOH	no LOH	amplification
GSM405443	-0.486639715	-0.653204227	0.0605	57	0.98	1	GBM	IV	NA	NA	amplification
GSM405312	-0.491071311	-0.659152647	0.0293	61	1.02	1	GBM	IV	NA	NA	amplification
GSM405226	-0.512661405	-0.688132486	0.0028	49	0.28	1	OLIGOASTROCYTOMA	III	no LOH	LOH	amplification
GSM405474	-0.524231599	-0.703662865	0.0344	61	0.29	1	GBM	IV	NA	NA	amplification
GSM405390	-0.554141148	-0.743809699	0.0917	70	0.02	1	OLIGOASTROCYTOMA	III	NA	NA	NA
GSM405405	-0.581116167	-0.780017587	0.0126	71	0.61	1	GBM	IV	no LOH	LOH	NA
GSM405267	-0.591581464	-0.794064892	0.0358	53	0.65	1	GBM	IV	no LOH	NA	NA
GSM405292	-0.605376456	-0.812581563	0	66	1.11	1	GBM	IV	NA	NA	amplification
GSM405347	-0.616268217	-0.827201299	0.0143	43	0.19	1	OLIGOASTROCYTOMA	III	NA	NA	amplification
GSM405428	-0.622239739	-0.835216722	0.0052	71	0.79	1	GBM	IV	no LOH	no LOH	amplification
GSM405376	-0.637951306	-0.856305963	0.016	53	1.85	1	GBM	IV	no LOH	NA	amplification
GSM405289	-0.67705098	-0.908788469	0.003	37	0.19	1	ASTROCYTOMA	III	NA	NA	amplification
GSM405352	-0.715537781	-0.960448333	0.0752	70	0.4	1	GBM	IV	NA	NA	amplification

Table-S3. Probesets in the NNI8 Stem vs Tumor Gene Signature

Probeset ID	Entrez Gene ID	Gene Symbol	Description	Log Fold Change
1553635_s_at	200132	TCTEX1D1	Tctex1 domain containing 1	-6.215791136
209156_s_at	1292	COL6A2	collagen, type VI, alpha 2	-6.493620158
209448_at	10553	HTATIP2	HIV-1 Tat interactive protein 2, 30kDa	-6.42297587
222484_s_at	9547	CXCL14	chemokine (C-X-C motif) ligand 14	-8.105582051
202018_s_at	4057	LTF	lactotransferrin	-8.54583883
230422_at	2359	FPR3	formyl peptide receptor 3	-7.35868863
203032_s_at	2271	FH	fumarate hydratase	6.389162912
204122_at	7305	TYROBP	TYRO protein tyrosine kinase binding protein	-7.451463342
213975_s_at	4069	LYZ	lysozyme	-8.567997622
204570_at	1346	COX7A1	cytochrome c oxidase subunit VIIa polypeptide 1 (muscle)	-6.10959307
204158_s_at	10312	TCIRG1	T-cell, immune regulator 1, ATPase, H+ transporting, lysosomal V0 subunit A3	-6.005341469
209183_s_at	11067	C10orf10	chromosome 10 open reading frame 10	-6.05532165
209047_at	358	AQP1	aquaporin 1 (Colton blood group)	-6.969067359
205572_at	285	ANGPT2	angiopoietin 2	-7.511111563
236034_at	285	ANGPT2	angiopoietin 2	-6.482834194
235639_at	28513	CDH19	cadherin 19, type 2	6.235154529
209901_x_at	199	AIF1	allograft inflammatory factor 1	-6.32542485
213095_x_at	199	AIF1	allograft inflammatory factor 1	-7.499645133
215051_x_at	199	AIF1	allograft inflammatory factor 1	-7.64616928
1555460_a_at	25800	SLC39A6	solute carrier family 39 (zinc transporter), member 6	6.466383357
220311_at	29104	N6AMT1	N-6 adenine-specific DNA methyltransferase 1 (putative)	6.090119758
203240_at	8857	FCGBP	Fc fragment of IgG binding protein	-6.279670112
202628_s_at	5054	SERPINE1	serpin peptidase inhibitor, clade E (nexin, plasminogen activator inhibitor type 1), member 1	-6.169187776
201743_at	929	CD14	CD14 molecule	-9.061228844
225400_at	116461	TSEN15	tRNA splicing endonuclease 15 homolog (S. cerevisiae)	6.564806667
219386_s_at	56833	SLAMF8	SLAM family member 8	-6.439653705
218345_at	55365	TMEM176A	transmembrane protein 176A	-7.028336131
219167_at	51285	RASL12	RAS-like, family 12	-7.447403055
225502_at	81704	DOCK8	dedicator of cytokinesis 8	-6.431728356

234023_s_at	55835	CENPJ	centromere protein J	6.500186173
209619_at	972	CD74	CD74 molecule, major histocompatibility complex, class II invariant chain	-6.392605538
223434_at	2635	GBP3	guanylate binding protein 3	-7.428950443
207054_at	3617	IMPG1	interphotoreceptor matrix proteoglycan 1	-7.236493758
205374_at	6588	SLN	sarcolipin	-6.139099986
203535_at	6280	S100A9	S100 calcium binding protein A9	-6.508034002
203571_s_at	10974	C10orf116	chromosome 10 open reading frame 116	-6.322842462
204128_s_at	5983	RFC3	replication factor C (activator 1) 3, 38kDa	6.363690078
218559_s_at	9935	MAFB	v-maf musculoaponeurotic fibrosarcoma oncogene homolog B (avian)	-6.671432912
201842_s_at	2202	EFEMP1	EGF containing fibulin-like extracellular matrix protein 1	-6.040243322
212268_at	1992	SERPINB1	serpin peptidase inhibitor, clade B (ovalbumin), member 1	-6.972772922
209723_at	5272	SERPINB9	serpin peptidase inhibitor, clade B (ovalbumin), member 9	-6.55138368
223620_at	2857	GPR34	G protein-coupled receptor 34	-7.926594277
219607_s_at	51338	MS4A4A	membrane-spanning 4-domains, subfamily A, member 4	-8.180055654
226034_at	1846	DUSP4	dual specificity phosphatase 4	6.838468179
225314_at	132299	OCIAD2	OCIA domain containing 2	-8.275917817
204990_s_at	3691	ITGB4	integrin, beta 4	-6.364422156
203854_at	3426	CFI	complement factor I	-6.363714998
202310_s_at	1277	COL1A1	collagen, type I, alpha 1	-7.130038944
1556499_s_at	1277	COL1A1	collagen, type I, alpha 1	-9.238542552
213566_at	6039	RNASE6	ribonuclease, RNase A family, k6	-7.823580016
204482_at	7122	CLDN5	claudin 5	-6.460963571
221816_s_at	51131	PHF11	PHD finger protein 11	-6.825731298
239132_at	4842	NOS1	nitric oxide synthase 1 (neuronal)	-6.386282534
209395_at	1116	CHI3L1	chitinase 3-like 1 (cartilage glycoprotein-39)	-10.14439331
209396_s_at	1116	CHI3L1	chitinase 3-like 1 (cartilage glycoprotein-39)	-9.362700349
219719_at	51751	HIGD1B	HIG1 hypoxia inducible domain family, member 1B	-6.669433848
203540_at	2670	GFAP	glial fibrillary acidic protein	-7.35128303
201721_s_at	7805	LAPTM5	lysosomal protein transmembrane 5	-6.25877809
232887_at	644139	PIRT	phosphoinositide-interacting regulator of transient receptor potential channels	-6.331567906
204787_at	11326	VSIG4	V-set and immunoglobulin domain containing 4	-7.189520229
208161_s_at	8714	ABCC3	ATP-binding cassette, sub-family C (CFTR/MRP), member 3	-6.929235405
210055_at	7253	TSHR	thyroid stimulating hormone receptor	-6.141153984

202859_x_at	3576	IL8	interleukin 8	-8.035544596
235417_at	90853	SPOCD1	SPOC domain containing 1	-6.444542888
203835_at	2615	LRRC32	leucine rich repeat containing 32	-6.267902391
202238_s_at	4837	NNMT	nicotinamide N-methyltransferase	-6.6617682
202237_at	4837	NNMT	nicotinamide N-methyltransferase	-7.208303354
229391_s_at	441168	FAM26F	family with sequence similarity 26, member F	-6.297620939
223467_at	51655	RASD1	RAS, dexamethasone-induced 1	-8.103012345
239461_at	117248	GALNTL2	UDP-N-acetyl-alpha-D-galactosamine:polypeptide N-acetylgalactosaminyltransferase-like 2	-7.696742518
228501_at	117248	GALNTL2	UDP-N-acetyl-alpha-D-galactosamine:polypeptide N-acetylgalactosaminyltransferase-like 2	-6.995008809
205786_s_at	3684	ITGAM	integrin, alpha M (complement component 3 receptor 3 subunit)	-6.272756493
208747_s_at	716	C1S	complement component 1, s subcomponent	-8.132346089
201859_at	5552	SRGN	serglycin	-8.765885577
201858_s_at	5552	SRGN	serglycin	-8.111413158
207397_s_at	3239	HOXD13	homeobox D13	6.35025642
1568604_a_at	8618	CADPS	Ca++-dependent secretion activator	-7.030383795
231068_at	146802	SLC47A2	solute carrier family 47, member 2	-8.52812485
215049_x_at	9332	CD163	CD163 molecule	-7.402833043
218729_at	56925	LXN	latexin	-6.457187984
209875_s_at	6696	SPP1	secreted phosphoprotein 1	-7.285379742
200986_at	710	SERPING1	serpin peptidase inhibitor, clade G (C1 inhibitor), member 1	-8.060359753
225353_s_at	714	C1QC	complement component 1, q subcomponent, C chain	-7.877615852
202953_at	713	C1QB	complement component 1, q subcomponent, B chain	-9.175565222

Table-S4. Results from Pathway Activation Score, Log Rank and Cox Regression analysis (NNI-8 GPC versus primary tumor gene signature)

Dataset	Connectivity Maps Analysis						Log Rank *p*-value	Multivariate Cox		Univariate Cox	
	# of probes	# of samples	(+)	(-)	total (+)(-)	%(+)(-)		Hazard Ratio	*p*-value	Hazard Ratio	*p*-value
REMBRANDT	84	298	80	54	134	44.97	0.007	0.671 (0.455-0.989)	0.044	0.596 (0.406-0.874)	0.008
Gravendeel	84	276	86	77	163	59.06	0.0007	0.691 (0.488-0.977)	0.036	0.567 (0.407-0.791)	0.0008

(+) represent patients with concordance to GPC signature; (-) represent patients with inverse gene expression relationship to GPC signature

Table-S5A. Activation scores, associated p-value and metadata of Rembrandt samples identified as (+) or (-) based on the NNI-8 GPC versus primary tumor signature

Samples	Activation Score	Normalized Score	p-value	Age	Survival (mths)	Status	Histology	Grade
E08021	1.522597165	1	0	40	81.5	1	OLIGODENDROGLIOMA	III
E09448	1.422752629	0.934424851	0	60	229.1	1	OLIGODENDROGLIOMA	III
HF0891	1.303831733	0.856320873	0	35	28.8	1	GBM	IV
HF0142	1.288468221	0.84623054	0	25	0.3	1	GBM	IV
HF0066	1.216406036	0.798902076	0	50	9.1	1	GBM	IV
E10110	1.176753544	0.772859408	0	50	23.1	1	GBM	IV
HF0996	1.119487883	0.735248895	0	50	120.5	0	GBM	IV
E09804	1.103850023	0.724978378	0	70	42.4	0	OLIGODENDROGLIOMA	II
HF1136	1.084938272	0.712557659	0	35	45.3	1	ASTROCYTOMA	III
HF0108	1.077128487	0.707428407	0	35	132	0	ASTROCYTOMA	III
HF1227	1.074604481	0.705770709	0	50	251.7	0	OLIGODENDROGLIOMA	II
E10105	1.067544582	0.701133961	0	40	1.1	NA	ASTROCYTOMA	III
E09278	1.050937357	0.690226792	0	40	36.6	0	GBM	IV
HF0920	1.049199817	0.689085624	0	40	1	1	OLIGODENDROGLIOMA	II

E09867	1.04340192	0.685277724	0	75	38.7	0	OLIGODENDROGLIOMA	II
E09690	1.029117513	0.675896118	0	75	62.3	0	GBM	IV
E09893	1.027983539	0.675151355	0	40	111.9	1	OLIGODENDROGLIOMA	III
E09394	1.019807956	0.669781857	0	30	51.7	1	MIXED	III
HF1628	1.007590306	0.66175764	0	70	14.6	1	GBM	IV
E09802	0.99482396	0.653373054	0	80	32.2	1	GBM	IV
HF0184	0.987032465	0.648255814	0	65	12	1	OLIGODENDROGLIOMA	III
HF0975	0.978033836	0.642345762	0	60	36.5	1	ASTROCYTOMA	III
HF0251	0.974357567	0.63993129	0	65	22.7	1	OLIGODENDROGLIOMA	III
HF1382	0.962780064	0.632327503	0	35	48.3	1	GBM	IV
HF1511	0.960128029	0.63058572	0	25	56.6	1	ASTROCYTOMA	II
E09722	0.958006401	0.629192293	0	50	28.5	1	GBM	IV
HF1587	0.919524463	0.603918412	0	30	75.3	0	ASTROCYTOMA	III
HF0180	0.911165981	0.598428791	0.0105	35	0.3	1	GBM	IV
HF1677	0.903978052	0.593707957	0	50	63.5	0	ASTROCYTOMA	II
E09656	0.891229995	0.585335383	0	65	34.1	1	OLIGODENDROGLIOMA	III
HF1551	0.888523091	0.583557563	0	30	70.9	0	ASTROCYTOMA	II
E10299	0.878079561	0.576698539	0	40	44.6	0	ASTROCYTOMA	II/III
HF1613	0.870233196	0.571545262	0	35	66.8	1	ASTROCYTOMA	III
E10013	0.860045725	0.564854411	5.00E-04	55	4.9	1	GBM	IV
E09855	0.850022862	0.55827167	0.0247	25	38.4	0	ASTROCYTOMA	III
E10252B	0.846566072	0.556001345	0	55	53	1	GBM	IV
E09988	0.84526749	0.555148472	0	70	64.6	1	OLIGODENDROGLIOMA	III
HF0702	0.831184271	0.545899001	0.0011	50	8.5	1	ASTROCYTOMA	III
E09818	0.829263832	0.544637709	0	30	38.1	0	ASTROCYTOMA	II/III
E09997	0.827471422	0.543460504	0	35	46.9	0	ASTROCYTOMA	II/III
E09966	0.822496571	0.540193158	0.002	55	17.7	1	ASTROCYTOMA	III
HF1469	0.821326017	0.539424371	0	25	22.2	1	GBM	IV
HF1640	0.81911294	0.537970882	0	50	5.5	1	GBM	IV
HF1295	0.80175583	0.526571209	0	55	19.1	1	ASTROCYTOMA	III
E09688	0.800877915	0.525994618	0	55	50.8	1	MIXED	II
E10267	0.789062643	0.518234672	0	75	12	1	GBM	IV
HF0408	0.770900777	0.506306458	0.0032	30	15.8	1	GBM	IV

E09454	0.760987654	0.499795791	0	55	18	1	GBM	IV
HF1344	0.758536808	0.498186143	0	60	9	1	ASTROCYTOMA	II
E10262	0.755884774	0.496444359	0.0074	50	18	1	GBM	IV
E09569	0.738052126	0.484732366	0	70	37.4	1	GBM	IV
E10211	0.736131687	0.483471074	0	85	28.4	1	GBM	IV
E09920	0.725761317	0.4766601	0.0074	25	59.4	1	ASTROCYTOMA	III
E10271	0.722981253	0.47483423	0.0044	30	12.5	1	GBM	IV
HF1191	0.715116598	0.469668941	6.00E-04	25	0.3	1	GBM	IV
E09959	0.713580247	0.468659908	0	50	46.4	1	ASTROCYTOMA	III
HF0966	0.709958848	0.466281472	2.00E-04	50	137.7	0	ASTROCYTOMA	III
E50123	0.674183813	0.442785412	0	30	17.5	1	GBM	IV
E10001	0.672610882	0.441752354	0	50	8.7	1	OLIGODENDROGLIOMA	III
HF0960	0.669666209	0.439818374	0	45	88.7	1	OLIGODENDROGLIOMA	II
E10252	0.666575217	0.437788295	0	55	53	1	GBM	IV
HF1490	0.665532693	0.437103594	0.0025	65	4	1	ASTROCYTOMA	III
HF0990	0.651906722	0.42815443	0	NA	88.3	1	GBM	IV
E09860	0.621490626	0.408177974	0	40	36.8	0	OLIGODENDROGLIOMA	II
HF1338	0.604572474	0.397066596	0	35	5.9	1	GBM	IV
E09956	0.604444444	0.39698251	0	70	21	1	GBM	IV
HF0963	0.566035665	0.371756679	0.009	10	10.6	1	GBM	IV
E09610	0.565743027	0.371564482	0.0243	55	12.5	1	GBM	IV
HF1057	0.554513032	0.364188929	0.0021	55	24.5	1	OLIGODENDROGLIOMA	III
E09623	0.547379973	0.359504132	3.00E-04	50	20.7	1	GBM	IV
E10184	0.541033379	0.355335864	0	30	28.3	1	GBM	IV
HF1487	0.530132602	0.348176533	0	50	9.9	1	OLIGODENDROGLIOMA	II
E09921	0.511476909	0.335923986	0	40	36.4	0	ASTROCYTOMA	II/III
HF0442.5	0.509044353	0.33432635	0.0137	30	19.6	1	GBM	IV
HF0992	0.496607225	0.326157986	2.00E-04	30	20	1	GBM	IV
E10144	0.477750343	0.313773304	0.0012	50	25.9	1	GBM	IV
E10138	0.459789666	0.301977225	2.00E-04	25	46.9	0	ASTROCYTOMA	II/III
E09801	0.459021491	0.301472708	5.00E-04	30	42.5	1	ASTROCYTOMA	III
HF0654	0.387965249	0.25480492	0.0299	20	14.6	1	GBM	IV
HF1357	0.382094193	0.250948972	0.0141	40	30.8	1	OLIGODENDROGLIOMA	III

HF0816	-0.432245085	-0.40731102	0.0376	60	46.7	1	OLIGODENDROGLIOMA	III
E09471	-0.454631916	-0.428406467	0.0028	70	27.2	1	ASTROCYTOMA	II
HF1534	-0.478372199	-0.450777291	7.00E-04	20	7.8	1	GBM	IV
E10226	-0.53223594	-0.501533901	0.0285	65	18.7	1	GBM	IV
E10031	-0.545569273	-0.514098101	0.0032	55	27.5	1	GBM	IV
HF0316	-0.551641518	-0.519820068	0	40	73.4	1	ASTROCYTOMA	II
HF0954.2	-0.593379058	-0.559149978	0	70	11	1	ASTROCYTOMA	III
HF0606	-0.612821216	-0.577470615	0	30	76.8	1	ASTROCYTOMA	II
E09451	-0.636707819	-0.599979318	0	60	5.3	1	GBM	IV
HF0024	-0.649272977	-0.611819655	0	45	5.8	1	GBM	IV
E09664	-0.661088249	-0.622953363	0.0094	40	27.1	1	OLIGODENDROGLIOMA	II/III
E09673	-0.665441244	-0.627055255	0	45	213.8	0	ASTROCYTOMA	II
E10158	-0.667142204	-0.628658095	0	70	40.6	0	GBM	IV
HF0844	-0.672281664	-0.633501086	0	30	63.8	1	ASTROCYTOMA	II
HF1538	-0.68349337	-0.644066044	0	55	3.2	1	GBM	IV
E10193	-0.687242798	-0.647599187	0	50	34.2	NA	GBM	IV
HF1671	-0.689437586	-0.649667368	0	50	13.3	1	GBM	IV
E10284	-0.691687243	-0.651787253	0	55	4.8	1	GBM	IV
HF1077	-0.697960677	-0.657698804	0	45	73.4	1	GBM	IV
HF1137	-0.711074531	-0.670056186	0	35	18.3	1	GBM	IV
E09430	-0.715354367	-0.674089139	0	45	32	1	GBM	IV
HF0543	-0.715628715	-0.674347661	0	30	67.6	0	GBM	IV
E09483	-0.715829904	-0.674537244	0	65	10.3	1	GBM	IV
E10514	-0.716671239	-0.675330047	0	75	23.7	1	GBM	IV
HF0089	-0.72698674	-0.685050498	0	65	7.9	1	ASTROCYTOMA	III
E10551	-0.734192958	-0.691841026	0	65	12.3	1	GBM	IV
E09661	-0.739515318	-0.696856365	0	65	48.5	0	OLIGODENDROGLIOMA	II
E10488	-0.758774577	-0.715004653	0	55	21.9	1	GBM	IV
E10103	-0.764389575	-0.72029575	0	50	3.3	1	ASTROCYTOMA	II/III
E09930	-0.772565158	-0.727999724	0	50	5.1	1	GBM	IV
E09531	-0.773699131	-0.729068284	0	55	19.3	1	ASTROCYTOMA	II/III
HF1178	-0.788367627	-0.742890628	0	35	15.8	1	GBM	IV
HF0936	-0.797567444	-0.751559753	0	55	5.1	1	ASTROCYTOMA	II

E09649	-0.804773663	-0.758350281	0	70	9.7	1	GBM	IV
HF0757	-0.813644262	-0.766709179	0	40	74.9	1	ASTROCYTOMA	II
HF0460	-0.816899863	-0.769776981	0	45	10.7	1	OLIGODENDROGLIOMA	III
HF1246	-0.829721079	-0.781858605	0	65	0.2	1	ASTROCYTOMA	II
E09602	-0.841481481	-0.792940609	0	60	4.1	1	GBM	IV
E10227	-0.845834476	-0.797042501	0	45	12.6	1	GBM	IV
E09239	-0.849419296	-0.80042053	0	30	63.3	1	ASTROCYTOMA	III
E09331	-0.864618198	-0.814742684	0	55	38.9	0	GBM	IV
E10290	-0.880951075	-0.830133398	0	30	6.9	1	GBM	IV
E10077	-0.88698674	-0.835820896	0	55	25.8	1	GBM	IV
E10300	-0.88870599	-0.837440971	0	60	9.4	1	GBM	IV
E09334	-0.89223594	-0.840767295	0	50	85.2	1	MIXED	III
E10305	-0.90434385	-0.852176761	0	40	10.1	1	GBM	IV
HF1585	-0.910068587	-0.857571266	0	25	19.9	1	GBM	IV
HF0953	-0.940283493	-0.886043225	0	35	44.6	1	ASTROCYTOMA	II
E09348	-0.942075903	-0.887732239	0	35	18.5	1	GBM	IV
E10002	-0.944691358	-0.890196822	0	55	8.4	1	GBM	IV
HF1356	-1.01733882	-0.958653614	0	50	13.5	1	GBM	IV
HF0608	-1.035354367	-0.975629933	0	50	10.6	1	ASTROCYTOMA	II
HF1220	-1.039433013	-0.979473303	0	35	10.4	1	GBM	IV
E09759	-1.061216278	-1	0	45	20.1	1	GBM	IV

Table-S5B. Activation scores, associated p-value and metadata of Gravendeel samples identified as (+) or (-) based on the NNI-8 GPC versus primary tumor signature

Samples	Activation Score	Normalized Score	p-value	Age	Survival (yrs)	Status	Histology	Grade	CHR1p	CHR19q	IDH1	EGFR
GSM405467	1.226995885	1	0	43.9	1.34	1	OLIGODENDROGLIOMA	III	no LOH	no LOH	mutation	wild type
GSM405476	1.216186557	0.991190412	0	64.97	1.31	1	OLIGOASTROCYTOMA	III	no LOH	no LOH	no mutation	amplification
GSM405475	1.200091449	0.978072921	0	33.74	1.05	1	GBM	IV	NA	NA	no mutation	wild type

GSM405431	1.147946959	0.935575232	0	80.65	0.92	1	GBM	IV	no LOH	no LOH	no mutation	wild type
GSM405210	1.13399177	0.924201771	0	38.53	10.28	1	OLIGODENDROGLIOMA	III	LOH	LOH	mutation	wild type
GSM405399	1.132766347	0.923203053	0	52.07	1.18	1	OLIGOASTROCYTOMA	III	no LOH	NA	no mutation	amplification
GSM405349	1.128376772	0.919625555	0	24.42	2.41	1	GBM	IV	NA	NA	no mutation	wild type
GSM405246	1.126127115	0.917792088	0	32.59	6.31	1	GBM	IV	LOH	LOH	mutation	NA
GSM405369	1.106776406	0.902021286	0	50.34	4.13	1	GBM	IV	LOH	LOH	mutation	wild type
GSM405201	1.089437586	0.887890171	0	44.57	9.82	1	OLIGODENDROGLIOMA	III	LOH	LOH	mutation	NA
GSM405208	1.088834019	0.887398265	0	51.4	3.04	1	OLIGODENDROGLIOMA	III	LOH	LOH	mutation	wild type
GSM405338	1.064581619	0.867632591	0	50.23	7.96	1	OLIGODENDROGLIOMA	II	LOH	LOH	mutation	wild type
GSM405370	1.054485597	0.859404347	0	46.52	1.61	1	GBM	IV	no LOH	no LOH	no mutation	wild type
GSM405323	1.005102881	0.819157499	0	58.78	0.62	1	GBM	IV	NA	NA	no mutation	amplification
GSM405319	1.003950617	0.818218406	0	53.65	5.62	1	OLIGODENDROGLIOMA	III	LOH	LOH	mutation	NA
GSM405257	1.000164609	0.815132815	0	46.04	10.86	0	OLIGODENDROGLIOMA	III	LOH	LOH	mutation	wild type
GSM405437	0.981545496	0.799958263	0	51.63	3.44	0	OLIGODENDROGLIOMA	II	NA	NA	mutation	NA
GSM405378	0.975290352	0.794860329	0	57.22	0	1	OLIGODENDROGLIOMA	II	NA	NA	no mutation	wild type
GSM405382	0.972491998	0.792579674	0	44.15	4.86	1	OLIGOASTROCYTOMA	III	LOH	LOH	NA	NA
GSM405227	0.967773205	0.788733864	0	48.1	4.77	1	OLIGODENDROGLIOMA	III	NA	NA	NA	NA
GSM405449	0.95820759	0.780937901	0	45.39	2.02	1	OLIGODENDROGLIOMA	III	LOH	LOH	no mutation	wild type
GSM405247	0.941362597	0.767209254	0	39.36	1.59	1	GBM	IV	no LOH	no LOH	no mutation	NA
GSM405420	0.939899406	0.766016755	0	49.94	3	1	OLIGODENDROGLIOMA	III	no LOH	no LOH	mutation	wild type
GSM405327	0.937796068	0.764302537	0	66.86	3.3	1	OLIGODENDROGLIOMA	III	LOH	LOH	mutation	wild type
GSM405329	0.936406036	0.763169663	0	60.33	5.02	1	OLIGODENDROGLIOMA	III	LOH	LOH	mutation	NA
GSM405212	0.936296296	0.763080225	0	23.33	17.49	1	OLIGODENDROGLIOMA	III	LOH	LOH	no mutation	wild type
GSM405204	0.929382716	0.757445667	0	33.89	8.59	1	OLIGODENDROGLIOMA	III	LOH	LOH	no mutation	wild type
GSM405283	0.896223137	0.730420654	0	38.07	4.07	1	OLIGOASTROCYTOMA	III	LOH	LOH	NA	wild type

GSM405234	0.882725194	0.719419849	0	57.68	0.62	1	GBM	IV	NA	NA	NA	NA
GSM405347	0.875793324	0.713770384	0	43.11	0.19	1	OLIGOASTROCYTOMA	III	NA	NA	mutation	amplification
GSM405441	0.871568358	0.710327043	0	44.74	3.27	0	OLIGODENDROGLIOMA	II	LOH	LOH	no mutation	wild type
GSM405308	0.868696845	0.707986763	0	47.4	3.1	0	GBM	IV	NA	NA	mutation	NA
GSM405377	0.859625057	0.700593268	0.007 1	41.98	0.6	1	OLIGODENDROGLIOMA	III	LOH	LOH	no mutation	NA
GSM405434	0.848870599	0.691828399	0	67.01	0.24	1	GBM	IV	NA	NA	NA	NA
GSM405386	0.84528578	0.688906776	0	53.85	3.76	1	OLIGODENDROGLIOMA	II	LOH	LOH	mutation	wild type
GSM405232	0.844078647	0.687922965	0	35.7	0.98	1	GBM	IV	no LOH	no LOH	mutation	wild type
GSM405223	0.839561043	0.684241123	0	53.26	1.92	1	GBM	IV	NA	NA	no mutation	amplification
GSM405207	0.835976223	0.6813195	0	44.41	8.12	1	OLIGODENDROGLIOMA	III	LOH	LOH	no mutation	wild type
GSM405366	0.833836305	0.67957547	0	75.13	2.21	1	OLIGODENDROGLIOMA	III	LOH	LOH	mutation	wild type
GSM405388	0.817704618	0.666428167	0	78.52	0.53	1	OLIGOASTROCYTOMA	III	no LOH	no LOH	no mutation	amplification
GSM405337	0.816479195	0.665429449	0	15.02	0.28	1	GBM	IV	NA	NA	no mutation	amplification
GSM405344	0.81571102	0.664803387	0	34.71	1.19	1	OLIGODENDROGLIOMA	II	partial LOH	no LOH	no mutation	wild type
GSM405253	0.794549611	0.647556867	4.00E -04	34.84	12.56	0	GBM	IV	no LOH	no LOH	no mutation	NA
GSM405330	0.794494742	0.647512149	0	33.12	0.71	1	GBM	IV	no LOH	NA	mutation	wild type
GSM405380	0.786465478	0.640968309	0	39.99	6.04	1	OLIGODENDROGLIOMA	III	LOH	LOH	mutation	wild type
GSM405289	0.767480567	0.625495632	0	37.44	0.19	1	ASTROCYTOMA	III	NA	NA	no mutation	amplification
GSM405341	0.766620942	0.624795039	0.072	71.11	0.63	1	OLIGOASTROCYTOMA	III	NA	NA	mutation	amplification
GSM405316	0.742386831	0.605044272	0	40.06	10.34	1	OLIGOASTROCYTOMA	III	NA	NA	no mutation	wild type
GSM405461	0.737997257	0.601466774	0	49.14	0.76	1	GBM	IV	LOH	LOH	no mutation	wild type
GSM405318	0.725358939	0.591166562	0	62.46	6.21	0	OLIGODENDROGLIOMA	III	no LOH	no LOH	mutation	NA
GSM405383	0.711970736	0.580255195	0.029	37.6	1.32	1	ASTROCYTOMA	II	no LOH	no LOH	no mutation	wild type

GSM405231	0.707599451	0.576692604	0.0017	62.96	1.26	1	GBM	IV	no LOH	no LOH	NA	NA
GSM405312	0.697082762	0.568121516	0	61.31	1.02	1	GBM	IV	NA	NA	no mutation	amplification
GSM405292	0.685980796	0.559073428	0	65.52	1.11	1	GBM	IV	NA	NA	no mutation	amplification
GSM405396	0.682414266	0.556166711	2.00E-04	77.31	0.02	1	GBM	IV	no LOH	no LOH	mutation	NA
GSM405309	0.682359396	0.556121993	0.004	54.6	0.26	1	GBM	IV	NA	NA	mutation	NA
GSM405220	0.668971193	0.545210625	0	54.12	1.27	1	GBM	IV	NA	NA	no mutation	wild type
GSM405225	0.667636031	0.54412247	0	31.56	3.47	1	OLIGOASTROCYTOMA	III	no LOH	no LOH	NA	wild type
GSM405249	0.660027435	0.537921474	0	23.02	0.04	1	GBM	IV	NA	NA	mutation	wild type
GSM405468	0.65395519	0.532972602	0	33.48	7.04	0	PILOCYTIC ASTROCYTOMA	I	NA	NA	no mutation	NA
GSM405215	0.651083676	0.530632323	0.0056	51.44	2.3	1	GBM	IV	no LOH	no LOH	no mutation	NA
GSM405460	0.644554184	0.525310795	0	52.52	0.48	1	OLIGODENDROGLIOMA	III	no LOH	no LOH	no mutation	amplification
GSM405303	0.643219021	0.52422264	0.0055	56.64	0.55	1	GBM	IV	NA	NA	no mutation	NA
GSM405352	0.638372199	0.520272486	0	69.95	0.4	1	GBM	IV	NA	NA	no mutation	amplification
GSM405427	0.633763146	0.516516114	0.0014	50.83	1.53	1	GBM	IV	NA	NA	NA	NA
GSM405262	0.63122085	0.514444146	0.0062	43.26	2.89	1	GBM	IV	NA	NA	no mutation	amplification
GSM405392	0.616680384	0.502593686	0.0161	48.35	0.47	1	GBM	IV	NA	no LOH	NA	NA
GSM405284	0.613260174	0.499806219	0	57.7	1.6	1	OLIGOASTROCYTOMA	III	no LOH	no LOH	NA	amplification
GSM405242	0.60696845	0.494678472	0.0119	30.33	0.18	1	GBM	IV	NA	NA	NA	NA
GSM405363	0.605724737	0.493664848	2.00E-04	48.84	9.79	1	GBM	IV	no LOH	no LOH	mutation	wild type
GSM405385	0.602487426	0.491026444	0	34.78	1.26	0	GBM	IV	no LOH	NA	mutation	NA
GSM405391	0.599725652	0.488775601	0.0071	55.55	1.05	1	GBM	IV	no LOH	no LOH	NA	NA
GSM405355	0.598171011	0.487508571	0.013	73.19	1.19	1	ASTROCYTOMA	II	NA	NA	no mutation	NA
GSM405222	0.590507545	0.481262857	0.0074	54.06	1.3	1	GBM	IV	NA	NA	NA	NA

GSM405372	0.572748057	0.466788898	0	37.12	3.32	1	GBM	IV	LOH	LOH	NA	NA
GSM405294	0.565852766	0.461169245	0	56.41	0.8	1	GBM	IV	partial LOH	partial LOH	no mutation	amplification
GSM405281	0.561847279	0.457904779	0	37.12	3.32	1	ASTROCYTOMA	III	NA	NA	no mutation	NA
GSM405205	0.557274806	0.454178219	0.006	48.03	3.24	1	OLIGODENDROGLIOMA	III	LOH	LOH	mutation	wild type
GSM405302	0.543557385	0.442998539	0.0107	41.39	0.74	1	GBM	IV	NA	NA	no mutation	amplification
GSM405339	0.53907636	0.43934651	9.00E-04	78.08	NA	0	GBM	IV	NA	NA	no mutation	amplification
GSM405419	0.518829447	0.422845303	0.0073	36.27	2.93	1	GBM	IV	NA	NA	mutation	wild type
GSM405483	0.50780064	0.41385684	6.00E-04	32.35	0.19	0	PILOCYTIC ASTROCYTOMA	I	NA	NA	no mutation	NA
GSM405362	0.507123914	0.41330531	4.00E-04	38.11	1.06	1	GBM	IV	no LOH	no LOH	no mutation	NA
GSM405422	0.494759945	0.403228692	1.00E-04	70.67	0.91	1	GBM	IV	no LOH	no LOH	no mutation	NA
GSM405325	0.468020119	0.381435769	4.00E-04	42.98	3.65	1	OLIGOASTROCYTOMA	III	NA	NA	mutation	wild type
GSM405203	0.458655693	0.373803774	0	38.58	8.92	1	OLIGODENDROGLIOMA	III	LOH	LOH	no mutation	wild type
GSM405452	-0.405048011	-0.352486153	0.0119	71.02	0.35	1	GBM	IV	NA	NA	no mutation	wild type
GSM405464	-0.452857796	-0.394091806	1.00E-04	54.72	0.56	1	GBM	IV	NA	NA	no mutation	NA
GSM405299	-0.475189758	-0.413525817	0.0032	54.94	1.75	1	GBM	IV	NA	NA	NA	NA
GSM405238	-0.516140832	-0.449162794	0.056	37.25	0.94	1	GBM	IV	NA	NA	no mutation	NA
GSM405417	-0.530644719	-0.461784555	2.00E-04	77.31	0.02	1	GBM	IV	no LOH	no LOH	NA	NA
GSM405361	-0.531028807	-0.462118801	0	79.19	1.64	1	OLIGODENDROGLIOMA	III	no LOH	no LOH	no mutation	wild type
GSM405368	-0.55473251	-0.482746546	0	32.14	1.81	1	GBM	IV	NA	NA	NA	NA
GSM405321	-0.555390947	-0.483319539	0	33.83	3.97	1	ASTROCYTOMA	III	NA	NA	mutation	wild type

GSM405446	-0.558408779	-0.485945757	0.0111	68.18	0.73	1	GBM	IV	NA	no LOH	mutation	NA
GSM405470	-0.56354824	-0.490418285	0	31.72	1.92	1	GBM	IV	NA	NA	mutation	NA
GSM405445	-0.563712849	-0.490561533	7.00E-04	56.15	3.33	0	OLIGODENDROGLIOMA	III	no LOH	no LOH	no mutation	NA
GSM405304	-0.570132602	-0.496148214	0	66.39	0.56	1	GBM	IV	NA	NA	no mutation	NA
GSM405340	-0.574833105	-0.500238747	0.0366	52.88	5.56	0	GBM	IV	no LOH	no LOH	mutation	wild type
GSM405455	-0.587288523	-0.511077863	0	55.49	0.23	1	GBM	IV	NA	NA	mutation	NA
GSM405277	-0.590525834	-0.513895079	0	43.89	2.76	1	ASTROCYTOMA	III	NA	NA	mutation	wild type
GSM405450	-0.593854595	-0.516791876	1.00E-04	36.66	13.3	0	OLIGOASTROCYTOMA	III	NA	NA	NA	NA
GSM405443	-0.610992227	-0.531705609	0.0318	56.62	0.98	1	GBM	IV	NA	NA	no mutation	amplification
GSM405402	-0.611028807	-0.531737442	0	23.72	4.55	0	ASTROCYTOMA	II	no LOH	NA	no mutation	amplification
GSM405263	-0.611394604	-0.532055771	0	61.74	1.55	1	GBM	IV	NA	NA	no mutation	wild type
GSM405453	-0.612985825	-0.533440504	0	70.23	0.21	1	GBM	IV	NA	no LOH	no mutation	amplification
GSM405296	-0.614302698	-0.53458649	0.0168	41.09	0.29	1	GBM	IV	no LOH	no LOH	no mutation	wild type
GSM405400	-0.630855053	-0.548990896	0.0028	49.64	0.45	1	ASTROCYTOMA	III	no LOH	NA	no mutation	wild type
GSM405268	-0.631458619	-0.549516139	0	48.04	0.64	1	GBM	IV	no LOH	no LOH	no mutation	amplification
GSM405273	-0.632556013	-0.550471128	0	56.42	0.54	1	OLIGOASTROCYTOMA	III	NA	NA	no mutation	NA
GSM405271	-0.643895748	-0.560339339	0	69.89	0.3	1	GBM	IV	NA	NA	NA	NA
GSM405365	-0.66085048	-0.575093907	0	64.29	2.66	1	GBM	IV	no LOH	no LOH	no mutation	NA

GSM405211	-0.661234568	-0.575428153	0.0023	34.93	1.83	1	OLIGODENDROGLIOMA	III	LOH	LOH	mutation	NA
GSM405214	-0.664252401	-0.578054371	0	37.84	1.5	1	GBM	IV	no LOH	no LOH	no mutation	wild type
GSM405348	-0.674659351	-0.587110842	0.0011	11.72	0.03	0	PILOCYTIC ASTROCYTOMA	I	NA	NA	NA	NA
GSM405295	-0.679890261	-0.591662953	0.0011	41.77	1.99	1	ASTROCYTOMA	III	NA	NA	NA	NA
GSM405218	-0.693315043	-0.603345642	0	32.36	0.64	1	GBM	IV	no LOH	no LOH	no mutation	amplification
GSM405334	-0.700429813	-0.609537149	0	57.01	1.47	1	OLIGODENDROGLIOMA	III	no LOH	no LOH	NA	wild type
GSM405393	-0.701874714	-0.61079455	0	70.67	0.08	1	GBM	IV	NA	NA	no mutation	NA
GSM405390	-0.70266118	-0.611478958	0.0261	70.07	0.02	1	OLIGOASTROCYTOMA	III	NA	NA	no mutation	NA
GSM405375	-0.706191129	-0.614550837	0	67.03	0.06	1	GBM	IV	no LOH	NA	no mutation	NA
GSM405463	-0.710983082	-0.618720952	0	65.53	2.22	1	GBM	IV	NA	no LOH	no mutation	wild type
GSM405261	-0.71303155	-0.620503597	0	60.46	0.98	1	OLIGODENDROGLIOMA	III	no LOH	no LOH	mutation	NA
GSM405477	-0.71478738	-0.622031578	0	73.64	0.11	1	GBM	IV	NA	NA	NA	NA
GSM405471	-0.721572931	-0.627936589	0	78.12	0.15	1	GBM	IV	NA	NA	mutation	NA
GSM405290	-0.738692273	-0.642834405	0	45.5	1.16	1	GBM	IV	NA	NA	NA	NA
GSM405288	-0.742021033	-0.645731203	0	41.93	1.53	1	OLIGOASTROCYTOMA	III	no LOH	no LOH	NA	wild type
GSM405364	-0.746977595	-0.650044566	0	37.61	9.85	1	OLIGODENDROGLIOMA	III	LOH	LOH	mutation	wild type
GSM405397	-0.748861454	-0.651683963	0.0187	60.36	0.35	1	GBM	IV	no LOH	no LOH	no mutation	amplification
GSM405240	-0.771504344	-0.671388553	0.0049	33.09	6.62	0	GBM	IV	no LOH	no LOH	mutation	NA
GSM405447	-0.782130773	-0.680636022	0	59.03	2.79	1	GBM	IV	no LOH	no LOH	NA	NA

GSM405301	-0.785788752	-0.683819316	0	65.35	0.3	1	GBM	IV	NA	NA	NA	NA
GSM405233	-0.79310471	-0.690185904	0	51.64	0.86	1	GBM	IV	NA	NA	no mutation	wild type
GSM405472	-0.796360311	-0.693019036	0	62.11	0.34	1	GBM	IV	NA	NA	mutation	NA
GSM405241	-0.811650663	-0.706325205	0	55.98	0.16	1	GBM	IV	NA	NA	NA	NA
GSM405236	-0.829208962	-0.721605017	0	52.2	1.03	1	GBM	IV	NA	NA	no mutation	NA
GSM405407	-0.844938272	-0.735293181	0	81.18	0.82	1	ASTROCYTOMA	III	no LOH	no LOH	no mutation	NA
GSM405259	-0.864252401	-0.752100974	0	64.01	0.41	1	ASTROCYTOMA	III	NA	NA	no mutation	NA
GSM405442	-0.866758116	-0.754281531	0	63.61	0.3	1	GBM	IV	NA	NA	no mutation	wild type
GSM405243	-0.868221308	-0.755554848	0	61.33	0.88	1	GBM	IV	NA	NA	NA	NA
GSM405423	-0.871129401	-0.758085567	0	35.67	6.12	1	ASTROCYTOMA	III	LOH	no LOH	mutation	NA
GSM405421	-0.872812071	-0.759549882	0	38.4	6.08	0	ASTROCYTOMA	III	no LOH	no LOH	no mutation	wild type
GSM405457	-0.879048925	-0.764977399	0	70.98	0.3	1	OLIGODENDROGLIOMA	III	no LOH	no LOH	no mutation	wild type
GSM405282	-0.889638775	-0.774193035	0	51.92	0.12	1	GBM	IV	NA	NA	no mutation	NA
GSM405412	-0.897759488	-0.781259948	0	55.71	0.65	1	GBM	IV	NA	no LOH	no mutation	NA
GSM405320	-0.902039323	-0.784984402	0	70.28	0.6	1	GBM	IV	NA	NA	no mutation	wild type
GSM405416	-0.912757202	-0.794311453	0	64.26	0.34	1	GBM	IV	NA	NA	NA	NA
GSM405353	-0.918573388	-0.799372891	0	55.39	0.7	1	GBM	IV	NA	NA	no mutation	amplification
GSM405426	-0.920859625	-0.80136245	0	67.1	0.05	1	GBM	IV	NA	NA	mutation	wild type

GSM405415	-0.933004115	-0.811930986	0	67.48	0.5	1	GBM	IV	no LOH	no LOH	no mutation	NA
GSM405374	-0.940448102	-0.81840899	0	58.58	1.21	1	GBM	IV	LOH	LOH	no mutation	wild type
GSM405456	-0.94083219	-0.818743236	0	52.5	NA	0	GBM	IV	NA	NA	no mutation	NA
GSM405278	-0.947105624	-0.824202585	0	58.23	0.73	1	GBM	IV	NA	NA	no mutation	amplification
GSM405313	-0.963090992	-0.83811358	0	32.5	3.31	1	GBM	IV	NA	NA	mutation	wild type
GSM405235	-0.969108368	-0.843350099	0	71.09	0.21	1	GBM	IV	NA	NA	no mutation	NA
GSM405245	-0.97561957	-0.849016362	0	37.98	1.4	1	GBM	IV	no LOH	NA	no mutation	NA
GSM405293	-1.006474623	-0.875867448	0	63.73	0.88	1	GBM	IV	NA	NA	mutation	amplification
GSM405403	-1.025624143	-0.892531992	0	38.42	0.04	1	ASTROCYTOMA	III	NA	NA	NA	NA
GSM405430	-1.052967535	-0.916327115	0	61.1	0.35	1	GBM	IV	no LOH	no LOH	no mutation	wild type
GSM405265	-1.082524005	-0.942048131	0	32.14	1.81	1	ASTROCYTOMA	III	NA	NA	no mutation	wild type
GSM405459	-1.102222222	-0.95919017	0	64.28	1.14	1	GBM	IV	no LOH	no LOH	no mutation	NA
GSM405479	-1.102807499	-0.959699497	0	63.3	0.38	1	GBM	IV	NA	NA	mutation	amplification

Table-S6. Confusion Matrix for cross validation of Phillips Classification signature

		Predicted			
		Mesenchymal	**Proneural**	**Proliferative**	**Class Error Rate**
Actual	**Mesenchymal**	30	0	5	0.14285714
	Proneural	2	34	1	0.08108108
	Proliferative	4	0	24	0.14285714
	Overall Error Rate				0.12

Table-S7. 50 compounds from Eli Lilly targets common oncologic pathways. Table of 50 small molecules from Eli Lilly, showing the targeting of common oncologic pathways in our GPCs.

Compound No.	Targets
1	Gamma-secretase
2	Gamma-secretase
20	Gamma-secretase
3	PPARα, PPARγ
16	PPARα, PPARγ
4	PI3Kα
31	mTOR, PI3Kα
42	mTOR, PI3Kα
43	mTOR, PI3Kα
46	mTOR, PI3Kα
7	mTOR
5	GSK3β, CDK2, CDK4
8	GSK3β, CDK1, CDK2
6	GSK3β > PKCβ (~ 10×)
9	GSK3β, CDK2, CDK4, PKCα/β
12	GSK3β > IKKα (~ 10×)
14	GSK3β
24	CDK1, CDK2, CDK4, CDK6
37	CDK1, CDK4, CDK9
39	CDK1, TAK1
40	CDK1, CDK9, TAK1
44	CDK9 > CDK7 (~ 10×)
45	CDK9
48	CDK9
19	AurA, TAK1
11	p70s6, PKAα, AKT
41	p70s6, PKA, PKCβ2, PKCε
33	p70s6, PLK1, FLT3
22	PLK1, PLK3
35	PLK1, PLK3
50	PLK1, PLK3
25	ABL1, FLT3
23	ABL1, EphB4, FLT3, DDR2, FGFR1, KDR
27	ABL1, EphB2 > EphB4 (~ 10×)
36	EphB4, EphB2, FGFR1/3
32	JAK2 >> AurA/B, FGFR1/3, JAK3 (~ 20-40×)
13	TGFβR1
29	TGFβR1
10	TGFβR1, p38α-MAPK
17	p38α/β-MAPK
18	p38α/β-MAPK
21	p38α/β-MAPK
15	MMP13
38	MMP2, 3, 12, 13

26	AR, GR, PR
34	AR
28	HH/smo
30	HH/smo
49	HH/smo
47	cMET

SUPPLEMENTARY FIGURES

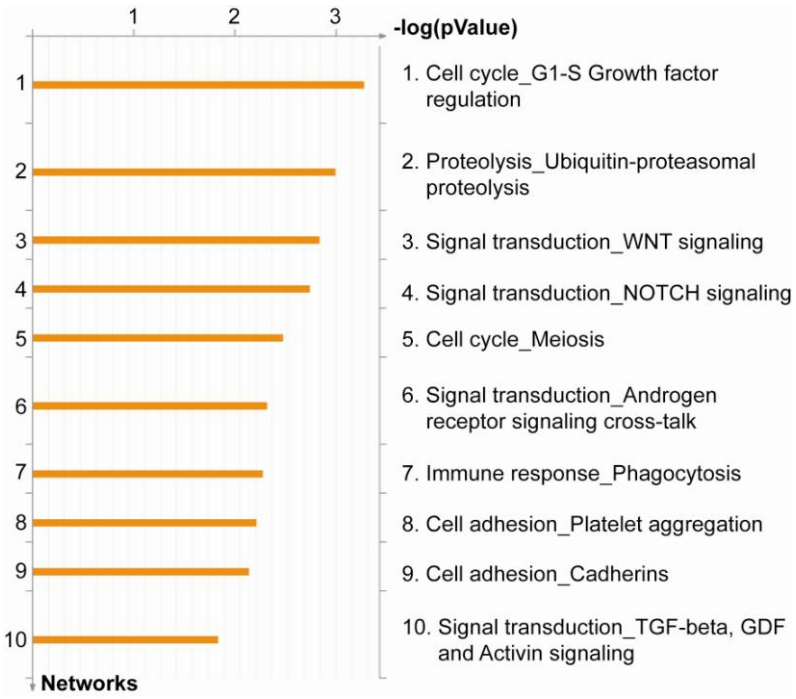

Figure-S1A. Top 10 process networks generated from oligodendroglial GPC gene signature using GeneGo analysis. The "oligodendroglial GPC gene signature" was enriched in the Notch, Wnt and TGFβ signaling.

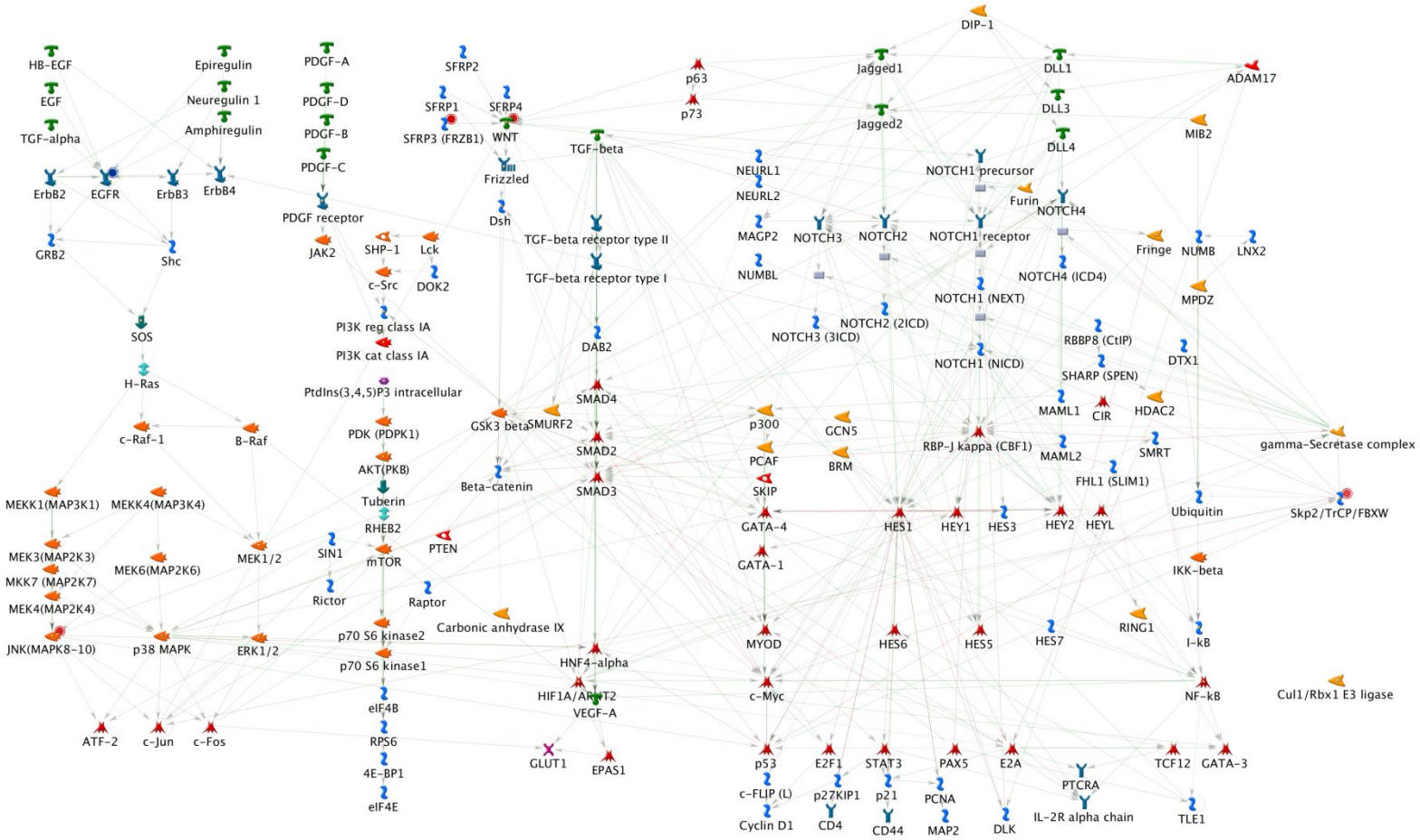

Figure-S1B. Notch signaling identified from GeneGo Process Network. Red circles indicate the 4 key genes (JNK, SFRP3, WNT, Skp2/TrCP/FBXW) up-regulated while blue circles indicate the key gene (EGFR) down-regulated in the OA GPC signature. All other genes shown depict the network of genes affected by these key genes.

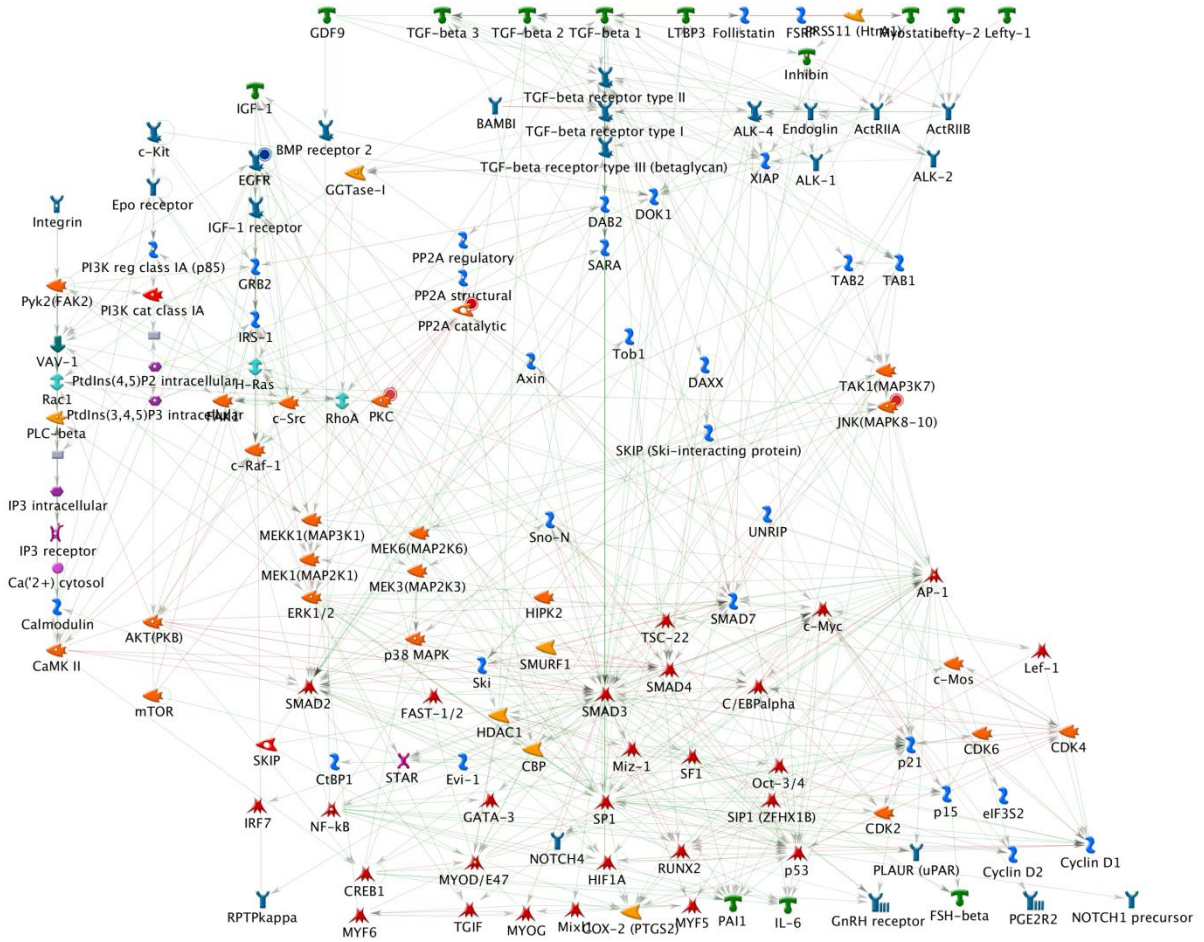

Figure-S1C. TGFβ, GDF and Activin signaling identified from GeneGo Process Network. Red circles indicate the 3 key genes (PKC, PP2A, JNK) up-regulated while blue circles indicate the key gene (EGFR) down-regulated in the OA GPC signature. All other genes shown depict the network of genes affected by these key genes.

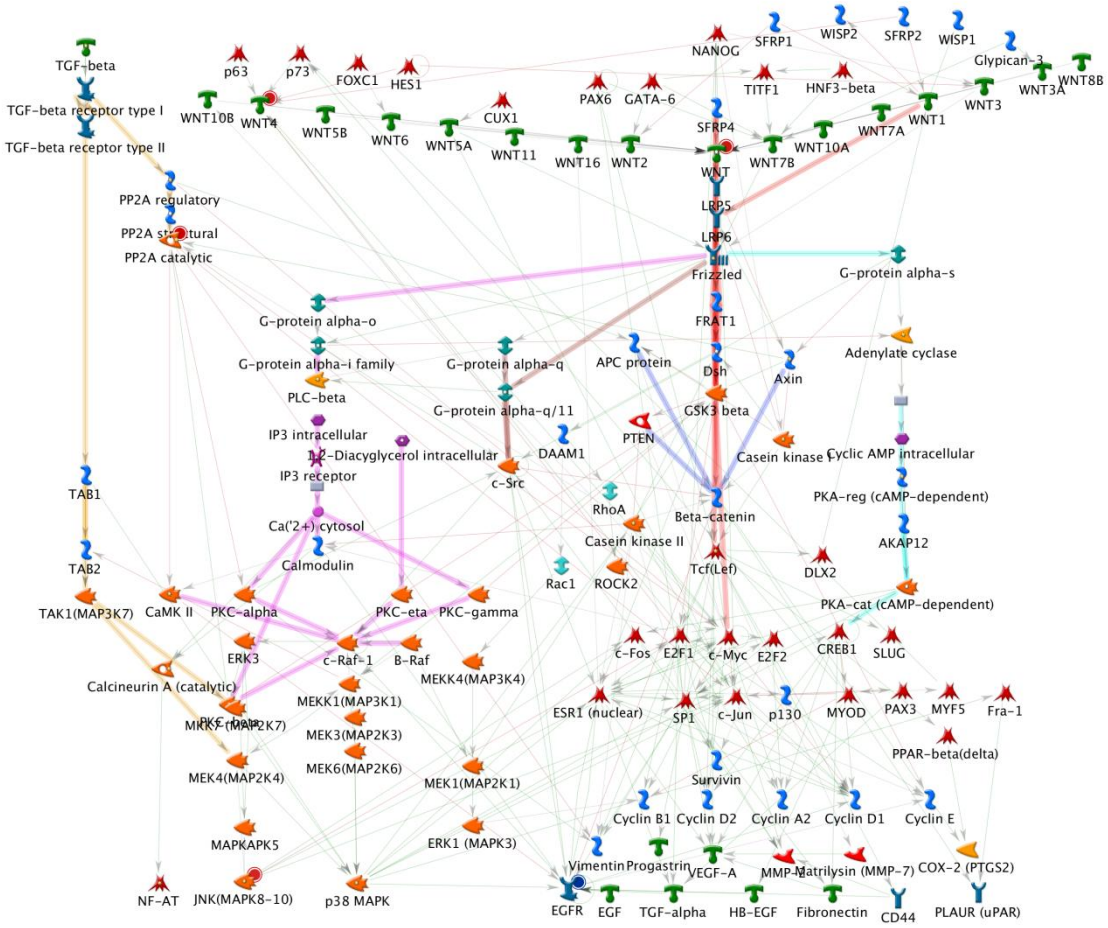

Figure-S1D. WNT signaling identified from GeneGo Process Network. Red circles indicate the 4 key genes (JNK, PP2A, WNT, WNT4) up-regulated while blue circles indicate the key gene (EGFR) down-regulated in the OA GPC signature. All other genes shown depict the network of genes affected by these key genes.

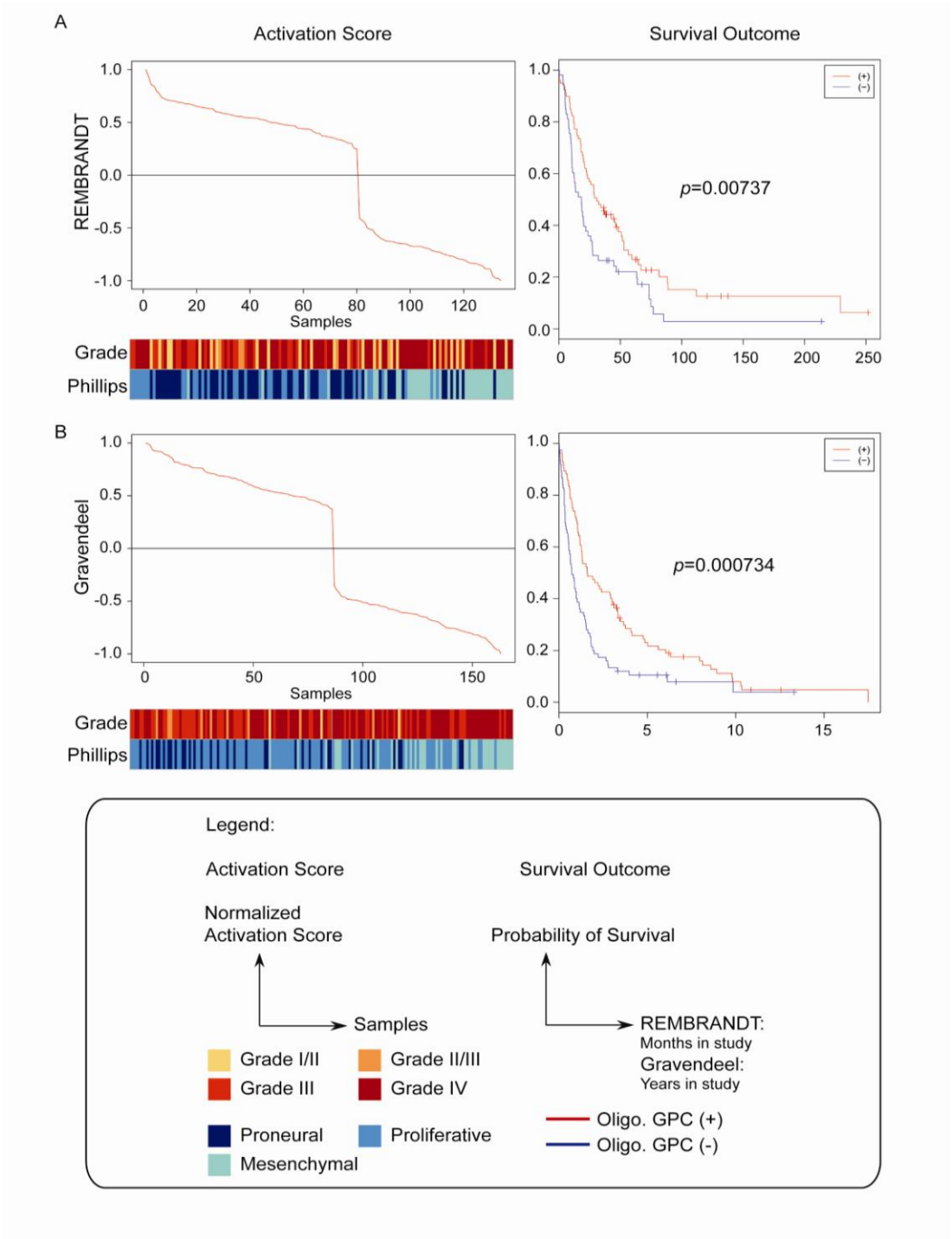

Figure-S2. "NNI-8 GPC versus primary tumor" gene signature stratifies patient survival. Patient survival is shown in all glioma patients. Tumor grade ("Grade") and molecular classification ("Phillips"[10]) distribution corresponding to (+) and (-) classes is shown below the activation score graphs.

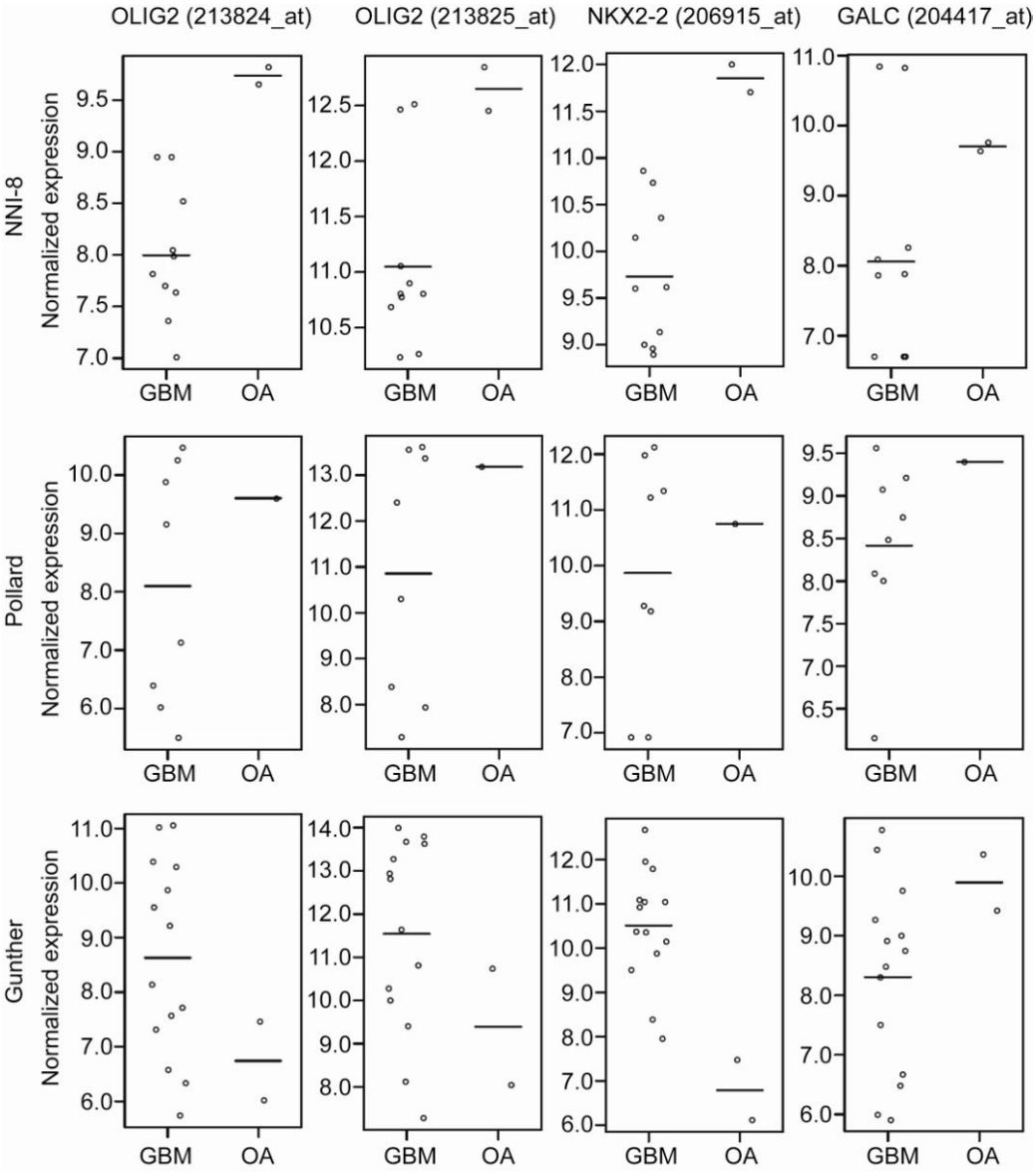

Figure-S3. Oligodendroglial GPCs express OPC markers. Oligodendroglial tumor GPCs (OA) of NNI-8 and Pollard reflect higher immature OPC marker expression[167], Olig2, Nkx2.2 and GalC, in comparison to GBM GPCs (GBM). The Gunther line expresses mature oligodendrocyte marker, GalC, and may reflect its diagnosis as a GBM with oligodendroglial features